DISSERTATION / DOCTORAL THESIS

Titel der Dissertation /Title of the Doctoral Thesis

„Dispersion Relations and the Muon g – 2 Hadronic Light-by-Light Contribution in Multiple Kinematic Regions"

verfasst von / submitted by

Jan Lüdtke, B.Sc. M.Sc.

angestrebter akademischer Grad / in partial fulfilment of the requirements for the degree of

Doktor der Naturwissenschaften (Dr.rer.nat.)

Wien, 2023 / Vienna 2023

Studienkennzahl lt. Studienblatt / degree programme code as it appears on the student record sheet:	A 796 605 411
Dissertationsgebiet lt. Studienblatt / field of study as it appears on the student record sheet:	Physik
Betreut von / Supervisor:	Ass.-Prof. Dr. Massimiliano Procura

Abstract

The muon anomalous magnetic moment has been drawing great interest due to a long-standing tension between its Standard Model evaluation and highly precise measurements. In order to match the increased accuracy of forthcoming experimental results and ultimately establish size and nature of the discrepancy, progress has to be made on the theory side in terms of accurate predictions with reliable uncertainty estimates. The focus of this thesis lies on improving the data-driven dispersive evaluation of the hadronic light-by-light (HLbL) contribution to the muon $g-2$, which is responsible for a substantial part of the uncertainty in the present Standard Model prediction. While the dispersive HLbL determination is under firm control at low energies, the contribution from the transition regions between this and the regimes where short-distance constraints (SDCs) are valid is less understood and causes the bulk of the uncertainty.

We provide a new framework to combine the dispersive low-energy input on HLbL with all known constraints in regions where perturbative QCD and operator product expansions are valid. Instead of having to rely on hadronic model calculations, we smoothly connect these multiple kinematic regions through general interpolants. This leads to an independent evaluation of the effect of SDCs on HLbL and, crucially, provides robust uncertainty estimates. We find that intermediate states with masses between 1 and 2 GeV play a key role in reducing the theory error on HLbL.

However, in the established dispersive formalism, in which the photon virtualities are kept fixed, not all these contributions are accessible. We thus develop a new dispersive framework for HLbL that enables the evaluation of effects from intermediate states with spin larger or equal to two and masses in the 1–2 GeV range, for which only model estimates with no reliable theory error exist. At variance with the established dispersive approach, we employ dispersion relations directly in the limit of a soft external photon, which corresponds to the magnetic field entering the definition of $g-2$. We first discuss the formalism for a simpler case than HLbL, namely the correlator of two vector currents and one axial-vector current, which is closely related to one particular SDC for HLbL. Afterwards, we apply our novel approach to HLbL and work out the effects of single-particle intermediate states. For two-pion intermediate states, the dispersive treatments of new sub-processes are required and we therefore present a detailed analysis of $\pi\pi \to \gamma\pi\pi$ in the soft-photon limit. This paves the way for a model-independent inclusion of $\pi\pi$ D-waves and tensor mesons into HLbL and thus for a reduction of the uncertainty of this contribution to the muon $g-2$.

Zusammenfassung

Das anomale magnetische Moment des Myons erhält große Beachtung, da es seit langem eine Abweichung zwischen Berechnungen im Standardmodell und hochpräzisen Messungen aufweist. Um mit der erhöhten Genauigkeit bevorstehender experimenteller Ergebnisse mitzuhalten und letztlich die Größe und Art der Diskrepanz feststellen zu können, werden genauere theoretische Berechnungen mit verlässlichen Fehlern benötigt. Ziel dieser Arbeit ist es, die datenbasierte dispersive Bestimmung des Hadronic Light-by-Light (HLbL)-Beitrags zum $g-2$ des Myons zu verbessern, der einen wesentlichen Teil zur Unsicherheit der Standardmodell-Vorhersage beiträgt. Während die dispersive HLbL-Bestimmung bei niedrigen Energien solide ist, wird der Beitrag der Übergangsregionen zu den Bereichen, wo Short-Distance Constraints (SDCs) gültig sind, weniger gut verstanden und verantwortlich für den größten Teil des Fehlers.

Diese Arbeit führt eine neue Methode ein, den dispersiven Niedrigenergieinput zu HLbL mit jenen Regionen zu kombinieren, in denen perturbative QCD und Operatorproduktentwicklungen gültig sind. Die verschiedenen Energieregionen werden mit glatten Interpolationsfunktionen verknüpft, ohne auf hadronische Modelle angewiesen zu sein. Auf diese Weise wird der Effekt von SDCs auf HLbL bestimmt und insbesondere eine robuste Fehlerabschätzung ermöglicht. Die Untersuchung zeigt, dass Zwischenzustände mit Massen zwischen 1 und 2 GeV eine entscheidende Rolle spielen, um den Fehler von HLbL zu reduzieren.

Im etablierten dispersiven Zugang, bei dem die Virtualitäten der Photonen festgehalten werden, sind jedoch nicht alle diese Zustände zugänglich. Daher wird in dieser Arbeit ein neuer dispersiver Formalismus für HLbL entwickelt, der es erlaubt, den Effekt von Zwischenzuständen mit Spin zwei oder größer und Massen zwischen 1 und 2 GeV zu berechnen, für die es bisher nur Modellabschätzungen ohne zuverlässige Fehler gibt. Im Gegensatz zum etablierten Zugang, werden hier Dispersionsrelationen im Limes eines weichen Photons verwendet, das zum magnetischen Feld in der Definition des $g-2$ gehört. Der Formalismus wird zunächst für einen einfacheren Fall als HLbL diskutiert: den Korrelator von zwei Vektorströmen und einem Axialvektorstrom, der unter anderem in einem bestimmten SDC für HLbL benötigt wird. Anschließend wird die neuartige Methode auf HLbL angewendet und die Effekte von Einteilchenzwischenzuständen berechnet. Für Zwei-Pion-Zwischenzustände werden dispersive Beschreibungen neuer Unterprozesse benötigt. Daher wird eine detaillierte Analyse von $\pi\pi \to \gamma\pi\pi$ für ein weiches Photon präsentiert. Das ebnet den Weg, $\pi\pi$-D-Wellen und Tensormesonen modellunabhängig in die Berechnung von HLbL zu integrieren und so die Unsicherheiten seines Beitrags zu $g-2$ zu reduzieren.

Acknowledgments

First and foremost I am grateful to my thesis supervisor Massimiliano Procura for offering me the possibility to work on such a fascinating topic, for his constant support and for carefully reading this thesis. Furthermore, I want to thank our close collaborator Peter Stoffer who has been involved in the largest part of the work presented here. The regular meetings with both of them were particularly enlightening and countless new ideas were developed during them.

I thank all members of the particle physics group at the University of Vienna for warmly welcoming me when I entered it in 2018. I have always been enjoying the chats about both physics and non-physics topics and the diversity of the subjects covered in the group broadened my mind. A special thanks goes to Michael Adam for joining the work on the muon $g-2$, which gave me the chance to have more frequent discussions on the topics I have been working on. I am also particularly thankful to my office mate Angelika Widl for the pleasant working atmosphere and for sharing her informative insights about the early spread of Covid-19.

I thank Gilberto Colangelo, Martin Hoferichter, Josef Leutgeb and Anton Rebhan for useful discussions on several aspects of the work. I am particularly grateful to Gilberto Colangelo and Anton Rebhan for accepting to review my thesis. Support by the FWF-DACH Grant I 3845-N27 and by the FWF doctoral program Particles and Interactions, project no. W1252-N27, is gratefully acknowledged.

Finally, I thank my family for their invaluable support. In spite of the large distance and the travel restrictions during the pandemic, my parents Iris and Bernd as well as my brother Nico have always stayed in close contact with me and have given advises whenever needed. The greatest acknowledgment goes to my wife Christina for her love and encouragement.

Contents

List of Tables

List of Figures

List of Abbreviations

ABJ	Adler–Bell–Jackiw
BNL	Brookhaven National Laboratory
BTT	Bardeen–Tung–Tarrach
CHPS	Colangelo–Hoferichter–Procura–Stoffer
DSE	Dyson–Schwinger equation
FNAL	Fermilab National Accelerator Laboratory
HLbL	hadronic light-by-light
hQCD	holographic QCD
HVP	hadronic vacuum polarization
HW	hard-wall model
J-PARC	Japan Proton Accelerating Complex
LO	leading order
MV	Melnikov–Vainshtein
NLO	next-to-leading order
NNLO	next-to-next-to-leading order
NWA	narrow-width approximation
OPE	operator product expansion
pQCD	perturbative quantum chromodynamics
QCD	quantum chromodynamics
QED	quantum electrodynamics
QFT	quantum field theory
RχT	Resonance Chiral Theory
SDC	short-distance constraint
SM	standard model
SW	soft-wall model
TFF	transition form factor
VFF	vector form factor
VMD	vector-meson dominance
VVA correlator	correlator of two vector currents and an axial-vector current
χPT	Chiral perturbation theory

1 Introduction

The anomalous magnetic moment of the muon a_μ has been receiving particular attention since the measurement at the Brookhaven National Laboratory (BNL) experiment E821 [1] observed a tension compared to the Standard Model (SM) prediction at the time, see Refs. [1, 2] and references therein. Since then, the SM prediction has been considerably improved and in 2020 a consensus on the status of the efforts has been reached among the global community as summarized by the White Paper, Ref. [3]. According to this, the most up-to-date full SM evaluation is [3–23]

$$a_\mu^{\text{SM}} = (116\,591\,810 \pm 43) \times 10^{-11} \,. \tag{1.1}$$

In the meantime, the new E989 experiment at the Fermilab National Accelerator Laboratory (FNAL) got undergoing with the final goal to improve the precision reached at BNL by a factor of 4 [24]. The first published measurement in 2021 [25–28] updates the experimental world average to

$$a_\mu^{\text{exp}} = (116\,592\,061 \pm 41) \times 10^{-11} \,, \tag{1.2}$$

which differs from Eq. (1.1) by $4.2\,\sigma$. To determine the source of this tension and to make full use of the expected four-fold improvement of the experimental measurement, it is crucial to achieve advances in the SM prediction both in precision and reliability. Recent progress in this direction has been made, which includes analyses that point towards a reduction of the tension [29–36]. These are presently under intense scrutiny [37].

While the bulk of the SM prediction is given by pure quantum electrodynamics (QED) contributions, its uncertainty is almost entirely due to strong-interaction effects described by quantum chromodynamics (QCD). The most important ones, namely hadronic vacuum

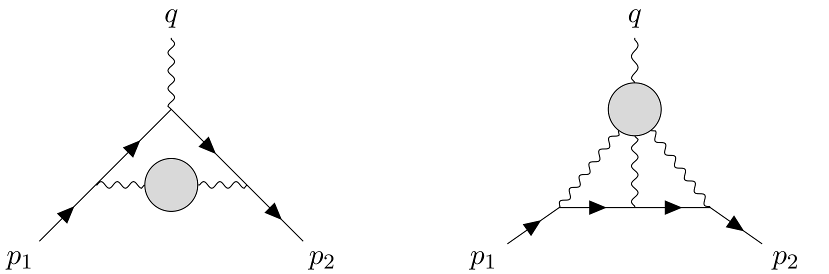

Figure 1.1: The two most important hadronic effects: leading-order HVP on the left and HLbL on the right. The blobs denote arbitrary effects due to the strong interaction.

polarization (HVP) and hadronic light-by-light scattering (HLbL), are shown in Fig. 1.1. At present, these are not yet known at the precision required to match the projected goal of the final experimental results at Fermilab. Ref. [3] reviews and combines calculations of both HVP and HLbL, each in a data-driven dispersive formalism and from lattice QCD. The goal of this thesis is to improve the data-driven determination of HLbL, which involves the interaction of four photons due to the strong force. Its evaluation in Ref. [3] is based on the dispersive formalism developed in Refs. [17,38,39]. In that framework, the effects of the dominant exclusive intermediate states are expressed in terms of simpler sub-processes, given through hadronic form factors and scattering amplitudes. In order to capture the collective effect of suppressed heavier intermediate states, a matching to short-distance constraints (SDCs) [21,40–46], derived from perturbative QCD (pQCD) and the operator product expansion (OPE) [15,20,21,40,47–49], has to be performed.

While the evaluation of effects from the lightest intermediate states is under excellent control both conceptually and numerically [16–19,39,50,51], the main uncertainties of the data-driven HLbL estimate given in Ref. [3] are due to the effect of resonances in the 1–2 GeV range, which can currently only be estimated in the context of hadronic models [15,41–44,52–57], and the incorporation of SDCs at high energies. Both points will be addressed in this thesis.

We begin with a review of both the principle underlying the a_μ measurements and the status of its SM prediction in Ch. 2. The example of HVP is used to introduce the concepts and notation needed in the following chapters and an introduction to the data-driven evaluation of HLbL and its current status and limitations is given.

In Ch. 3, we turn to the combination of SDCs with the low-energy dispersive representation. We review the constraints and implementations available in the literature. Then, we provide a novel approach that for the first time does not rely on a specific hadronic model in the intermediate energy range. Instead, we use interpolants with parameters fixed from the SDCs and a smooth matching to the low-energy representation. This allows us to efficiently study the uncertainties and determine which additional input would be required to reduce them. This chapter is based on Ref. [45].

We find that in order to significantly reduce the uncertainty on HLbL, good control over the effects of additional intermediate states with masses between 1 and 2 GeV is mandatory. However, besides the lack of experimental input to determine the required form factors, intermediate states of spin two and larger also suffer from theoretical issues. In the currently employed dispersive formalism, the hadronic blob in the diagram in Fig. 1.1 is expressed in terms of a redundant set of scalar functions free of kinematic singularities and zeros. In order to avoid these redundancies, one then changes to a non-redundant basis set, but at the cost of introducing kinematic singularities. The form of these singularities is such that the scalar functions still fulfill standard dispersion relations, but the results due to individual exclusive intermediate states are singular in certain kinematic limits.

The fact that the Lorentz structures in the decomposition of the HLbL tensor have different mass dimensions allows one to derive sum rules, which ensure that the residues of the kinematic poles vanish. However, these sum rules are only guaranteed to be fulfilled once the full infinite tower of intermediate states is summed up. Results for individual intermediate states do contain these poles, which when plugged into the $g-2$ diagram lead to divergent results. In order to avoid this, one could choose a scheme to subtract the poles from the integrand. However, as long as the partial sum included in a calculation does not fulfill the sum rules, the obtained result will strongly depend on the chosen subtraction scheme and it is unclear which scheme should be preferred.

In this thesis, we develop a novel dispersive formalism that is free of these issues. In the limit where the momentum of the external photon, q_4, vanishes, a Lorentz basis of tensor structures free of kinematic singularities and zeros exists. Thus, writing dispersion relations in this limit gives finite well-defined results for any individual intermediate state without the need to specify an arbitrary subtraction scheme. However, the constraints from unitarity are more difficult to implement in this setup. The origin of this is that in the limit $q_4 \to 0$, two channels differing by whether the soft photon is incoming or outgoing are not kinematically separable any more.

In order to concentrate on this new aspect without having to deal with the complicated Lorentz structure of HLbL, we first consider a simpler process with a soft photon in Ch. 4, namely the correlator of two vector currents and an axial-vector current (VVA). This allows us to study in detail the new dispersive formalism and its relation to the one that is currently used for HLbL. Except for this being an important step towards an application to HLbL, the VVA correlator is also interesting for two other reasons: it is needed for the hadronic electroweak contribution to a_μ, which can currently only be evaluated through hadronic models [6, 58, 59], and for a particular SDC for HLbL [15, 21]. We discuss both applications in this chapter.

Having understood the simpler case of VVA, we return to HLbL in Ch. 5 and perform important steps in the application of the new formalism also in this case. We first explain in more detail the issues with higher-spin intermediate states in the established formalism and why the new approach is ideally suited to avoid them. Then, we derive results for single-particle intermediate states including tensor mesons and show which sub-processes are needed for a calculation of two-pion contributions. An essential result is that the issues with redundancies does not reenter through the tensor decompositions of the sub-processes. Finally, in this chapter, we focus on another difficulty that did not show up in VVA: the hadronic blob in the HLbL diagram does not contain charged particles and thus is finite in the soft-photon limit, but this is not true for all sub-processes appearing in the unitarity relations. Crucially, however, the form of these singularities is fully determined by the corresponding process without the soft photon, which makes it possible to demonstrate their cancellation analytically and separately for each considered intermediate state. The content of this chapter except for Sec. 5.3 is published in Ref. [60].

In Ch. 6, we then focus on the process $\pi\pi \to \gamma\pi\pi$ for a soft photon, which is a necessary input for the two-pion contribution to HLbL in the new dispersive formalism. We demonstrate explicitly that the soft-photon singularities cancel out and show how the five-point kinematics can be reduced to four-point kinematics by an expansion in the soft-photon momentum. Afterwards, we derive integral equations of the Khuri–Treiman type and present a numerical implementation including $\pi\pi$-scattering D-waves. This paves the way for a similar study of the second important so-far unknown sub-process, $\gamma^*\gamma^* \to \gamma\pi\pi$, for which our results are required as input, and finally the two-pion intermediate state to HLbL. In addition, both studies will strongly profit from the theoretical advances made in Chs. 4–6. They thus represent important steps towards the goal of incorporating $\pi\pi$ D-waves into HLbL.

Ch. 7 is devoted to conclusions and outlook.

2 The Anomalous Magnetic Moment of the Muon

The magnetic moment of the electron played an essential role in establishing QED as the microscopic theory for interactions between matter and electromagnetic fields [61, 62]. Later, the SM was completed by including also the weak [63–65] and strong [66, 67] interactions and the last SM particle, the Higgs boson, was discovered at the LHC in 2012 [68]. However, the SM, despite being incredibly successful in describing a huge variety of experiments, does not offer explanations for neutrino masses, dark matter or the observed matter-antimatter asymmetry. This implies that it eventually has to be replaced by another theory and it might be that lepton magnetic moments turn out crucial in its development again.

A point-like particle at rest has only one characteristic axis, its spin $\boldsymbol{S}$. Due to rotational symmetry, any static magnetic dipole moment $\boldsymbol{\mu}$ thus must be along that axis and we can define the particle's gyromagnetic factor or g-factor g through[1]

$$\boldsymbol{\mu} = g\frac{Qe}{2m}\boldsymbol{S}\,, \tag{2.1}$$

where Q is the particle's charge in units of e ($Q = -1$ for charged leptons) and m its mass.

The Dirac equation coupled minimally to the electromagnetic field

$$(\mathrm{i}\not{D} - m)\psi(x) = 0 \tag{2.2}$$

leads to $g = 2$. At this point, one could add a term proportional to $\sigma^{\mu\nu}F_{\mu\nu}\psi(x)$ that would modify g, but this would correspond to a non-renormalizable operator in the corresponding Lagrangian density. Indeed, $g = 2$ turns out to be approximately fulfilled at sub-percent precision for the electron and the muon, which motivates the definition of the anomaly as

$$a = \frac{g-2}{2}\,. \tag{2.3}$$

In 1947, a measurement of the ground state hyperfine splitting of hydrogen [61] found a non-vanishing value for the anomalous magnetic moment of the electron a_e. While this was first attributed to an underestimated uncertainty in the fine-structure constant, Schwinger showed that this experimental result is compatible with a correction to the electron's g-factor

[1] We use natural units with $\hbar = c = 1$ throughout this thesis.

calculated in the newly developed theory of QED [62]. This success had a great impact in establishing QED, and relativistic quantum field theory (QFT) in general, as the framework to describe the fundamental interactions of elementary particles.

In the following decades, both measurements and theory predictions steadily improved so that by now all sectors of the SM are probed in the comparison. The precision of the experimental PDG world average [69]

$$a_e^{\mathrm{exp}} = (115\,965\,218\,076 \pm 28) \times 10^{-14} \tag{2.4}$$

based on Refs. [70, 71] has reached the incredible precision of 0.24 ppb. However, the SM prediction is currently affected by a $5.4\,\sigma$ tension between two measurements of the fine-structure constant based on ^{133}Cs [72] or ^{87}Rb [73] atoms. This demands further investigations to allow for a stringent comparison against the experimental result.

Assuming lepton-flavor universal couplings of the new physics to the SM, the muon anomalous magnetic moment a_μ is more sensitive to virtual effects from heavy particles of mass M compared to the electron due to the approximate scaling (up to logarithms)

$$\frac{\delta a_l}{a_l} \sim \frac{m_l^2}{M^2}\,. \tag{2.5}$$

Heavy new physics would thus have a 40 000 times larger effect on a_μ compared to a_e and the slightly less precise experimental world average given in Eq. (1.2) with a precision of 0.35 ppm is still 30 times more sensitive to heavy new physics than a_e^{exp}. The comparison with the 2020 theory consensus [3] in Eq. (1.1), which will be reviewed in Sec. 2.2, indeed shows a $4.2\,\sigma$ tension. This result is currently under scrutiny due to recent results from lattice QCD for the HVP contribution to a_μ represented through the diagram on the left-hand side of Fig. 1.1 (see Sec. 2.2 for its precise definition), which are in tension with the corresponding data-driven evaluation [29]. Resolving this issue, as well as generally reducing the uncertainties on the experimental and theory side is crucial to determine whether the observed tension is due to new physics.

In principle, the anomalous magnetic moment of the τ-lepton would be even more sensitive to heavy new physics. However, the short lifetime of the τ makes it impossible to perform a measurement of the type discussed in the next section. Nevertheless, a number of ideas exist how to measure a_τ indirectly at a much lower level of precision compared to a_e and a_μ, see Ref. [74] and references therein. A measurement sensitive to $a_\tau \neq 0$ seems also feasible at the LHC in the near future [75, 76], while for significantly higher precision polarized lepton colliders are needed [77].

In this chapter, we review the basics of the experimental measurement as well as the SM calculation—with particular focus on the most challenging hadronic contributions. In the course of this, we introduce many concepts that will be needed throughout this thesis.

2.1 Measurement

The early muon $g-2$ experiments at CERN [78–84], the modern BNL [1] and FNAL [24–28] experiments as well as the planned experiment at the Japan Proton Accelerator Complex (J-PARC) [85] all follow the same principle. One starts with injecting a beam of muons polarized in the direction of motion, produced from charged-pion decay, into a uniform magnetic field perpendicular to the momentum of the muons. Due to the Lorentz force, the muons travel through the magnetic field in circles (or spirals) with cyclotron frequency

$$\omega_{\mathrm{c}} = \frac{eB}{m_\mu \gamma}\,, \tag{2.6}$$

where B is the strength of the magnetic field and γ the Lorentz factor of the muon beam.

At the same time, the magnetic field also leads to a Larmor precession of the muons' spins with frequency

$$\omega_{\mathrm{L}} = \frac{eB}{m_\mu \gamma}(1 + \gamma a_\mu)\,, \tag{2.7}$$

which implies a precession frequency of the spin relative to the momentum of

$$\omega_{\mathrm{a}} = \omega_{\mathrm{L}} - \omega_{\mathrm{c}} = \frac{eB}{m_\mu} a_\mu\,. \tag{2.8}$$

This anomalous precession frequency is directly proportional to the anomalous magnetic moment a_μ, which increases the precision by a factor of about 850 compared to a measurement of g_μ.

After some time, the muons decay into electrons and neutrinos and the parity violating nature of the weak interaction leads to the decay electrons being preferentially emitted in the direction of the muon spin in the center-of-mass frame. In the laboratory frame, this makes the electrons on average having higher energy if momentum and spin are aligned compared to them being anti-aligned. Thus, the number of electrons with energies above some threshold oscillates with the frequency ω_{a} as a function of time. Together with a precise measurement of the magnetic field, this allows to achieve the high precision required for an accurate test of the SM.

In practice, it is impossible to have a pure uniform magnetic field and no electric fields. At the planned experiment at J-PARC, an effort is made to reduce electric fields and inhomogeneities in the magnetic field as much as possible. This is achieved by using a low-energy ($\sim 210\,\mathrm{MeV}$) muon beam, which allows to keep the radius of the muon orbits below $1\,\mathrm{m}$. This approach is complementary to the BNL and FNAL experiments, where higher-energy muons are used. Then, an electric quadrupole field is needed to keep the muons on their tracks. This field perpendicular to the muon's momenta has the effect of adding another term to Eq. (2.8)

$$\boldsymbol{\omega}_{\mathrm{a}} = \frac{e}{m_\mu c}\left[a_\mu \boldsymbol{B} - \left(a_\mu - \frac{1}{\gamma^2 - 1}\right)\frac{\boldsymbol{v} \times \boldsymbol{E}}{c^2}\right]. \tag{2.9}$$

Here, the components of the vector-valued frequency perpendicular to the magnetic field describe an oscillation around the circular path. By choosing the "magic" energy of 3.098 GeV, corresponding to $\gamma \approx 29.3$, the round bracket in this equation vanishes and the formula reduces to Eq. (2.8).

In both setups, additional corrections with systematic uncertainties have to be applied. These are e.g. due to non-uniformity of the magnetic field, field components parallel to the direction of the momentum, deviations from the magic momentum and beam dynamics. The importance of the individual corrections differs significantly between the two approaches, which would make the J-PARC experiment a valuable cross-check of the BNL and FNAL results.

The final result of the BNL experiment [1] (updated for the latest value of the magnetic moment ratio μ_μ/μ_p [86]) reads

$$a_\mu^{\mathrm{BNL}} = (116\,592\,089 \pm 63) \times 10^{-11} \,. \tag{2.10}$$

Since 2018 the FNAL experiment is taking data with the goal of reducing this uncertainty by a factor of 4 to 16×10^{-11} [24]. The analysis of run 1 has been completed in 2021 with the result [25–28]

$$a_\mu^{\mathrm{FNAL,run1}} = (116\,592\,040 \pm 54) \times 10^{-11} \,, \tag{2.11}$$

whose uncertainty is statistically dominated and thus improvable by data from further runs. The number given in Eq. (1.2) is the world average that arises as the combination of these two experimental results. The goal of the J-PARC experiment is to obtain an independent measurement with a precision of $\sim 50 \times 10^{-11}$ [85], comparable to the individual measurements at BNL and FNAL run 1. The uncertainty is expected to be statistically dominated and thus improvable by acquiring additional data.

2.2 The Muon $g-2$ in the Standard Model

In this section, we review the status of the SM prediction of the muon $g-2$. The two most important hadronic contributions, which are responsible for the bulk of the SM theory uncertainty, will be explained in more detail in the following sections. In 2020, the $g-2$ Theory Initiative has reached a worldwide consensus on the current status of the SM predictions, which is summarized in detail in the White Paper Ref. [3]. The prospects for the future can be found in Ref. [37] and a more pedagogical introduction to the topic is given in the book by Jegerlehner [56].

We consider the matrix element of an electromagnetic vector current $j_{\mathrm{em}}^\mu = \sum_f Q_f \bar{\psi}_f \gamma^\mu \psi_f$, where the sum runs over fermions with charge eQ_f, between muon states with momenta $p_{1/2}$ and helicities $r_{1/2}$

$$\langle \mu^-(p_2, r_2)| \, j_{\mathrm{em}}^\mu(0) \, |\mu^-(p_1, r_1)\rangle = \mathrm{i}\bar{u}(p_2, r_2)\Gamma^\mu u(p_1, r_1) \,. \tag{2.12}$$

Here $\bar{u}$ and u are momentum-space spinors and Γ^μ a Hermitian momentum-dependent matrix in Dirac space. Using Lorentz covariance and the Ward identity $q_\mu \bar{u}(p_2, r_2)\Gamma^\mu u(p_1, r_1) = 0$ with $q = p_1 - p_2$, the vertex function can be expressed in terms of 4 scalar form factors (see e.g. Sec. 3.3 of Ref. [56])

$$\Gamma^\mu = \gamma^\mu F_{\mathrm{E}}(q^2) + \left(\gamma^\mu - \frac{2mq^\mu}{q^2}\right)\gamma_5 F_{\mathrm{A}}(q^2) + \mathrm{i}\sigma^{\mu\nu}\frac{q_\nu}{2m}F_{\mathrm{M}}(q^2) + \sigma^{\mu\nu}\frac{q_\nu}{2m}\gamma_5 F_{\mathrm{D}}(q^2)\,. \tag{2.13}$$

We notice that the decomposition is automatically independent of $p_1 + p_2$ as expected from translational invariance.

The first form factor in Eq. (2.13) is called electric form factor and its normalization corresponds to the charge of the muon in units of e, which is fixed as a renormalization condition, $F_{\mathrm{E}}(0) = 1$. The anapole moment F_{A} is P violating and vanishes at $q^2 = 0$. The anomalous magnetic moment is given by the magnetic form factor at $q^2 = 0$, $F_{\mathrm{M}}(0) = a_\mu$, and the normalization of the CP violating form factor F_{D} is related to an electric dipole moment d_μ, $F_{\mathrm{D}}(0) = -2md_\mu$. The relations to the non-relativistic definitions of the dipole moments are obtained by considering the non-relativistic limits of the corresponding terms in the interaction Hamiltonian. At tree level only $F_{\mathrm{E}}(q^2) = 1$ is non-vanishing so that the standard muon-photon vertex factor is obtained. In pure QED, which conserves P and CP, F_{A} and F_{D} vanish, but they receive small finite contributions if also the weak interaction is included.

The calculation of a_μ in some QFT like the SM usually starts from the renormalized muon-photon vertex, which is then projected onto the magnetic form factor at $q^2 = 0$. Since this calculation is done at the amplitude level, sets of renormalized loop diagrams for the vertex that fulfill the Ward identity lead to well-defined contributions to a_μ with no interference effects to be considered. This allows one to split the SM calculation into three separate sectors:

- diagrams involving only leptons and photons (QED),
- diagrams involving at least one electroweak gauge boson or Higgs boson (electroweak) and
- diagrams without electroweak gauge nor Higgs bosons, but with strongly interacting particles (hadronic).

In this separation, diagrams involving both electroweak effects and strongly interacting particles have been conveniently labeled as electroweak in order to make the contributions from this sector gauge-anomaly free and thus finite.

The contribution to each sector can be written as a series in the fine-structure constant α. The smallness of α leads to a pattern of rapid convergence, which enables the calculations to reach the necessary sub-ppm precision. Numerical results for each contribution as they have been compiled in Ref. [3] can be found in Tab. 2.1 and are briefly reviewed in the following.

Contribution	value$\times 10^{11}$	error$\times 10^{11}$
Experiment	116 592 061	41
QED	116 584 718.931	0.104
Electroweak	153.6	1.0
HVP LO	6931	40
HVP NLO	−98.3	0.7
HVP NNLO	12.4	0.1
HLbL LO	90	17
HLbL NLO	2	1
Sum SM	116 591 810	43

Table 2.1: The experimental world average based on Refs. [1, 25] for a_μ compared against the different contributions to the SM prediction as compiled in Ref. [3] as well as their sum.

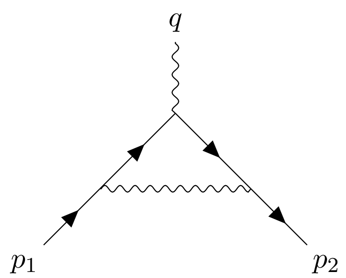

Figure 2.1: The only 1-loop QED contribution to a_μ.

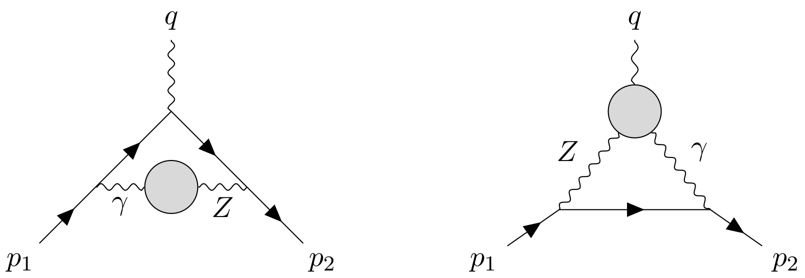

Figure 2.2: The relevant mixed electroweak and strong diagrams. The blobs denote arbitrary effects due to the strong interaction.

The QED contribution is by far the largest, responsible for more than 99.99 % of the full SM prediction. The leading one-loop diagram Fig. 2.1 has first been calculated by Schwinger [62] with the famous result

$$a_e^{\mathrm{QED},1} = \frac{\alpha}{2\pi} \,. \tag{2.14}$$

QED diagrams involving only one lepton species are mass-independent and universal for e, μ and τ. In the case of a_e, they dominate since diagrams involving muons are suppressed by an approximate factor m_e^2/m_μ^2, see Eq. (2.5), and similarly for τ-leptons. The mass-independent terms have been calculated analytically to 3 loops. The 4-loop result is known semi-analytically [87] and the 5-loop contribution has been calculated numerically [5].[2] The diagrams involving closed loops of different lepton flavors depend on the ratios of lepton masses. While τ loops come with suppression factors m_μ^2/m_τ^2, electron-loop diagrams are in general enhanced by $\log(m_\mu/m_e)$, which make these contributions larger than the corresponding mass-independent contributions at the same order. A complete numerical 5-loop computation is available [4] and despite the stronger logarithmic enhancement at higher orders, the series still appears convergent at this order and an RGE estimate of the enhanced part of the 6-loop contribution [4] confirms this pattern. The uncertainty of the QED contribution is dominated by the unknown 6-loop term compared to smaller uncertainties due to α, lepton-mass ratios and the numerical integration uncertainties in the 4-loop mass-dependent and the 5-loop part. Nevertheless, this sector appears to be under excellent control with negligible uncertainties even if the other sectors and the experimental determination improve in the next years as expected.

The electroweak contribution is suppressed compared to the QED sector due to the large masses of the W, Z and Higgs bosons. A determination with a precision of 5–10 % would currently be sufficient, but the quoted uncertainty is even below 1 %. It results from a 2-loop computation where only some small terms suppressed by M_Z^2/m_t^2 or $(1-4\sin\theta_W^2)$ have

[2] There is a $4.8\,\sigma$ discrepancy in the 5-loop diagrams without lepton loops between Ref. [5] and Ref. [88]. While this discrepancy on the order of 6×10^{-14} starts to become relevant in the electron case, it gives a negligible contribution to the uncertainty for the muon.

been neglected (see Ref. [7] and references therein) and a logarithmic estimate of the 3-loop contribution [6]. The uncertainty is now completely dominated by electroweak diagrams involving strongly interacting particles, most importantly the two diagrams in Fig. 2.2. For these, a perturbative expansion in α_s is not applicable due to the low scale set by the muon mass. While the γZ-blob in the diagram on the left can be related to the cross section $\sigma(e^+e^- \to \text{hadrons})$ as will be explained below for HVP, for the $\gamma\gamma Z$-blob in the diagram on the right one had to resort to a hadronic model [6, 58, 59]. The uncertainty of this model is difficult to estimate and we will provide an evaluation with reduced model dependence for the u- and d-quark contributions based on dispersion relations in Ch. 4 of this thesis. The result is slightly shifted with respect to the model estimates, but compatible within uncertainties, so that the smallness of this contribution is confirmed.

Also the hadronic contributions can be expanded in a series in α, but the strong-interaction effects have to be treated non-perturbatively due to the low scale set by the muon mass. We therefore represent these contributions as QED diagrams with hadronic blobs, effective photon vertices mediated by quarks and gluons. The leading effect in this category appears at order α^2 and is given by the left diagram in Fig. 1.1. It is called leading-order (LO) HVP since the hadronic blob in this case contributes to the photon 2-point function, related to the running of α. Its effect on a_μ is large compared to the uncertainty aimed at, see Tab. 2.1, so that a challenging sub-percent accuracy is required. As will be explained in Sec. 2.3, this contribution can be related to the cross section $\sigma(e^+e^- \to \text{hadrons})$ via a dispersion relation. A dedicated experimental program at e^+e^- colliders with center-of-mass energies of about 1–10 GeV has allowed to reach the precision quoted in the table, but further improvements are required to match the projected advances in the experimental determination of a_μ and further scrutiny is demanded in view of the current discrepancy compared to lattice QCD.

Recently lattice QCD calculations of the HVP contribution have become competitive. Since at the time of the White Paper their accuracy was still inferior compared to the dispersive evaluations, they were not included in the final estimates in Tab. 2.1. Since then, however, the BMW collaboration has published results with sub-percent precision [29] and parts of this result have been cross-checked by RBC/UKQCD [30], ETMC [31, 32], the Mainz group [33] and Fermilab Lattice/MILC/HPQCD [34, 35]. The comparison against the data-driven evaluation shows a $2.1\,\sigma$ discrepancy and replacing the HVP value in the White Paper SM prediction by the BMW lattice result would reduce the discrepancy with experiment to merely $1.5\,\sigma$. Efforts to improve and compare data-driven and lattice evaluations are ongoing, see e.g. Refs. [36, 89–92] for recent studies.

At order α^3, there are diagrams involving the hadronic 2-point function and an additional photon or lepton loop and diagrams with two insertions of HVP. Both these contributions are called "HVP NLO" (next-to-leading order) in Tab. 2.1 and lead to a small, but significant negative correction [13]. Since this can again be related to the precisely known cross section $\sigma(e^+e^- \to \text{hadrons})$, the uncertainty of this contribution is negligible.

At the same order in α, also the leading insertion of the hadronic 4-point function contributes through the diagram in the right part of Fig. 1.1, which defines the hadronic light-by-light scattering (HLbL) contribution. Its data-driven evaluation using dispersion relations has been pioneered in Refs. [17, 38, 39]. In this CHPS formalism, the HLbL contribution to a_μ is expressed through a multitude of hadronic form factors and scattering amplitudes in contrast to the much simpler HVP, which only depends on a single cross section. Nevertheless, this formalism allowed for the first time to model-independently define and calculate the most important contributions to HLbL and assign well-defined and small uncertainties to them. Suppressed contributions are more difficult to calculate due to a lack of data needed as input and challenges in the formalism. Input from pQCD and the OPE can be used to constrain these suppressed contributions [15, 20, 21, 40, 46–49, 93, 94]. We will provide a framework to systematically implement these constraints in Ch. 3 and develop a novel dispersive formalism for the VVA-correlator that is needed as input in one particular SDC in Ch. 4. Conceptual difficulties connected to including higher-spin intermediate states in HLbL will be addressed in Ch. 5.

The CHPS framework will be reviewed in Sec. 2.4. The number in Tab. 2.1 is an average of a dispersive data-driven evaluation and a lattice QCD calculation [22], which in this case agree. Also the updated result from the lattice [95, 96] agrees with the phenomenological number. This makes HLbL appear under good control, but a reduction of the uncertainty by a factor of ~ 2 is required to match the upcoming results from the FNAL experiment.

Hadronic contributions at order α^4 are also included in the SM prediction of Ref. [3], see "HVP NNLO" (next-to-next-to-leading order) and "HLbL NLO" in Tab. 2.1. These effects are small and, due to the efforts made in the lower-order hadronic diagrams as well as Refs. [14, 23], known with sufficient precision. The only hadronic correction at order α^4 that was not considered in Ref. [3] has recently been shown to be negligible [97].

2.3 Data-Driven evaluation of Hadronic Vacuum Polarization

Here, we provide an introduction to the dispersive formalism in the case of HVP in order to set up concepts and notation that will be crucial in our discussion of the more complicated HLbL, which is the subject of this thesis. We focus on the aspects relevant to HLbL and refrain from giving detailed discussions of electromagnetic corrections and the statistical aspects of the combination of data from different experiments, which are crucial for a precise determination of the HVP contribution to a_μ.

2.3.1 Matrix element and tensor decomposition

The hadronic blob in the HVP diagram in Fig. 1.1 is determined by the S-matrix element (with unity subtracted) of off-shell photon states

$$S_{\gamma\gamma} = \langle \gamma^*(-q_1, \lambda_1) | \gamma^*(q_2, \lambda_2) \rangle := \langle \gamma^*(-q_1, \lambda_1), \mathrm{in} | \, (S - 1) \, | \gamma^*(q_2, \lambda_2), \mathrm{in} \rangle \ . \tag{2.15}$$

Using LSZ reduction for the two photons, we obtain to leading order in α

$$S_{\gamma\gamma} = -e^2 \epsilon_\mu^{\lambda_1}(-q_1)^* \epsilon_\nu^{\lambda_2}(q_2) \int \mathrm{d}^4x \, \mathrm{d}^4y e^{\mathrm{i} q_1 \cdot x} e^{\mathrm{i} q_2 \cdot y} \, \langle 0 | \, T\{ j^\mu_{\mathrm{em}}(x) j^\nu_{\mathrm{em}}(y) \} \, | 0 \rangle \tag{2.16}$$

with the electromagnetic current of light quarks[3]

$$j^\mu_{\mathrm{em}}(x) = \bar{\psi}(x) \mathcal{Q} \gamma^\mu \psi(x) \,, \quad \psi = (u, d, s)^T \,, \quad \mathcal{Q} = \frac{1}{3} \, \mathrm{diag}(2, -1, -1) \,. \tag{2.17}$$

Next, we use translational symmetry and shift the integration variable

$$\begin{aligned} S_{\gamma\gamma} &= -e^2 \epsilon_\mu^{\lambda_1}(-q_1)^* \epsilon_\nu^{\lambda_2}(q_2) \int \mathrm{d}^4x \, \mathrm{d}^4y e^{\mathrm{i} q_1 \cdot x} e^{\mathrm{i} q_2 \cdot y} \, \langle 0 | \, T\{ j^\mu_{\mathrm{em}}(x - y) j^\nu_{\mathrm{em}}(0) \} \, | 0 \rangle \\ &= -e^2 \epsilon_\mu^{\lambda_1}(-q_1)^* \epsilon_\nu^{\lambda_2}(q_2) \int \mathrm{d}^4y e^{\mathrm{i}(q_1 + q_2) \cdot y} \int \mathrm{d}^4x e^{\mathrm{i} q_1 \cdot x} \, \langle 0 | \, T\{ j^\mu_{\mathrm{em}}(x) j^\nu_{\mathrm{em}}(0) \} \, | 0 \rangle \\ &= -e^2 \epsilon_\mu^{\lambda_1}(-q_1)^* \epsilon_\nu^{\lambda_2}(q_2) (2\pi)^4 \delta^{(4)}(q_1 + q_2) \int \mathrm{d}^4x e^{\mathrm{i} q_1 \cdot x} \, \langle 0 | \, T\{ j^\mu_{\mathrm{em}}(x) j^\nu_{\mathrm{em}}(0) \} \, | 0 \rangle \\ &= \mathrm{i} e^2 \epsilon_\mu^{\lambda_1}(-q_1)^* \epsilon_\nu^{\lambda_2}(q_2) (2\pi)^4 \delta^{(4)}(q_1 + q_2) \Pi^{\mu\nu}(q_1) \,, \end{aligned} \tag{2.18}$$

where in the last line we have defined the vacuum polarization tensor[4]

$$\Pi^{\mu\nu}(q) = \mathrm{i} \int \mathrm{d}^4x e^{\mathrm{i} q \cdot x} \, \langle 0 | \, T\{ j^\mu_{\mathrm{em}}(x) j^\nu_{\mathrm{em}}(0) \} \, | 0 \rangle \ . \tag{2.19}$$

Lorentz invariance allows for only 2 independent Lorentz structures, $q^\mu q^\nu$ and $g^{\mu\nu}$ and the Ward identities $q_\mu \Pi^{\mu\nu}(q) = q_\nu \Pi^{\mu\nu}(q) = 0$ following from electromagnetic gauge invariance demand the coefficient of one linear combination to vanish. As a result, one obtains

$$\Pi^{\mu\nu}(q) = \left(q^2 g^{\mu\nu} - q^\mu q^\nu \right) \Pi(q^2) \tag{2.20}$$

with a scalar function $\Pi(q^2)$.

In the next section, we will use the unitarity of the S-matrix to derive an expression for the imaginary part in terms of sub-processes. Afterwards, the real part will be related to the imaginary part through the analyticity properties of $\Pi(q^2)$.

[3]The contribution from heavy quarks to a_μ is suppressed, see Eq. (2.5). While for HVP these contributions are still important, for HLbL the c-quark only gives a small contribution and b- and t-quark contributions are negligible at the current level of precision. We thus focus on the three light quarks in this thesis.

[4]This differs by a factor $-e^2$ from the standard definition. With this choice, the expressions are more similar to the HLbL case discussed in the next section.

2.3.2 Constraints from Unitarity

For probabilities to be conserved, it is necessary that the S-matrix is unitary, i.e. $SS^\dagger = 1$. Using the definition of the T-matrix $S = 1 + \mathrm{i}T$, one obtains

$$\mathrm{i}(T^\dagger - T) = TT^\dagger\,. \tag{2.21}$$

Sandwiching this equation between (in or out) states gives

$$\mathrm{i}(\langle a|\, T^\dagger\, |b\rangle - \langle a|\, T\, |b\rangle) = \langle a|\, T^\dagger T\, |b\rangle = \sum_c \langle a|\, T\, |c\rangle\, \langle c|\, T^\dagger\, |b\rangle\ , \tag{2.22}$$

where a complete set of states $|c\rangle$ has been inserted in the last equation.

Due to time-reversal and Lorentz invariance, the QCD S-matrix is symmetric[5] and this property also applies to the T-matrix, i.e. $T^T = T$, which leads to

$$2\,\mathrm{Im}\,\langle a|\, T\, |b\rangle = \sum_c \langle a|\, T\, |c\rangle\, \langle b|\, T\, |c\rangle^*\ . \tag{2.23}$$

With our notation $\langle f|i\rangle = \langle f, \mathrm{in}|\, (S-1)\, |i, \mathrm{in}\rangle = \langle f, \mathrm{in}|\, \mathrm{i}T\, |i, \mathrm{in}\rangle$, this can be written as

$$\mathrm{Im}\left[-\mathrm{i}\,\langle f|i\rangle\right] = \sum_c \frac{1}{2S_c}\left(\prod_{i=1}^{N_c}\int \widetilde{\mathrm{d}p_i}\right)\langle i|c, \{p_i\}\rangle^*\,\langle f|c, \{p_i\}\rangle\ , \tag{2.24}$$

which we will refer to as a unitarity relation in the following. Here, S_c is the symmetry factor of the state $|c, \{p_i\}\rangle$ depending on the N_c momenta p_i and

$$\widetilde{\mathrm{d}p_i} = \frac{\mathrm{d}^3 p_i}{(2\pi)^3 2p_i^0} \qquad \text{with} \qquad p_i^0 = \sqrt{\boldsymbol{p}_i^2 + m^2} \tag{2.25}$$

the Lorentz-invariant integration measure. Since the left-hand side of Eq. (2.24) is real, the same has to be true for the product of matrix elements on the right-hand side. This implies that the complex conjugation can also be moved to the other matrix element.

Applying this to $S_{\gamma\gamma}$ gives

$$\mathrm{Im}[\mathrm{i}S_{\gamma\gamma}] = \frac{1}{2}\sum_n \frac{1}{S_n}\left(\prod_{i=1}^{N_n}\int \widetilde{\mathrm{d}p_i}\right)\langle\gamma^*(-q_1,\lambda_1)|n,\{p_i\}\rangle^*\,\langle\gamma^*(q_2,\lambda_2)|n,\{p_i\}\rangle\ . \tag{2.26}$$

With the definition of the amplitude

$$\langle\gamma^*(q,\lambda), \mathrm{in}|\, T\, |n, \{p_i\}, \mathrm{in}\rangle = (2\pi)^4\delta^{(4)}\left(q - \sum_i p_i\right)\epsilon_\mu^\lambda(q)\mathcal{M}^\mu_{\gamma^* n}(q)\,, \tag{2.27}$$

[5] Strictly speaking, this is only true in the case of spinless particles. In the case of particles with non-vanishing integer spin, transposition of the S-matrix complex conjugates all polarization vectors/tensors. For that reason, any polarization vectors in the matrix element on the left-hand side of Eq. (2.23) are not included in the imaginary part. This is precisely what is needed in Eq. (2.26) to cancel the polarization vectors and obtain Eq. (2.28). For compactness of the notation, in the following it is always understood that polarization vectors are outside the imaginary part.

this becomes

$$\mathrm{Im}\,\Pi^{\mu\nu}(q_1) = -\frac{1}{2e^2}\sum_n \frac{1}{S_n}\left(\prod_{i=1}^{N_n}\int\widetilde{\mathrm{d}p_i}\right)(2\pi)^4\delta^{(4)}\left(-q_1-\sum_i p_i\right)\mathcal{M}^{\mu}_{\gamma^* n}(-q_1)^*\mathcal{M}^{\nu}_{\gamma^* n}(-q_1)\,. \tag{2.28}$$

By contraction with $g^{\mu\nu}$, one can project onto Π

$$\mathrm{Im}\,\Pi = -\frac{1}{6q_1^2e^2}\sum_n \frac{1}{S_n}\left(\prod_{i=1}^{N_n}\int\widetilde{\mathrm{d}p_i}\right)(2\pi)^4\delta^{(4)}\left(-q_1-\sum_i p_i\right)\mathcal{M}^{\mu}_{\gamma^* n}(-q_1)^*\mathcal{M}_{\gamma^* n\mu}(-q_1)\,. \tag{2.29}$$

This is the desired relation between the imaginary part of the correlator in terms of the sub-processes $\gamma^* \to X$ with some hadronic state X. These can be accessed experimentally at e^+e^- colliders by studying the cross sections $\sigma(e^+e^- \to \gamma^* \to X)$. A direct experimental determination of Π would instead require a measurement of $e^+e^- \to \gamma^* \to l^+l^-$ with some charged lepton l. In order to study Π in this process, one needs to be sensitive to the interference of the HVP insertion in the photon propagator with the tree-level QED diagram. This contribution to $\sigma(e^+e^- \to l^+l^-)$ is of order α^3, whereas $\sigma(e^+e^- \to \gamma^* \to X)$ starts at order α^2, which implies that roughly 2 orders of magnitude less e^+e^- collisions are needed to reach the required precision in the hadronic cross section compared to the leptonic one. Nevertheless, a direct measurement in the similar t-channel process $\mu^+e^- \to \mu^+e^-$ is planned at the proposed MUonE experiment at CERN [98–101] and would then provide a complementary and more direct determination of a_μ^{HVP} independent of the dispersive and lattice ones.

It is even possible to express the right-hand side of Eq. (2.29) in terms of the total cross section of hadron production at e^+e^- collisions

$$\mathrm{Im}\,\Pi = \frac{1}{16\pi^2\alpha^2}\frac{q_1^4\sigma_e(q_1^2)}{q_1^2+2m_e^2}\sigma(e^+e^- \to \text{hadrons}) \tag{2.30}$$

so that in principle no exclusive hadronic channels are needed. In practice, at low energies the exclusive channels are measured individually and added up, whereas at sufficiently high energies one switches to an inclusive measurement.

2.3.3 Dispersive reconstruction of the real part and contribution to a_μ

Having expressed the imaginary part in terms of an experimentally accessible cross section, one can exploit the analytic properties of Π to also determine its real part. Π is a function of the photon virtuality $q^2 = s$, which we now treat as a complex variable. The principle of maximal analyticity says that T-matrix elements are analytic functions of the kinematic invariants they depend on, except for the cuts and poles demanded by unitarity. Since the tensor structure relating $\Pi(s)$ to the T-matrix element $-\mathrm{i}S_{\gamma\gamma}$ is non-singular, this property carries over to $\Pi(s)$ and we can express it via Cauchy's integral formula

$$\Pi(s) = \frac{1}{2\pi \mathrm{i}} \oint_\Gamma \mathrm{d}s' \frac{\Pi(s')}{s' - s - \mathrm{i}\epsilon} \tag{2.31}$$

with a closed path Γ encircling the point s once in the positively oriented direction without crossing or encircling any singularity of $\Pi(s)$. We have inserted an $\mathrm{i}\epsilon$ in the denominator such that for real s the physical value of $\Pi(s)$ above the cut is obtained.

Since all singularities of $\Pi(s)$ lie on the positive real axis, we can move the path to infinity everywhere except for the real axis. If $\Pi(s)$ tended to 0 at $|s| \to \infty$, one could neglect the large circle and obtain

$$\Pi(s) = \frac{1}{2\pi \mathrm{i}} \int_{s_{\mathrm{thr}}}^{\infty} \mathrm{d}s' \frac{\Pi(s' + \mathrm{i}\epsilon) - \Pi(s' - \mathrm{i}\epsilon)}{s' - s - \mathrm{i}\epsilon} \,. \tag{2.32}$$

Since instead the asymptotic behavior is $\Pi(s) = \mathcal{O}(s^0)$, the previous equation does not hold, but one can perform a subtraction by writing a dispersion relation for $(\Pi(s) - \Pi(0))/s$. This function does not have additional singularities, but now behaves as $\mathcal{O}(s^{-1})$ asymptotically. One obtains

$$\Pi(s) = \Pi(0) + \frac{q^2}{2\pi \mathrm{i}} \int_{s_{\mathrm{thr}}}^{\infty} \mathrm{d}s' \frac{\Pi(s' + \mathrm{i}\epsilon) - \Pi(s' - \mathrm{i}\epsilon)}{s'(s' - s - \mathrm{i}\epsilon)} \,, \tag{2.33}$$

i.e. in order to improve the high-energy behavior of the dispersion relation one has to introduce a subtraction constant $\Pi(0)$ that is not determined by unitarity and analyticity.

Finally, the Schwarz' reflection principle relates the discontinuity over the cut to the imaginary part

$$\Pi(s + \mathrm{i}\epsilon) - \Pi(s - \mathrm{i}\epsilon) = 2\mathrm{i}\, \mathrm{Im}\, \Pi(s) \,, \tag{2.34}$$

so that

$$\Pi(s) = \Pi(0) + \frac{s}{\pi} \int_{s_{\mathrm{thr}}}^{\infty} \mathrm{d}s' \frac{\mathrm{Im}\, \Pi(s')}{s'(s' - s - \mathrm{i}\epsilon)} \,, \tag{2.35}$$

which allows us to calculate $\Pi(s)$ solely in terms of the cross section $\sigma(e^+e^- \to \text{hadrons})$ and the subtraction constant $\Pi(0)$. In the on-shell scheme, which is conventionally used for a_μ, $\Pi(0) = 0$.

The full Feynman-gauge photon propagator arises from a Dyson series of self-energy insertions

$$\begin{aligned} \mathrm{i}D^{\mu\nu}(q^2) &= \frac{-\mathrm{i}g^{\mu\nu}}{q^2(1 - e^2\Pi(q^2))} = \frac{-\mathrm{i}g^{\mu\nu}}{q^2} - \frac{\mathrm{i}e^2\Pi(q^2)g^{\mu\nu}}{q^2} + \mathcal{O}(e^4) \\ &= \frac{-\mathrm{i}g^{\mu\nu}}{q^2} + \frac{1}{\pi} \int_{s_{\mathrm{thr}}}^{\infty} \mathrm{d}s \frac{-\mathrm{i}e^2 g^{\mu\nu}}{s(s - q^2)} \,\mathrm{Im}\, \Pi(s) + \mathcal{O}(e^4) \,. \end{aligned} \tag{2.36}$$

If we plug this series into the diagram in Fig. 2.1, the first term amounts to the 1-loop QED contribution, the second one to the vacuum polarization contributions at order α^2 and the higher order terms to multiple insertions of vacuum polarization. For the order α^2 term we are interested in, the dispersion integral can be pulled out of the loop integral, which then takes the form of Fig. 2.1 with a photon of mass $\sqrt{s}$. We thus obtain a dispersive representation of the HVP contribution to a_μ

$$\begin{aligned} a_\mu^{\mathrm{HVP}} &= 4\pi\alpha\frac{1}{\pi}\int_{s_{\mathrm{thr}}}^{\infty}\frac{\mathrm{d}s}{s}a_\mu^{\mathrm{QED},1}(\sqrt{s})\,\mathrm{Im}\,\Pi(s) \\ &= \frac{\alpha^2}{3\pi^2}\int_{s_{\mathrm{thr}}}^{\infty}\frac{\mathrm{d}s}{s}K(s)R(s)\,. \end{aligned} \tag{2.37}$$

Here, $a_\mu^{\mathrm{QED},1}(m)$ is the 1-loop QED contribution to a_μ with a photon mass m and in the second line we have plugged in the imaginary part from Eq. (2.30) and brought the result to the form given in Ref. [3] with a kernel function $K(s)$ given in that reference, whose functional form makes the integrand peaked in the low-energy region. Furthermore,

$$R(s) = \frac{\sigma(e^+e^- \to \text{hadrons})}{\sigma_{\mathrm{pt}}}\,, \qquad \sigma_{\mathrm{pt}} = \frac{4\pi\alpha^2}{3s}\,. \tag{2.38}$$

With this expression, one only has to perform a single integral over the cross section $\sigma(e^+e^- \to \text{hadrons})$ to obtain a_μ^{HVP}. While experimental data are used in the low s region, at higher energies away from flavor thresholds, pQCD provides more precise input. There are two independent analyses of the available data, see Refs. [8, 12] and Refs. [9, 13], respectively. In addition, constraints from analyticity and unitarity on the lowest contributing hadronic states (2π, 3π and $\pi^0\gamma$) have been studied in Refs. [10, 11, 102]. The different results have been merged in Ref. [3] with the final result given in Tab. 2.1.

2.4 Data-Driven Evaluation of Hadronic Light-by-Light Scattering

HLbL has a long history of model calculations. The first full model-dependent evaluations were performed in Refs. [103–107]. For comprehensive reviews including partial calculations we refer to Refs. [56, 108, 109]. Due to intrinsic model dependence, the uncertainties of these models are difficult if not impossible to determine. This means that the quoted uncertainties are only educated guesses with no statistical definition.

Starting in 2014, a novel framework for a data-driven determination of HLbL based on dispersion relations has been developed [17,38,39]. Its goal is to obtain a reliable, systematically improvable determination of a_μ^{HLbL} in the spirit of the data-driven approach to HVP. We will summarize the definitions and results obtained in this formalism in the following. Alternative data-driven approaches to specific contributions to HLbL can be found in Refs. [110, 111].

2.4.1 HLbL tensor and Lorentz decomposition

The hadronic blob in the HLbL diagram (Fig. 1.1 left) is described by the fourth-rank vacuum polarization tensor for fully off-shell photon-photon scattering in pure QCD, called the HLbL tensor,

$$\Pi^{\mu\nu\lambda\sigma}(q_1,q_2,q_3) = -\mathrm{i}\int \mathrm{d}^4x\;\mathrm{d}^4y\;\mathrm{d}^4z\, e^{-\mathrm{i}(q_1\cdot x+q_2\cdot y+q_3\cdot z)}\,\langle 0|\,\mathrm{T}\{j^\mu_{\mathrm{em}}(x)j^\nu_{\mathrm{em}}(y)j^\lambda_{\mathrm{em}}(z)j^\sigma_{\mathrm{em}}(0)\}\,|0\rangle \tag{2.39}$$

with momenta q_1, q_2 and q_3 incoming and $q_4 = q_1+q_2+q_3$ outgoing.

Lorentz symmetry and parity allow for a decomposition into 138 structures, with the forms $g\,g$, $g\,q\,q$ and $q\,q\,q\,q$, where g is a metric tensor and q one of the three independent momenta.[6] The scalar functions multiplying these structures are free of kinematic singularities since the HLbL tensor is, but the Ward identities

$$\{q_1^\mu, q_2^\nu, q_3^\lambda, q_4^\sigma\}\Pi_{\mu\nu\lambda\sigma}(q_1,q_2,q_3) = 0 \tag{2.40}$$

lead to the vanishing of specific linear combinations, i.e. kinematic zeros.

Bardeen and Tung [112] introduced a method to systemically remove them in their studies of doubly-virtual Compton scattering, which has been applied to the HLbL tensor in Ref. [39]. One defines the projectors

$$I_{12}^{\mu\nu} := g^{\mu\nu} - \frac{q_2^\mu q_1^\nu}{q_1\cdot q_2}\,, \qquad\qquad I_{34}^{\lambda\sigma} := g^{\lambda\sigma} - \frac{q_4^\lambda q_3^\sigma}{q_3\cdot q_4} \tag{2.41}$$

which leave the HLbL tensor invariant as it respects the Ward identities, but project every Lorentz structure onto a gauge invariant one. This leaves only 43 structures non-zero.[7] These are still multiplied by the original scalar functions, so that no kinematic singularities have been introduced, but the zeros now manifest themselves as poles in $q_1\cdot q_2$ and $q_3\cdot q_4$ in the projected structures. These are at most quadratic in both scalar products. To remove them, one employs the following steps:

- remove as many double-double poles as possible by adding linear combinations of other structures with coefficients containing no poles,
- remove the remaining double-double poles by multiplying by $q_1\cdot q_2$ or $q_3\cdot q_4$,
- repeat the first two steps for poles of lower degree.

This procedure introduces zeros in the structures and thus poles in the scalar functions through the multiplication by $q_1\cdot q_2$ and $q_3\cdot q_4$. These correspond to degeneracies of the structures in the limits $q_1\cdot q_2\to 0$ or $q_3\cdot q_4\to 0$, where the structures do not represent a basis. Thus, additional structures have to be added [113], leading to a generating redundant "BTT" set of 54 Lorentz structures,

$$\Pi^{\mu\nu\lambda\sigma} = \sum_{i=1}^{54} T_i^{\mu\nu\lambda\sigma}\Pi_i\,, \tag{2.42}$$

[6] Conservation of parity forbids the appearance of an odd number of epsilon tensors.

[7] In 4 space-time dimensions, there are two relations between these structures reducing the number of independent ones to 41, which correspond to the 41 helicity amplitudes of fully off-shell photon-photon scattering.

which is manifestly gauge invariant, closed with respect to crossing relations and such that the scalar functions Π_i are free of kinematic singularities and zeros. The Π_i are functions of the Mandelstam variables

$$s = (q_1 + q_2)^2 , \qquad t = (q_1 + q_3)^2 , \qquad u = (q_1 - q_4)^2 , \tag{2.43}$$

two of which are independent due to the fact that $s + t + u = q_1^2 + q_2^2 + q_3^2 + q_4^2$, where q_i^2 denote the photon virtualities.

2.4.2 Master formula for the ontribution to the muon $g - 2$

The HLbL contribution to the vertex function involves a two-loop integration

$$\begin{aligned}\Gamma^{\sigma}_{\mathrm{HLbL}}(p_1, p_2) = -e^6 \int \frac{\mathrm{d}^4 q_1}{(2\pi)^4} \frac{\mathrm{d}^4 q_2}{(2\pi)^4} \gamma_\mu \frac{\not{p}_2 + \not{q}_1 + m_\mu}{(p_2 + q_1)^2 - m_\mu^2} \gamma_\lambda \frac{\not{p}_1 - \not{q}_2 + m_\mu}{(p_1 - q_2)^2 - m_\mu^2} \gamma_\nu \\ \times \frac{1}{q_1^2 q_2^2 (p_1 - p_2 - q_1 - q_2)^2} \Pi_{\mu\nu\lambda\sigma}(q_1, q_2, p_1 - p_2 - q_1 - q_2)\end{aligned} \tag{2.44}$$

with the HLbL tensor defined in Eq. (2.39). By projecting this onto the magnetic form factor [56, 114, 115], averaging over the spatial directions of k and expanding around $k = 0$, one arrives at

$$a_\mu^{\mathrm{HLbL}} = -\frac{1}{48 m_\mu} \mathrm{Tr}\{(\not{p} + m_\mu)[\gamma^\rho, \gamma^\sigma](\not{p} + m_\mu)\Gamma^{\mathrm{HLbL}}_{\rho\sigma}(p)\} , \tag{2.45}$$

where

$$\Gamma^{\mathrm{HLbL}}_{\rho\sigma}(p) = \frac{\partial}{\partial k^\sigma} \Gamma^{\mathrm{HLbL}}_{\ \rho}(p_1, p_2)\bigg|_{k=0} . \tag{2.46}$$

Next, the representation of the HLbL tensor in terms of the 54 BTT structures is plugged in. Due to the derivative and limit $k \to 0$ in Eq. (2.46), only 19 linear combinations of scalar functions give non-vanishing contributions to a_μ^{HLbL} and these are needed in the reduced kinematics

$$s = (q_1 + q_2)^2 , \quad t = q_2^2 , \quad u = q_1^2 , \quad q_1^2 , \quad q_2^2 , \quad q_3^2 = (q_1 + q_2)^2 , \quad k^2 = q_4^2 = 0 . \tag{2.47}$$

One can thus perform a basis change

$$\Pi^{\mu\nu\lambda\sigma} = \sum_{i=1}^{54} T_i^{\mu\nu\lambda\sigma} \Pi_i = \sum_{i=1}^{54} \hat{T}_i^{\mu\nu\lambda\sigma} \hat{\Pi}_i , \tag{2.48}$$

in such a way that the derivatives of only 19 structures $\hat{T}_i^{\mu\nu\lambda\sigma}$ are non-vanishing in the limit $k \to 0$. Thus, only the scalar functions $\hat{\Pi}_{g_i}$ with $\{g_i\} = \{1, \ldots, 11, 13, 14, 16, 17, 39, 50, 51, 54\}$

are needed to calculate a_μ. These scalar functions can be characterized by the six representatives

$$\begin{aligned}
\hat{\Pi}_1 &= \Pi_1 + q_1 \cdot q_2 \Pi_{47}\,, \\
\hat{\Pi}_4 &= \Pi_4 - q_1 \cdot q_3 \left(\Pi_{19} - \Pi_{42}\right) - q_2 \cdot q_3 \left(\Pi_{20} - \Pi_{43}\right) + q_1 \cdot q_3 q_2 \cdot q_3 \Pi_{31}\,, \\
\hat{\Pi}_7 &= \Pi_7 - \Pi_{19} + q_2 \cdot q_3 \Pi_{31}\,, \\
\hat{\Pi}_{17} &= \Pi_{17} + \Pi_{42} + \Pi_{43} - \Pi_{47}\,, \\
\hat{\Pi}_{39} &= \Pi_{39} + \Pi_{40} + \Pi_{46}\,, \\
\hat{\Pi}_{54} &= \Pi_{42} - \Pi_{43} + \Pi_{54}\,,
\end{aligned} \tag{2.49}$$

and the remaining ones are related to these via the crossing relations

$$\begin{aligned}
&\hat{\Pi}_2 = \mathcal{C}_{23}\hat{\Pi}_1\,, \quad \hat{\Pi}_3 = \mathcal{C}_{13}\hat{\Pi}_1\,, \quad \hat{\Pi}_5 = \mathcal{C}_{23}\hat{\Pi}_4\,, \quad \hat{\Pi}_6 = \mathcal{C}_{13}\hat{\Pi}_4\,, \\
&\hat{\Pi}_8 = \mathcal{C}_{12}\hat{\Pi}_7\,, \quad \hat{\Pi}_9 = \mathcal{C}_{12}\mathcal{C}_{13}\hat{\Pi}_7\,, \quad \hat{\Pi}_{10} = \mathcal{C}_{23}\hat{\Pi}_7\,, \quad \hat{\Pi}_{13} = \mathcal{C}_{13}\hat{\Pi}_7\,, \quad \hat{\Pi}_{14} = \mathcal{C}_{12}\mathcal{C}_{23}\hat{\Pi}_7\,, \\
&\hat{\Pi}_{11} = \mathcal{C}_{13}\hat{\Pi}_{17}\,, \quad \hat{\Pi}_{16} = \mathcal{C}_{23}\hat{\Pi}_{17}\,, \quad \hat{\Pi}_{50} = -\mathcal{C}_{23}\hat{\Pi}_{54}\,, \quad \hat{\Pi}_{51} = \mathcal{C}_{13}\hat{\Pi}_{54}\,,
\end{aligned} \tag{2.50}$$

where the crossing operator $\mathcal{C}_{ij}$ exchanges the photons i and j.

The trace in Eq. (2.45) can be calculated for each of these 19 structures. By exploiting the symmetry $q_1 \leftrightarrow -q_2$ of the integration measure and the product of propagators at $k = 0$, the number of independent scalar functions needed for a_μ can be further reduced to 12. After performing a Wick rotation to Euclidean momenta, 5 of the 8 integrals can be performed by angular averages using the technique of Gegenbauer polynomials [116, 117]. This leads to the master formula [17]

$$a_\mu^{\mathrm{HLbL}} = \frac{2\alpha^3}{3\pi^2} \int_0^\infty \mathrm{d}Q_1 \int_0^\infty \mathrm{d}Q_2 \int_{-1}^1 \mathrm{d}\tau \sqrt{1-\tau^2}\, Q_1^3 Q_2^3 \sum_{i=1}^{12} T_i(Q_1, Q_2, \tau)\, \bar{\Pi}_i(Q_1, Q_2, \tau)\,, \tag{2.51}$$

where $Q_{1,2}$ denote the magnitudes of the Euclidean loop four-momenta, $Q_{1,2} = \sqrt{-q_{1,2}^2}$, and τ is the cosine of the angle between these vectors. The scalar functions $\bar{\Pi}_i$ are a subset of the previous $\hat{\Pi}_i$ for $k = 0$ and 6 of the $\bar{\Pi}_i$ are related to the other 6 by the crossing relations Eq. (2.50). The analytic expressions of the integration kernels T_i are given in Ref. [17]. Further details on the derivation of the master formula can also be found in Ref. [118].

Parameterizing the three-dimensional integration domain by the coordinates [119]

$$\Sigma \in [0, \infty)\,, \quad r \in [0, 1]\,, \quad \phi \in [0, 2\pi]\,, \tag{2.52}$$

which are related to the non-vanishing photon virtualities by

$$\begin{aligned}
Q_1^2 &= \frac{\Sigma}{3}\left(1 - \frac{r}{2}\cos\phi - \frac{r}{2}\sqrt{3}\sin\phi\right)\,, \\
Q_2^2 &= \frac{\Sigma}{3}\left(1 - \frac{r}{2}\cos\phi + \frac{r}{2}\sqrt{3}\sin\phi\right)\,, \\
Q_3^2 &= Q_1^2 + 2Q_1Q_2\tau + Q_2^2 = \frac{\Sigma}{3}\left(1 + r\cos\phi\right)\,,
\end{aligned} \tag{2.53}$$

will prove very useful in the discussion about asymptotic constraints on HLbL in Ch. 3. The master formula in Eq. (2.51) then takes the form

$$a_\mu^{\mathrm{HLbL}} = \frac{\alpha^3}{432\pi^2}\int_0^\infty \mathrm{d}\Sigma\,\Sigma^3 \int_0^1 \mathrm{d}r\, r\sqrt{1-r^2}\int_0^{2\pi}\mathrm{d}\phi \sum_{i=1}^{12} T_i(\Sigma,r,\phi)\bar{\Pi}_i(\Sigma,r,\phi)\,, \tag{2.54}$$

where $T_i(\Sigma,r,\phi) = T_i(Q_1^2(\Sigma,r,\phi), Q_2^2(\Sigma,r,\phi), Q_3^2(\Sigma,r,\phi))$ and similarly for $\bar{\Pi}_i(\Sigma,r,\phi)$.

In terms of the Q_i^2 coordinates, the integration domain amounts to a cone with tip at the origin. In terms of (Σ,r,ϕ), a given point in this cone is specified by the distance Σ to the tip of the point's projection on the symmetry axis ($\Sigma = Q_1^2+Q_2^2+Q_3^2$), and by the polar coordinates r and ϕ on the plane containing the point and orthogonal to the symmetry axis, normalized such that $r=1$ corresponds to the surface of the cone.

2.4.3 Dispersive reconstruction

The scalar functions Π_i are free of kinematic singularities so that they are analytic in the complex kinematic invariants except for the singularities demanded by unitarity. One can therefore use the unitarity relation Eq. (2.24) to reconstruct the imaginary part from on-shell intermediate states and then use a dispersion relation to obtain the real part. Of course, it is crucial that this dispersion relation is unsubtracted to obtain a parameter-free prediction for a_μ^{HLbL}.

The HLbL scalar functions depend on four q_i^2 and two independent Mandelstam variables. One therefore has to choose which variables should be kept fixed when writing the dispersion relation. Here we review the approach introduced in Ref. [39], namely dispersion relations in the Mandelstam variables keeping the four photon virtualities fixed.

The s-channel pole residues and discontinuities are determined from the unitarity relation

$$\begin{aligned}&\mathrm{Im}_s\left(-\mathrm{i}\,\langle\gamma^*(-q_3,\lambda_3)\gamma^*(q_4,\lambda_4)|\gamma^*(q_1,\lambda_1)\gamma^*(q_2,\lambda_2)\rangle\right)\\ &=\sum_n \frac{1}{2S_n}\left(\prod_{i=1}^{N_n}\int\widetilde{\mathrm{d}p_i}\right)\langle\gamma^*(q_1,\lambda_1)\gamma^*(q_2,\lambda_2)|n;\{p_i\}\rangle^*\,\langle\gamma^*(-q_3,\lambda_3)\gamma^*(q_4,\lambda_4)|n;\{p_i\}\rangle\,.\end{aligned} \tag{2.55}$$

Individual contributions to the HLbL tensor can then be calculated by fixing the state n. Selecting the π^0-state leads to

$$\begin{aligned}&\mathrm{Im}_s^\pi\left(-\mathrm{i}\,\langle\gamma^*(-q_3,\lambda_3)\gamma^*(q_4,\lambda_4)|\gamma^*(q_1,\lambda_1)\gamma^*(q_2,\lambda_2)\rangle\right)\\ &=\frac{1}{2}\int\widetilde{\mathrm{d}p}\,\langle\gamma^*(q_1,\lambda_1)\gamma^*(q_2,\lambda_2)|\pi^0(p)\rangle^*\,\langle\gamma^*(-q_3,\lambda_3)\gamma^*(q_4,\lambda_4)|\pi^0(p)\rangle\end{aligned} \tag{2.56}$$

and the matrix elements evaluate to

$$\begin{aligned}
&\langle\gamma^*(-q_3,\lambda_3)\gamma^*(q_4,\lambda_4)|\gamma^*(q_1,\lambda_1)\gamma^*(q_2,\lambda_2)\rangle \\
&\quad = \mathrm{i}e^4(2\pi)^4\delta^{(4)}(q_1+q_2+q_3-q_4)\epsilon_\mu^{\lambda_1}(q_1)\epsilon_\nu^{\lambda_2}(q_2)\epsilon_\lambda^{\lambda_3}(-q_3)^*\epsilon_\sigma^{\lambda_4}(q_4)^*\Pi^{\mu\nu\lambda\sigma}(q_1,q_2,q_3)\,, \\
&\langle\gamma^*(q_1,\lambda_1)\gamma^*(q_2,\lambda_2)|\pi^0(p)\rangle \\
&\quad = \mathrm{i}e(2\pi)^4\delta^{(4)}(q_1+q_2-p)\epsilon_\mu^{\lambda_1}(q_1)^*\epsilon_\nu^{\lambda_2}(q_2)^*\epsilon^{\mu\nu\lambda\sigma}q_{1\alpha}q_{2\beta}F_{\pi\gamma^*\gamma^*}(q_1^2,q_2^2)\,,
\end{aligned} \tag{2.57}$$

where we have introduced the pion transition form factor (TFF) defined by

$$\mathrm{i}\int \mathrm{d}^4x\, e^{\mathrm{i}q_1\cdot x}\,\langle 0|\,\mathrm{T}\{j_\mu(x)j_\nu(0)\}\,|\pi^0(q_1+q_2)\rangle = \epsilon_{\mu\nu\alpha\beta}q_1^\alpha q_2^\beta F_{\pi\gamma^*\gamma^*}(q_1^2,q_2^2) \tag{2.58}$$

with $\epsilon^{0123}=+1$. Plugging this in, leads to

$$\begin{aligned}
&\mathrm{Im}_s^\pi\,\Pi^{\mu\nu\lambda\sigma}(q_1,q_2,q_3) \\
&\quad = -\frac{1}{2}\int\widetilde{\mathrm{d}p}(2\pi)^4\delta^{(4)}(q_1+q_2-p)\epsilon_{\mu\nu\alpha\beta}\epsilon_{\lambda\sigma\delta\gamma}q_{1\alpha}q_{2\beta}q_{3\delta}q_{4\gamma}F_{\pi\gamma^*\gamma^*}(q_1^2,q_2^2)F_{\pi\gamma^*\gamma^*}(q_3^2,q_4^2) \\
&\quad = -\pi\delta(s-m_\pi^2)\epsilon_{\mu\nu\alpha\beta}\epsilon_{\lambda\sigma\delta\gamma}q_{1\alpha}q_{2\beta}q_{3\delta}q_{4\gamma}F_{\pi\gamma^*\gamma^*}(q_1^2,q_2^2)F_{\pi\gamma^*\gamma^*}(q_3^2,q_4^2) \\
&\quad = -\pi\delta(s-m_\pi^2)T_1^{\mu\nu\lambda\sigma}F_{\pi\gamma^*\gamma^*}(q_1^2,q_2^2)F_{\pi\gamma^*\gamma^*}(q_3^2,q_4^2)\,.
\end{aligned} \tag{2.59}$$

One thus only gets a contribution to the first scalar function. Similar results can be obtained for the π^0-pole in the t- and u-channels, which only contribute to $\mathrm{Im}_t\,\Pi_2$ and $\mathrm{Im}_u\,\Pi_3$, respectively.

The fixed-t dispersion relation contains integrals over the s- and u-channel cuts due to $u=q_1^2+q_2^2+q_3^2+q_4^2-s-t$

$$\Pi_i(s,t,u;q_i^2) = c_i^t + \int\mathrm{d}s'\frac{\mathrm{Im}_s\,\Pi_i(s',t,u';q_i^2)}{s'-s} + \int\mathrm{d}u'\frac{\mathrm{Im}_u\,\Pi_i(s',t,u';q_i^2)}{u'-u}\,, \tag{2.60}$$

where c_i^t only accounts for t-channel poles and does not represent a subtraction constant. Plugging in the results for the π^0 intermediate state and also accounting for the t-channel pole in the fixed-s and fixed-u relations, one obtains

$$\begin{aligned}
\Pi_1^{\pi^0\text{-pole}}(s,t,u) &= \frac{F_{\pi^0\gamma^*\gamma^*}(q_1^2,q_2^2)F_{\pi^0\gamma^*\gamma^*}(q_3^2,q_4^2)}{s-m_\pi^2} \\
\Pi_2^{\pi^0\text{-pole}}(s,t,u) &= \frac{F_{\pi^0\gamma^*\gamma^*}(q_1^2,q_3^2)F_{\pi^0\gamma^*\gamma^*}(q_2^2,q_4^2)}{t-m_\pi^2} \\
\Pi_3^{\pi^0\text{-pole}}(s,t,u) &= \frac{F_{\pi^0\gamma^*\gamma^*}(q_1^2,q_4^2)F_{\pi^0\gamma^*\gamma^*}(q_2^2,q_3^2)}{u-m_\pi^2}
\end{aligned} \tag{2.61}$$

and there are no contributions to the other scalar functions.

In the master formula, the π^0-pole only contributes to $\bar{\Pi}_{1,2}$, which fulfill

$$\bar{\Pi}_2 = \mathcal{C}_{23}[\bar{\Pi}_1]\,, \qquad\qquad \mathcal{C}_{12}[\bar{\Pi}_1] = \bar{\Pi}_1\,. \tag{2.62}$$

The contribution to $\bar{\Pi}_1$ reads

$$\bar{\Pi}_1^{\pi^0\text{-pole}} = -\frac{F_{\pi^0\gamma^*\gamma^*}(-Q_1^2, -Q_2^2) F_{\pi^0\gamma^*\gamma^*}(-Q_3^2, 0)}{Q_3^2 + m_\pi^2} \,. \tag{2.63}$$

Evaluating the master formula Eq. (2.51) using $\bar{\Pi}_{1,2}^{\pi^0\text{-pole}}$ defines the pion-pole contribution $a_\mu^{\pi^0\text{-pole}}$. The space-like singly-virtual and doubly-virtual π^0 TFFs have been reconstructed via a data-driven dispersive approach that takes into account all singularities due to 2π and 3π states in Refs. [18, 50, 120]. SDCs have been accounted for by adding to the spectral density a contribution from pQCD and an effective pole has been used to ensure the correct normalization, $F_{\pi\gamma^*\gamma^*}(0,0)$. The representation has also been used to predict the branching ratio $\mathrm{BR}[\pi^0 \to e^+e^-]$ in Ref. [121]. Using this input, one obtains

$$a_{\mu,\text{disp}}^{\pi^0\text{-pole}} = 62.6^{+3.0}_{-2.5} \times 10^{-11} \,. \tag{2.64}$$

This result agrees with other recent determinations based on lattice QCD [19], Canterbury approximants [16], Dyson-Schwinger equations (DSEs) [122, 123] and holographic QCD (hQCD) models [41, 43, 44, 124].

The η/η'-pole contributions to a_μ can be determined analogously resulting in Eq. (2.63) with the pion TFFs replaced by η/η' TFFs.[8] A dispersive analysis of the doubly-virtual η/η' TFFs has not been completed yet,[9] but the method of Canterbury approximants in Ref. [16] provides data-driven determinations and associated uncertainties also for the η/η' TFFs with the results

$$\begin{aligned} a_{\mu,\text{Can}}^{\eta\text{-pole}} &= (16.3 \pm 1.4) \times 10^{-11} \,, \\ a_{\mu,\text{Can}}^{\eta'\text{-pole}} &= (14.5 \pm 1.9) \times 10^{-11} \,. \end{aligned} \tag{2.65}$$

The pion box is singled out by selecting two-pion states in the unitarity relation Eq. (2.55) and selecting the pion pole in the crossed channel unitarity relation for the $\gamma^*\gamma^* \to 2\pi$ amplitudes. It then can be shown that this definition of the pion box exactly amounts to the pion box in scalar QED dressed with pion vector form factors (VFF) [39]. Using a dispersive representation for the pion VFF, this amounts to [17]

$$a_\mu^{\pi\text{-box}} = (-15.9 \pm 0.2) \times 10^{-11} \,. \tag{2.66}$$

[8] Strictly speaking, only states consiting of stable particles (within QCD) should be considered in the sum in Eq. (2.55), whereas η and η' mesons can decay to multi-pion states with at least 3 pions (away from the isospin limit). Their very small widths compared to their masses, however, allow to approximate these states by stable particles. To avoid double-counting, their contributions have to be subtracted from 3-pion states once calculated or estimated.

[9] The dispersive formalism for the singly-virtual η/η' TFF has been established [125, 126] and progress has been made towards the determination of the doubly-virtual isovector contribution [127–129].

Similarly, the charged-kaon box depends on the kaon VFF. Using a representation based on DSEs [130], one obtains a very small contribution to a_μ [3]

$$a_\mu^{K^+\text{-box}} = (-0.46 \pm 0.02) \times 10^{-11}\,, \tag{2.67}$$

where the uncertainty corresponds to variations of the model parameters. The neutral-kaon box is completely negligible [3].

Two-pion intermediate states with multi-pion contributions to at least one of the $\gamma^*\gamma^* \to 2\pi$ sub-amplitudes were considered in Ref. [17]. To this end, the helicity-partial waves of $\gamma^*\gamma^* \to 2\pi$ were calculated from generalized Roy–Steiner equations restricted to the S-wave in the two-pion system with a pion-pole left-hand cut. For the $\pi\pi$-scattering phase shifts, input from the inverse-amplitude method was used, which allows to cut off the $f_0(980)$ and heavier scalar resonances in a clean way. This lead to

$$a_{\mu,S\text{-wave}}^{\pi\pi,\pi\text{-pole LHC}} = (-8 \pm 1) \times 10^{-11}\,, \tag{2.68}$$

which includes the effect of the $f_0(500)$ resonance. The results for the lightest intermediate states discussed here are compatible with previous model evaluations [108, 109], but drastically improve both precision and reliability of error estimates.

States with higher multiplicity can currently only be estimated under the assumption that they are saturated by resonances using a narrow-width approximation (NWA). In the dispersive reconstruction, single-particle intermediate states of mass m are associated with poles at $Q_i^2 = -m^2$ with the residue given by TFFs for on-shell mesons. Let us compare the impact on the scalar functions Π_i of two such states of different masses $m_{1,2}$. The ratio of the two contributions contains a factor

$$\frac{Q_i^2 + m_1^2}{Q_j^2 + m_2^2} = \frac{m_1^2}{m_2^2} + \mathcal{O}(Q_i^2, Q_j^2)\,, \tag{2.69}$$

which shows that heavier states are suppressed at small $\Sigma = Q_1^2 + Q_2^2 + Q_3^2$. As soon as one of the momenta becomes comparable to the larger mass, no such suppression occurs any more.[10] This effect is of course modified by the numerator in $\bar{\Pi}_i$, which encodes information on the strength of the coupling to two (off-shell) photons, but it still helps us identify which states *can* be relevant at specific energy scales and which not.

Heavier pseudoscalars contribute to the scalar functions exactly as the light pseudoscalars with the TFFs and the mass replaced accordingly. Conversely, the couplings of scalars, axials and tensors to off-shell photons have different decompositions into TFFs [131]. As already mentioned, sum rules were derived in Ref. [17], which are needed to obtain finite and unambiguous results for a_μ^{HLbL}, see Sec. 5.1.1. These sum rules are not satisfied for individual

[10] This argument obviously also holds if the denominator of the heavier state gets replaced by m_i^2 as for the axial-meson longitudinal contribution in Eq. (3.36) below (see also Ref. [55]).

intermediate states except for single-pseudoscalar states, but only for the infinite tower of states. The scalar contribution is free of kinematic singularities and they can be avoided also for the axial-vector meson contribution by choosing another basis [46]. Starting from spin 2, kinematic singularities in individual contributions are unavoidable in the established formalism by making use of only the minimal set of sum rules. In contrast, the complementary dispersive approach introduced in Ch. 5 and Ref. [60] is manifestly free of this type of singularities.

3 Effects of Longitudinal Short-Distance Constraints on the Hadronic Light-by-Light Contribution to the Muon $g-2$

The data-driven approach to HLbL introduced in Sec. 2.4 allows one to calculate the effects of the most important intermediate states in terms of experimentally accessible quantities. However, it is impossible to perform such analyses for the infinite tower of contributions and approximations have to be made instead. According to Ref. [3], these approximations currently dominate the uncertainty of the SM prediction of a_μ^{HLbL}.

According to the argument at the end of Sec. 2.4.3, these heavier intermediate states contribute significantly only at sufficiently large Q_i^2. In the regimes where some or all of the Q_i^2 are much larger than Λ_{QCD}^2, the OPE and pQCD can be used to calculate the scalar functions as we will review in the next section. This leads to the so-called SDCs that are valid in regions where unitarity ceases to be fully predictive.

Since the master formula integrals run only over space-like photon virtualities and all unitarity cuts and poles are in the time-like region, the scalar functions are analytic in the relevant domain. The idea of the approach presented in this chapter is thus to construct functions that smoothly connect the known regimes, i.e. the low-energy region and the various regions where SDCs are valid. The goal is to quantify how much information can be gained using this input only without reference to hadronic models for the complicated treatment of heavier intermediate states. In addition, we perform a detailed uncertainty estimate to assess which part of the input has to be improved to obtain a more precise result.

We focus the study on the longitudinal components of HLbL, i.e. the scalar functions $\bar{\Pi}_{1,2}$. The reason for this is two-fold: first, these scalar functions are numerically the most important, especially due to the large effects of the light pseudoscalar-pole contributions. We therefore expect to be able to capture in this way the largest part of the effect on a_μ^{HLbL} due to SDCs. Second, the transversal asymmetric asymptotic SDC is less restrictive due to non-perturbative corrections absent in the longitudinal counterpart. Nevertheless, the developed method is very general and we expect a similar analysis for the remaining scalar functions to be possible with only minor modifications.

In the following section, we review the relevant SDCs and discuss some of their implications on the following calculations. We also discuss how these SDCs are fulfilled in available hadronic models. In Sec. 3.2, we show how the different SDCs can be connected to obtain a representation valid at large $\Sigma = Q_1^2 + Q_2^2 + Q_3^2$ before interpolating between this and the low-energy domain in Sec. 3.3. Sec. 3.4 is then devoted to the numerical analysis before we conclude this chapter in Sec. 3.5. The content of this chapter has been published in Ref. [45].

3.1 Short-distance constraints on HLbL

In this section, we review the asymptotic constraints on the BTT scalar functions available in the literature and make first steps towards their implementation in the subsequent sections. The fully asymptotic limit, where all q_i are space-like and large is dominated by the pQCD quark loop. However, since in the evaluation of a_μ^{HLbL} one photon is soft ($q_4 \approx 0$), this limit is not particularly useful for its evaluation. For $q_4 \approx 0$ and $Q_1^2 \sim Q_2^2 \sim Q_3^2 \gg \{\Lambda_{\text{QCD}}^2, m_q^2\}$, an OPE in a background external field can be employed [20, 47, 48]. In the limit where $q_4 \approx 0$ and $Q_1^2 \sim Q_2^2 \gg \{Q_3^2, \Lambda_{\text{QCD}}^2, m_q^2\}$ and the corresponding crossed versions, a standard OPE can be used to relate the HLbL tensor to the VVA correlator, which is constrained by the Adler–Bell–Jackiw anomaly and non-renormalization theorems [15, 21, 40, 49] (see also Refs. [55,94] and Ch. 4). The limit $Q_1^2 \gg \{Q_2^2, Q_3^2, Q_4^2, \Lambda_{\text{QCD}}^2, m_q^2\}$ is far outside the integration domain in the master formula and thus again not important for a_μ^{HLbL}.

In the reduced kinematics Eq. (2.47) after the Wick rotation to Euclidean momenta, both relevant asymptotic limits correspond to $\Sigma \to \infty$ but for different values of r and ϕ: the asymmetric limit $Q_1^2 \sim Q_2^2 \gg Q_3^2$ corresponds to $r = 1$ and $\phi = \pi$ while the symmetric configuration $Q_1^2 \sim Q_2^2 \sim Q_3^2$ occurs in a neighborhood of $r = 0$ (see Fig. 3.1).

3.1.1 The asymmetric asymptotic region: Melnikov–Vainshtein constraint

We now review the definition of a constraint on the HLbL tensor that is valid if two virtualities are comparable and much larger than both the third virtuality and Λ_{QCD}. This was first considered by Melnikov and Vainshtein and we thus denote it as MV constraint.

We consider the HLbL tensor as defined in Eq. (2.39) after the Wick rotation has been performed, i.e. for Euclidean momenta, in the regime where $\hat{q} \equiv (q_1 - q_2)/2$ is large. The leading contributions to the integral in Eq. (2.39) then comes from $x \approx y$ and the product of electromagnetic currents in the matrix element can be expanded around $x = y$. We consider the tensor operator

$$\Pi^{\mu\nu}(q_1, q_2) = \mathrm{i} \int \mathrm{d}^4x \; \mathrm{d}^4y \, e^{-\mathrm{i}(q_1\cdot x + q_2\cdot y)} \, \mathrm{T}\{j_{\text{em}}^\mu(x) j_{\text{em}}^\nu(y)\} \, , \tag{3.1}$$

which we want to expand into a series of local operators. Operators with the lowest mass dimension are multiplied by the largest power of $\hat{q}$ and thus dominate at large $\hat{q}$.[1] The

[1] This is in contrast with an OPE in Minkowski space, where operators of lower twist dominate due to the non-positive-definiteness of the scalar product.

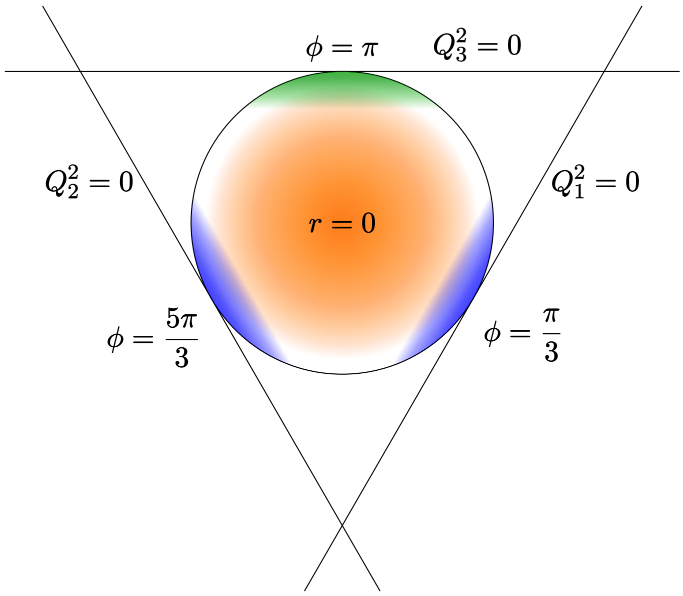

Figure 3.1: The circle represents the boundary of the $g-2$ integration domain for a fixed value of Σ. The angles $\phi = \pi/3$, $\phi = \pi$ and $\phi = 5\pi/3$ correspond to $Q_2^2 = Q_3^2$, $Q_1^2 = Q_2^2$ and $Q_1^2 = Q_3^2$, respectively. The colored regions indicate where SDCs on $\bar{\Pi}_1$ hold at large Σ. In the green region, the OPE relates $\bar{\Pi}_1$ to the VVA correlator at leading order, whereas the LO OPE gives a vanishing result for $\bar{\Pi}_1$ in the blue regions. The pQCD constraint is valid in the orange domain.

operator of lowest dimension is the unit operator, which, however, amounts to a disconnected contribution when inserted into the HLbL tensor. The next operator has dimension 3 and is the di-quark operator, which due to chiral symmetry and charge conjugation can only appear in the form of an axial-vector current[2]

$$j_5^\mu(x) = \bar{\psi}(x)\mathcal{Q}^2\gamma^\mu\gamma_5\psi(x)\,, \tag{3.2}$$

where the quadratic dependence on the charge matrix (defined in Eq. (2.17)) follows from the linear dependence on $\mathcal{Q}$ of the two vector currents. Due to parity conservation, this current furthermore needs to be contracted with an epsilon tensor.

Since the pre-factor (Wilson coefficient) is independent of the states between which the operator is evaluated, we can compute both the two-vector-current and the axial-vector-current operators between single-quark states and match the coefficients. For $q_1 + q_2 \neq 0$, where the unit operator does not contribute, one obtains (see e.g. Refs. [15, 21])

$$\Pi^{\mu\nu}(q_1, q_2) = \int \mathrm{d}^4 z\, e^{-\mathrm{i}(q_1+q_2)\cdot z}\left(-\frac{2\mathrm{i}}{\hat{q}^2}\epsilon^{\mu\nu\alpha\beta}\hat{q}_\alpha j_{5\beta}(z)\right) + \dots\,. \tag{3.3}$$

[2] The scalar density $\bar{\psi}(x)\mathcal{Q}^2\psi(x)$ cannot contribute in the chiral limit and therefore is necessarily multiplied by a light quark mass, which effectively increases its dimension by one unit.

The ellipsis denotes sub-leading terms suppressed by powers of $\{|q_1+q_2|/|\hat{q}|,\, \Lambda_{\text{QCD}}/|\hat{q}|\}$. This result implies that, at leading order in the OPE and at leading order in α_s, the HLbL tensor can be expressed in terms of the correlator of two vector currents and an axial current,

$$\begin{aligned}\Pi_{\mu\nu\lambda\sigma}(q_1,q_2,q_3) &= \frac{2\mathrm{i}}{\hat{q}^2}\epsilon_{\mu\nu\alpha\beta}\hat{q}^\alpha \int \mathrm{d}^4x\,\mathrm{d}^4y\, e^{-\mathrm{i}q_3\cdot x}e^{\mathrm{i}q_4\cdot y}\,\langle 0|\,\mathrm{T}\{j_\lambda(x)j_\sigma(y)j_5^\beta(0)\}\,|0\rangle \\ &= \frac{2}{\hat{q}^2}\epsilon_{\mu\nu\alpha\beta}\hat{q}^\alpha \mathcal{W}_{\lambda\sigma}{}^{\beta}(-q_3,q_4) \\ &= \frac{8}{\hat{q}^2}\epsilon_{\mu\nu\alpha\beta}\hat{q}^\alpha \sum_{a=3,8,0} C_a^2(\mathcal{W}^{(a)})_{\lambda\sigma}{}^{\beta}(-q_3,q_4)\end{aligned} \tag{3.4}$$

for $Q_1^2\sim Q_2^2\gg\{Q_3^2,Q_4^2,\Lambda_{\text{QCD}}^2\}$, where in the second line we have inserted the definition of the hadronic VVA correlator

$$\mathcal{W}_{\mu\nu\rho}(q_1,q_2) = \mathrm{i}\int \mathrm{d}^4x \int \mathrm{d}^4y\, e^{\mathrm{i}(q_1\cdot x+q_2\cdot y)}\,\langle 0|\,\mathrm{T}\{j_\mu^{\text{em}}(x)j_\nu^{\text{em}}(y)j_\rho^5(0)\}\,|0\rangle \tag{3.5}$$

with the three outgoing momenta q_1, q_2 and $q_3=-q_1-q_2$ and in the third line we have employed its flavor decomposition into isovector ($a=3$), flavor-octet ($a=8$) and flavor-singlet ($a=0$) components[3] as derived in Ref. [21]. The numerical coefficients $C_a=\mathrm{Tr}(\mathcal{Q}^2\lambda_a)/2$ with λ^a the Gell-Mann matrices and $\lambda^0=\sqrt{2/3}\,\mathbb{1}$ follow from the flavor decomposition of the quark-charge matrix and explicitly read

$$C_3=\frac{1}{6}\,, \qquad C_8=\frac{1}{6\sqrt{3}}\,, \qquad C_0=\frac{2}{3\sqrt{6}}\,. \tag{3.6}$$

The VVA correlator can be decomposed into Lorentz structures (see e.g. Ref. [132]). For this, we start by writing down all Lorentz structures compatible with Lorentz symmetry and invariance under parity, which requires a Levi-Civita tensor in each term

$$\begin{aligned}&\{\epsilon^{\mu\nu\rho\alpha}q_{1\alpha}\,,\epsilon^{\mu\nu\rho\alpha}q_{2\alpha}\,,\epsilon^{\mu\nu\alpha\beta}q_{1\alpha}q_{2\beta}q_1^\rho\,,\epsilon^{\mu\nu\alpha\beta}q_{1\alpha}q_{2\beta}q_2^\rho\,,\\ &\epsilon^{\mu\rho\alpha\beta}q_{1\alpha}q_{2\beta}q_1^\nu\,,\epsilon^{\mu\rho\alpha\beta}q_{1\alpha}q_{2\beta}q_2^\nu\,,\epsilon^{\nu\rho\alpha\beta}q_{1\alpha}q_{2\beta}q_1^\mu\,,\epsilon^{\nu\rho\alpha\beta}q_{1\alpha}q_{2\beta}q_2^\mu\}\,.\end{aligned} \tag{3.7}$$

Since antisymmetric tensors of rank larger than 4 vanish in four dimensions, two structures can be expressed as linear combinations of the others and can thus be dropped. We choose to eliminate the 6th and 7th structures. Additionally, the Ward identities

$$q_{1\mu}(\mathcal{W}^{(a)})^{\mu\nu\rho}(q_1,q_2) = q_{2\nu}(\mathcal{W}^{(a)})^{\mu\nu\rho}(q_1,q_2) = 0 \tag{3.8}$$

[3] See Sec. 4.1.1 for more details.

allow us to reduce the number of independent Lorentz structures to 4. These can be chosen as[4]

$$\begin{aligned}\{t_L^{\mu\nu\rho}, t_+^{\mu\nu\rho}, t_-^{\mu\nu\rho}, \tilde{t}_-^{\mu\nu\rho}\} = \{&-\epsilon^{\mu\nu\alpha\beta} q_{1\alpha} q_{2\beta}(q_1+q_2)^\rho \,, \\ &\epsilon^{\mu\rho\alpha\beta} q_1^\nu q_{1\alpha} q_{2\beta} - \epsilon^{\nu\rho\alpha\beta} q_2^\mu q_{1\alpha} q_{2\beta} - q_1\cdot q_2 \epsilon^{\mu\nu\rho\alpha}(q_1-q_2)_\alpha \\ &- \frac{2q_1\cdot q_2}{(q_1+q_2)^2}\epsilon^{\mu\nu\alpha\beta} q_{1\alpha} q_{2\beta}(q_1+q_2)^\rho \,, \\ &\left((q_1-q_2)^\rho - \frac{q_1^2-q_2^2}{(q_1+q_2)^2}(q_1+q_2)^\rho\right)\epsilon^{\mu\nu\alpha\beta} q_{1\alpha} q_{2\beta} \,, \\ &\epsilon^{\mu\rho\alpha\beta} q_1^\nu q_{1\alpha} q_{2\beta} + \epsilon^{\nu\rho\alpha\beta} q_2^\mu q_{1\alpha} q_{2\beta} - q_1\cdot q_2 \epsilon^{\mu\nu\rho\alpha}(q_1+q_2)_\alpha\}\end{aligned} \tag{3.9}$$

and the three-point function then reads

$$\begin{aligned}(\mathcal{W}^{(a)})^{\mu\nu\rho}(q_1,q_2) = -\frac{1}{8\pi}\Big[&w_L^{(a)}(q_1^2,q_2^2,(q_1+q_2)^2) t_L^{\mu\nu\rho} + w_T^{+(a)}(q_1^2,q_2^2,(q_1+q_2)^2) t_+^{\mu\nu\rho} \\ &+ w_T^{-(a)}(q_1^2,q_2^2,(q_1+q_2)^2) t_-^{\mu\nu\rho} + \tilde{w}_T^{-(a)}(q_1^2,q_2^2,(q_1+q_2)^2)\tilde{t}_-^{\mu\nu\rho}\Big] \,.\end{aligned} \tag{3.10}$$

The Lorentz structures are chosen such that the first is longitudinal and the latter three are transversal with respect to the axial current.

After projection onto the BTT scalar functions, one observes that w_L determines the asymptotic behavior of $\bar{\Pi}_{1,2}$ in the asymmetric region, while the transversal functions fix the other scalar functions entering the master formula [21]. For this reason, we call also the scalar functions and the corresponding contributions to a_μ^{HLbL} longitudinal and transversal. In the chiral limit, the longitudinal function is fixed by the axial Adler–Bell–Jackiw (ABJ) anomaly [133, 134]

$$w_L^{(a)}(q_1^2,q_2^2,(q_1+q_2)^2) = \frac{2N_c}{(q_1+q_2)^2} \,, \tag{3.11}$$

where only the singlet component receives corrections from the gluonic $U(1)$ anomaly.

Plugging this into the result from the BTT decomposition, we arrive at

$$\bar{\Pi}_1^{(a),\mathrm{OPE}}(Q^2,Q^2,Q_3^2) = -\frac{2N_c C_a^2}{\pi^2 Q^2 Q_3^2} \quad \text{for} \quad a=\{3,8,0\} \,. \tag{3.12}$$

This equation holds in the chiral limit, neglecting the anomalous contribution in the singlet channel and in the kinematic limit $Q_1^2 \sim Q_2^2 \equiv Q^2 \gg Q_3^2 \gg \Lambda_{\mathrm{QCD}}^2$. For the non-singlet components ($a = 3, 8$), since perturbative [135] as well as non-perturbative [136] corrections are absent in the chiral limit, the hierarchy between Λ_{QCD}^2 and Q_3^2 can be dropped. In the singlet case, the gluonic $U(1)$ anomaly modifies the result. Thus the hierarchy can only be dropped at leading order in the large-N_c expansion, where the anomaly vanishes. Furthermore, in the

[4]See Refs. [55, 94] for a discussion of the relevance of the kinematic singularities at $(q_1+q_2)^2 = 0$. In Ch. 4, we will use a decomposition free of kinematic singularities.

crossed kinematics ($Q_2^2 \sim Q_3^2 \gg Q_1^2$ and $Q_1^2 \sim Q_3^2 \gg Q_2^2$), the leading-order OPE contributions to $\bar{\Pi}_1$ vanish.

Let us now compare $\bar{\Pi}_1^{(a),\,\mathrm{OPE}}$ against the pseudoscalar pole contributions, focusing on the pion pole first. In the chiral limit and using the fact that [137, 138]

$$\lim_{Q^2\to\infty} Q^2 F_{\pi\gamma^*\gamma^*}(-Q^2,-Q^2) = 4C_3 F_\pi \tag{3.13}$$

at leading order in α_s, one finds

$$\lim_{Q^2\to\infty} Q^2 \bar{\Pi}_1^{\pi^0\text{-pole}}(Q^2,Q^2,Q_3^2) = -4C_3 F_\pi \frac{F_{\pi\gamma^*\gamma^*}(-Q_3^2,0)}{Q_3^2}\,. \tag{3.14}$$

This expression has a pole at $Q_3^2 = 0$ since $F_{\pi\gamma^*\gamma^*}(0,0) = 3C_3/(2\pi^2 F_\pi)$. The location of this pole as well as its residue agree with $\bar{\Pi}_1^{(3),\,\mathrm{OPE}}$ in Eq. (3.12), which is consistent with the pion being the only massless isovector state in the chiral limit. The agreement between the OPE result and the pion pole has to stay in place also if perturbative corrections are included in both $\bar{\Pi}_1^{(a),\mathrm{OPE}}$ and the asymptotic limit of the pion TFF to the same order.

For finite quark masses, the pole in $\bar{\Pi}_1^{\pi^0\text{-pole}}$ is shifted from $Q_3^2 = 0$ to $Q_3^2 = -m_\pi^2$, which lies outside the integration domain for a_μ^{HLbL}. The closest point in the integration region for fixed asymptotic Σ (see Fig. 3.1) is at $Q_3^2 = 0$, where

$$\lim_{Q^2\to\infty} Q^2 \bar{\Pi}_1^{\pi^0\text{-pole}}(Q^2,Q^2,0) = -4C_3 F_\pi \frac{F_{\pi\gamma^*\gamma^*}(0,0)}{m_\pi^2} = -\frac{6C_3^2}{\pi^2 m_\pi^2}\,. \tag{3.15}$$

This is still close to the actual pole, which leads to the enhancement by m_π^{-2}. Since no other contribution receives the same enhancement, the last expression is expected to provide an excellent approximation to the true $\bar{\Pi}_1^{(3)}$ in the specified limit.[5] We observe that the OPE result, which is derived in the chiral limit, reproduces Eq. (3.15) if the pole position is shifted by the pion mass as dictated by the pion pole contribution

$$\lim_{Q^2\to\infty} Q^2 \bar{\Pi}_1^{(3)}(Q^2,Q^2,Q_3^2) = -\frac{6C_3^2}{\pi^2(Q_3^2+m_\pi^2)}\,. \tag{3.16}$$

This is also consistent with the OPE result in Eq. (3.12) for $Q^2 \gg Q_3^2 \gg \Lambda_{\mathrm{QCD}}^2$, where chiral corrections are sub-leading.

We extend the last relation to the η/η' channels and write

$$\lim_{Q^2\to\infty} Q^2 \bar{\Pi}_1^{(a)}(Q^2,Q^2,Q_3^2) = -\frac{6C_{\mathrm{PS}}^2}{\pi^2(Q_3^2+m_{\mathrm{PS}}^2)}\,. \tag{3.17}$$

Here $C_\pi = C_3$ but $C_{\eta/\eta'}$ cannot be directly identified with $C_{0/8}$ due to η-η'-mixing. In analogy to the pion channel, we assume that ground-state single-pseudoscalar exchanges dominate

[5] At variance with the MV model of Ref. [15], we do not neglect the momentum dependence of the singly-virtual TFF and we allow for the contribution from other states besides the pion at finite Q_3^2.

$\bar{\Pi}_1^{(8/0)-\eta/\eta'}(Q^2,Q^2,0)$, despite the fact that the η/η' poles are further away from $Q_3^2=0$. This assumption implies that $C_{\eta/\eta'}$ can be read off from the pole contributions

$$\lim_{Q^2\to\infty} Q^2\bar{\Pi}_1^{\eta/\eta'\text{-pole}}(Q^2,Q^2,0) = -\frac{6C_{\eta/\eta'}^2}{\pi^2 m_{\eta/\eta'}^2}\,. \tag{3.18}$$

One can show that in the chiral limit and at leading order in α_s [21]

$$\lim_{Q_3^2\to 0}\lim_{Q^2\to\infty} Q^2Q_3^2\left(\bar{\Pi}_1^{\eta\text{-pole}}(Q^2,Q^2,Q_3^2)+\bar{\Pi}_1^{\eta'\text{-pole}}(Q^2,Q^2,Q_3^2)\right) = -\frac{6(C_8^2+C_0^2)}{\pi^2}\,. \tag{3.19}$$

At this point, we note that, besides the α_s corrections to the TFFs and OPE coefficient discussed in Sec. 3.1.2, which affect all ground-state pseudoscalars in the same way, the $U(1)$ anomaly induces a running of the flavor singlet decay constant [139–141]. This running leads to an incomplete cancellation between the decay constants in the symmetric asymptotic and the real photon limits, which has a sizable impact due to the large scale separation [142, 143].

Since $\bar{\Pi}_1^{\eta/\eta'\text{-pole}}$ can be expressed in terms of TFFs analogously to Eq. (2.63), assuming that corrections due to non-vanishing meson masses are negligible both in the real photon limit and in the symmetric asymptotic limit of the η/η' TFFs, Eqs. (3.17–3.19) together imply

$$C_\eta^2 + C_{\eta'}^2 = C_8^2 + C_0^2 \tag{3.20}$$

up to the above-mentioned anomaly-induced scale-dependence, which leads to a violation of this equality (cf. Sec. 3.4.2).

For $Q_3^2 \gg \Lambda_{\text{QCD}}^2$, the additional Q_3^2-suppression of the singly-virtual TFF leads to a mismatch between the pseudoscalar pole contributions and the OPE constraint and other states beyond ground-state pseudoscalars have to be responsible for saturating the constraint. In Sec. 3.1.4, we will review some hadronic models that achieve this saturation. In Secs. 3.2–3.4, we will, however, show that sufficiently precise results for a_μ^{long} can also be achieved without explicit model assumptions on the coupling of heavier intermediate states to photons.

3.1.2 α_s corrections to the OPE

The derivation of Eq. (3.3) has been performed at leading order in α_s. Since no other operator of dimension 3 can appear in the OPE of two vector currents, α_s corrections only affect the OPE coefficient of the axial-vector current. Thus, the NLO version of Eq. (3.3) is

$$\Pi^{\mu\nu}(q_1,q_2) = \int \mathrm{d}^4z\, e^{-i(q_1+q_2)\cdot z}\left(-\frac{2i}{\hat{q}^2}\left(1+\frac{\alpha_s}{\pi}C\right)\epsilon^{\mu\nu\alpha\beta}\hat{q}_\alpha j_{5\beta}(z) + \mathcal{O}\left(\hat{q}^{-2}\right)\right), \tag{3.21}$$

where C is a real number.

C can be easily computed by observing that the two-current operator not only enters the HLbL tensor, but also the pion TFF (see Eq. (2.58)). Thus, any perturbative correction to

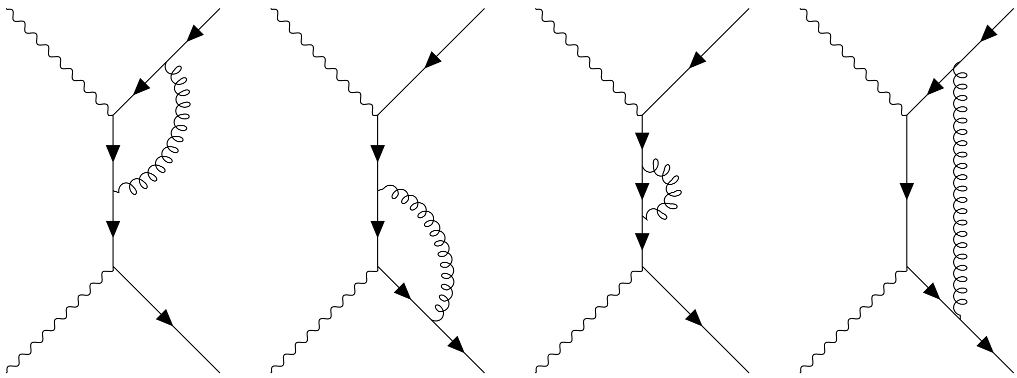

Figure 3.2: Diagrams contributing to the matrix element $\langle q(p_1)|\, \Pi^{\mu\nu}(q_1, q_2)\, |q(p_2)\rangle$ at NLO without wave-function renormalization. In addition there are the same diagrams with the photons crossed. Solid lines represent quarks, wiggly lines photons and curled lines gluons.

the OPE Wilson coefficient automatically implies the same perturbative correction to the symmetric limit of the pion TFF and vice versa and C can be determined from the pion TFF asymptotics. This also guarantees that the OPE result Eq. (3.12) agrees with the pion pole in the chiral limit for $Q_3^2 = 0$ exactly to all orders.

At leading order in the OPE, the asymptotic TFF can be written as

$$F_{\pi\gamma^*\gamma^*}(-Q_1^2, -Q_2^2) = \int_0^1 \mathrm{d}u\, T(Q_1^2, Q_2^2, u)\phi_\pi(u) \tag{3.22}$$

where $T(Q_1^2, Q_2^2, u)$ is the perturbativly calculable hard scattering kernel, $\phi_\pi(u)$ the pion distribution amplitude and the integral runs over the momentum distribution among the partons in the quark anti-quark Fock state of the pion. In the symmetric limit $Q_1^2 = Q_2^2$ the hard scattering kernel is independent of u and thus can be pulled out of the integral. The normalization of the pion distribution amplitude, $\int_0^1 \mathrm{d}u\, \phi_\pi(u) = 1$, then fixes the integral. With the hard scattering kernel calculated to NLO in Ref. [144], this leads to [18]

$$F_{\pi\gamma^*\gamma^*}(-Q^2, -Q^2) = \left(1 - \frac{\alpha_s}{\pi} + \mathcal{O}\left(\alpha_s^2\right)\right) \frac{2F_\pi}{3Q^2} + \mathcal{O}\left(Q^{-4}\right) . \tag{3.23}$$

From this, we read off $C = -1$.

As this result disagrees with Ref. [145], we computed the single-quark matrix element of Eq. (3.3) to NLO. The Feynman diagrams contributing to $\langle q(p_1)|\, \Pi^{\mu\nu}(q_1, q_2)\, |q(p_2)\rangle$ can be found in Fig. 3.2 and have to be calculated with the standard QCD Feynman rules. The UV-divergences of the first two diagrams are canceled by vertex renormalization and that of the third by quark wave function renormalization, whereas the last diagram is UV finite. The result has to be expanded to leading order in $1/|\hat{q}|$.

However, also the single-quark matrix element of the right-hand side of Eq. (3.3) has to be calculated to NLO. For this we need $\langle q(p_1)|\, j_5^\beta\, |q(p_2)\rangle$ to $\mathcal{O}(\alpha_s)$, the relevant diagram for which

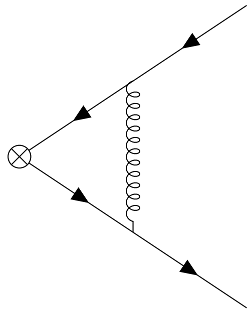

Figure 3.3: Diagrams contributing to the matrix element $\langle q(p_1)|\, j_5^\beta(z)\, |q(p_2)\rangle$ at NLO without wave-function renormalization. Solid lines represent quarks and curled lines gluons.

is displayed in Fig. 3.3. This is also needed to cancel the IR divergences of the fourth diagram in Fig. 3.2 in the massless limit, which is leading in $1/|\hat{q}|$. To evaluate this diagram in dimensional regularization, one needs a prescription for the treatment of γ_5 in $d \neq 4$. The presence of the axial anomaly shows that one cannot simply require $\{\gamma_\mu, \gamma_5\} = 0$ and $\mathrm{Tr}(\gamma_\mu\gamma_\nu\gamma_\lambda\gamma_\sigma) = 4\mathrm{i}\epsilon_{\mu\nu\lambda\sigma}$ to remain valid as this would allow the singlet vector and axial-vector currents to be conserved simultaneously. Instead, 't Hooft and Veltman [146] proposed to use

$$\gamma_5 = \frac{1}{4!}\epsilon_{\mu\nu\lambda\sigma}\gamma^\mu\gamma^\nu\gamma^\lambda\gamma^\sigma \tag{3.24}$$

and pull the ϵ-tensor out of the d-dimensional integral. This leads to $\{\gamma_\mu, \gamma_5\} = 2\hat{\gamma}_\mu\gamma_5$, where $\hat{\gamma}_\mu$ vanishes if $\mu \in \{0, 1, 2, 3\}$ and equals γ_μ otherwise. This approach was later formalized by Breitenlohner and Maison [147].

Using this scheme, one finds that the axial current is renormalized not only by the wave-function renormalization of the fermions, which make the matrix element finite, but also by a finite renormalization for the non-anomalous Ward identity (cf. Ref. [144])

$$\Gamma_5^\mu(p_2 - p_1)_\mu = (\not{p}_1 - \Sigma(p_1))\gamma_5 + \gamma_5(\not{p}_2 - \Sigma(p_2)) \tag{3.25}$$

to hold, where Γ_5^μ is the 1PI matrix element of the axial current with quark momenta p_1 and p_2 and $\Sigma(p)$ the quark self-energy.

Putting everything together, this calculation confirms $C = -1$. It follows that the NLO version of Eq. (3.17) reads

$$\lim_{Q^2\to\infty} Q^2\bar{\Pi}_1^{(a)}(Q^2, Q^2, Q_3^2) = -\frac{6C_P^2}{\pi^2(Q_3^2 + m_P^2)}\left(1 - \frac{\alpha_s}{\pi}\right). \tag{3.26}$$

This result has later also been confirmed in Ref. [49]. In this reference also higher-order terms in the OPE have been considered. For $q_3^2 \gg \Lambda_{\mathrm{QCD}}^2$, one can use perturbative input for the matrix elements appearing therein and doing this, the properly expanded result from the perturbative quark loop is recovered. At smaller values of q_3^2, these matrix elements are non-perturbative and Ref. [49] does not provide an evaluation. We will thus not consider these corrections in the following.

3.1.3 The symmetric asymptotic limit: perturbative QCD constraints

In Refs. [20, 47, 48], the behavior of the HLbL tensor in the regime where three photon virtualities are large, whereas the fourth is on-shell as needed for a_μ^{HLbL}, has been investigated. It has been argued there that the standard OPE with the pQCD quark loop at leading order is not applicable due to the small momentum scale entering via the external photon.

Instead, the authors of Refs. [20,47,48] have considered an alternative OPE in the presence of an external electromagnetic background field. In this formalism, the soft photon can either couple to a hard quark line or soft degrees of freedom through non-perturbative operators with the quantum numbers of the external field. For the calculation one first factors out the external photon from the matrix element at small q_4

$$\mathrm{i}\epsilon_\sigma(-q_4)\Pi^{\mu\nu\lambda\sigma}(q_1,q_2,q_3) = -\Pi_F^{\mu\nu\lambda\rho\sigma}(q_1,q_2)\,\langle 0|\,F_{\rho\sigma}\,|\gamma^*(-q_4)\rangle = -\mathrm{i}q_{4\rho}\epsilon_\sigma(-q_4)\Pi_F^{\mu\nu\lambda[\rho\sigma]}(q_1,q_2)\,, \tag{3.27}$$

where $[\rho\sigma]$ indicates antisymmetrization. The matrix element $\Pi_F^{\mu\nu\lambda\rho\sigma}(q_1,q_2)$ is independent of the soft momentum q_4 and can be calculated perturbatively through the OPE in a background field.

At leading order in this OPE, the external field couples to a hard quark line through modification of the quark propagator. At leading order in α_s, this exactly leads to the massless quark loop result in standard pQCD. The expression for $\bar{\Pi}_1$ reads

$$\begin{aligned}
\bar{\Pi}_1^{\mathrm{pQCD}}(q_1^2,q_2^2,q_3^2) &= \frac{N_c\,\mathrm{Tr}\,\mathcal{Q}^4}{16\pi^2}\int_0^1\mathrm{d}x\int_0^{1-x}\mathrm{d}y\,I_1(x,y) = \frac{1}{24\pi^2}\int_0^1\mathrm{d}x\int_0^{1-x}\mathrm{d}y\,I_1(x,y)\,,\\
I_1(x,y) &= -\frac{16x(1-x-y)}{\Delta_{132}^2} - \frac{16xy(1-2x)(1-2y)}{\Delta_{132}\Delta_{32}}\,,\\
\Delta_{ijk} &= m_q^2 - xyq_i^2 - x(1-x-y)q_j^2 - y(1-x-y)q_k^2\,,\\
\Delta_{ij} &= m_q^2 - x(1-x)q_i^2 - y(1-y)q_j^2\,,
\end{aligned} \tag{3.28}$$

where we have kept a non-zero quark mass despite the fact that quark-mass effects are intertwined with non-perturbative higher-order contributions in this regime. The expressions for the other scalar functions can be found in Ref. [21].

At NLO in the OPE, the photon couples to the diagram through the di-quark operator with quantum numbers of the external field

$$\langle\bar{q}\sigma_{\alpha\beta}q\rangle = \mathcal{Q}_q F_{\alpha\beta} X_q \tag{3.29}$$

with the charge $\mathcal{Q}_q$ of the quark q and the tensor coefficients related to the magnetic susceptibility X_q. Due to chiral symmetry, the result is additionally suppressed by one power of the light quark masses. This together with the small numerical values of the tensor coefficients leads to a very small contribution to a_μ^{HLbL} if the integrals in the master formula are restricted to reasonably large momenta. Operators at dimension 4 are not suppressed by quark masses, but their effect on a_μ^{HLbL} is similarly small [47]. In the following, we will only make use of the leading-order result. Perturbative α_s-corrections to the quark loop have been calculated in Ref. [48]. The full result up to two loops is complicated, but to a good approximation it is given by $(1-\alpha_s/\pi)$ times the leading-order expression.

In the symmetric limit, neglecting terms that are suppressed by powers of m_q^2/Q^2, the leading order result in both the OPE and α_s takes the form

$$\bar{\Pi}_1^{\text{pQCD}}(Q^2,Q^2,Q^2) = \sum_{a=3,8,0} \bar{\Pi}_1^{(a),\,\text{pQCD}}(Q^2,Q^2,Q^2) = \sum_{a=3,8,0} -\frac{4N_c C_a^2}{3\pi^2 Q^4}\,, \tag{3.30}$$

where we have chosen to adopt the same flavor decomposition as for the asymmetric OPE case, Eq. (3.12). However, Eq. (3.28) is expected to be a good approximation also away from the fully symmetric configuration as long as large logarithms of ratios of momenta are absent. Since $\bar{\Pi}_1^{P\text{-pole}}$ decays like Q^{-6}, (towers of) hadronic contributions beyond ground-state pseudoscalar poles have to be responsible for the behavior shown by Eq. (3.30).

In order to saturate the pQCD result in the isosinglet channels, we need coefficients $C_{\eta/\eta'}^{\text{pQCD}}$ satisfying

$$C_8^2 + C_0^2 = \left(C_\eta^{\text{pQCD}}\right)^2 + \left(C_{\eta'}^{\text{pQCD}}\right)^2 . \tag{3.31}$$

Since Eq. (3.20) is violated, we define

$$\left(C_{\eta/\eta'}^{\text{pQCD}}\right)^2 = (1+\delta_0)C_{\eta/\eta'}^2\,, \tag{3.32}$$

where the parameter δ_0 is chosen such that Eq. (3.31) holds.

3.1.4 Saturation of SDCs within hadronic models

In this section, we discuss general constraints on hadronic models saturating the SDCs introduced above and review models, which at least partly achieve a saturation. The numerical results of these models are compared to ours in Secs. 3.4.3 and 3.4.4.

Both the asymmetric SDC for finite Q_3^2 as well as the symmetric asymptotic constraint on a_μ^{HLBL} cannot be saturated by the pseudoscalar poles alone, which decay too fast in the respective limits. In fact, no finite number of single-particle intermediate states can saturate the limits as the coupling between these mesons and the photons is subject to SDCs as well [131, 148, 149] (see e.g. Ref. [150] where the analogous case of a three-point function is treated explicitly). For this reason, only infinite towers of states can saturate the limits, where the non-commutativity of the limits on the virtualities and the infinite sum over the states can make the tower contribution decay more slowly than any individual contribution. Hadronic models are needed to estimate the effects of these towers of intermediate states.

It is evident from the derivation in Sec. 3.1.1 that the asymmetric OPE constraint can only be saturated by states that couple to the axial current. In the single-particle sector, the only available states are pseudoscalars and axials. In the chiral limit, massive pseudoscalars cannot couple to the axial current for the following reason: consider the vaccum-to-massive-pseudoscalar matrix element of the axial current

$$\langle 0|\, A_\mu^{(a)}(x)\, |P(k)\rangle = \mathrm{i} k_\mu F_P^{(a)}\,, \tag{3.33}$$

where $A_\mu^{(a)}(x) = \bar{\psi}(x)\gamma_\mu\gamma_5\lambda^a\psi(x)/2$ are the flavor components of the axial current and $F_P^{(a)}$ is the decay constant of the pseudoscalar. In the chiral limit and for $a \neq 0$, the axial current is conserved, so that the derivative must vanish

$$\langle 0|\, \partial^\mu A_\mu(x)\, |P(k)\rangle = k^2 F_P = m_P^2 F_P = 0\,. \tag{3.34}$$

This can only be satisfied if either the mass vanishes in the chiral limit (as for the ground-state pseudoscalars) or the decay constant tends to zero in the chiral limit. The latter has to be the case for excited pseudoscalars, which thus do not couple to the axial current as evident from Eq. (3.33). For this reason, only an infinite tower of axials can saturate the asymmetric SDC in the chiral limit, whereas away from the chiral limit excited pseudoscalars can also contribute.

Together with the first derivation of the asymmetric asymptotic constraint, the authors of Ref. [15] have also presented a model to saturate it (see also Refs. [21, 93]). They use only one multiplet each of pseudoscalars and axials, but modify their forms compared to the dispersive framework reviewed in Sec. 2.4. The longitudinal constraint is saturated by the pseudoscalars with the singly-virtual TFF set to a constant. This substantially changes the form of the scalar function in the low-energy region, where the pseudoscalar poles in the dispersive definition are known to dominate. With this prescription, the parametric Q-dependence in the symmetric regime is compatible with the pQCD quark-loop result, but the coefficient is too large. In the transversal sector, a vector-meson dominance (VMD) model for axials, again without the singly-virtual TFF, is employed to saturate the asymmetric constraint.

More recently, two other model-based approaches were considered to saturate the SDCs. In Refs. [21, 40], the longitudinal constraints are saturated by infinite towers of excited pseudoscalars in a large-N_c-inspired Regge model, away from the chiral limit. In this model, the masses of both pseudoscalars and vector mesons are assumed to follow Regge trajectories

$$m^2_{P(n),\mathrm{V}(n)} = \hat{m}^2_{P,\mathrm{V}} + n\sigma^2_{P,\mathrm{V}}\,, \tag{3.35}$$

where the intercept $\hat{m}^2_{P,\mathrm{V}}$ and the slope $\sigma^2_{P,\mathrm{V}}$ are determined from the measured spectra. It is further assumed that the nth excited pseudoscalar couples only to the nth excited vector mesons. Then VMD-like models with six free parameters are constructed for the TFFs and five of them are chosen to satisfy the following conditions:

- normalization of the ground-state (π^0, η, η') TFFs at vanishing virtualities,

- Brodsky-Lepage limit for the ground-state TFFs,
- symmetric asymptotic limit for the ground-state TFFs,
- asymmetric OPE constraint for the longitudinal part of the HLbL tensor and
- symmetric pQCD constraint for the longitudinal part of the HLbL tensor.

The remaining free parameter is fitted to the ground-state TFFs using the dispersive pion TFF [18, 50] for the model in the isovector channel and data in the isoscalar channels. It has also been checked that the two-photon couplings of the excited pseudoscalars are compatible with experimental constraints where available.

To reduce the model-dependence of the approach, the result for $\bar{\Pi}_1$ is replaced by the pQCD quark-loop result for $Q_i > Q_{\text{match}}$ for all $i \in \{1,2,3\}$. Minimizing the combined uncertainty of the Regge model below the matching point and the quark-loop result above it, the preferred matching scale is determined to be around $Q_{\text{match}} = 1.7\,\text{GeV}$.

Refs. [41–44, 151] on the other hand have investigated how axials can contribute to a saturation of SDCs within holographic models for QCD. These models are based on the AdS/CFT conjecture [152] that relates a theory of gravity in $d+1$ dimensional anti-de Sitter space to a strongly interacting conformal field theory in d dimensions. To model the non-perturbative QCD dynamics, a five-dimensional $U(N_f) \times U(N_f)$ Yang-Mills theory in curved space-time is employed. The extra dimension is cut-off either by a hard boundary (hard-wall model, HW) or smoothly by a dilaton field (soft-wall model, SW) to break conformal symmetry in the infrared. Different mechanisms are employed to also break chiral and axial symmetry. In this way, one obtains models with Regge spectra for pseudoscalar, vector and axial-vector mesons.[6] In Refs. [41, 43, 44, 124] these models have been applied to the pseudoscalar TFFs finding results compatible with the dispersive and data-driven determinations from Refs. [16, 18, 50].

In these models, the contribution to $\bar{\Pi}_1$ of an axial meson of mass M_A in the flavor channel a can be written as[7]

$$\bar{\Pi}_1^{(a),\,\text{axial}} = -\frac{9\,C_a^2}{16\pi^4 M_A^2}\left[Q_1^2\,A(Q_1^2,Q_2^2) + Q_2^2\,A(Q_2^2,Q_1^2)\right]A(Q_3^2,0)\,, \tag{3.36}$$

where $A(Q_1^2,Q_2^2)$ is the axial TFF. While each individual contribution falls off too fast in the asymptotic regimes to saturate the OPE and pQCD constraints, one can analytically show that the infinite tower behaves differently and indeed has the correct Q-dependence. Together with the pseudoscalar contributions, these models can satisfy Eq. (3.12) with the full Q_3^2-dependence as long as $Q_3^2 \ll Q^2$ and accordingly also for the transversal OPE constraints. In the pQCD

[6] Models without chiral symmetry breaking only include ground-state pseudoscalars in agreement with chiral symmetry.

[7] See, however, our comment in Sec. 2.4.3 about the intrinsic model dependence of such a contribution.

regime, the parametric Q-dependence is again correct, but if the parameters are fixed to satisfy the OPE constraint, the coefficient is too small [41, 43]. This could be corrected by other contributions to the pQCD behavior not calculated so far in the holographic models [41].

3.2 Interpolating between asymptotic constraints

From this section on, we entirely focus on the longitudinal part of a_μ^{HLbL}, for which the master formula Eq. (2.54) reduces to

$$a_\mu^{\mathrm{long}} = \frac{\alpha^3}{432\pi^2}\int_0^\infty \mathrm{d}\Sigma \int_0^1 \mathrm{d}r \int_0^{2\pi} \mathrm{d}\phi \Sigma^3\, r\sqrt{1-r^2}\left[T_1(\Sigma,r,\phi) + T_2\left(\Sigma,r,\phi+\frac{2\pi}{3}\right)\right]\bar{\Pi}_1(\Sigma,r,\phi)\,. \tag{3.37}$$

The hadronic dynamics is solely contained in the scalar function $\bar{\Pi}_1$. The low-energy region of this function, i.e. the region where all virtualities Q_i^2 are simultaneously small, is well approximated by the contributions of the lightest states only, as argued in Sec. 2.4.3. We will use this input in some part of the three-dimensional integration domain including the origin as we are going to specify later. As already pointed out, if two or three of the virtualities get large, the SDCs derived in the previous section can only be saturated by infinite towers of intermediate states. However, experimental input on these towers is very scarce and constrained to the few lightest states, which introduces uncontrolled uncertainties into model-based estimates as explained in Sec. 3.1.4. Our approach instead is to construct general functions compatible with all SDCs by construction and smoothly connecting to the well-known low-energy region.

To this end, we approximate the true $\bar{\Pi}_1(\Sigma, r, \phi)$ following a two-step procedure. We first select functional forms that are valid for asymptotic Σ and are compatible with the constraints discussed in the previous section. We then interpolate between this set of functions and various representations of $\bar{\Pi}_1$ at small Σ determined by single-particle intermediate states. Here we work at leading order in α_s. Perturbative corrections will be discussed in our numerical analysis in Sec. 3.4.

We first focus on the constraints at the central points of their respective region of validity in the plane for asymptotic Σ depicted in Fig. 3.1. The OPE result in Eq. (3.17) is valid for $Q_1^2 = Q_2^2 \gg Q_3^2$ or equivalently $(r,\phi) = (1,\pi)$. It imposes a Σ^{-2} fall-off for non-zero Q_3^2 and a pole in the coefficient function at $Q_3^2 = -m_P^2$, slightly outside the integration domain, but approaching it as $\Sigma \to \infty$. The sub-leading results in the crossed kinematics $Q_1^2 = Q_3^2 \gg Q_2^2$ and $Q_2^2 = Q_3^2 \gg Q_1^2$ are also consistent with a Σ^{-2} behavior, but without poles close to $Q_1^2 = 0$ or $Q_2^2 = 0$. In the symmetric limit $Q_1^2 = Q_2^2 = Q_3^2$, Eq. (3.30) holds, which also has a Σ^{-2} behavior.

These constraints are all compatible with

$$\bar{\Pi}_1^{(a),\text{ asymp}'} = -\frac{4N_cC_P^2}{\pi^2(Q_3^2+m_P^2)(Q_1^2+Q_2^2+Q_3^2)} = -\frac{12N_cC_P^2}{\pi^2\Sigma(3m_P^2+\Sigma+\Sigma r\cos\phi)} \tag{3.38}$$

if $C_P = C_P^{\mathrm{pQCD}}$. Thus, Eq. (3.38) interpolates between symmetric and asymmetric asymptotic limits. According to Sec. 3.1.3, δ_0 parameterizes the anomaly corrections to the singlet VVA correlator and the resulting shift in C_P^{pQCD} with respect to C_P. A term proportional to Σ^{-2} and independent of r and ϕ is suppressed with respect to Eq. (3.38) at $Q_3^2 = 0$, where $\bar{\Pi}_1^{(a),\text{ asymp}'}$ behaves as $(m_P^2\Sigma)^{-1}$. Thus, the addition of such a term modifies the behavior in the pQCD regime while not spoiling compatibility with the OPE constraint. To account for a non-vanishing δ_0, we subtract $12N_c\delta_0 C_{\eta/\eta'}^2/(\pi^2\Sigma^2)$ from Eq. (3.38) in the case of η/η', which leads to

$$-\frac{12N_cC_P^2}{\pi^2\Sigma(3m_P^2+\Sigma+\Sigma r\cos\phi)} - \frac{12N_c\delta_0C_P^2}{\pi^2\Sigma^2} \xrightarrow[\Sigma\gg m_P^2]{r=0} -\frac{12N_cC_P^2(1+\delta_0)}{\pi^2\Sigma} = -\frac{12N_c(C_P^{\mathrm{pQCD}})^2}{\pi^2\Sigma} \tag{3.39}$$

in the symmetric asymptotic regime.

Obviously, the choice made in Eq. (3.38) and the exact form of the singlet correction are not unique and we are free to add a generic function such that the interpolant still satisfies the constraints. This function cannot decay more slowly than Σ^{-2} for any (r,ϕ) region of finite size in order for the a_μ^{long} integral to converge. Conversely, a function decaying faster than Σ^{-2} would not have a non-negligible effect at asymptotic Σ compared to Eq. (3.38), so that the function has to be Σ^{-2} times a coefficient depending on r and ϕ. This coefficient should be an analytic function of r and ϕ without poles at $r \leq 1$ since $\bar{\Pi}_1$ is free of kinematic singularities and dynamical ones can only appear at negative Q_i^2. Therefore it can be approximated by a Taylor series in $r\cos\phi$ and $r\sin\phi$ truncated after order M. In total, this lets us write

$$\begin{aligned}
\bar{\Pi}_1^{(3),\text{ asymp}} &= \bar{\Pi}_1^{(3),\text{ asymp}'} + \frac{12N_cC_\pi^2}{\pi^2\Sigma^2}\sum_{i=0}^{M}\sum_{j=0}^{M}\frac{1}{i!\,j!}a_{i,j}(r\cos\phi)^i(r\sin\phi)^j\,, \\
\bar{\Pi}_1^{(8/0)-\eta/\eta',\text{ asymp}} &= \bar{\Pi}_1^{(8/0)-\eta/\eta',\text{ asymp}'} - \frac{36\delta_0C_{\eta/\eta'}^2}{\pi^2\Sigma^2} \\
&\quad + \frac{12N_cC_{\eta/\eta'}^2}{\pi^2\Sigma^2}\sum_{i=0}^{M}\sum_{j=0}^{M}\frac{1}{i!\,j!}a_{i,j}(r\cos\phi)^i(r\sin\phi)^j\,,
\end{aligned} \tag{3.40}$$

where

$$a_{0,0} = 0\,,\quad a_{i,2j+1} = 0 \tag{3.41}$$

for integer j, due to the pQCD constraint and crossing symmetry.

Up to now, we have applied the quark-loop result only at $r = 0$. The fact that Eq. (3.28) holds also in a neighborhood of this point can be used to fix the coefficients $a_{i,j}$. To this end, we fitted the asymptotic expressions Eq. (3.40) at fixed asymptotic Σ with $M = 2$ to the quark loop result Eq. (3.28). In the isosinglet cases, the fit is performed for the sum of the two cases to remove the dependence on $\eta-\eta'$-mixing and the anomaly correction in η/η' channels leads to different results compared to the pion channel.

We restricted the fits to $r < 0.9$, where the maximal ratio of two squared momenta is 14.7. Since $\ln(14.7) \approx 2.7$, no large logarithms appear in this regime and we can assume the convergence of fixed-order pQCD. We chose a grid of equally separated points in this circle $\{(r_i, \phi_i)\}$ and minimized the sum of the relative squared differences between our interpolant and the leading-order quark-loop expression

$$\chi^2 = \lim_{\Sigma\to\infty} \sum_{i=0}^{N} \left(\frac{\bar{\Pi}_1^{(a),\text{ asymp}}(\Sigma, r_i, \phi_i) - \bar{\Pi}_1^{(a),\text{ pQCD}}(\Sigma, r_i, \phi_i)}{\bar{\Pi}_1^{(a),\text{ pQCD}}(\Sigma, r_i, \phi_i)} \right)^2 . \tag{3.42}$$

The resulting 5 dimensionless fit parameters in the pion channel read

$$a_{1,0} = -0.170\ , \quad a_{2,0} = 0.094\ , \quad a_{0,2} = -0.554\ , \quad a_{1,2} = -0.169\ , \quad a_{2,2} = -0.756 \tag{3.43}$$

and are all at most $\mathcal{O}(1)$, as expected since in Eq. (3.40) they parameterize relative corrections. In the η and η' channels, the fit yields

$$a_{1,0} = -0.017\ , \quad a_{2,0} = -0.201\ , \quad a_{0,2} = -0.621\ , \quad a_{1,2} = -0.339\ , \quad a_{2,2} = -0.642 \tag{3.44}$$

for $\delta_0 = 0.101$ as determined from the Canterbury TFFs, see Sec. 3.4.2. In Sec. 3.4.1.2 we will discuss uncertainties due to the chosen fitting range, the number of parameters in the fit and α_s corrections to the asymptotic constraints.

3.3 Interpolating between low and high energies

The next step is to smoothly connect our representation of $\bar{\Pi}_1$ for $\Sigma \gg \{\Lambda^2_{\text{QCD}}, m_P^2, \dots\}$ given by Eq. (3.40) to an accurate low-energy description. We achieve this by adding suitable terms to $\bar{\Pi}_1^{(a),\text{ asymp}}$ that are sub-leading at large Σ. For each choice of r and ϕ, the coefficients of these terms are then matched onto an input low-energy representation of $\bar{\Pi}_1$ at a suitably defined surface $\Sigma^{\text{match}}(r, \phi)$. In Sec. 3.3.2, we discuss the construction of Σ^{match} and how it is related to the mass scale at which intermediate states beyond the ones explicitly considered start to affect $\bar{\Pi}_1$. Sec. 3.3.3 is devoted to a discussion of the convergence of the interpolants.

3.3.1 Interpolation functions and matching procedure

For $\Sigma > \Sigma^{\text{match}}$, we consider the following two interpolation functions

$$\begin{aligned}
\bar{\Pi}_1^{(a),\text{ int 1}}(\Sigma, r, \phi) &= \bar{\Pi}_1^{(a),\text{ asymp}}(\Sigma, r, \phi) \left(1 + \sum_{i=1}^{N} b_i(r, \phi)\Sigma^{-i}\right) , \\
\bar{\Pi}_1^{(a),\text{ int 2}}(\Sigma, r, \phi) &= \bar{\Pi}_1^{(a),\text{ asymp}}(\Sigma, r, \phi) \left(1 + \sum_{i=1}^{N} b_i(r, \phi)\Sigma^{-i}\right)^{-1} ,
\end{aligned} \tag{3.45}$$

whose leading terms at asymptotic Σ are given in Eq. (3.40), whereas below the matching surface we set $\bar{\Pi}_1^{(a),\text{ int }1/2} = \bar{\Pi}_1^{P\text{-pole}}$. In Sec. 3.3.3, we will show that these functions converge to the true $\bar{\Pi}_1^{(a)}$ in the limit $N \to \infty$ when matched to exact low-energy input using the convergence property of a Taylor series. The two different forms given in Eq. (3.45) will be used to estimate the sensitivity of our numerical results on the specific choice of interpolation between low and high energies.

The coefficients $b_i(r,\phi)$ are fixed from the requirement that the $\bar{\Pi}_1^{(a),\text{ int i}}$ have the same value and the same $N-1$ Σ-derivatives as the low-energy representation if evaluated at $\Sigma = \Sigma^{\text{match}}(r,\phi)$ for each (r,ϕ). No expansion is performed in r and ϕ, which is crucial to obtain a smooth transition to the low-energy regime.

Determining the optimal value of N is a non-trivial issue. On the one hand, larger values of N seem to be preferable since the true $\bar{\Pi}_1$ is analytic for space-like momenta and thus all derivatives are continuous. On the other hand, matching many derivatives leads to a function that is almost saturated by the low-energy input contribution up to considerably higher energies than $\Sigma^{\text{match}}(r,\phi)$. Since it is desirable to match at least one derivative in order to have $\bar{\Pi}_1$ differentiable at the matching point, we will use $N \in \{2,3\}$ in order to estimate the dependence on N.

Interpolation functions with a logarithmic dependence on Σ are not forbidden. This can stem, for example, from non-perturbative corrections leading to terms like $\ln(Q_i^2/M^2)$, where M is some non-perturbative mass scale. In fact, the Regge model considered in Refs. [21, 40] leads to interpolants containing terms like $Q^{-4}\ln(Q^2/\sigma^2)$ for $Q_i^2 = Q^2 \to \infty$, where σ^2 could e.g. be the Regge slope of the excited pseudoscalar masses. In order to allow for such a logarithmic approach of the asymptotic expression, we additionally consider the alternative interpolant

$$\bar{\Pi}_1^{(a),\text{ int }3}(\Sigma,r,\phi) = \bar{\Pi}_1^{(a),\text{ asymp}}(\Sigma,r,\phi)\left[1 + b_1(r,\phi)\Sigma^{-1}\ln\left(\frac{\Sigma}{\Lambda_{\text{QCD}}^2}\right) + \sum_{i=1}^{N-1} b_{i+1}(r,\phi)\Sigma^{-i}\right] \tag{3.46}$$

and use again $N \in \{2,3\}$. We note that this interpolant is independent of the numerical value of Λ_{QCD}, a change of which can be absorbed into b_2.

The b_1-term in this interpolant leads to a slower approach of the asymptotic representation $\bar{\Pi}_1^{(a),\text{ asymp}}(\Sigma,r,\phi)$ of this interpolant compared to the polynomial behaviors of interpolants 1 and 2. Terms with a logarithmic dependence on Σ multiplied by a higher power of Σ^{-1}, however, do not modify the leading behavior of approaching the asymptotic expression and are thus expected to have a negligible numerical effect.

3.3.2 The matching surface Σ^{match}

The remaining crucial ingredient in our procedure is the function $\Sigma^{\text{match}}(r,\phi)$, which determines the value of Σ at which the matching is performed for given r and ϕ. Choosing it too low leads to important modifications of $\bar{\Pi}_1^{(a)}$ at low energies with consequent overestimation of $a_\mu^{(a)}$.[8] Conversely, choosing Σ^{match} too high assumes the low-energy input to dominate beyond what is expected according to mass and phase-space considerations and thus leads to underestimate $a_\mu^{(a)}$.

For small values of Q_3^2, the π^0, η, η' poles are assumed to dominate independently of $Q_{1,2}^2$, due to the pole at $Q_3^2 = -m_P^2$ (see Secs. 2.4.3 and 3.1.1). This implies that no matching is needed in this regime, i.e. $\Sigma^{\text{match}}(1,\pi) = \infty$. The most general function that is analytic for all (r,ϕ) except for a (first-order) pole at $(r,\phi) = (1,\pi)$ can be written as

$$\Sigma^{\text{match}}(r,\phi) = \frac{3m^2}{1 + r\cos\phi}\left(1 + P(r\cos\phi, r\sin\phi)\right) , \tag{3.47}$$

where m^2 determines the matching scale at $r = 0$ and P is an analytic function with two arguments and vanishing at the origin. The transformation property of $\bar{\Pi}_1$ under crossing specified in Eq. (2.62) restricts P to be even in its second argument.

The parameter m^2 sets the absolute mass scale of Σ^{match} and should thus be related to the masses of the states affecting $\bar{\Pi}_1$ beyond the ones explicitly included, namely π^0, η, η' here. In the following, we will assume that contributions to $\bar{\Pi}_1$ in the $g-2$ kinematics stemming from multi-particle intermediate states are dominated by narrow resonances while non-resonant effects lead to negligible corrections to the matching procedure and can be simply added to our final results.[9] This is realized for example in the large-N_c limit of pure QCD: since the short-distance expressions for $\bar{\Pi}_1$ in both symmetric and asymmetric limits scale like N_c, these can indeed be saturated by single-meson exchanges (see Ref. [153]). Non-resonant contributions from multi-hadron intermediate states (like 2π, $2K$, $\pi\eta$, 3π, $\ldots$) are sub-leading for large N_c and thus cannot contribute to the SDCs. Since scalar mesons have no impact on $\bar{\Pi}_1$, the lightest states beyond the ground-state pseudoscalars that are the most relevant at small Q_3^2 (see Sec. 2.4.3) are the axial mesons like $a_1(1260)$ and the tensor mesons like $f_2(1270)$, with masses in the 1–2 GeV region, whose effects on a_μ^{HLbL} can presently be estimated only using hadronic models, see, however, the advances made in Ch. 5 and Ref. [60].

For $P(x,y) = 0$, $\Sigma = \Sigma^{\text{match}}$ corresponds to $Q_3^2 = m^2$. Since a state of mass M ceases to be suppressed by the denominator $(Q_3^2 + M^2)$ compared to lighter states when Q_3^2 approaches M^2, m^2 should be chosen well below M^2. At the same time, it should not be taken too small, because we do not expect any large contribution to $\bar{\Pi}_1$ at $Q_3^2 \ll M^2$. We thus regard $m^2 = 0.5\ \text{GeV}^2$ as a good starting point for our analysis. In Sec. 3.4.1.4, we will discuss a

[8]We denote by $a_\mu^{(a)}$ the result of the integral in Eq. (3.37) for $\bar{\Pi}_1 \equiv \bar{\Pi}_1^{(a)}$.

[9]We have checked the effects of the inclusion of the pion-loop contribution to $\bar{\Pi}_1$ [17] in the low-energy representation. Since the two-pion state contains a five-dimensional representation of the isospin group, a full decomposition into $\bar{\Pi}_1^{(a)}$ is not possible. However, even if its complete contribution is added to the isovector channel, we find that at the current level of precision it is irrelevant whether the pion loop is included in the matching procedure or not.

range of choices for this parameter. The function P has to be analytic and can thus be Taylor expanded around the origin. We truncate the expansion after order M and thus write

$$P(x,y) = \sum_{i=0}^{M}\sum_{j=0}^{M} \frac{1}{i!\; j!} p_{i,j}\; x^i y^j\,. \tag{3.48}$$

In order for P to vanish at the origin and be even in its second argument, the Taylor coefficients have to fulfill

$$p_{0,0} = 0 \quad \text{and} \quad p_{i,2n+1} = 0\,. \tag{3.49}$$

The remaining coefficients are unknown and in Sec. 3.4.1.4 we will estimate the uncertainty of our result due to this ignorance by a Monte Carlo sampling.

3.3.3 Convergence of the interpolants

In this section, we discuss under which conditions our interpolants in Eqs. (3.45) and (3.46) converge to the true $\bar{\Pi}_1^{(a)}$ as $N \to \infty$. To this end, we assume that $\bar{\Pi}_1^{(a)}$ is known exactly in the region below the matching surface, i.e. for $\Sigma < \Sigma^{\text{match}}(r,\phi)$, and that $\bar{\Pi}_1^{(a)} \to \bar{\Pi}_1^{(a),\text{ asymp}}$ for asymptotic Σ.

The scalar function $\bar{\Pi}_1^{(a)}$ is free of kinematic singularities and analytic except for poles and branch cuts for configurations where the real part of at least one Q_i^2 is negative. For fixed (r,ϕ) with $0 \leq r < 1$ and $0 \leq \phi < 2\pi$, $\bar{\Pi}_1^{(a)}$ is an analytic function of Σ except for poles due to single-particle intermediate states and branch cuts due to multi-particle intermediate states for $\mathrm{Re}(\Sigma) < 0$. $\bar{\Pi}_1^{(a),\text{ asymp}}$ for fixed (r,ϕ) is also an analytic function except for isolated poles at $\Sigma \leq 0$ (see Eq. (3.40)). The ratio $\bar{\Pi}_1^{(a)}/\bar{\Pi}_1^{(a),\text{ asymp}}$ therefore has the same singularities as $\bar{\Pi}_1^{(a)}$ and has a pole at the zero of $\bar{\Pi}_1^{(a),\text{ asymp}}$, which we assume to be at $\Sigma^{\text{pole}} < \Sigma^{\text{match}}$. We can thus write the ratio as a Taylor series in Σ^{-1} at $(\Sigma^{\text{match}})^{-1}$,

$$\frac{\bar{\Pi}_1^{(a)}(\Sigma)}{\bar{\Pi}_1^{(a),\text{ asymp}}(\Sigma)} = \sum_{i=0}^{\infty} a_i \left(\frac{1}{\Sigma} - \frac{1}{\Sigma^{\text{match}}}\right)^i . \tag{3.50}$$

This series converges for $\Sigma^{-1} \in (2(\Sigma^{\text{match}})^{-1} - (\Sigma^{\text{pole}})^{-1}, (\Sigma^{\text{pole}})^{-1})$ or equivalently for $\Sigma \in (\Sigma^{\text{pole}}, \infty)$ if the relation $\Sigma^{\text{pole}} < \Sigma^{\text{match}}/2$ holds, which will be checked below. Since the ratio $\bar{\Pi}_1^{(a)}/\bar{\Pi}_1^{(a),\text{ asymp}}$ approaches 1 as $\Sigma \to \infty$, we also know that

$$\sum_{i=0}^{\infty} a_i \left(-\Sigma^{\text{match}}\right)^{-i} = 1\,. \tag{3.51}$$

We can thus write

$$\begin{aligned}\bar{\Pi}_1^{(a)}(\Sigma) &= \bar{\Pi}_1^{(a),\text{ asymp}}(\Sigma) \sum_{i=0}^{\infty} a_i \left(\frac{1}{\Sigma} - \frac{1}{\Sigma^{\text{match}}}\right)^i \\ &= \bar{\Pi}_1^{(a),\text{ asymp}}(\Sigma) \sum_{i=0}^{\infty} b_i \Sigma^{-i}\,, \end{aligned} \tag{3.52}$$

where the b_i are linear combinations of the a_i with coefficients depending on Σ^{match}. In particular, $b_0 = 1$ due to Eq. (3.51). Eq. (3.52) shows that $\bar{\Pi}_1^{(a),\text{ int 1}}$ converges to the true $\bar{\Pi}_1^{(a)}$ for $N \to \infty$ if $\Sigma^{\text{pole}} < \Sigma^{\text{match}}/2$ for all (r, ϕ) in the HLbL integration domain and $\Sigma > \Sigma^{\text{pole}}$. In the applications of our method, N is limited to rather low values since $\bar{\Pi}_1^{(a)}$ and its derivatives at the matching surface are determined only from the π^0, η, η'-poles (and additionally from the lightest axial in Sec. 3.4.4).

Let us now examine under which conditions the zero in $\bar{\Pi}_1^{(a),\text{ asymp}}$ occurs for $\Sigma^{\text{pole}} < \Sigma^{\text{match}}/2$. This relation is independent of the low-energy input but depends on the pseudoscalar mass in $\bar{\Pi}_1^{(a),\text{ asymp}}$ and especially the anomaly correction δ_0. For $P(x, y) = 0$ in Σ^{match} and $m^2 = 0.5\,\text{GeV}^2$, the zero in $\bar{\Pi}_1^{(a),\text{ asymp}}$ is at sufficiently low Σ for all flavor channels and all (r, ϕ). For $\bar{\Pi}_1^{(3),\text{ asymp}}$, m^2 can be reduced down to $0.0019\,\text{GeV}^2$ without violating the requirement $\Sigma^{\text{pole}} < \Sigma^{\text{match}}/2$, while for the iso-singlet cases there is no zero for positive Σ in $\bar{\Pi}_1^{(8/0)-\eta/\eta',\text{ asymp}}$ allowing all values for m. In all cases, this does not place a serious limitation on the values for m we will consider in the uncertainty estimation in Sec. 3.4.1.4. The effect of the polynomial $P(x, y)$ will also be discussed in Sec. 3.4.1.4, where we will find that also there the requirement is not restrictive.

Since $\bar{\Pi}_1^{(a),\text{ asymp}}$ for fixed (r, ϕ) in the integration domain has poles only for $\Sigma \leq 0$ and $\bar{\Pi}_1^{(a)}$ has no kinematic zero, also the ratio $\bar{\Pi}_1^{(a),\text{ asymp}}/\bar{\Pi}_1^{(a)}$ can be expanded in Σ^{-1} at positive $(\Sigma^{\text{match}})^{-1}$. The same line of arguments thus proves the convergence of interpolant 2 in Eq. (3.45) for $N \to \infty$ and the requirement $\Sigma^{\text{pole}} < \Sigma^{\text{match}}/2$ is trivially fulfilled due to $\Sigma^{\text{pole}} = 0$. The convergence of interpolant 3 given in Eq. (3.46) easily follows from that of interpolant 1 because the logarithmic term can be written as a Taylor series at finite $(\Sigma^{\text{match}})^{-1}$ so that the parameter b_1 in Eq. (3.46) is redundant as $N \to \infty$.

3.4 Numerical results and error analysis

In this section, we present the numerical results from the interpolants constructed in the previous sections for a_μ^{long}. We start in Sec. 3.4.1 with the isovector channel under the assumption that the low-energy region is well described by the pion pole alone. Special attention is paid to the estimation of the various sources of uncertainties. In Sec. 3.4.2, we apply the same procedure to the isoscalar channels with the η and η' poles at low energies, respectively. Since the holographic models reviewed in Sec. 3.1.4 predict a sizable contribution from the lightest axial multiplet in the low-energy region, in Sec. 3.4.4 we present an analysis including the holographic isoscalar $a_1(1260)$ contribution together with the pion pole in the isovector channel. Despite the model-dependence inherent to the definition of such a state in the dispersive formalism as mentioned in Sec. 2.4.3, this shows that input from further states can easily be included in our formalism.

We define the contribution to $a_\mu^{(a)}$ due to the SDCs as the difference

$$\Delta a_\mu^{(a)} = a_\mu^{(a)} - a_\mu^{\text{le-input}}\,, \tag{3.53}$$

where $a_\mu^{\text{le-input}}$ is the result from using the low-energy input state(s) in the master formula. For a_μ^{HLbL}, ultimately the sum $a_\mu^{(a)} = a_\mu^{\text{le-input}} + \Delta a_\mu^{(a)}$ is relevant and should agree between different determinations. This implies that any comparison of results for $\Delta a_\mu^{(a)}$ only makes sense if the low-energy input and thus $a_\mu^{\text{le-input}}$ is the same. Including more and more states in the low-energy input, which less and less contribute below the matching surface, increases $a_\mu^{\text{le-input}}$ and decreases $a_\mu^{(a)}$ in such a way that the sum $a_\mu^{(a)} = a_\mu^{\text{le-input}} + \Delta a_\mu^{(a)}$ converges.

3.4.1 The isovector channel

The isovector channel is characterized by a large contribution from the pion pole constituting the largest individual piece to a_μ^{HLbL}. Due to the small pion mass compared to other hadronic scales, its main effect is on the low-energy region of $\bar{\Pi}_1^{(3)}$. It is under excellent control both theoretically as well as numerically as we have reviewed in Sec. 2.4.3. The high-energy behavior of this contribution is controlled by the asymptotic behavior of the TFFs calculable from QCD directly and it can thus neither saturate the asymmetric nor the symmetric SDC on $\bar{\Pi}_1^{(3)}$.

The lightest one-particle intermediate state beyond the π^0 in this channel is the $a_1(1260)$, whose effect at low energies is suppressed by the large mass gap. While it still has a non-negligible influence on $\bar{\Pi}_1^{(3)}$ in the holographic models of Ref. [41, 42], this contribution is not well-known and will be assumed to be sufficiently suppressed in the low-energy region to be dropped there (see Sec. 3.4.4 for an analysis including model information on this state). The same will be assumed for tensor mesons, whereas the pion loop and other non-resonant two-pion contributions are sub-leading in large-N_c and can thus be ignored in an analysis of the saturation of SDCs, which are leading in large-N_c themselves.

The numerical dominance of the isovector channel at low energies due to the pion pole does not imply that the same holds true at intermediate and high energies. In fact, the values of C_a in Eq. (3.6) make the flavor singlet channel the numerically most important one in the asymptotic region where meson masses can be neglected, i.e. for $Q_i^2 \gg \Lambda_{\text{QCD}}^2$.

The starting point for our numerical analysis is a "reference" set of assumptions and input parameters. From these we will calculate a reference result and the impact of modifications to the assumptions and parameters will be assessed by modifying them one by one in the next sections. In this way, we will obtain a number of individual uncertainties, which will be combined in Sec. 3.4.1.5 to define our final result. This procedure allows us also to examine how the estimate of the effects of SDCs would be improved by more precise information on the pion pole, the contributions from states with masses around 1–2 GeV and the asymptotic regime, which each would reduce a subset of the individual uncertainties.

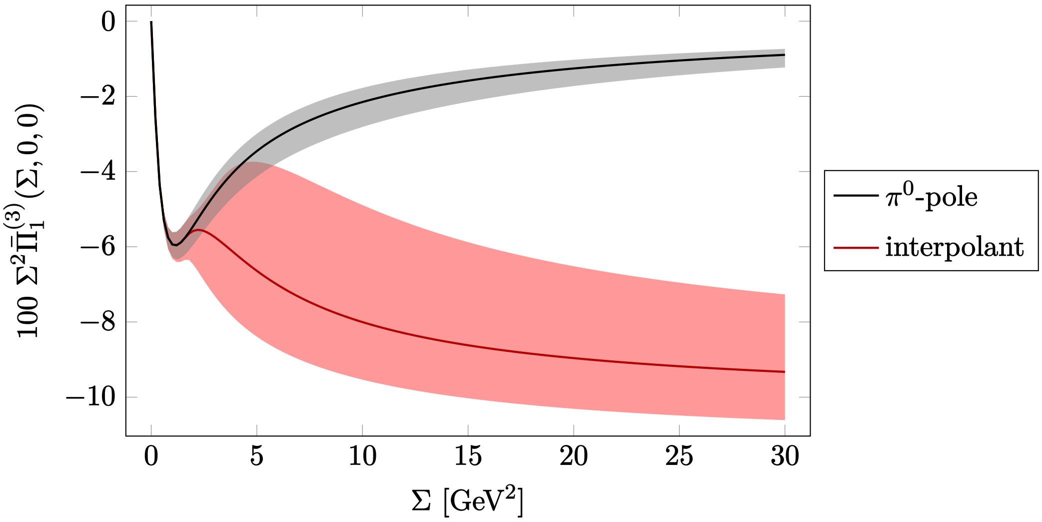

Figure 3.4: The pion pole contribution and associated uncertainty from Refs. [18, 50] vs. the reference interpolant and its error band which includes all sources of uncertainty considered in the present analysis (see discussion in Secs. 3.4.1.1–3.4.1.4 below).

As low-energy reference input, we took the dispersive π^0 singly- and doubly-virtual TFFs [18, 50]. As reference interpolating function, we used $\bar{\Pi}_1^{(3),\text{ int }1}$ with $N = 3$ (see Eq. (3.45)), which turned out to yield results that are central in the range spanned by the interpolants 1, 2 and 3 and $N \in \{2, 3\}$ (cf. Eqs. (3.62) below). The asymptotic function is given in Eq. (3.40) with the parameters from the fit to the pQCD quark loop result given in Eq.(3.43). α_s corrections to the SDCs will be included in the uncertainty together with the perturbative corrections to the dispersive pion TFF. For the matching surface, we used Eq. (3.47) with $P(x, y) = 0$ and $m^2_{\text{ref}} = 0.5\,\text{GeV}^2$. The resulting function, which we call $\bar{\Pi}_1^{(3),\text{ ref}}$, is shown in Fig. 3.4 for $r = 0$ together with the uncertainty band for the interpolants that we are going to discuss in the next sections. One can see there that at low energies the interpolant is given by the pion pole contribution including the error band. At higher energies, the interpolant leaves the pion pole and converges to the asymptotic expression. The uncertainty band opens there and covers many different forms of $\bar{\Pi}_1^{(3)}$ reflecting the poor knowledge in the intermediate energy region.

Our reference outcome for the contribution to a_μ^{long} due to the longitudinal SDCs in the isovector channel is

$$\Delta a_\mu^{(3),\text{ ref}} = a_\mu^{(3),\text{ ref}} - a_{\mu,\text{disp}}^{\pi^0\text{-pole}} = 2.56 \times 10^{-11}\,, \tag{3.54}$$

where $a_\mu^{(3),\text{ ref}}$ comes from using $\bar{\Pi}_1^{(3),\text{ ref}}$ in the master formula Eq. (3.37), and $a_{\mu,\text{disp}}^{\pi^0\text{-pole}}$ is given in Eq. (2.64) according to Refs. [18, 50]. In Sec. 3.4.1.5 we will argue that our final result does not strongly depend on the choice of the reference set of parameters.

3.4.1.1 Pion TFF uncertainties

We start our discussion of the uncertainties that we attach to the reference result Eq. (3.54) with those of the pion TFF. In Refs. [18, 50], the uncertainty of the pion-pole contribution receives four contributions: one related to the normalization in the real-photon limit, which is taken from the PrimEx experiment [154], one to the dispersive formalism and the fits and one each to the singly- and doubly-virtual asymptotic behaviors. The individual uncertainties are then added in quadrature to obtain the result quoted in Eq. (2.64). The space-like TFF is available as a table of points (Q_1^2, Q_2^2) with the central values and the individual uncertainties for each point.

To propagate the errors of the pion TFF to our result, we calculated $\Delta a_\mu^{(3),\text{ ref}}$ using the boundary values of the error bands for the individual error sources in the pion TFF in the low-energy input to $a_\mu^{(3)}$ and $a_{\mu,\text{disp}}^{\pi^0\text{-pole}}$. Then we added the individual uncertainties in quadrature, both for the upward and the downward errors. We obtained

$$\delta_{\text{TFF}}^{+}\Delta a_\mu^{(3)} = 0.06\times 10^{-11}\,, \qquad \delta_{\text{TFF}}^{-}\Delta a_\mu^{(3)} = 0.13\times 10^{-11} \tag{3.55}$$

for the uncertainties in the two directions, which correspond to the asymmetric error of the dispersive π^0 TFF. Both values are dominated by the error in the asymmetric asymptotic limit of the π^0 TFF, which covers a large range due to the conflicting high-energy data from the BaBar and Belle experiments [155, 156]. Given the smallness of $\delta_{\text{TFF}}^{\pm}\Delta a_\mu^{(3)}$, the (negative) correlation between them and the uncertainties of $a_{\mu,\text{disp}}^{\pi^0\text{-pole}}$ can be safely neglected when calculating $a_\mu^{(3)} = a_\mu^{\pi^0\text{-pole}} + \Delta a_\mu^{(3)}$.

In order to study the impact of different pion TFF parameterizations, we compared the previous results against the ones obtained using, both for the construction of the interpolant and the evaluation of $a_\mu^{\pi^0\text{-pole}}$, the C_2^1 Canterbury approximant with $a_{\pi;1,1} = 2b_\pi^2$ of Ref. [16] and the TFF calculated from DSEs [122]. We obtained

$$\Delta a_\mu^{(3),\text{ Can}} = 2.60\times 10^{-11} \quad\text{and}\quad \Delta a_\mu^{(3),\text{ DSE}} = 2.52\times 10^{-11}\,, \tag{3.56}$$

which are both compatible with the reference result within the range given above. We conclude that the outcome of our analysis is very robust against changes in the TFF input and that the present knowledge of the pion TFF is sufficient for our purposes.

3.4.1.2 Asymptotic uncertainties

Here, we consider the uncertainties in $\bar{\Pi}_1^{(3),\text{ asymp}}$ (see Eq. (3.40)), which are related to

- the choices made in the fit to the quark-loop result that lead to Eq. (3.43), namely the degree M of the polynomial and the radius $r_{\max}$ of the fitting domain;
- α_s corrections to the OPE constraint as given by Eq. (3.26);

- α_s corrections to the quark loop.

We start by discussing the fit to the quark-loop result. In Sec. 3.2, we chose $M=2$, which reduces the χ^2 in Eq. (3.42) by roughly a factor of 40 compared to $M=1$. Considering a larger value of M gives an estimate of the errors made by approximating the pQCD result by a polynomial at $r<r_{\text{max}}$ at fixed asymptotic Σ and by extrapolating to the regime $r>r_{\text{max}}$, which is unknown except for the OPE constraints. Choosing $M=3$ shifts the result for $\Delta a_\mu^{(3)}$ by only 0.02×10^{-11} indicating that the truncation at $M=2$ is sufficient. We also studied the effects of a substantial reduction of the radius, namely from $r_{\text{max}}=0.9$ down to $r_{\text{max}}=0.5$, where no logarithm of ratios of squared momenta is larger than 1. We found that this leads to a small shift (0.07×10^{-11}). We did not consider $r_{\text{max}}>0.9$ since fixed-order pQCD is not expected to converge for r close to 1 due to large logarithms. Combining linearly the shifts due to an increase of M and a reduction of r_{max} leads to

$$\delta_{\text{pQCD fit}}\Delta a_\mu^{(3)} = 0.09\times 10^{-11}\,, \tag{3.57}$$

which we will use as the (symmetric) uncertainty due to the quark-loop fit with respect to the reference contribution of longitudinal SDCs to the pion pole input in Eq. (3.54).

Next, we turn to the estimate of the separate perturbative corrections to either the OPE or the pQCD result. To obtain meaningful uncertainties, it is crucial to apply the corrections only in their respective regions of validity and not to extrapolate the corrections out of that region in an uncontrolled way. Therefore, for asymptotic Σ we write (cf. Eq. (3.26))

$$\bar{\Pi}_1^{(3),\,\text{asymp},\,\delta\text{OPE}} = \bar{\Pi}_1^{(3),\,\text{asymp}}\left[1-\frac{\alpha_s(\mu^2=Q_1^2+Q_2^2)}{\pi}\,\theta\!\left(A-\frac{Q_3^2}{Q_1^2+Q_2^2}\right)\right] \tag{3.58}$$

with the leading-order function $\bar{\Pi}_1^{(3),\,\text{asymp}}$ given in Eq. (3.40). Here, the Heaviside step function θ ensures that the perturbative correction only affects a region around $Q_3^2=0$, whose size can be varied via the free parameter A. By setting $A=1/29$, this region does not extend into the $r<0.9$ domain. The choice of the renormalization scale μ^2 is the same as in Ref. [18]. In our numerical analysis, for the running of α_s we used the three-flavor one-loop beta function and matched to $\alpha_s(\mu^2=M_\tau^2)=0.35$ since energies much larger than $M_\tau=1.777\,\text{GeV}$ are irrelevant numerically for a_μ^{HLbL}.

According to the discussion in Sec. 3.1.1, the OPE constraint in the chiral limit is saturated by the pion pole at $Q_3^2=0$ to all orders in perturbation theory. For this reason in a consistent analysis the OPE coefficient and the pion TFF in the symmetric limit should be taken at the same perturbative accuracy. Hence we replaced in Eq. (3.45) $\bar{\Pi}_1^{(3),\,\text{asymp}}$ by $\bar{\Pi}_1^{(3),\,\text{asymp},\,\delta\text{OPE}}$ and matched the correspondingly modified $\bar{\Pi}_1^{(3),\,\text{int 1}}$ to the pion-pole contribution with TFFs including $\mathcal{O}(\alpha_s)$ effects [18,144].[10] Using this interpolant and this pion-pole result, our outcome

[10]We thank Bai-Long Hoid for kindly providing us with a numerical representation of the dispersive pion TFF with $\mathcal{O}(\alpha_s)$ corrections.

for $\Delta a_\mu^{(3)}$ is larger than the reference result Eq. (3.54) by

$$\delta^{+}_{\text{NLO OPE}}\Delta a_\mu^{(3)} = 0.01 \times 10^{-11}\,. \tag{3.59}$$

For $A = 1/3$, the domain where the correction applies extends down to $r = 0.25$, but nevertheless the shift of $\Delta a_\mu^{(3)}$ turns out to be -0.05×10^{-11} and thus still negligible. The smallness of these shifts can be understood from the large values of Σ^{match} in the region where these perturbative corrections apply. For this reason, the effect is almost completely included in the pion pole contribution, where its impact is also small [18].

The NLO calculation of the quark loop in Ref. [48] shows that also in the symmetric regime the correction is close to an overall factor $-\alpha_s/\pi$ for all r and ϕ. Thus, instead of using the result of the full two-loop calculation, we approximate it by

$$\bar{\Pi}_1^{(3),\text{ asymp, }\delta\text{pQCD}} = \bar{\Pi}_1^{(3),\text{ asymp}}\left(1 - \frac{\alpha_s(\mu^2 = \Sigma)}{\pi}\theta\left(r_{\max} - r\right)\right)\,, \tag{3.60}$$

and as in the leading-order quark loop fit, we set $r_{\max} = 0.9$. Using this expression in Eq. (3.45) for the matching to the pion pole with leading-order dispersive TFF, we obtained a shift of -0.18×10^{-11} compared to the reference result. Even when inflating this uncertainty by a factor of 2 to account for different values of $r_{\max}$, scale-variations and the error due to using an approximation for the two-loop result,

$$\delta^{-}_{\text{NLO pQCD}}\Delta a_\mu^{(3)} = 0.36 \times 10^{-11} \tag{3.61}$$

this effect is still sufficiently small compared to the current precision goal. Notice that as opposed to our prescription in Ref. [45], we now use an uncertainty only in the negative direction since the α_s-correction in Ref. [48] is clearly negative. In principle with the NLO result available, it would be preferable to directly interpolate between the NLO expressions for the OPE and the quark loop. The discontinuous functions employed here only serve to provide a rough estimate of NLO effects, which given their smallness appears sufficient.

3.4.1.3 Choice of interpolation functions

In Eqs. (3.45) and (3.46), we introduced three different interpolation functions, characterized by two or three free parameters to be matched to the low-energy representation. The corresponding results for the contribution from longitudinal SCDs are

$$\begin{aligned}
\Delta a_\mu^{(3),\text{ int 1, }N=2} &= 3.18 \times 10^{-11}\,, & \Delta a_\mu^{(3),\text{ int 1, }N=3} &= 2.56 \times 10^{-11}\,,\\
\Delta a_\mu^{(3),\text{ int 2, }N=2} &= 2.75 \times 10^{-11}\,, & \Delta a_\mu^{(3),\text{ int 2, }N=3} &= 2.16 \times 10^{-11}\,,\\
\Delta a_\mu^{(3),\text{ int 3, }N=2} &= 2.69 \times 10^{-11}\,, & \Delta a_\mu^{(3),\text{ int 3, }N=3} &= 1.94 \times 10^{-11}\,,
\end{aligned} \tag{3.62}$$

where $\Delta a_\mu^{(3),\text{ int 1, }N=3} = \Delta a_\mu^{(3),\text{ ref}}$ given by Eq. (3.54) has been included for completeness.

We observe that the slower logarithmic approach to the asymptotic limits in interpolant 3 leads to smaller results, especially when compared to the similar interpolant 1. Setting

$$\delta_{\text{int}}\Delta a_\mu^{(3)} = 0.62 \times 10^{-11}\,, \tag{3.63}$$

all values listed above are within the range $\Delta a_\mu^{(3),\,\text{ref}} \pm \delta_{\text{int}}\Delta a_\mu^{(3)}$.

3.4.1.4 Choice of $\Sigma^{\text{match}}(r,\phi)$

The function $\Sigma^{\text{match}}(r,\phi)$ in Eq. (3.47) contains the mass parameter m and the polynomial $P(x,y)$, which has been set equal to zero so far. We have argued in Sec. 3.3.2 that m should be chosen considerably smaller than the mass M of the lightest resonances contributing to $\bar{\Pi}_1$ in addition to the ground-state pseudoscalar mesons. For this reason, for the reference interpolant we set $m^2 = 0.5\,\text{GeV}^2$. Here we discuss the effects of alternative choices for this parameter within a range between m_{min} and m_{max}.

Since according to Sec. 3.3.2 a conservative choice for the upper end of the range is $m_{\text{max}} \simeq M$, we set $m^2_{\text{max}} = 1\,\text{GeV}^2$. In order to determine an appropriate value for m_{min}, one has to estimate isovector contributions beyond the π^0-pole. Following our argument in Sec. 3.3.2, it is sufficient to restrict ourselves to single-particle intermediate states and focus on the one giving the largest effect at energies around m. We assumed this to be given by the pseudoscalar $\pi(1300)$ for the following reasons. Models for tensor mesons around 1 GeV give similar or smaller contributions to a_μ^{HLbL} [52,53,157]. For ground-state axials, recent studies based on different approximations and hadronic models yield quite different numerical results, see e.g. Refs. [41–44,52,54], leading to large uncertainties. If future model-independent analyses show that axial-meson exchanges are responsible for significant effects in $\bar{\Pi}_1^{(3)}$ also at relatively small momenta, then these contributions should be added to the pion pole before the matching is performed since our procedure relies on a sufficiently precise knowledge of $\bar{\Pi}_1^{(3)}$ below $\Sigma^{\text{match}}(r,\phi)$. Neglecting issues related to model dependence, in Sec. 3.4.4 we will discuss the inclusion in our procedure of information from hQCD on the lightest axial meson.

As for the light pseudoscalars, the interaction of $\pi(1300)$ with two photons can be described by a TFF, which determines the contribution to $\bar{\Pi}_1$ as in Eq. (2.63). As input for the $\pi(1300)$ TFF we resorted to Resonance Chiral Theory (RχT). RχT is an extension of Chiral Perturbation Theory (χPT) including one multiplet each of scalar, pseudoscalar, vector and axial-vector resonances with parameters typically fixed from SDCs [158]. The $\pi(1300)$ TFF belongs to the odd-intrinsic parity sector, which has first been considered in Ref. [159] and it has been calculated to read

$$F_{\pi(1300)\gamma^*\gamma^*}(q_1^2,q_2^2) = \frac{8\sqrt{2}}{3}F_V\frac{\sqrt{2}\kappa_3^{PV}(2M_V^2-q_1^2-q_2^2) - F_V\kappa^{VVP}}{(q_1^2-M_V^2)(q_2^2-M_V^2)}\,. \tag{3.64}$$

Here, we used $F_V = F_\rho = 146.3\,\text{MeV}$ for the vector-meson decay constant and $M_V = M_\rho = 775\,\text{MeV}$ for its mass. The parameter κ_3^{PV} also appears in the π^0 TFF and can be fixed by

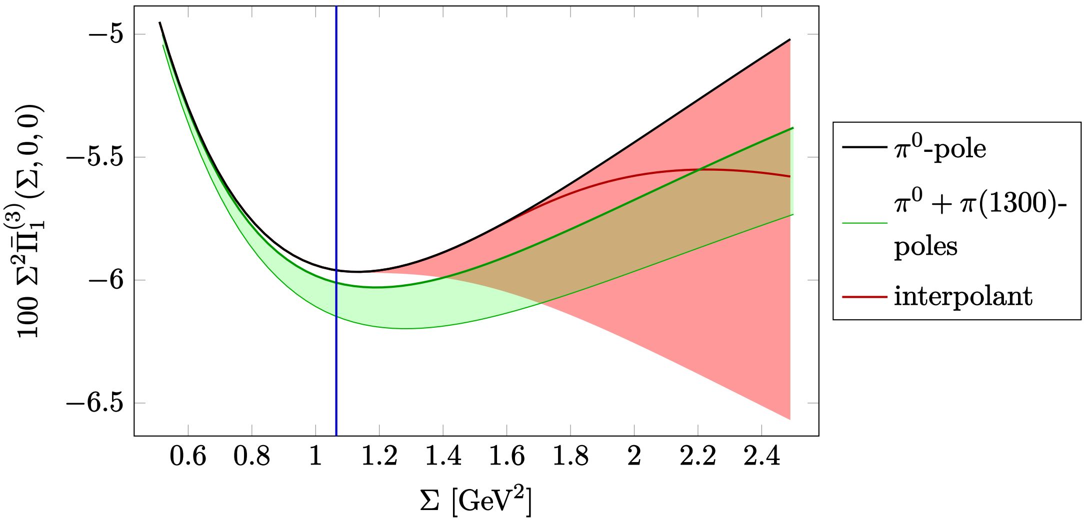

Figure 3.5: The dispersive pion pole contribution and the reference interpolant with error band corresponding to the various choices of the parameter m. The blue line indicates the value of the matching surface for $m^2 = m^2_{\text{min}}$. The green band shows the sum of the π^0- and $\pi(1300)$-pole contributions, where the latter has been calculated using input from RχT and phenomenology, including errors.

imposing the Brodsky–Lepage condition $F_{\pi^0\gamma^*\gamma^*}(-Q^2,0) = 2F_\pi/Q^2 + \mathcal{O}(Q^{-4})$ on it to be $\kappa_3^{PV} = -0.056$. Having fixed everything except κ^{VVP}, we can impose the two-real-photon limit of the excited pion TFF to be in the range $F_{\pi(1300)\gamma^*\gamma^*}(0,0) \in [0, 0.0544]\text{GeV}^{-1}$, argued for in Ref. [21] based on experimental results [160, 161].

Our procedure to determine m_{min} can be illustrated by means of Fig. 3.5. Given a value of m_{min}, at large enough Σ, the range of interpolants (orange band) spanned by $m \in [m_{\text{min}}, m_{\text{max}}]$ safely includes the green band representing the sum of the contributions from π^0 and $\pi(1300)$, including errors on the latter due to the range for $F_{\pi(1300)\gamma^*\gamma^*}(0,0)$. Since this is not the case at small Σ, the contribution to a_μ^{long} from this region is underestimated in our approach. To gauge this effect, we calculated the integral in Eq. (3.37) with

$$\bar{\Pi}_1 = \bar{\Pi}_1^{\pi^0\text{-pole}} + \bar{\Pi}_1^{\pi(1300)\text{-pole}} - \bar{\Pi}_1^{(3),\text{ int}}(m = m_{\text{min}}) \tag{3.65}$$

using the maximal $\pi(1300)$ contribution, i.e. $F_{\pi(1300)\gamma^*\gamma^*}(0,0) = 0.0544\,\text{GeV}^{-1}$, and restricting the Σ-domain to the region below the point where the bands start to fully overlap (as a function of r and ϕ). This integral gives the missed contribution $a_\mu^{(3),\text{ missed}}$ at a fixed m_{min}. Repeating this calculation for different values of m_{min} yields the function $a_\mu^{(3),\text{ missed}}(m_{\text{min}})$ and by inverting this, we determined m_{min} by fixing $a_\mu^{(3),\text{ missed}}$ to values well below the accuracy goal set by forthcoming experimental results. For $a_\mu^{(3),\text{ missed}} = 0.5\times 10^{-11}$, we obtained $m^2_{\text{min},\,1} = 0.35\,\text{GeV}^2$ and for $a_\mu^{(3),\text{ missed}} = 0.2\times 10^{-11}$, $m^2_{\text{min},\,2} = 0.13\,\text{GeV}^2$.

Numerically, $m_{\max} = 1\,\text{GeV}$ leads to the shift $\delta_m^- \Delta a_\mu^{(3)} = 1.20 \times 10^{-11}$ and the two values $m_{\text{min, 1}}$ and $m_{\text{min, 2}}$ yield $\delta_{m,1}^{+\prime} \Delta a_\mu^{(3)} = 0.81 \times 10^{-11}$ and $\delta_{m,2}^{+\prime} \Delta a_\mu^{(3)} = 3.66 \times 10^{-11}$, respectively. If we add $a_\mu^{(3),\text{ missed}}(m_{\text{min},1/2})$ to the latter numbers, we obtain the conservative estimates

$$\delta_m^- \Delta a_\mu^{(3)} = 1.20 \times 10^{-11}\,, \quad \delta_{m,1}^{+} \Delta a_\mu^{(3)} = 1.31 \times 10^{-11}\,, \quad \delta_{m,2}^{+} \Delta a_\mu^{(3)} = 3.86 \times 10^{-11}\,. \tag{3.66}$$

In the following, we will use $\delta_{m,1}^{+} \Delta a_\mu^{(3)}$ for the main results and keep $\delta_{m,2}^{+} \Delta a_\mu^{(3)}$ as an alternative, even more conservative uncertainty.

We also considered a different parameterization for the $\pi(1300)$ TFF, namely the one given by the Regge model in Refs. [21,40]. Using the empirical $m_{\pi(1300)} = 1.30\,\text{GeV}$ instead of the Regge-model value of 1.36 GeV used in these references and following the same procedure discussed above, we obtained $m^2_{\text{min, 1}} = 0.53\,\text{GeV}^2$ and $m^2_{\text{min, 2}} = 0.20\,\text{GeV}^2$. This leads to[11]

$$\delta_{m,1}^{+} \Delta a_\mu^{(3)} = 0.36 \times 10^{-11}\,, \qquad \delta_{m,2}^{+} \Delta a_\mu^{(3)} = 2.63 \times 10^{-11}\,, \tag{3.67}$$

where we again added a_μ^{missed} to the uncertainties in the upward direction. For our final result we use the more conservative uncertainty estimates given in Eq. (3.66).

Next, we studied the effects of the polynomial P in $\Sigma^{\text{match}}(r,\phi)$. In Eq. (3.48), this was written as a polynomial with the coefficients $p_{i,j}$. These are unknown, but since they are dimensionless, they should be of $\mathcal{O}(1)$. We therefore set $M = 2$ and sampled the five coefficients not constrained by Eq. (3.49) according to standard normal distributions. Since the pion pole gives an excellent approximation of $\bar{\Pi}_1$ for very small Σ at any (r,ϕ), we only allowed for parameter sets giving $\Sigma^{\text{match}}(r,\phi) > \Sigma_t$ for all (r,ϕ), where Σ_t is defined as the smallest value of Σ such that

$$\frac{\bar{\Pi}_1^{\pi(1300)\text{-pole}}(\Sigma,r,\phi)}{\bar{\Pi}_1^{\pi^0\text{-pole}}(\Sigma,r,\phi)} = 0.02 \tag{3.68}$$

holds for some (r,ϕ). With $\bar{\Pi}_1^{\pi(1300)\text{-pole}}$ calculated using RχT, we obtained $\Sigma_t = 0.57\,\text{GeV}^2$. This condition ensures that there are no large contributions from our interpolation at points where RχT predicts a very small excited pion contribution. We have also checked that in the Monte Carlo sampling of the polynomial $P(x,y)$, the requirement $\Sigma^{\text{pole}} < \Sigma^{\text{match}}/2$ needed for the convergence of the interpolant as derived in Sec. 3.3.3 does not lead to a further constraint beyond $\Sigma^{\text{match}}(r,\phi) > \Sigma_t$.

From 10 200 sets of coefficients, we obtained the distribution of results for $\Delta a_\mu^{(3)}$ shown in Fig. 3.6. It is characterized by a peak slightly shifted to smaller values compared to the reference result and asymmetric tails. To quantify the uncertainty related to the polynomial P, we read off the 16 % quantiles from both sides, which would correspond to 1σ errors for a Gaussian distribution, and subtract the reference result. This gives

$$\delta_{P(x,y)}^{+} \Delta a_\mu^{(3)} = 0.39 \times 10^{-11}\,, \qquad \delta_{P(x,y)}^{-} \Delta a_\mu^{(3)} = 0.32 \times 10^{-11}\,. \tag{3.69}$$

[11] Notice that in this case $m_{\text{min, 1}} > m_{\text{ref}}$ and thus $\delta_{m,1}^{+\prime} \Delta a_\mu^{(3)} < 0$.

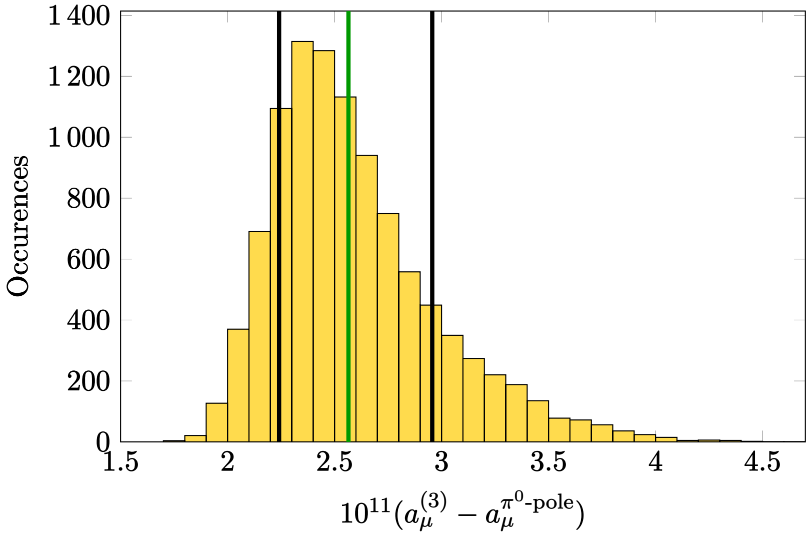

Figure 3.6: Histogram of the shifts of $a_\mu^{(3)}$ due to longitudinal short-distance constraints in the isovector channel for a sample of 10 200 sets of parameters in the polynomial $P(x,y)$ in Σ^{match}. The green line indicates the result for $P(x,y) = 0$, i.e. the reference result, and the black lines indicate the boundaries of the error range.

As these results originated from a probabilistic procedure, repeating the calculation would lead to a different result. To quantify these statistical uncertainties without having to repeat this computationally costly calculation several times, we resorted to the bootstrap method [162]. This means that we sampled 10 200 numbers from the 10 200 entries of the histogram, where the same entry can be drawn multiple times. From this new sample we again calculated the quantiles. Repeating this many times produces a distribution, the standard deviation of which estimates the statistical uncertainty of the quantiles. We obtained 0.003×10^{-11} and 0.008×10^{-11} for the statistical uncertainties of the two quantiles and consequently conclude that the numbers in Eq. (3.69) would not considerably change if the calculation were repeated. In addition, we performed computations with $M = 3$ and moderate changes in the value of the ratio in Eq. (3.68) and found that the results are stable against such variations.

3.4.1.5 Estimate of the effects of longitudinal SDCs in the isovector channel

The π^0-column of Tab. 3.1 collects all uncertainties in our estimate of the effects of longitudinal SDCs in the isovector channel as described in the previous subsections. By combining them in quadrature, we get

$$\delta^+_{\text{tot}}\Delta a_\mu^{(3)} = 1.50 \times 10^{-11}\,, \qquad \delta^-_{\text{tot}}\Delta a_\mu^{(3)} = 1.44 \times 10^{-11}\,. \tag{3.70}$$

	π^0	η	η'
$\Delta a_{\mu,\text{ref}} \times 10^{11}$	2.56	2.58	3.91
$\delta_{\text{TFF}} \Delta a_\mu \times 10^{11}$	${}^{+0.06}_{-0.13}$	0.47	0.30
$\delta_{\text{pQCD fit}} \Delta a_\mu \times 10^{11}$	0.09	0.08	0.14
$\delta_{\text{NLO OPE}} \Delta a_\mu \times 10^{11}$	${}^{+0.01}_{-0.00}$	${}^{+0.01}_{-0.00}$	${}^{+0.02}_{-0.00}$
$\delta_{\text{NLO pQCD}} \Delta a_\mu \times 10^{11}$	${}^{+0.00}_{-0.36}$	${}^{+0.00}_{-0.36}$	${}^{+0.00}_{-0.55}$
$\delta_{\text{int}} \Delta a_\mu \times 10^{11}$	0.62	${}^{+0.61}_{-0.65}$	${}^{+0.74}_{-0.84}$
$\delta_{m,1} \Delta a_\mu \times 10^{11}$	${}^{+1.31}_{-1.20}$	${}^{+1.27}_{-1.17}$	${}^{+1.68}_{-1.60}$
$\delta_{P(x,y)} \Delta a_\mu \times 10^{11}$	${}^{+0.39}_{-0.32}$	${}^{+0.31}_{-0.33}$	${}^{+0.32}_{-0.43}$
$\delta_{\text{tot}} \Delta a_\mu \times 10^{11}$	${}^{+1.50}_{-1.44}$	${}^{+1.52}_{-1.50}$	${}^{+1.90}_{-1.97}$
$\Delta a_\mu \times 10^{11}$	2.6 ± 1.5	2.6 ± 1.5	3.9 ± 1.9

Table 3.1: The effects on a_μ^{HLbL} of longitudinal SDCs assuming that the low-energy region is dominated by ground-state pseudoscalar poles, whose contributions are taken as input. In each flavor channel, the results are presented as the shifts $\Delta a_{\mu,\text{ref}}$ with respect to the pole contributions for a specific reference set of parameters and a list of uncertainties corresponding to different choices for each of these parameters. In the last two rows, these uncertainties are added in quadrature and the final range is symmetrized. See main text for details.

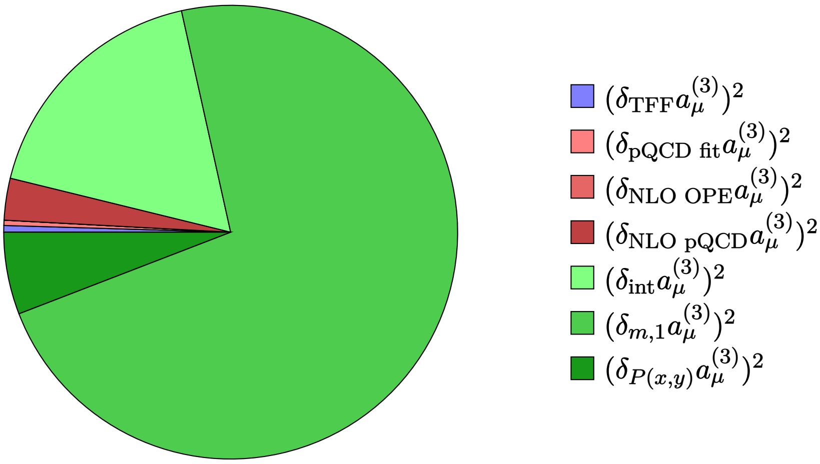

Figure 3.7: Relative contributions to the total uncertainty in the isovector channel. For asymmetric errors the mean of the squared errors is used.

Since we do not regard the reference parameterization as the central value, we symmetrized the uncertainty to finally obtain the range

$$\Delta a_\mu^{(3)} = (2.6 \pm 1.5) \times 10^{-11} \,. \tag{3.71}$$

Using instead $\delta^+_{m,2} \Delta a_\mu^{(3)}$ in Eq. (3.66), the final result would be $(3.8 \pm 2.7) \times 10^{-11}$. Notice that, despite the fact that it likely overestimates the range of longitudinal short-distance effects, this interval is still definitely compatible with the current precision goal.

Fig. 3.7 shows the contributions to the quadratic error from the different sources discussed above. The different shades of green therein correspond to uncertainties related to the interpolation between low and high energies, which dominate the total uncertainty. An especially crucial role is played by the choice of m, the scale at which the matching between the low-energy representation of $\bar{\Pi}_1$ and the interpolant is performed. The uncertainties δ_{int}, δ_m and $\delta_{P(x,y)}$ could be reduced by additional low-energy input concerning further intermediate states and higher-order terms in the symmetric and asymmetric OPEs, see Refs. [20, 47, 49], which would help constrain the coefficients $b_i(r, \phi)$ in the interpolants in Eqs. (3.45) and(3.46). The uncertainties related to the asymptotic behavior of $\bar{\Pi}_1^{(3)}$ are shown in red and only give a small contribution to the total uncertainty showing that fully including NLO effects in the interpolation will not considerably reduce the uncertainty. Nevertheless, the calculation in Ref. [48] was important to exclude the possibility of large perturbative corrections. The uncertainty related to the pion TFF input is shown in blue and completely negligible for the total uncertainty.

We have also checked that our results are robust against the choice of different reference sets of parameters. For example, if we set m_{ref} equal to the previous boundary values for the uncertainty in the reference configuration, namely $m^2_{\text{ref}} = 0.35\,\text{GeV}^2$ and $m^2_{\text{ref}} = 1\,\text{GeV}^2$ and choose $m^2 \in [0.35, 1]\mathrm{GeV}^2$ as the range for the error estimation as before, we get

$$\Delta a_\mu^{(3),\ m^2_{\mathrm{ref}}=0.35\,\mathrm{GeV}^2} = (2.8 \pm 1.6) \times 10^{-11}\,, \quad \Delta a_\mu^{(3),\ m^2_{\mathrm{ref}}=1.00\,\mathrm{GeV}^2} = (2.4 \pm 1.5) \times 10^{-11}\,, \tag{3.72}$$

where all other sources of uncertainty are included as before, but varying the parameters with respect to the new reference set. We obtained similar results by selecting as reference different interpolants or different values of the number of free parameters N contained therein. The symmetrization of the uncertainty is crucial to arrive at that conclusion as otherwise the central value would shift considerably.

3.4.2 The isoscalar contributions

In this section, the procedure presented above for the isovector case is applied to the isoscalar channels with η/η'-poles as low-energy input. In our analysis, we employed the Canterbury TFFs from Ref. [16] in the reference interpolant.[12] We determined the parameters encoding $\eta-\eta'$-mixing as explained in Secs. 3.1.1 and 3.1.3 and obtained

$$C_\eta = 0.164\,, \qquad C_{\eta'} = 0.219\,, \qquad \delta_0 = 0.110\,, \tag{3.73}$$

which shows that δ_0 is indeed sizable.

Following the same procedure for the construction of the reference interpolant as in Sec. 3.4.1, we found

$$\Delta a^\eta_{\mu,\mathrm{ref}} = 2.58 \times 10^{-11}\,, \qquad \Delta a^{\eta'}_{\mu,\mathrm{ref}} = 3.91 \times 10^{-11}\,. \tag{3.74}$$

The uncertainty estimation proceeds in the same way as in the isovector channel up to minor modifications. Since error bands for the doubly-virtual TFFs in all kinematic configurations are not available in the literature, we estimated uncertainties by considering another TFF representation, namely the one based on DSE [122]. This yields $\Delta a^\eta_{\mu,\mathrm{ref}} = 2.11 \times 10^{-11}$ and $\Delta a^{\eta'}_{\mu,\mathrm{ref}} = 4.20 \times 10^{-11}$. The fact that individual results for η and η' channels differ by 18 and 8 %, but the sum only by 3 % can be understood by comparing the mixing parameters

$$C^{\mathrm{DSE}}_\eta = 0.148\,, \qquad C^{\mathrm{DSE}}_{\eta'} = 0.228\,, \qquad \delta^{\mathrm{DSE}}_0 = 0.127\,, \tag{3.75}$$

against those obtained from the Canterbury parameterization. These coefficients enter the asymptotic functions $\bar{\Pi}_1^{(8/0)-\eta/\eta',\ \mathrm{asymp}}$ quadratically, which leads to a reshuffling between $a_\mu^{(8/0)-\eta}$ and $a_\mu^{(8/0)-\eta'}$. Due to Eq. (3.20), this effect drops out in the sum up to the anomaly correction affecting the OPE regime. As TFF contribution to the uncertainty on $\Delta a_\mu^{(8/0)-\eta/\eta'}$ we took the absolute value of the differences between the results from the Canterbury and DSE

[12] In the conventions of Ref. [16], we used the C^1_2 approximant with $a_{\eta/\eta';1,1} = 2b^2_{\eta/\eta'}$ as for the pion.

TFFs for the individual channels and note that this probably overestimates the uncertainty for the sum of the channels due to the reshuffling.

Since NLO results are not available for the η/η' TFFs, we estimated the NLO OPE uncertainty by simply rescaling the one in the pion channel by the ratio of the reference outcomes. Due to the smallness of this uncertainty, this is expected to be sufficiently accurate.

For the range $[m_{\min}, m_{\max}]$ and the minimal allowed value Σ_t for Σ^{match} in the Monte Carlo simulation for $P(x,y)$, we took the results from the isovector channel. We rescaled the $\pi(1300)$ term below the matching surface by the ratio of reference results when adding this contribution to $\delta_m a_\mu^{(8/0)-\eta/\eta'}$. This is justified by the fact that the first excited pseudoscalars in the three flavor channels have similar masses, despite the large mass difference of the pseudo-Goldstone bosons.

All results are collected in Tab. 3.1 and our final estimate for the longitudinal short-distance effects in $a_\mu^{(8/0)-\eta/\eta'}$ reads

$$\Delta a_\mu^{(8/0)-\eta} = (2.6 \pm 1.5) \times 10^{-11}\,, \qquad \Delta a_\mu^{(8/0)-\eta'} = (3.9 \pm 1.9) \times 10^{-11}\,. \tag{3.76}$$

The difference in the uncertainty of the η'-channel compared to Ref. [45] is due to Ref. [48] showing that the NLO correction to the quark loop is negative, which only affects this channel at the quoted accuracy. The relative contributions to the uncertainties are similar to the pion case illustrated in Fig. 3.7. A more precise description of $\eta - \eta'$-mixing would of course help better separate the two isoscalar channels but would not play an important role in their sum leading to negligible shifts in the total contribution from longitudinal SDCs.

3.4.3 Sum over flavor channels and comparison with literature

Under the assumption that the three ground-state pseudoscalar mesons dominate the low-energy region of $\bar{\Pi}_1^{(3)}$, we can add the results of the two previous sections to obtain our estimate for the effect of longitudinal SDCs on the HLbL contribution to a_μ. The result is

$$\Delta a_\mu^{\text{long}} = \Delta a_\mu^{(3)} + \Delta a_\mu^{(8/0)-\eta} + \Delta a_\mu^{(8/0)-\eta'} = (9.1 \pm 4.9) \times 10^{-11}\,, \tag{3.77}$$

where we have combined the three uncertainties linearly since they originate from the same sources in all three channels and are thus expected to be strongly correlated.

This result is remarkably close to what is expected based on flavor symmetry considerations. If the $U(3)$ symmetry emerging in the combined chiral and large-N_c limit is assumed, then $\Delta a_\mu^{(8/0)-\eta} + \Delta a_\mu^{(8/0)-\eta'} = 3\Delta a_\mu^{(3)}$. Using our isovector result and adding linearly a standard 30 % uncertainty for $U(3)$ breaking effects, we obtain

$$\Delta a_\mu^{\text{long}} = (10.4 \pm 8.3) \times 10^{-11}\,. \tag{3.78}$$

For this reason we do not expect that a more refined analysis of the subtler isosinglet contributions is going to change substantially our final results Eq. (3.77).

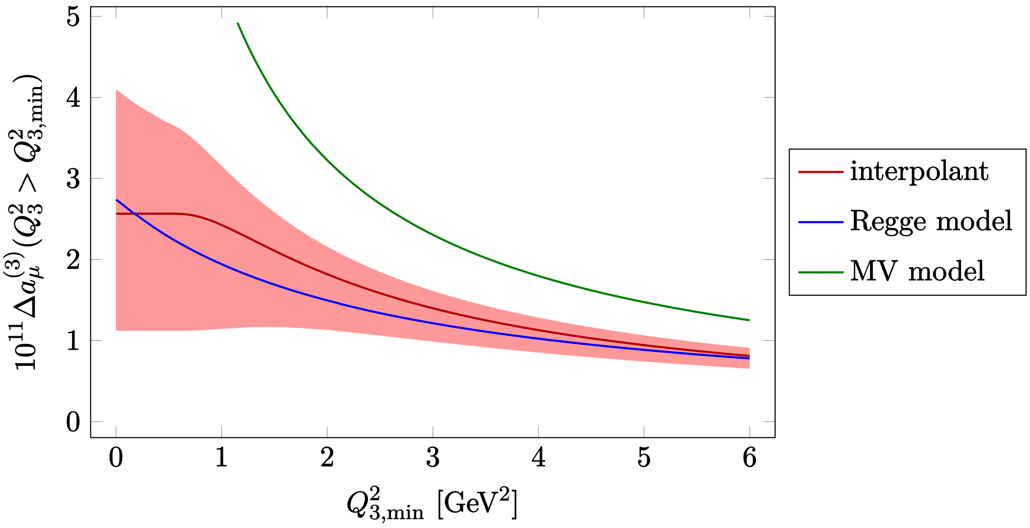

Figure 3.8: $\Delta a_\mu^{(3)}$ as a function of a lower cutoff on Q_3^2 in Eq. (3.37): our reference result and corresponding error band against the tower of excited pseudoscalars in the large-N_c Regge model 1 of Refs. [21, 40] and the curve from the MV model [15] evaluated using the up-to-date dispersive pion TFF. At small non-vanishing $Q_{3,\text{min}}^2$, our reference curve is constant due to the finite Σ^{match}, which for $P(x, y) = 0$ corresponds to $m^2 = Q_3^2 = \text{const.}$, whereas the Regge model has a slope due to the absence of such a cutoff. The upper end of our error band shows a slope because of the inclusion of the $\pi(1300)$ contribution in that region.

Our result can directly be compared to the Regge model of Refs. [21, 40] (see Sec. 3.1.4). As in our calculation, there it is assumed that the excited pseudoscalars give the dominant contribution to $\bar{\Pi}_1^{(a)}$ in the intermediate energy region, whereas in the regime where all virtualities are large both approaches are independent of the mechanism for the saturation of the SDC due to the matching to the quark loop in the Regge model. Their outcome is $\Delta a_\mu^{\text{long}} = (13 \pm 6) \times 10^{-11}$, which is well compatible with ours within errors. For the η'-channel, the Regge model yields $\Delta a_\mu^{(8/0)-\eta'} = (6.5 \pm 2.0) \times 10^{-11}$, which is somewhat larger than our result but still compatible within errors.[13] This can partly be explained by the different value for $C_{\eta'}$ used in Refs. [21, 40], namely $C_{\eta'} = 0.239$, which results from imposing that Eq. (3.20) holds exactly.

Fig. 3.8 shows $\Delta a_\mu^{(3)}$ as a function of a lower cutoff on Q_3^2 in our approach as well as the large-N_c Regge model 1 of Refs. [21, 40]. In order to obtain this plot, we calculated the integral in Eq. (3.37) as a function of a lower limit on Q_3^2 (which depends on Σ, r and ϕ) for both the

[13] The quoted result does not include the matching to the pQCD quark loop, which has only been performed for the sum of all channels in Refs. [21, 40].

full $a_\mu^{(3)}$ as well as the pion pole contribution (cf. Eq. (3.54)). The Regge model result lies within our error band for all $Q^2_{3,\text{min}}$.

Our estimate of longitudinal short-distance effects as well as the one in Refs. [21, 40] are smaller than the shift obtained in Ref. [15], $\Delta a_\mu^{\text{long}} = 23.5 \times 10^{-11}$, which even increases to about 38×10^{-11} if up-to-date TFF input is used [21]. These large values are due to two features of the MV model: the fact that the singly-virtual TFF is set to a constant over the whole integration region and not only in the OPE regime, and the fact that in the symmetric asymptotic limit the parametric momentum dependence is correct but its coefficient is too large. Both of these features can be clearly seen in Fig. 3.8 and are responsible for the discrepancies in the slope at small $Q^2_{3,\text{min}}$ and the values at large $Q^2_{3,\text{min}}$, respectively.

Refs. [41–44] have studied how the inclusion of an infinite tower of axial-vector mesons could help satisfy the OPE SDCs, focusing for this purpose on the relevant TFFs in the context of hQCD models. The most realistic model in Ref. [44] finds that the tower of axial-vector mesons gives a contribution of 31×10^{-11} and 34×10^{-11} depending on the way the model parameters are fixed, of which about 18×10^{-11} and 20×10^{-11} is attributed to a_μ^{long}, respectively. Thus, the results of this study appear to be at the high end of our range in Eq. (3.77). However, we stress that comparing these numbers with our result is not properly justified. Indeed, while in the holographic models the parametric Σ-dependences implied by pQCD and the OPE in the respective limits are correctly reproduced, the coefficients thereof are typically too small. In addition, the lightest multiplet of axials significantly alters $\bar{\Pi}_1$ at small photon virtualities, which implies that in our approach its contribution should be included in the low-energy representation. This aspect will be discussed in the next section, also to show how information on additional states in the 1–2 GeV region can be incorporated in our analysis.

3.4.4 Including ground-state axial mesons from hQCD at low energies

In the holographic models studied in Refs. [41–44], the lightest axial multiplet gives a substantial contribution to the low-energy region, which, if confirmed by a model-independent dispersive analysis, has to be included in the low-energy input in our approach. Conversely, the excited axials are sufficiently heavy that their effect below Σ^{match} is negligible. Focusing on the isovector channel again, we here illustrate the application of our procedure to the case of the inclusion of axial-meson input.

Among the various scenarios analyzed in Ref. [42], the hard-wall model by Hirn and Sanz (HW2) [163], which was also studied in Ref. [41] with different parameters, reproduces best the measured mass, the measured equivalent two-photon decay width and the singly virtual momentum dependence measured by L3 for the lightest multiplet [164, 165]. Furthermore, it yields asymptotic axial TFFs whose momentum dependence is consistent with the behavior derived in Ref. [131]. The infinite tower of axials has the correct momentum scaling in the MV regime, but the coefficient is 38 % too small [42]. Given also the relative simplicity of this model, we focus on this in the following, although the more involved models in Refs. [43,44] are more realistic.

The lightest isovector axial-vector meson, the a_1, contributes $a_{\mu,\text{HW2}}^{a_1} = 3.3 \times 10^{-11}$ to a_μ^{long} in this model. The rest of the tower of isovector axial mesons adds $\Delta a_\mu^{(3),\ A,\ \text{HW2}} = 0.8 \times 10^{-11}$ to this, implying that in this framework about 80 % of the total effect comes from the lightest state.[14] Almost half of the ground-state contribution is from the region below Σ^{match} (for the reference interpolant), whereas only about 10 % of the tower's effect comes from that region.

We matched the interpolant in Eq. (3.45) to the contributions from the pion and the holographic a_1 with the reference set of assumptions in Sec. 3.4.1. A subtlety arises in the regime of asymptotic $Q_1^2 \sim Q_2^2$ and $Q_3^2 \approx 0$. There, the low-energy input and the asymptotic representation Eq. (3.40) are simultaneously valid due to $\Sigma^{\text{match}}(1,\pi) = \infty$. However, in Sec. 3.2 we included chiral corrections by demanding consistency with the ground-state pseudoscalar pole contributions only, which due to the close-by poles at $Q_3^2 = -m_P^2$ are enhanced in this regime. Nevertheless, the a_1 gives a correction, which we included by shifting C_π^2 by 1.7 %. To avoid a modification in the quark-loop regime, we added a Σ^{-2} term independent of r and ϕ similarly to the anomaly correction in the isoscalar channels in Sec. 3.2. We obtained

$$\Delta a_\mu^{(3),\ A} = a_\mu^{(3),\ A} - a_{\mu,\text{disp}}^{\pi^0\text{-pole}} - a_{\mu,\text{HW2}}^{a_1} = 1.9 \times 10^{-11} \,. \tag{3.79}$$

This result is more than twice as large as the resummed tower in HW2, $\Delta a_\mu^{(3),\ A,\ \text{HW2}}$, but the significance of this discrepancy could only be assessed by a more sophisticated analysis including uncertainties, which is beyond the scope of this work. However, in the holographic model the infinite tower of axials does not fully saturate the pQCD nor the OPE constraints, which suggests that additional degrees of freedom besides axials should be included in a more realistic model, which could reduce the discrepancy.

We then considered the choice of parameters made in Ref. [41] and referred to as HW2(UV-fit) in Ref. [42]. This model is constructed to obey the OPE constraint exactly, but fails to describe low-energy physics like the ρ-meson mass, the pion TFF and the axial TFFs measured by L3. The longitudinal contribution from the a_1 in this case amounts to $a_{\mu,\ \text{HW2(UV-fit)}}^{a_1} = 3.4 \times 10^{-11}$ and the tower of states increases the value by $\Delta a_\mu^{(3),\ A,\text{HW2(UV-fit)}} = 0.8 \times 10^{-11}$. Our reference interpolant leads to $\Delta a_\mu^{(3),\ A} = 1.4 \times 10^{-11}$, which is again larger than the model result. However, also in HW2(UV-fit) the pQCD constraint is not fully satisfied by the tower of axials.

Neglecting issues related to intrinsic model dependence in the low-energy input, our method based on interpolants that by construction satisfy all constraints indicates that the effects of longitudinal SDCs are relatively small compared to the dominant low-energy contributions, and what is crucial in order to achieve higher precision is to gain control over the latter. We stress that a reliable prediction for the effect of SDCs on a_μ^{long} with a robust uncertainty estimate

[14]We thank Josef Leutgeb for checking these numbers and the ones for HW2(UV-fit) below.

requires model-independent input information, which is not available for the ground-state axial-vector mesons yet.

3.5 Conclusions

In this chapter, we introduced a novel approach [45] to incorporate longitudinal SDCs into the calculation of the HLbL contribution to the muon $g-2$. At variance with the previous estimates based on hadronic models, we constructed general functions interpolating between low-, mixed- and high-energy regions, without resorting to specify which and how hadronic intermediate states are responsible for saturating the constraints. Furthermore, our method allows us also to study in detail the role played by parameters and assumptions in a transparent and numerically efficient way.

Our main premise is that an accurate low-energy representation of the longitudinal function $\bar{\Pi}_1(Q_1^2, Q_2^2, Q_3^2)$ entering the HLbL integral can be obtained by taking into account only intermediate states that are under good theoretical and numerical control. For the π^0, due to the location of its pole, the form of this low-energy representation can be straightforwardly extended even to large Q_1^2 and Q_2^2 as long as Q_3^2 stays small. Using available input for the π^0-pole term, we found that the shift due to longitudinal SDCs on the isovector part of a_μ^{HLbL} is in the range $(2.6 \pm 1.5) \times 10^{-11}$. By including in the analysis also the isoscalar components, which the η- and η'-poles are assumed to dominate at low energies, we obtained that longitudinal SDCs increase a_μ^{HLbL} by $(9.1 \pm 4.9) \times 10^{-11}$ in total. The quoted ranges encompass uncertainties in the low-energy input, perturbative corrections and fitting errors at asymptotic momenta, parametric variations of the functional form of the interpolants and of the matching surface, at which these functions are matched to the low-energy input, with the latter dominating the total uncertainty. Thus, according to our analysis, infinite towers of states heavier than 1 GeV, albeit crucial for the saturation of SDCs, give a relatively small contribution to a_μ^{HLbL} and this effect can be estimated with sufficient precision using our method. Conversely, states with masses around 1 GeV contributing significantly to the low-energy region play a decisive role also in a precision determination of short-distance effects.

Our result for the effects of longitudinal SDCs on a_μ^{HLbL} agrees with recent model estimates [21, 40], fulfills the accuracy goal set by the forthcoming experimental results and is significantly smaller than the earlier model result of Ref. [15], especially if up-to-date TFF input is used. Furthermore, neglecting issues concerning intrinsic model dependence and the fact that hQCD calculations in Refs. [41–44,151] do not completely saturate the SDCs, we find in agreement with these studies that the infinite tower of axials has a relatively small impact on the longitudinal part of a_μ^{HLbL} if the lightest multiplet is treated explicitly as a low-energy contribution.

We expect that model-independent information on further intermediate states can be incorporated in our approach once these become available. In that respect, we expect the novel dispersive approach introduced in Ch. 5 and Ref. [60] to provide useful input. We do not expect large shifts nor a significant reduction of the uncertainties from including the higher-order corrections to asymptotic expressions derived in Refs. [20, 47–49], given the small contributions of the perturbative uncertainties in our analysis and the sparse knowledge of the non-perturbative matrix elements that appear in these expressions. Furthermore, our method might be generalized to the case of transversal SDCs. Therefore, the approach described in this chapter paves the way for a combination of all available low- and high-energy information on HLbL into one model-independent, accurate numerical estimate of this contribution to the muon $g-2$.

4 Dispersive Reconstruction of the VVA Correlator in the Soft-Photon Limit

One result of the analysis in the previous chapter was that control over intermediate states with masses between 1 and 2 GeV is crucial to significantly reduce the current uncertainties of the HLbL contribution to the muon $g-2$. In principle, multi-pion and multi-kaon states contribute in that region and it is currently impossible to describe these in a model-independent way. Instead, a more realistic approach is to assume that significant contributions only come from resonantly enhanced regions and that the effect of the resonances is well described by the NWA.

Two issues currently limit progress in this direction. On the one hand, data on heavier resonances are scarce and on the other hand the inclusion of states with spin 2 and larger is prevented by kinematic singularities within the CHPS approach that only cancel once an appropriate set of states is included such that sum rules are fulfilled, see Sec. 5.1.1 below for a precise statement of the problem. In Ch. 5, we will provide a solution to the latter by constructing a novel formalism for HLbL based on dispersion relations for the scalar functions $\bar{\Pi}_i$ directly in the limit $q_4 = 0$.

In order to introduce this formalism, we first develop it for the simpler case of the VVA correlator in this chapter. As we have seen in Sec. 3.1.1, this correlator is closely related to HLbL through the MV SDC Eq. (3.4). In addition, the VVA correlator is also required as input for the electroweak contribution to a_μ depicted in the diagram on the right-hand side

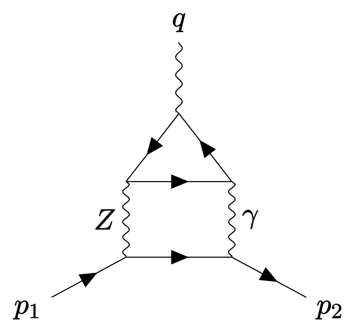

Figure 4.1: Lepton-loop diagram that has to be added to the hadronic VVA contribution to a_μ (right-hand side diagram in Fig. 2.2) to obtain a finite effect on a_μ.

of Fig. 2.2. In order to ensure gauge-anomaly cancellation needed to obtain a finite result, the lepton-loop contribution in Fig. 4.1 has to be added. We use our dispersive result for the hadronic VVA correlator to obtain an evaluation of this contribution due to the first family of leptons, $a_\mu^{\text{VVA}}[u,d,e]$, with reduced model dependence compared to Ref. [6].

After introducing the VVA Green's function and its tensor decomposition, we work out the new dispersive formalism including pseudoscalar, axial-vector and vector poles as well as two-pion rescattering. Afterwards, we compare it to the formalism with fixed photon virtualities, the analog of the CHPS framework for HLbL, first analytically and then numerically for the isovector part of the correlator taking into account SDCs. We compare our results against the currently used models and calculate $a_\mu^{\text{VVA}}[u,d,e]$.

4.1 The VVA Green's function

4.1.1 Kinematics and matrix element

First, we review some relevant definitions and results that can be found e.g. in Ref. [94] and adapt them to our notation. The VVA correlator is given in Eq. (3.5), but here we use the axial-vector current

$$j_\mu^5(x) = \bar\psi(x)\mathcal{Q}_5\gamma_\mu\gamma_5\psi(x)\,. \tag{4.1}$$

The flavor matrix $\mathcal{Q}_5$ amounts to $\mathcal{Q}^2$ in the context of the SDC for HLbL, reducing the definition to Eq. (3.2), and $2I_3 = \text{diag}(1,-1,-1)$ with the weak isospin I_3 for the electroweak contribution to $g-2$, where the axial current couples to a Z boson (see Sec. 4.1.3). In both cases, the axial current can be written in terms of its flavor components according to

$$j_\mu^5(x) = \sum_{a=3,8,0} 2C_a j_\mu^{5(a)}(x)\,, \qquad j_\mu^{5(a)}(x) = \bar\psi(x)\frac{\lambda^a}{2}\gamma_\mu\gamma_5\psi(x)\,. \tag{4.2}$$

The coefficients C_a are given by $C_a = \text{Tr}(Q_5\lambda_a)/2$, explicitly Eq. (3.6) for the SDC for HLbL and

$$C_3 = 1\,, \qquad C_8 = \frac{1}{\sqrt{3}}\,, \qquad C_0 = -\frac{1}{\sqrt{6}} \tag{4.3}$$

for the electroweak contribution to a_μ. We define flavor components of the VVA correlator as

$$\mathcal{W}^{(a)}_{\mu\nu\rho}(q_1,q_2) = \text{i}\int \text{d}^4x \int \text{d}^4y\, e^{\text{i}(q_1\cdot x+q_2\cdot y)}\,\langle 0|\,\text{T}\{j_\mu^{\text{em}}(x)j_\nu^{\text{em}}(y)j_\rho^{5(a)}(0)\}\,|0\rangle\,. \tag{4.4}$$

The Ward identities for the VVA correlator read

$$\{q_1^\mu, q_2^\nu\}\mathcal{W}^{(a)}_{\mu\nu\rho}(q_1,q_2) = \{0,0\}\,, \quad (q_1+q_2)^\rho\mathcal{W}^{(a)}_{\mu\nu\rho}(q_1,q_2) = \mathcal{A}^{(a)}\epsilon_{\mu\nu\alpha\beta}q_1^\alpha q_2^\beta\,, \tag{4.5}$$

where $\mathcal{A}^{(a)} = N_c\,\text{Tr}(\mathcal{Q}^2\lambda^a)/(4\pi^2)$ according to the QED axial anomaly and the second identity receives corrections from quark masses and the gluon anomaly. The full correlator fulfills the Ward identities with $\mathcal{A} = \sum_a 2C_a\mathcal{A}^{(a)}$ in the anomalous one. The anomalous Ward identity has been checked up to three loops in pQCD [166].

4.1.2 Tensor decomposition

In Ref. [94], a decomposition of $\mathcal{W}_{\mu\nu\rho}(q_1, q_2)$ into independent Lorentz structures free of kinematic singularities and zeros has been given:

$$
\begin{aligned}
\mathcal{W}^{\mu\nu\rho}(q_1,q_2) &= \sum_{i=0}^{3} \mathcal{W}_i(q_1^2, q_2^2, (q_1+q_2)^2)\tau_i^{\mu\nu\rho}(q_1,q_2)\,,\\
\tau_0^{\mu\nu\rho}(q_1,q_2) &= \epsilon^{\mu\nu\alpha\beta} q_{1\alpha} q_{2\beta}(q_1+q_2)^\rho\,,\\
\tau_1^{\mu\nu\rho}(q_1,q_2) &= \epsilon^{\mu\nu\alpha\beta} q_{1\alpha} q_{2\beta}(q_1-q_2)^\rho\,,\\
\tau_2^{\mu\nu\rho}(q_1,q_2) &= q_1^\nu \epsilon^{\mu\rho\alpha\beta} q_{1\alpha} q_{2\beta} - q_2^\mu \epsilon^{\nu\rho\alpha\beta} q_{1\alpha} q_{2\beta} - (q_1\cdot q_2)\epsilon^{\mu\nu\rho\alpha}(q_1-q_2)_\alpha\,,\\
\tau_3^{\mu\nu\rho}(q_1,q_2) &= q_1^\mu \epsilon^{\nu\rho\alpha\beta} q_{1\alpha} q_{2\beta} + q_2^\nu \epsilon^{\mu\rho\alpha\beta} q_{1\alpha} q_{2\beta} - q_1^2 \epsilon^{\mu\nu\rho\alpha} q_{2\alpha} - q_2^2 \epsilon^{\mu\nu\rho\alpha} q_{1\alpha}\,.
\end{aligned}
\tag{4.6}
$$

The Lorentz structures fulfill the crossing relations

$$
\mathcal{C}_{12}[\tau_0^{\mu\nu\rho}] = \tau_0^{\mu\nu\rho}\,,\quad \mathcal{C}_{12}[\tau_1^{\mu\nu\rho}] = -\tau_1^{\mu\nu\rho}\,,\quad \mathcal{C}_{12}[\tau_2^{\mu\nu\rho}] = \tau_2^{\mu\nu\rho}\,,\quad \mathcal{C}_{12}[\tau_3^{\mu\nu\rho}] = -\tau_3^{\mu\nu\rho}\,,
\tag{4.7}
$$

where the crossing operator is defined by $\mathcal{C}_{12}[f] := f(\mu \leftrightarrow \nu, q_1 \leftrightarrow q_2)$.

An equivalent decomposition has been obtained in Ref. [131] in the context of the axial-meson TFF by using the BTT recipe, see Sec. 2.4.1. These structures are related to the ones of Ref. [94] by

$$
\begin{aligned}
\tau_0^{\mu\nu\rho}(q_1,q_2) &= \bar{T}_3^{\mu\nu\rho}(q_1,q_2)\,,\\
\tau_1^{\mu\nu\rho}(q_1,q_2) &= T_1^{\mu\nu\rho}(q_1,q_2)\,,\\
\tau_2^{\mu\nu\rho}(q_1,q_2) &= \bar{T}_3^{\mu\nu\rho}(q_1,q_2) - T_2^{\mu\nu\rho}(q_1,q_2) + T_3^{\mu\nu\rho}(q_1,q_2)\,,\\
\tau_3^{\mu\nu\rho}(q_1,q_2) &= -T_2^{\mu\nu\rho}(q_1,q_2) - T_3^{\mu\nu\rho}(q_1,q_2)\,,
\end{aligned}
\tag{4.8}
$$

where we made use of the Schouten identity.

In the context of the MV SDC on HLbL, we have introduced a tensor decomposition of the VVA correlator in Eq. (3.10). The tensor structures appearing there can also be written in terms of ones in Eq. (4.6)

$$
\begin{aligned}
\tau_0^{\mu\nu\rho}(q_1,q_2) &= -t_L^{\mu\nu\rho}\,,\\
\tau_1^{\mu\nu\rho}(q_1,q_2) &= -\frac{q_1^2-q_2^2}{(q_1+q_2)^2} t_L^{\mu\nu\rho} + t_-^{\mu\nu\rho}\,,\\
\tau_2^{\mu\nu\rho}(q_1,q_2) &= -\frac{2q_1\cdot q_2}{(q_1+q_2)^2} t_L^{\mu\nu\rho} + t_+^{\mu\nu\rho}\,,\\
\tau_3^{\mu\nu\rho}(q_1,q_2) &= \frac{q_1^2-q_2^2}{(q_1+q_2)^2} t_L^{\mu\nu\rho} - t_-^{\mu\nu\rho} + \tilde{t}_-^{\mu\nu\rho}\,.
\end{aligned}
\tag{4.9}
$$

The poles in these equations represent kinematic singularities in the tensor decomposition Eq. (3.10). For this reason, these structures are not suited for a dispersive analysis.

For both the MV constraint in HLbL and the electroweak contribution to a_μ, we need the VVA correlator for small q_2 up to linear order. Expanding the Lorentz structures gives $\tau_i^{\mu\nu\rho}(q_1, q_2) = q_{2\sigma}\tau_i^{\mu\nu\rho\sigma}(q_1) + \mathcal{O}(q_2^2)$ with the new Lorentz tensors

$$\begin{aligned}
\tau_0^{\mu\nu\rho\sigma}(q_1) &= \tau_1^{\mu\nu\rho\sigma}(q_1) = \epsilon^{\mu\nu\alpha\sigma} q_{1\alpha} q_1^\rho \,, \\
\tau_2^{\mu\nu\rho\sigma}(q_1) &= \epsilon^{\mu\rho\alpha\sigma} q_1^\nu q_{1\alpha} - \epsilon^{\mu\nu\rho\alpha} q_1^\sigma q_{1\alpha} \,, \\
\tau_3^{\mu\nu\rho\sigma}(q_1) &= \epsilon^{\nu\rho\alpha\sigma} q_1^\mu q_{1\alpha} - q_1^2 \epsilon^{\mu\nu\rho\sigma} \,.
\end{aligned} \tag{4.10}$$

Since $\tau_0^{\mu\nu\rho\sigma}(q_1) = \tau_1^{\mu\nu\rho\sigma}(q_1)$ and $\tau_3^{\mu\nu\rho\sigma}(q_1) = \tau_2^{\mu\nu\rho\sigma}(q_1) - \tau_1^{\mu\nu\rho\sigma}(q_1)$, in this kinematic limit there are only two independent Lorentz structures. Thus, we can write

$$\mathcal{W}^{\mu\nu\rho}(q_1, q_2) = \sum_{i=1}^{2} \tilde{\mathcal{W}}_i(q_1^2) q_{2\sigma} \tau_i^{\mu\nu\rho\sigma}(q_1) + \mathcal{O}(q_2^2) \tag{4.11}$$

and the new scalar functions

$$\tilde{\mathcal{W}}_1(q^2) = \tilde{\mathcal{W}}_1(q^2, 0, q^2) \,, \qquad \tilde{\mathcal{W}}_2(q^2) = \tilde{\mathcal{W}}_2(q^2, 0, q^2) \,, \tag{4.12}$$

are related to the previous ones by

$$\begin{aligned}
\tilde{\mathcal{W}}_1(q_1^2, q_2^2, q_3^2) &:= \mathcal{W}_0(q_1^2, q_2^2, q_3^2) + \mathcal{W}_1(q_1^2, q_2^2, q_3^2) - \mathcal{W}_3(q_1^2, q_2^2, q_3^2) \,, \\
\tilde{\mathcal{W}}_2(q_1^2, q_2^2, q_3^2) &:= \mathcal{W}_2(q_1^2, q_2^2, q_3^2) + \mathcal{W}_3(q_1^2, q_2^2, q_3^2) \,.
\end{aligned} \tag{4.13}$$

Due to their properties with respect to the axial-vector current

$$(q_{1\rho} q_{1\rho'} - q_1^2 g_{\rho\rho'}) \tau_1^{\mu\nu\rho\sigma}(q_1) = 0 \,, \quad q_{1\rho} \tau_2^{\mu\nu\rho\sigma}(q_1) = 0 \,, \tag{4.14}$$

the function $\tilde{\mathcal{W}}_1$ is called the longitudinal and $\tilde{\mathcal{W}}_2$ the transversal component.

The anomalous Ward identity in Eq. (4.5) fixes the longitudinal function in the chiral limit and when the gluon anomaly is neglected:

$$\tilde{\mathcal{W}}_1(q^2) = \frac{\mathcal{A}}{q^2} \,. \tag{4.15}$$

We see that it contains a massless pole in q^2, which can only be dynamical since we started from a basis free of kinematic singularities. The only massless states in the chiral limit and without the gluon anomaly are the pseudo-Goldstone bosons and the η' and due to the diagonal flavor structure only the π^0, η and η' can contribute, each according to the coefficients C_a if mixing is neglected.

The non-renormalization theorem for the transversal component derived in Ref. [167] translates into

$$\tilde{\mathcal{W}}_2(q^2) = -\frac{\mathcal{A}}{2q^2} \,. \tag{4.16}$$

However, in contrast to Eq. (4.15), this equation receives non-perturbative corrections even in the chiral limit and hence is valid only for $-q^2 \gg \Lambda_{\mathrm{QCD}}^2$, where quark-mass effects are suppressed, see Sec. 4.5.1 below.

4.1.3 Connection with the hadronic electroweak contribution to a_μ

The VVA correlator is needed as input for one diagram in the electroweak contribution to a_μ, namely the one shown on the right-hand side of Fig. 2.2. Due to Furry's theorem [168], only the axial component of the Z-boson contributes and as for HLbL, the blob is only needed for a soft external photon. Thus, the dispersive representations of the functions $\tilde{\mathcal{W}}_i(q^2)$ that will be derived in Secs. 4.2 and 4.3 can be directly used to evaluate this diagram.

Analogously to the Master formula for HLbL in Eq. (2.51), also this diagram can be reduced to an integral over space-like values for the arguments of the scalar functions [56]

$$a_\mu^{\mathrm{VVA}} = \int_0^{\Lambda^2} \mathrm{d}Q^2 \left[K_1(Q^2)\tilde{\mathcal{W}}_1(-Q^2) + K_2(Q^2)\tilde{\mathcal{W}}_2(-Q^2)\right] , \tag{4.17}$$

where the cut-off Λ^2 should be taken to ∞ in the end. The form of the kernel functions $K_i(Q^2)$ depends on the gauge chosen for the electroweak part of the diagram since only the sum of all diagrams at a given order in the electroweak couplings is gauge invariant. In the unitary gauge, the kernel functions read [56]

$$\begin{aligned} K_1(Q^2) &= -\frac{G_\mu \alpha Q^2}{12\sqrt{2}\pi}\left[\left(\frac{Q^2}{m_\mu^2} - 2\right)\left(1 - \sqrt{1 + \frac{4m_\mu^2}{Q^2}}\right) + 2\right] , \\ K_2(Q^2) &= -\frac{G_\mu \alpha Q^2}{12\sqrt{2}\pi}\frac{M_Z^2}{M_Z^2 + Q^2}\left[\left(\frac{Q^2}{m_\mu^2} + 4\right)\left(1 - \sqrt{1 + \frac{4m_\mu^2}{Q^2}}\right) + 2\right] . \end{aligned} \tag{4.18}$$

Since the axial part of the Z boson couples to fermions according to their weak isospin, the functions $\tilde{\mathcal{W}}_i$ are needed here for the axial current in Eq. (4.1) with $\mathcal{Q}_5 = 2I_3$ as already mentioned in Sec. 4.1.1.

Both kernel functions go to constants for large Q^2 and the OPE predicts that the scalar functions $\tilde{\mathcal{W}}_i$ behave as $1/Q^2$, see Sec. 4.5.1. Thus, the integrals in Eq. (4.17) diverge logarithmically in the limit $\Lambda^2 \to \infty$. However, if we consider a complete family of fermions, the leading term in the $1/Q^2$ expansion drops out due to the gauge anomaly cancellation condition

$$\sum_f N_f I_3^f Q_f^2 = 0 , \tag{4.19}$$

where the sum runs over all quarks and leptons of one family, $N_f = 3$ for quarks and 1 for leptons, I_3^f is the fermion's weak isospin and Q_f its charge. This makes a_μ^{VVA} finite in the limit $\Lambda \to \infty$. For this reason, it is crucial that the leading OPE constraint on the VVA correlator is implemented exactly.

The contribution from a charged lepton is given, to leading order in α, through the loop diagram in Fig. 4.1, which yields

$$\tilde{\mathcal{W}}_1^l(q^2) = -2\tilde{\mathcal{W}}_2^l(q^2) = -\frac{1}{2\pi^2}\int_0^1 \mathrm{d}x \frac{x(1-x)}{x(1-x)q^2 - m_f^2} . \tag{4.20}$$

In our numerical study in Sec. 4.6, we will focus on the first-family contribution to a_μ^{VVA}. Since $2I_3$ restricted to the first family coincides with the third Pauli matrix, this exactly corresponds to twice the isovector part of the axial current together with the electron-loop contribution.

4.1.4 Hadronic models for the VVA correlator

So far, the VVA correlator and the corresponding contribution to a_μ have only been calculated using hadronic models. For the compilation in Ref. [3], a simple model due to Czarnecki, Marciano and Vainshtein [6], containing only pseudoscalar, axial-vector and vector poles has been used. For the isovector component, it takes the form

$$\begin{aligned}\tilde{\mathcal{W}}_{1,\mathrm{CMV}}^{(3)}(q^2) &= \frac{1}{4\pi^2(q^2-m_\pi^2)}\,,\\ \tilde{\mathcal{W}}_{2,\mathrm{CMV}}^{(3)}(q^2) &= \frac{1}{8\pi^2}\frac{1}{m_{a_1}^2-m_\rho^2}\left(\frac{m_\rho^2-m_\pi^2}{q^2-m_{a_1}^2}-\frac{m_{a_1}^2-m_\pi^2}{q^2-m_\rho^2}\right)\,. \end{aligned}\tag{4.21}$$

The residues of the poles have been fixed from the OPE constraints introduced in Sec. 4.5.1 below. For the contribution to a_μ from the first family of quarks and leptons, the model leads to[1]

$$a_{\mu,\mathrm{CMV}}^{\mathrm{VVA},L}[u,d,e] = -0.94\times 10^{-11}\,, \qquad a_{\mu,\mathrm{CMV}}^{\mathrm{VVA},T}[u,d,e] = -1.33\times 10^{-11}\,, \tag{4.22}$$

where the two results correspond to the longitudinal and transversal contribution, i.e. the contribution from $\tilde{\mathcal{W}}_1$ and $\tilde{\mathcal{W}}_2$, respectively. Ref. [6] quotes an uncertainty estimate of $\pm 0.2\times 10^{-11}$ for the sum based on generously varying the ρ and a_1 masses.

Refs. [41, 42] discuss holographic models for the axial-vector meson contributions to a_μ. We consider here the model introduced in Ref. [163] and called HW2 in Ref. [42]. In order to obtain the correct asymptotic limit, we use the anomaly, $N_c = 3$ and F_π to fix the parameters, which is called HW2(UV-fit) in Ref. [42] and set 2 in Ref. [41]. Formulae for the singly-virtual VVA scalar functions can be found in Ref. [41]

$$\begin{aligned}\tilde{\mathcal{W}}_{1,\mathrm{hQCD}}^{3}(-Q^2) &= -\frac{1}{4\pi^2 Q^2}\left(1-\frac{m_\pi^2}{Q^2+m_\pi^2}\tilde{F}_{\pi^0\gamma^*\gamma^*}(-Q^2,0)\right)\,,\\ \tilde{\mathcal{W}}_{2,\mathrm{hQCD}}^{3}(-Q^2) &= \frac{1}{8\pi^2 Q^2}-\frac{z_0^2}{16\pi^2}\left(\frac{K_0(\sqrt{Q^2}z_0)}{I_0(\sqrt{Q^2}z_0)}+\frac{K_1(\sqrt{Q^2}z_0)}{I_1(\sqrt{Q^2}z_0)}\right) \end{aligned}\tag{4.23}$$

with the Bessel functions K_i and I_i, the size of the holographic dimension $z_0 \approx 2.42\,\mathrm{GeV}^{-1}$ and the normalized pion TFF

$$\tilde{F}_{\pi^0\gamma^*\gamma^*}(-Q^2,0) = \int_0^{z_0}\mathrm{d}z\frac{2z}{z_0^2}\sqrt{Q^2}z\left(K_1(\sqrt{Q^2}z)+\frac{K_0(\sqrt{Q^2}z_0)}{I_0(\sqrt{Q^2}z_0)}I_1(\sqrt{Q^2}z)\right)\,. \tag{4.24}$$

[1] In Ref. [6], the electron mass as well as terms suppressed by m_μ^2/m_ρ^2 have been neglected in the Q^2 integral. This explains the difference to the numbers quoted there $a_{\mu,\mathrm{CMV}}^{\mathrm{VVA},L}[u,d,e] = -0.96\times 10^{-11}$ and $a_{\mu,\mathrm{CMV}}^{\mathrm{VVA},T}[u,d,e] = -1.32\times 10^{-11}$.

	$4\pi^2\,\mathrm{Res}\left(\tilde{\mathcal{W}}^{(3)}_{1,\mathrm{hQCD}}, m_i^2\right)$		$8\pi^2\,\mathrm{Res}\left(\tilde{\mathcal{W}}^{(3)}_{2,\mathrm{hQCD}}, m_i^2\right)$	
n	π	ρ	a_1	ρ
0	1.0204	-0.0208	6.16	-3.71
1	—	4.9×10^{-4}	11.10	-8.64
2	—	-6.5×10^{-5}	16.04	-13.57
3	—	1.6×10^{-5}	20.97	-18.51

Table 4.1: Residues of the lightest poles in the two isoscalar scalar functions in hQCD. n is the radial excitation and ρ stands for all vector mesons from the multiplet.

These functions have the correct leading asymptotic behavior due to the anomaly and the non-renormalization theorem, but do not include the effects of non-vanishing condensates [41]. This model leads to

$$a_{\mu,\,\mathrm{hQCD}}^{\mathrm{VVA},L}[u,d,e] = -0.90 \times 10^{-11}\,, \qquad a_{\mu,\,\mathrm{hQCD}}^{\mathrm{VVA},T}[u,d,e] = -1.29 \times 10^{-11}\,. \tag{4.25}$$

Given the large hadron masses in the holographic model [42] and the very different analytic form of this model compared to the CMV one, these values are surprisingly close to the ones of Ref. [6].

In the time-like region, the holographic functions have series of poles on the real axis since the model is constructed in the large-N_c limit. $\tilde{\mathcal{W}}_1^3$ contains a pion pole and a tower of vector-meson poles, whereas $\tilde{\mathcal{W}}_2^3$ contains towers of vector-meson and axial-vector meson poles. The masses of these states are, however, $SU(3)$ symmetric and typically too large [42]. E.g. the mass of the lightest vector meson is 0.99 GeV, which is considerably larger than m_ρ, but similar to m_ϕ. Similarly, the mass of the lightest axial meson is 1.57 GeV and thus larger than any of the masses in the lightest multiplet.

The residues of the lightest poles can be found in Tab. 4.1. We can see there that the pion pole completely dominates the first scalar function and the vector-meson poles only give small corrections to it. This is consistent with the pion pole being the only contribution in the chiral limit. Conversely, in the second scalar function, the whole tower of vector and axial-vector poles is important and the residues even increase with n. Thus, an intricate cancellation between the infinite towers of axial-vector and vector poles is needed to reach the space-like asymptotic value in Eq. (4.16). A similar—but simpler—cancellation is also built into the model in Eq. (4.21), where both the a_1 and the ρ pole have large residues with opposite sign.

4.2 Dispersion relations in $g-2$ kinematics

We now turn to the dispersive description of the two VVA scalar functions, comparing a formalism in $g-2$ kinematics, developed in this section, with a formalism in which the virtualities are kept fixed, the latter will be introduced in Sec. 4.3 below.

The asymptotic behavior of the scalar functions $\tilde{\mathcal{W}}_i(q_1^2)$ for large space-like momenta $q^2=-Q^2$ follows from the OPE (see Sec. 4.5.1). The leading term predicts

$$\tilde{\mathcal{W}}_i(-Q^2) \propto \frac{1}{Q^2}\left[1+\mathcal{O}\left(\frac{m_q^2}{Q^2},\frac{\Lambda_{\mathrm{QCD}}^2}{Q^2}\right)\right] \tag{4.26}$$

for both functions. We assume that this falloff remains true in the time-like region, which allows us to write an unsubtracted dispersion relation for the scalar functions $\tilde{\mathcal{W}}_i(q_1^2)$ in $g-2$ kinematics:

$$\tilde{\mathcal{W}}_i(q^2) = \frac{1}{\pi}\int \mathrm{d}s \frac{\operatorname{Im}\tilde{\mathcal{W}}_i(s)}{s-q^2-\mathrm{i}\epsilon}\,. \tag{4.27}$$

The imaginary parts of the scalar functions in $g-2$ kinematics $\operatorname{Im}\tilde{\mathcal{W}}_i(s)$ can be expressed in terms of the imaginary parts of the scalar functions $\tilde{\mathcal{W}}_i(q_1^2,q_2^2,q_3^2)$ in different physical regions:

$$\begin{aligned}
\operatorname{Im}\tilde{\mathcal{W}}_i(q_1^2) &= \frac{1}{2\mathrm{i}}\Big(\tilde{\mathcal{W}}_i(q_1^2+\mathrm{i}\epsilon,0,q_1^2+\mathrm{i}\epsilon)-\tilde{\mathcal{W}}_i(q_1^2-\mathrm{i}\epsilon,0,q_1^2-\mathrm{i}\epsilon)\Big)\\
&= \lim_{q_3^2\to q_1^2}\frac{1}{2\mathrm{i}}\Big(\tilde{\mathcal{W}}_i(q_1^2+\mathrm{i}\epsilon,0,q_3^2+\mathrm{i}\epsilon)-\tilde{\mathcal{W}}_i(q_1^2-\mathrm{i}\epsilon,0,q_3^2-\mathrm{i}\epsilon)\Big)\\
&= \lim_{q_3^2\to q_1^2}\frac{1}{2\mathrm{i}}\Big(\tilde{\mathcal{W}}_i(q_1^2+\mathrm{i}\epsilon,0,q_3^2+\mathrm{i}\epsilon)-\tilde{\mathcal{W}}_i(q_1^2+\mathrm{i}\epsilon,0,q_3^2-\mathrm{i}\epsilon)\\
&\qquad +\tilde{\mathcal{W}}_i(q_1^2+\mathrm{i}\epsilon,0,q_3^2-\mathrm{i}\epsilon)-\tilde{\mathcal{W}}_i(q_1^2-\mathrm{i}\epsilon,0,q_3^2-\mathrm{i}\epsilon)\Big)\\
&= \lim_{q_3^2\to q_1^2}\Bigg[\frac{1}{2\mathrm{i}}\Big(\tilde{\mathcal{W}}_i(q_1^2+\mathrm{i}\epsilon,0,q_3^2+\mathrm{i}\epsilon)-\tilde{\mathcal{W}}_i(q_1^2+\mathrm{i}\epsilon,0,q_3^2-\mathrm{i}\epsilon)\Big)\\
&\qquad +\left(\frac{1}{2\mathrm{i}}\Big(\tilde{\mathcal{W}}_i(q_1^2+\mathrm{i}\epsilon,0,q_3^2+\mathrm{i}\epsilon)-\tilde{\mathcal{W}}_i(q_1^2-\mathrm{i}\epsilon,0,q_3^2+\mathrm{i}\epsilon)\Big)\right)^*\Bigg]\\
&= \lim_{q_3^2\to q_1^2}\Big[\operatorname{Im}_3\tilde{\mathcal{W}}_i(q_1^2+\mathrm{i}\epsilon,0,q_3^2)+\Big(\operatorname{Im}_1\tilde{\mathcal{W}}_i(q_1^2,0,q_3^2+\mathrm{i}\epsilon)\Big)^*\Big]\,.
\end{aligned} \tag{4.28}$$

In this equation, Im_1 denotes the q_1^2-channel discontinuity analytically continued to $q_3^2+\mathrm{i}\epsilon$ and similarly for Im_3. Due to this analytic continuation, the discontinuities are in general complex quantities. In the third line of this equation, we could equally well have added and subtracted the function $\tilde{\mathcal{W}}_i(s-\mathrm{i}\epsilon,0,t+\mathrm{i}\epsilon)$, which would have resulted in having the complex conjugation on the other term. This is equivalent, because $\operatorname{Im}\tilde{\mathcal{W}}_i(s)$ is real. In general, due to the appearance of soft-photon singularities, the limit in Eq. (4.28) does not exist for the two individual discontinuities. Since this is not an issue for any of the contributions considered in this chapter, we defer a detailed discussion of soft-photon singularities to the case of HLbL in Sec. 5.3.

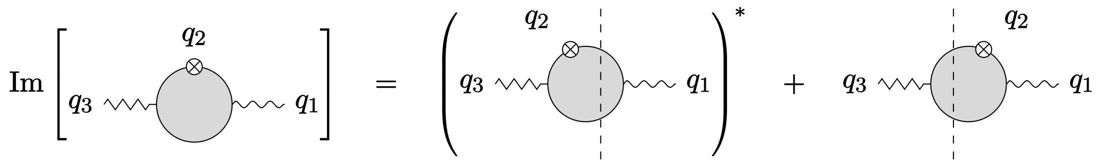

Figure 4.2: Unitarity cuts contributing to the discontinuity of the VVA function in the limit of $g-2$ kinematics. The axial current is denoted by a zigzag line, the off-shell photon by a wavy line and the static external electromagnetic field by a crossed circle.

Thus, the imaginary part in degenerate kinematics can be obtained as the sum of two cuts in general kinematics as illustrated in Fig. 4.2. This can be understood from the fact that the two cuts become kinematically indistinguishable in the limit $q_2 \to 0$.

We now consider the process $\gamma^*(-q_1)\gamma^*(-q_2) \to a^*(q_3)$, where a denotes an auxiliary axial-vector particle coupling to the axial current according to $-g_A a^\mu(x) j^5_\mu(x)$. The unitarity relation for this process takes the form

$$\begin{aligned}
&\mathrm{Im}_3 \left(-\mathrm{i}\,\langle a^*(q_3,\lambda_a)|\gamma^*(-q_1,\lambda_1)\gamma^*(-q_2,\lambda_2)\rangle\right) \\
&\quad = \sum_n \frac{1}{2S_n}\left(\prod_{i=1}^{N_n}\int \widetilde{\mathrm{d}p_i}\right) \langle\gamma^*(-q_1,\lambda_1)\gamma^*(-q_2,\lambda_2)|n;\{p_i\}\rangle^* \,\langle a^*(q_3,\lambda_a)|n;\{p_i\}\rangle \,. \qquad (4.29)
\end{aligned}$$

The imaginary part in this equation is given by the multivariate version of the Schwarz reflection principle as

$$\mathrm{Im}_3\, \tilde{\mathcal{W}}_i(q_1^2,0,q_3^2) = \frac{1}{2\mathrm{i}}\left(\tilde{\mathcal{W}}_i(q_1^2+\mathrm{i}\epsilon,0,q_3^2+\mathrm{i}\epsilon) - \tilde{\mathcal{W}}_i(q_1^2-\mathrm{i}\epsilon,0,q_3^2-\mathrm{i}\epsilon)\right) , \qquad (4.30)$$

whereas in Eq. (4.27), we need

$$\mathrm{Im}_3\, \tilde{\mathcal{W}}_i(q_1^2,0,q_3^2) = \frac{1}{2\mathrm{i}}\left(\tilde{\mathcal{W}}_i(q_1^2+\mathrm{i}\epsilon,0,q_3^2+\mathrm{i}\epsilon) - \tilde{\mathcal{W}}_i(q_1^2+\mathrm{i}\epsilon,0,q_3^2-\mathrm{i}\epsilon)\right) . \qquad (4.31)$$

This can be obtained by analytically continuing the unitarity relation in q_1 to a value below the branch point and then along the upper rim of the cut to the required value. In writing Eq. (4.29) we assume that this continuation has been performed.

Similarly, the unitarity relation in the q_1-channel reads

$$\begin{aligned}
&\mathrm{Im}_1 \left(-\mathrm{i}\,\langle\gamma^*(q_2,\lambda_2)a^*(q_3,\lambda_a)|\gamma^*(-q_1,\lambda_1)\rangle\right) \\
&\quad = \sum_n \frac{1}{2S_n}\left(\prod_{i=1}^{N_n}\int \widetilde{\mathrm{d}p_i}\right) \langle\gamma^*(-q_1,\lambda_1)|n;\{p_i\}\rangle^* \,\langle\gamma^*(q_2,\lambda_2)a^*(q_3,\lambda_a)|n;\{p_i\}\rangle \,, \qquad (4.32)
\end{aligned}$$

where a similar analytic continuation in q_3 is implicitly assumed. The two unitarity relations Eqs. (4.29) and (4.32) allow us to describe the two contributions to the discontinuity in the

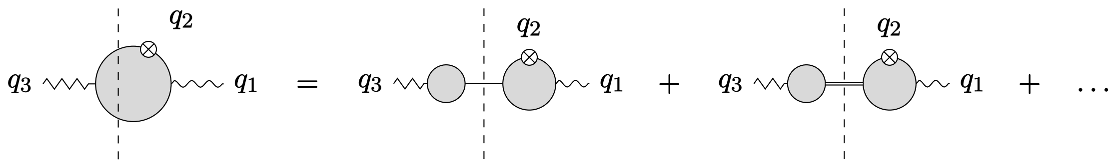

Figure 4.3: Pseudoscalar and axial-vector poles due to intermediate states in the unitarity relation Eq. (4.29). The normal line denotes a pseudoscalar meson and the double line a resonance, in this case an axial-vector meson.

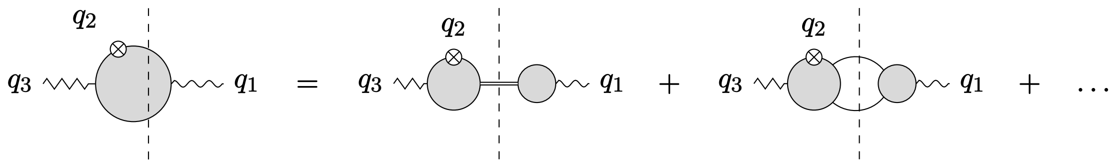

Figure 4.4: Vector poles and two-pion cuts due to intermediate states in the unitarity relation Eq. (4.32).

limit of $g-2$ kinematics in terms of a sum over intermediate states. In the following, we discuss pseudoscalar-, vector- and axial-pole contributions, as well as two-pion intermediate states, as shown in Figs. 4.3 and 4.4. Scalar mesons cannot appear in either discontinuity due to parity and current conservation, respectively. Also tensor mesons with $J^{PC} = 2^{++}$ couple neither to vector nor axial-vector currents and thus do not contribute.

In principle, only stable states (in pure QCD) should be considered in the sums over intermediate states. However, an explicit treatment of intermediate states with more than two particles is very challenging and we expect them to be numerically important only if resonantly enhanced. Many of these resonances, especially the important ones at relatively low energies, are reasonably narrow, i.e. $\Gamma \ll M$, so that we can approximate their effect using a NWA. Since we are only interested in the scalar functions at space-like momenta, the impact of the non-zero width is expected to be small. In this approximation, the resonances are stable and can be included in the unitarity relations instead of the corresponding multi-meson channel. Double counting is avoided by excluding single-particle states that already appear as resonances in the included multi-meson channels, e.g. the ρ-meson is included in the $\pi\pi$-scattering phase shift $\delta_1^1(s)$ that we will use in the numerical analysis below so that we do not include in addition a ρ-state in the NWA.

4.2.1 Pseudoscalar pole

A single pseudoscalar meson does not couple to an electromagnetic current and thus a one-pseudoscalar intermediate state can only appear in the unitarity relation in q_3, shown in Fig. 4.3. We thus single out this state in Eq. (4.29),

$$\begin{aligned}
&\mathrm{Im}_3^P \left(-\mathrm{i}\,\langle a^*(q_3,\lambda_a)|\gamma^*(-q_1,\lambda_1)\gamma^*(-q_2,\lambda_2)\rangle\right)\\
&= \frac{1}{2}\int \widetilde{\mathrm{d}p}\,\langle \gamma^*(-q_1,\lambda_1)\gamma^*(-q_2,\lambda_2)|P(p)\rangle^*\,\langle a^*(q_3,\lambda_a)|P(p)\rangle\,. \qquad (4.33)
\end{aligned}$$

We relate the two matrix elements to the pseudoscalar transition form factor (TFF) and decay constant, respectively,

$$\begin{aligned}
&\langle \gamma^*(-q_1,\lambda_1)\gamma^*(-q_2,\lambda_2)|P(p)\rangle\\
&= -e^2\epsilon_\mu^{\lambda_1}(-q_1)^*\epsilon_\nu^{\lambda_2}(-q_2)^*\int \mathrm{d}^4x\,\mathrm{d}^4y\,e^{-\mathrm{i}(q_1\cdot x+q_2\cdot y)}\,\langle 0|\,\mathrm{T}\{j^\mu_{\mathrm{em}}(x)j^\nu_{\mathrm{em}}(y)\}\,|P(p)\rangle\\
&= -e^2\epsilon_\mu^{\lambda_1}(-q_1)^*\epsilon_\nu^{\lambda_2}(-q_2)^*\int \mathrm{d}^4x\,\mathrm{d}^4y\,e^{-\mathrm{i}(q_1\cdot x+q_2\cdot y+p\cdot y)}\,\langle 0|\,\mathrm{T}\{j^\mu_{\mathrm{em}}(x-y)j^\nu_{\mathrm{em}}(0)\}\,|P(p)\rangle\\
&= -e^2\epsilon_\mu^{\lambda_1}(-q_1)^*\epsilon_\nu^{\lambda_2}(-q_2)^*\int \mathrm{d}^4x\,\mathrm{d}^4y\,e^{-\mathrm{i}y\cdot(q_1+q_2+p)}e^{-\mathrm{i}x\cdot q_1}\,\langle 0|\,\mathrm{T}\{j^\mu_{\mathrm{em}}(x)j^\nu_{\mathrm{em}}(0)\}\,|P(p)\rangle\\
&= -e^2\epsilon_\mu^{\lambda_1}(-q_1)^*\epsilon_\nu^{\lambda_2}(-q_2)^*(2\pi)^4\delta^{(4)}(q_1+q_2+p)\int \mathrm{d}^4x\,e^{-\mathrm{i}x\cdot q_1}\,\langle 0|\,\mathrm{T}\{j^\mu_{\mathrm{em}}(x)j^\nu_{\mathrm{em}}(0)\}\,|P(p)\rangle\\
&= \mathrm{i}e^2\epsilon_\mu^{\lambda_1}(-q_1)^*\epsilon_\nu^{\lambda_2}(-q_2)^*(2\pi)^4\delta^{(4)}(q_1+q_2+p)\epsilon^{\mu\nu\alpha\beta}q_{1\alpha}q_{2\beta}F_{P\gamma^*\gamma^*}(q_1^2,q_2^2) \qquad (4.34)
\end{aligned}$$

with the TFF definition in Eq. (2.58) generalized to other pseudoscalars and

$$\begin{aligned}
\langle a^*(q_3,\lambda_a)|P(p)\rangle &= -\mathrm{i}g_A\epsilon_\rho^{\lambda_a}(q_3)^*\int \mathrm{d}^4z\,e^{\mathrm{i}q_3\cdot z}\,\langle 0|\,j_5^\rho(z)\,|P(p)\rangle\\
&= -\mathrm{i}g_A\epsilon_\rho^{\lambda_a}(q_3)^*(2\pi)^4\delta^{(4)}(q_3-p)\,\langle 0|\,j_5^\rho(0)\,|P(p)\rangle\\
&= 2g_A\epsilon_\rho^{\lambda_a}(q_3)^*(2\pi)^4\delta^{(4)}(q_3-p)p^\rho\sum_a C_aF_P^a \qquad (4.35)
\end{aligned}$$

with a factor $2C_a$ from the flavor decomposition of the axial current. Inserting this into Eq. (4.33) gives

$$\begin{aligned}
&\mathrm{Im}_3^P\left(-\mathrm{i}e^2g_A(2\pi)^4\delta^{(4)}(q_1+q_2+q_3)\epsilon_\mu^{\lambda_1}(-q_1)\epsilon_\nu^{\lambda_2}(-q_2)\epsilon_\rho^{\lambda_a}(q_3)^*\mathcal{W}^{\mu\nu\rho}(q_1,q_2)\right)\\
&= -\mathrm{i}e^2g_A\epsilon_\mu^{\lambda_1}(-q_1)\epsilon_\nu^{\lambda_2}(-q_2)\epsilon_\rho^{\lambda_a}(q_3)^*(2\pi)^4\delta^{(4)}(q_1+q_2+q_3)\epsilon^{\mu\nu\alpha\beta}q_{1\alpha}q_{2\beta}\\
&\quad\times F_{P\gamma^*\gamma^*}(q_1^2,q_2^2)q_3^\rho\sum_a C_aF_P^a\int\widetilde{\mathrm{d}p}\,(2\pi)^4\delta^{(4)}(q_3-p)\,. \qquad (4.36)
\end{aligned}$$

The TFF is not complex conjugated here due to the analytic continuation to $q_{1/2}^2+\mathrm{i}\epsilon$. The integral is calculated in App. A.1, which leads to

$$\mathrm{Im}_3^P\,\mathcal{W}^{\mu\nu\rho}(q_1,q_2) = 2\epsilon^{\mu\nu\alpha\beta}q_{1\alpha}q_{2\beta}F_{P\gamma^*\gamma^*}(q_1^2,q_2^2)q_3^\rho\sum_a C_aF_P^a\pi\delta(q_3^2-m_P^2)\,. \qquad (4.37)$$

We expand this in q_2 to linear order

$$\begin{aligned}\mathrm{Im}_3^P\,\mathcal{W}^{\mu\nu\rho}(q_1,q_2) &= -2\pi\epsilon^{\mu\nu\alpha\beta}q_{1\alpha}q_{2\beta}q_1^\rho F_{P\gamma^*\gamma^*}(m_P^2,0)\sum_a C_a F_P^a\delta(q_1^2-m_P^2)+\mathcal{O}(q_2^2)\\ &= -2\pi\tau_1^{\mu\nu\rho\sigma}q_{2\sigma}F_{P\gamma^*\gamma^*}(m_P^2,0)\sum_a C_a F_P^a\delta(q_1^2-m_P^2)+\mathcal{O}(q_2^2)\end{aligned}\tag{4.38}$$

and obtain through projection onto the Lorentz structures in the limit $q_2\to 0$

$$\mathrm{Im}^P\,\tilde{\mathcal{W}}_i(q^2) = -2\pi F_{P\gamma^*\gamma^*}(m_P^2,0)\sum_a C_a F_P^a\delta(q^2-m_P^2)\delta_{i1}\,.\tag{4.39}$$

This can be plugged into the dispersion relation Eq. (4.27), from which we obtain the contribution of a single-pseudoscalar intermediate state to the longitudinal scalar function

$$\tilde{\mathcal{W}}_1^P(q^2) = 2\sum_a C_a F_P^a\frac{F_{P\gamma^*\gamma^*}(m_P^2,0)}{q^2-m_P^2}\,.\tag{4.40}$$

The transversal scalar function does not receive a contribution from a single-pseudoscalar intermediate state.

In the chiral limit (and neglecting the gluon anomaly in the singlet case), we have $m_P=0$ and $\sum\limits_P F_P^a F_{P\gamma^*\gamma^*}(0,0)=\frac{N_c}{4\pi^2}\,\mathrm{Tr}(\mathcal{Q}^2\lambda^a)$, which leads to

$$\sum_P\tilde{\mathcal{W}}_1^P(q^2) = \frac{N_c\sum_a C_a\,\mathrm{Tr}(\mathcal{Q}^2\lambda^a)}{2\pi^2q^2} = \frac{2\sum_a C_a\mathcal{A}^{(a)}}{q^2} = \frac{\mathcal{A}}{q^2}\,,\tag{4.41}$$

in agreement with Eq. (4.15). This shows that the pseudoscalar poles defined by this dispersion relation saturate $\tilde{\mathcal{W}}_1(q^2)$ in the chiral limit (and if the gluon anomaly is neglected) for arbitrary q^2 and the sum over all other contributions to $\tilde{\mathcal{W}}_1(q^2)$ has to vanish in this limit.

4.2.2 Axial-vector meson pole

Similar to the pseudoscalar pole, the axial-vector pole can only appear in the discontinuity in q_3^2, see Fig. 4.3. For the contribution to this discontinuity of a narrow axial-vector meson A, treated as an asymptotic state, we find

$$\begin{aligned}&\mathrm{Im}_3^A\left(-\mathrm{i}\,\langle a^*(q_3,\lambda_a)|\gamma^*(-q_1,\lambda_1)\gamma^*(-q_2,\lambda_2)\rangle\right)\\ &\quad=\frac{1}{2}\int\widetilde{\mathrm{d}p}\sum_{\lambda_A}\langle\gamma^*(-q_1,\lambda_1)\gamma^*(-q_2,\lambda_2)|A(p,\lambda_A)\rangle^*\,\langle a^*(q_3,\lambda_a)|A(p,\lambda_A)\rangle\,.\end{aligned}\tag{4.42}$$

The two matrix elements evaluate to

$$\begin{aligned}&\langle\gamma^*(-q_1,\lambda_1)\gamma^*(-q_2,\lambda_2)|A(p,\lambda_A)\rangle\\ &\quad=\mathrm{i}e^2\epsilon_\mu^{\lambda_1}(-q_1)^*\epsilon_\nu^{\lambda_2}(-q_2)^*\epsilon_\alpha^{\lambda_A}(p)(2\pi)^4\delta^{(4)}(q_1+q_2+p)\mathcal{M}^{\mu\nu\alpha}(-q_1,-q_2)\end{aligned}\tag{4.43}$$

and

$$\langle a^*(q_3,\lambda_a)|A(p,\lambda_A)\rangle = -2\mathrm{i}g_A\epsilon_\rho^{\lambda_a}(q_3)^*(2\pi)^4\delta^{(4)}(q_3-p)\sum_a C_a F_A^a m_A \epsilon^{\rho\lambda_M}(p) \tag{4.44}$$

in the notation of Ref. [131].

The polarization sum for the axial meson is given by

$$\sum_{\lambda_M}\epsilon_\alpha^{\lambda_A}(p)^*\epsilon_\beta^{\lambda_A}(p) = -g_{\alpha\beta}+\frac{p_\alpha p_\beta}{m_A^2}\,, \tag{4.45}$$

which leads to

$$\begin{aligned}\mathrm{Im}_3^A\,\mathcal{W}^{\mu\nu\rho}(q_1,q_2) &= -2\mathrm{i}\pi\delta\left((q_1+q_2)^2-m_A^2\right)\sum_a C_a F_A^a m_A \\ &\quad\times\left(-g_\alpha{}^\rho+\frac{(q_1+q_2)_\alpha(q_1+q_2)^\rho}{m_A^2}\right)\mathcal{M}^{\mu\nu\alpha}(-q_1,-q_2)^*\,.\end{aligned} \tag{4.46}$$

Using the decomposition of $\mathcal{M}^{\mu\nu\alpha}(q_1,q_2)$ in terms of TFFs [131], taking into account the analytic continuation to $q_{1/2}^2+\mathrm{i}\epsilon$, which removes the complex conjugation from the TFFs, and expanding in q_2, we arrive at

$$\mathrm{Im}_3^A\,\tilde{\mathcal{W}}_i(q^2) = 2\pi\delta(q^2-m_A^2)\sum_a C_a\frac{F_A^a}{m_A}\mathcal{F}_2^A(m_A^2,0)\delta_{i2}\,. \tag{4.47}$$

Plugging this into the dispersion relation leads to

$$\tilde{\mathcal{W}}_2^A(q^2) = -2\sum_a C_a\frac{F_A^a}{m_A}\frac{\mathcal{F}_2^A(m_A^2,0)}{q^2-m_A^2}\,. \tag{4.48}$$

As opposed to the pseudoscalar poles, the axial poles only contribute to the transversal scalar function.

4.2.3 Vector-meson poles

Vector-meson poles can only contribute to the discontinuity in q_1^2, shown in Fig. 4.4. While the ρ-meson will be described dispersively in terms of two-pion intermediate states discussed in Sec. 4.2.4 below, the very narrow ω and ϕ mesons can be described in a NWA. Together with the axial poles, this is expected to capture the most important effects of three-pion intermediate states in the main process. We first derive the contribution to VVA in terms of the sub-process, where one vector current is replaced by a vector meson, and afterwards dispersively reconstruct this sub-process.

4.2.3.1 Contribution to VVA

The contribution of a vector meson V to the sum over intermediate states in Eq. (4.32) is given by

$$\begin{aligned}&\mathrm{Im}_1^V\left(-\mathrm{i}\left\langle\gamma^*(q_2,\lambda_2)a^*(q_3,\lambda_A)|\gamma^*(-q_1,\lambda_1)\right\rangle\right)\\&\quad=\frac{1}{2}\int\widetilde{\mathrm{d}p}\sum_{\lambda_V}\left\langle\gamma^*(-q_1,\lambda_1)|V(p,\lambda_V)\right\rangle^*\left\langle\gamma^*(q_2,\lambda_2)a^*(q_3,\lambda_a)|V(p,\lambda_V)\right\rangle\,.\end{aligned}\tag{4.49}$$

The first matrix element on the right-hand side evaluates to

$$\left\langle\gamma^*(-q_1,\lambda_1)|V(p,\lambda_V)\right\rangle=-\mathrm{i}e\left(\epsilon^{\lambda_1}(-q_1)^*\cdot\epsilon^{\lambda_V}(p)\right)(2\pi)^4\delta^{(4)}(q_1+p)m_Vf_V\,,\tag{4.50}$$

where the vector decay constant is defined through

$$\langle 0|\,j_\mu(0)\,|V(p,\lambda_V)\rangle=m_Vf_V\epsilon_\mu^{\lambda_V}(p)\,.\tag{4.51}$$

The other matrix element can be written as

$$\begin{aligned}&\left\langle\gamma^*(q_2,\lambda_2)a^*(q_3,\lambda_a)|V(p,\lambda_V)\right\rangle\\&\quad=-eg_A\epsilon_\nu^{\lambda_2}(q_2)^*\epsilon_\rho^{\lambda_a}(q_3)^*(2\pi)^4\delta^{(4)}(q_2+q_3-p)\epsilon_\lambda^{\lambda_V}(p)\mathcal{V}^{\lambda\nu\rho}(-p,q_2)\end{aligned}\tag{4.52}$$

with

$$\epsilon_\lambda^{\lambda_V}(p)\mathcal{V}^{\lambda\nu\rho}(-p,q_2)=\int\mathrm{d}^4x e^{\mathrm{i}q_2\cdot x}\left\langle 0\right|T\{j_{\mathrm{em}}^\nu(x)j_5^\rho(0)\}\left|V(p,\lambda_V)\right\rangle\,.\tag{4.53}$$

The function $\mathcal{V}^{\lambda\rho\nu}(-p,q_2)$ has a similar tensor structure as the VVA correlator. The $U(1)_{\mathrm{em}}$ Ward identity for contraction with p_λ does not hold, but every observable will be contracted with the vector-meson polarization sum, which allows one to drop one structure. One off-shell photon is replaced by an on-shell massive vector meson with $p^2=m_V^2$. Hence, in contrast to the VVA correlator, terms involving $1/p^2=1/m_V^2$ do not constitute kinematic singularities. We obtain the BTT decomposition of the matrix element

$$\mathcal{V}^{\lambda\nu\rho}(-p,q_2)=\sum_{i=0}^{3}t_i^{\lambda\nu\rho}(-p,q_2)\mathcal{V}_i(q_2^2,(p-q_2)^2)\tag{4.54}$$

with the tensor structures

$$\begin{aligned}t_0^{\lambda\nu\rho}(-p,q_2)&=\epsilon^{\lambda\nu\alpha\beta}p_\alpha q_{2\beta}(p-q_2)^\rho=\tau_0^{\lambda\nu\rho}(-p,q_2)\,,\\t_1^{\lambda\nu\rho}(-p,q_2)&=\epsilon^{\lambda\nu\alpha\beta}p_\alpha q_{2\beta}(p+q_2)^\rho=\tau_1^{\lambda\nu\rho}(-p,q_2)\,,\\t_2^{\lambda\nu\rho}(-p,q_2)&=(p\cdot q_2)\epsilon^{\lambda\nu\rho\alpha}q_{2\alpha}-q_2^\lambda\epsilon^{\nu\rho\alpha\beta}p_\alpha q_{2\beta}\\&=\frac{1}{2}\left(\tau_1^{\lambda\nu\rho}(-p,q_2)-\tau_2^{\lambda\nu\rho}(-p,q_2)+\tau_3^{\lambda\nu\rho}(-p,q_2)\right)\,,\\t_3^{\lambda\nu\rho}(-p,q_2)&=\epsilon^{\lambda\nu\rho\alpha}q_{2\alpha}-\frac{\epsilon^{\nu\rho\alpha\beta}p_\alpha q_{2\beta}p^\lambda}{m_V^2}\\&=\frac{1}{2m_V^2}\left(\tau_0^{\lambda\nu\rho}(-p,q_2)-\tau_2^{\lambda\nu\rho}(-p,q_2)-\tau_3^{\lambda\nu\rho}(-p,q_2)\right)\,,\end{aligned}\tag{4.55}$$

which for an on-shell vector meson satisfy

$$\left(g^\mu_\lambda - \frac{p^\mu p_\lambda}{m_V^2}\right) t_i^{\lambda\nu\rho}(-p,q_2) = t_i^{\mu\nu\rho}(-p,q_2)\,. \tag{4.56}$$

In this decomposition, we have already dropped the unphysical additional tensor structure that vanishes upon contraction with the polarization sum. Since the tensor structures are simply linear combinations of the ones in Eq. (4.6), we could have also used those.

Putting everything together, we find

$$\begin{aligned}\mathrm{Im}_1^V\, \mathcal{W}^{\mu\nu\rho}(q_1,q_2) &= \pi\delta(q_1^2 - m_V^2) m_V f_V \mathcal{V}^{\lambda\nu\rho}(q_1,q_2)\left(-g^\mu_\lambda + \frac{q_1^\mu q_{1\lambda}}{m_V^2}\right)\\ &= -\pi\delta(q_1^2 - m_V^2) m_V f_V \mathcal{V}^{\mu\nu\rho}(q_1,q_2)\,,\end{aligned} \tag{4.57}$$

where we have used the polarization sum similar to Eq. (4.45) and the integral calculated in App. A.1.

Therefore, in $g-2$ kinematics we obtain

$$\mathrm{Im}^V\, \tilde{\mathcal{W}}_i(q^2) = -\pi\delta^{(4)}(q^2 - m_V^2) m_V f_V \tilde{\mathcal{V}}_i(0,m_V^2) \tag{4.58}$$

with

$$\begin{aligned}\tilde{\mathcal{V}}_1(0,q^2) &= \mathcal{V}_0(0,q^2) + \mathcal{V}_1(0,q^2) + \frac{1}{m_V^2}\mathcal{V}_3(0,q^2)\,,\\ \tilde{\mathcal{V}}_2(0,q^2) &= -\frac{1}{m_V^2}\mathcal{V}_3(0,q^2)\,.\end{aligned} \tag{4.59}$$

Plugging this into the dispersion relation and assuming that both f_V and $\tilde{\mathcal{V}}_i(0,m_V^2)$ are real, leads to

$$\tilde{\mathcal{W}}_i^V(q^2) = \frac{m_V f_V \tilde{\mathcal{V}}_i(0,m_V^2)}{q^2 - m_V^2}\,. \tag{4.60}$$

In analogy to the other contributions, we can also perform a flavor decomposition of the axial current in $\mathcal{V}^{\lambda\nu\rho}(-p,q_2)$, which gives

$$\tilde{\mathcal{W}}_i^V(q^2) = 2\sum_{a=3,8,0} \frac{m_V f_V C_a \tilde{\mathcal{V}}_i^{(a)}(0,m_V^2)}{q^2 - m_V^2}\,. \tag{4.61}$$

The constants $\tilde{\mathcal{V}}_i^{(a)}(0,m_V^2)$ are unknown. In the following section, we develop a dispersive formalism to evaluate them.

4.2.3.2 Dispersion relations for $\tilde{\mathcal{V}}_i(0,q^2)$

Here, we want to dispersively reconstruct the functions $\tilde{\mathcal{V}}_i(0,q^2)$, where the non-vanishing argument refers to the invariant mass associated with the axial current. In $g-2$ kinematics, i.e. with $q_2 = 0$ in Eq. (4.53), the on-shell vector meson fixes $p^2 = m_V^2$ leaving no free kinematic invariant. A dispersive reconstruction is thus impossible in that limit. Instead, we work with an on-shell photon $q_2^2 = 0$, but do not constrain the individual components of q_2. This makes $q_3^2 = (q_2 - p)^2$ the only unconstrained kinematic variable, in which a dispersion relation can be formulated.

The asymptotic scaling of the form factors $\mathcal{V}_i$ for large space-like virtualities can be worked out using Brodsky–Lepage methods [148, 149, 169], in close analogy to the case of meson TFFs derived in Ref. [131]. Assuming that the scaling [170] $\tilde{\mathcal{V}}_i \asymp 1/q_3^2$ translates into the time-like region, both form factors $\tilde{\mathcal{V}}_{1,2}$ can be described by unsubtracted dispersion relations:

$$\tilde{\mathcal{V}}_i(0, q_3^2) = \frac{1}{\pi} \int \mathrm{d}s \frac{\operatorname{Im} \tilde{\mathcal{V}}_i(0, s)}{s - q_3^2 - \mathrm{i}\epsilon} . \tag{4.62}$$

We consider discontinuities due to pseudoscalar and axial poles. The unitarity relation reads

$$\begin{aligned} &\operatorname{Im} \left[-\mathrm{i} \langle a^*(q_3, \lambda_a) | \gamma(-q_2, \lambda_2) V(p_V, \lambda_V) \rangle\right] \\ &\quad = \sum_n \frac{1}{2S_n} \left(\prod_{i=1}^{N_n} \int \widetilde{\mathrm{d}p_i} \right) \langle \gamma(-q_2, \lambda_2) V(p_V, \lambda_V) | n; \{p_i\} \rangle^* \langle a^*(q_3, \lambda_a) | n; \{p_i\} \rangle \end{aligned} \tag{4.63}$$

and a pseudoscalar meson P contributes

$$\begin{aligned} &\operatorname{Im}^P \left[-\mathrm{i} \langle a^*(q_3, \lambda_a) | \gamma(-q_2, \lambda_2) V(p_V, \lambda_V) \rangle\right] \\ &\quad = \frac{1}{2} \int \widetilde{\mathrm{d}p} \, \langle \gamma(-q_2, \lambda_2) V(p_V, \lambda_V) | P(p) \rangle^* \langle a^*(q_3, \lambda_a) | P(p) \rangle \end{aligned} \tag{4.64}$$

to the sum over intermediate states. The matrix elements take the form (cf. Eq. (4.52))

$$\begin{aligned} &\langle a^*(q_3, \lambda_a) | \gamma(-q_2, \lambda_2) V(p_V, \lambda_V) \rangle \\ &\quad = -e g_A \epsilon_\nu^{\lambda_2}(-q_2) \epsilon_\rho^{\lambda_a}(q_3)^* (2\pi)^4 \delta^{(4)}(q_2 + q_3 - p_V) \epsilon_\lambda^{\lambda_V}(p_V) \mathcal{V}^{\lambda\nu\rho}(-p_V, q_2) \end{aligned} \tag{4.65}$$

and

$$\begin{aligned} &\langle \gamma(-q_2, \lambda_2) V(p_V, \lambda_V) | P(p) \rangle \\ &\quad = -\mathrm{i} e \epsilon_\nu^{\lambda_2}(-q_2)^* (2\pi)^4 \delta^{(4)}(q_2 + p - p_V) \langle V(p_V, \lambda_V) | \, j^\nu(0) \, | P(p) \rangle , \end{aligned} \tag{4.66}$$

and the last one is given in Eq. (4.35). In analogy to the pseudoscalar TFF definition, we write the matrix element in Eq. (4.66) in terms of a single tensor structure

$$\langle V(p_V, \lambda_V) | \, j^\nu(0) \, | P(p) \rangle = \epsilon_\rho^{\lambda_V}(p_V)^* \epsilon^{\rho\nu\alpha\beta} p_{V\alpha} q_{2\beta} F_{VP} \tag{4.67}$$

with $q_2 = p_V - p$ and due to $q_2^2 = 0$, F_{VP} is a constant.

Plugging this in, we find

$$\operatorname{Im}^P \mathcal{V}^{\lambda\nu\rho}(-p_V, q_2) = 2\pi \delta(q_3^2 - m_P^2) \sum_a C_a F_P^a F_{VP} t_0^{\lambda\nu\rho}(-p_V, q_2) \tag{4.68}$$

and therefore

$$\mathrm{Im}^P\,\tilde{\mathcal{V}}_i(0,q_3^2) = 2\pi\delta(q_3^2-m_P^2)\sum_a C_a F_P^a F_{VP}\delta_{i1}\,. \tag{4.69}$$

The dispersion relation then gives

$$\tilde{\mathcal{V}}_i^{P\text{-pole}}(0,q_3^2) = -2\sum_a C_a F_P^a \frac{F_{VP}}{q_3^2-m_P^2}\delta_{i1}\,. \tag{4.70}$$

An axial-vector meson A contributes

$$\begin{aligned}&\mathrm{Im}^A\left[-\mathrm{i}\,\langle a^*(q_3,\lambda_a)|\gamma(-q_2,\lambda_2)V(p_V,\lambda_V)\rangle\right]\\ &\quad=\frac{1}{2}\sum_{\lambda_A}\int\widetilde{\mathrm{d}p}\,\langle\gamma(-q_2,\lambda_2)V(p_V,\lambda_V)|A(p,\lambda_A)\rangle^*\,\langle a^*(q_3,\lambda_a)|A(p,\lambda_A)\rangle\end{aligned} \tag{4.71}$$

to the sum over intermediate states. The matrix elements are given in Eqs. (4.65) and (4.44) as well as

$$\begin{aligned}&\langle\gamma(-q_2,\lambda_2)V(p_V,\lambda_V)|A(p,\lambda_A)\rangle\\ &\quad=-\mathrm{i}e\epsilon_\nu^{\lambda_2}(-q_2)^*(2\pi)^4\delta^{(4)}(p_V-q_2-p)\,\langle V(p_V,\lambda_V)|\,j^\nu(0)\,|A(p,\lambda_A)\rangle\,.\end{aligned} \tag{4.72}$$

We decompose the matrix element on the right-hand side in analogy to Eq. (4.54). Upon contraction with the polarization sum for an on-shell axial-vector meson, the first tensor structure $t_0^{\mu\nu\alpha}$ will project to zero and not contribute to observables. Hence, we can write

$$\langle V(p_V,\lambda_V)|\,j^\nu(0)\,|A(p,\lambda_A)\rangle = -\mathrm{i}\epsilon_\mu^{\lambda_V}(p_V)^*\epsilon_\alpha^{\lambda_A}(p)\sum_{i=1}^3 t_i^{\mu\nu\alpha}(p_V,-q_2)F_{VA}^i\,, \tag{4.73}$$

where $q_2=p_V-p$. As in the pseudoscalar case, F_{VA}^i are constants at $q_2^2=0$.

Combining everything, we obtain

$$\begin{aligned}\mathrm{Im}^A\,\mathcal{V}^{\lambda\nu\rho}(-p_V,q_2) &= 2\pi\delta(q_3^2-m_A^2)\left(-g_\alpha^\rho+\frac{q_{3\alpha}q_3^\rho}{m_A^2}\right)m_A\\ &\quad\times\sum_{i=1}^3 t_i^{\lambda\nu\alpha}(p_V,q_3-p_V)F_{VA}^i\sum_a C_a F_A^a\end{aligned} \tag{4.74}$$

and the projection onto the functions $\tilde{\mathcal{V}}_i$ gives

$$\begin{aligned}\mathrm{Im}^A\,\tilde{\mathcal{V}}_1(0,q_3^2) &= 2\pi\delta(q_3^2-m_A^2)\sum_a C_a F_A^a\frac{m_A^2-m_V^2}{m_A}\left(F_{VA}^1+\frac{1}{2}F_{VA}^2+\frac{F_{VA}^3}{m_V^2}\right),\\ \mathrm{Im}^A\,\tilde{\mathcal{V}}_2(0,q_3^2) &= -2\pi\delta(q_3^2-m_A^2)\sum_a C_a F_A^a\frac{m_A}{m_V^2}F_{VA}^3\,.\end{aligned} \tag{4.75}$$

The dispersion relation then leads to

$$\begin{aligned}\tilde{\mathcal{V}}_1^{A\text{-pole}}(0,q_3^2) &= 2\sum_a C_a F_A^a\frac{1}{m_A}\frac{m_V^2-m_A^2}{q_3^2-m_A^2}\left(F_{VA}^1+\frac{1}{2}F_{VA}^2+\frac{F_{VA}^3}{m_V^2}\right),\\ \tilde{\mathcal{V}}_2^{A\text{-pole}}(0,q_3^2) &= 2\sum_a C_a F_A^a\frac{m_A}{m_V^2}\frac{F_{VA}^3}{q_3^2-m_A^2}\,.\end{aligned} \tag{4.76}$$

The formalism is not predictive with respect to the constants F_{VP} and F^i_{VA}. They can be constrained by measurements of the partial decay widths $\Gamma_{V\to P\gamma}$ and $\Gamma_{A\to P\gamma}$ if available, see Sec. (4.6).

4.2.4 Two-pion intermediate state

The two-pion intermediate state cannot appear in $\mathrm{Im}_3\, \mathcal{W}^{\mu\nu\rho}(q_1,q_2)$ for the following reason. The unitarity relation involves the transition of an axial current to two pions. The corresponding matrix element depends on two momenta and has one uncontracted index. From parity conservation it follows that it has to involve a Levi-Civita tensor. At least three of its indices have to be contracted, but we have only two independent vectors available so that it has to vanish.

There is, however, a two-pion contribution to $\mathrm{Im}_1\, \mathcal{W}^{\mu\nu\rho}(q_1,q_2)$, see Fig. 4.4, which will be discussed in the following. We start with its contribution to the unitarity relation Eq. (4.32)

$$\begin{aligned}
&\mathrm{Im}_1^{\pi^+\pi^-}\left(-\mathrm{i}\,\langle\gamma^*(q_2,\lambda_2)a^*(q_3,\lambda_a)|\gamma^*(-q_1,\lambda_1)\rangle\right)\\
&\quad=\frac{1}{2}\int\widetilde{\mathrm{d}p_1}\widetilde{\mathrm{d}p_2}\,\langle\gamma^*(-q_1,\lambda_1)|\pi^+(p_1)\pi^-(p_2)\rangle^*\,\langle\gamma^*(q_2,\lambda_2)a^*(q_3,\lambda_a)|\pi^+(p_1)\pi^-(p_2)\rangle\ ,
\end{aligned}\tag{4.77}$$

where the photon only couples to a pure isospin $I=1$ $\pi\pi$ state, hence there is no $\pi^0\pi^0$ contribution.

The first matrix element can be related to the pion VFF

$$\begin{aligned}
&\langle\gamma^*(-q_1,\lambda_1)|\pi^+(p_1)\pi^-(p_2)\rangle\\
&\quad=-\mathrm{i}e\epsilon_\mu^{\lambda_1}(-q_1)^*\int\mathrm{d}^4x\,e^{-\mathrm{i}q_1\cdot x}\,\langle 0|\,j^\mu(x)\,|\pi^+(p_1)\pi^-(p_2)\rangle\\
&\quad=-\mathrm{i}e\epsilon_\mu^{\lambda_1}(-q_1)^*(2\pi)^4\delta^{(4)}(q_1+p_1+p_2)\,\langle 0|\,j^\mu(0)\,|\pi^+(p_1)\pi^-(p_2)\rangle\\
&\quad=\mathrm{i}e\epsilon_\mu^{\lambda_1}(-q_1)^*(2\pi)^4\delta^{(4)}(q_1+p_1+p_2)\,\langle\pi^+(-p_2)|\,j^\mu(0)\,|\pi^+(p_1)\rangle\\
&\quad=\mathrm{i}e\epsilon_\mu^{\lambda_1}(-q_1)^*(2\pi)^4\delta^{(4)}(q_1+p_1+p_2)(p_1-p_2)^\mu F_\pi^V\left((p_1+p_2)^2\right)\ ,
\end{aligned}\tag{4.78}$$

where the sign change in the third equation is due to the Condon–Shortley phase convention for the crossing of the charged pion.

With the isospin decomposition of the two-pion state

$$|\pi^+\pi^-\rangle=\frac{1}{\sqrt{6}}\,|2,0\rangle+\frac{1}{\sqrt{2}}\,|1,0\rangle+\frac{1}{\sqrt{3}}\,|0,0\rangle\ ,\tag{4.79}$$

we define the isospin $I=1$ projection

$$|\pi^+\pi^-\rangle_{I=1}=|1,0\rangle\,\langle 1,0|\pi^+\pi^-\rangle=\frac{1}{\sqrt{2}}\,|1,0\rangle\ ,\tag{4.80}$$

which is odd under pion crossing $p_1 \leftrightarrow p_2$. We write the matrix element as

$$\begin{aligned}
&\langle\gamma^*(q_2,\lambda_2)a^*(q_3,\lambda_a)|\pi^+(p_1)\pi^-(p_2)\rangle_{I=1} \\
&= -eg_A\epsilon_\nu^{\lambda_2}(q_2)^*\epsilon_\rho^{\lambda_a}(q_3)^*\int \mathrm{d}^4x\,\mathrm{d}^4y\, e^{\mathrm{i}q_2\cdot x}e^{\mathrm{i}q_3\cdot y}\,\langle 0|\,\mathrm{T}\{j^\nu_{\mathrm{em}}(x)j_5^\rho(y)\}\,|\pi^+(p_1)\pi^-(p_2)\rangle_{I=1} \\
&= -eg_A\epsilon_\nu^{\lambda_2}(q_2)^*\epsilon_\rho^{\lambda_a}(q_3)^*\int \mathrm{d}^4x\, e^{\mathrm{i}q_2\cdot x}(2\pi)^4\delta^{(4)}(q_2+q_3-p_1-p_2) \\
&\qquad \times \langle 0|\,\mathrm{T}\{j^\nu_{\mathrm{em}}(x)j_5^\rho(0)\}\,|\pi^+(p_1)\pi^-(p_2)\rangle_{I=1} \\
&= \mathrm{i}eg_A\epsilon_\nu^{\lambda_2}(q_2)^*\epsilon_\rho^{\lambda_a}(q_3)^*(2\pi)^4\delta^{(4)}(q_2+q_3-p_1-p_2)\mathcal{U}^{\nu\rho}(q_2,p_1,p_2)\,, \qquad (4.81)
\end{aligned}$$

where in the last line we have defined the matrix element

$$\mathcal{U}^{\nu\rho}(q_2,p_1,p_2) = \mathrm{i}\int \mathrm{d}^4x\, e^{\mathrm{i}q_2\cdot x}\,\langle 0|\,\mathrm{T}\{j^\nu_{\mathrm{em}}(x)j_5^\rho(0)\}\,|\pi^+(p_1)\pi^-(p_2)\rangle_{I=1}\,. \qquad (4.82)$$

Plugging the results for the two matrix elements into Eq. (4.77), we arrive at

$$\begin{aligned}
&\mathrm{Im}_1^{\pi^+\pi^-}\,\mathcal{W}^{\mu\nu\rho}(q_1,q_2) \\
&\quad = \frac{\mathrm{i}}{2}\int \widetilde{\mathrm{d}p_1}\widetilde{\mathrm{d}p_2}(2\pi)^4\delta^{(4)}(q_1+p_1+p_2)(p_1-p_2)^\mu F_\pi^V(q_1^2)^*\,\mathcal{U}^{\nu\rho}(q_2,p_1,p_2)\,, \qquad (4.83)
\end{aligned}$$

where we have taken into account that unitarity is used in the q_1^2-channel and thus no analytic continuation of the pion VFF is needed. The pion VFF is well known (see, e.g., Ref. [10]), but the matrix element $\mathcal{U}^{\nu\rho}$ has to be reconstructed dispersively. We will therefore concentrate on this matrix element in the following.

4.2.4.1 Tensor decomposition of the matrix element $\mathcal{U}^{\nu\rho}(q_2,p_1,p_2)$

We start with the tensor decomposition of the function $\mathcal{U}^{\nu\rho}(q_2,p_1,p_2)$ in general kinematics, employing again the BTT recipe. The tensor structures have to contain a Levi-Civita tensor due to conservation of parity. They depend on three independent momenta. Thus, there are nine tensor structures to start with

$$\begin{aligned}
&\{\epsilon^{\nu\rho\alpha\beta}q_{2\alpha}p_{1\beta}\,,\ \epsilon^{\nu\rho\alpha\beta}q_{2\alpha}p_{2\beta}\,,\ \epsilon^{\nu\rho\alpha\beta}p_{1\alpha}p_{2\beta}\,,\ \epsilon^{\nu\alpha\beta\gamma}q_{2\alpha}p_{1\beta}p_{2\gamma}q_2^\rho\,,\ \epsilon^{\nu\alpha\beta\gamma}q_{2\alpha}p_{1\beta}p_{2\gamma}p_1^\rho\,, \\
&\ \epsilon^{\nu\alpha\beta\gamma}q_{2\alpha}p_{1\beta}p_{2\gamma}p_2^\rho\,,\ \epsilon^{\rho\alpha\beta\gamma}q_{2\alpha}p_{1\beta}p_{2\gamma}q_2^\nu\,,\ \epsilon^{\rho\alpha\beta\gamma}q_{2\alpha}p_{1\beta}p_{2\gamma}p_1^\nu\,,\ \epsilon^{\rho\alpha\beta\gamma}q_{2\alpha}p_{1\beta}p_{2\gamma}p_2^\nu\}\,. \qquad (4.84)
\end{aligned}$$

The Ward identity $q_{2\nu}\mathcal{U}^{\nu\rho}(q_2,p_1,p_2)=0$ is implemented by contracting the tensor structures with the gauge projector $g_{\mu\nu}-q_{2\mu}q_{2\nu}/q_2^2$ and then the BTT procedure introduced in Sec. 2.4.1 is applied taking into account the Schouten identities. The tensor structures can be chosen as

$$\begin{aligned}
\{\tau^{\nu\rho}_{\mathcal{U},i}(q_2,p_1,p_2)\} = \{&\epsilon^{\nu\rho\alpha\beta}q_{2\alpha}p_{1\beta}, \epsilon^{\nu\rho\alpha\beta}q_{2\alpha}p_{2\beta}, \epsilon^{\nu\alpha\beta\gamma}q_{2\alpha}p_{1\beta}p_{2\gamma}q_2^\rho, \\
&\epsilon^{\nu\alpha\beta\gamma}q_{2\alpha}p_{1\beta}p_{2\gamma}p_1^\rho, \epsilon^{\nu\alpha\beta\gamma}q_{2\alpha}p_{1\beta}p_{2\gamma}p_2^\rho\} \qquad (4.85)
\end{aligned}$$

and we have checked that these remain independent in all kinematic limits so that no Tarrach structures have to be added. The matrix element $\mathcal{U}$ can thus be written as

$$\mathcal{U}^{\nu\rho}(q_2,p_1,p_2)=\sum_{i=1}^{5}\mathcal{U}_i\left((p_1+p_2)^2,(q_2-p_1)^2;q_2^2,q_3^2\right)\mathrm{i}\tau^{\nu\rho}_{\mathcal{U},i}(q_2,p_1,p_2)\,, \tag{4.86}$$

where $q_3=p_1+p_2-q_2$ is the momentum of the axial current. The scalar functions $\mathcal{U}_i$ are free of kinematic singularities and zeros and depend on the two virtualities and the Mandelstam variables of the process,

$$s=(p_1+p_2)^2\,,\quad t=(p_1-q_2)^2\,,\quad u=(p_2-q_2)^2\,,\quad s+t+u=2M_\pi^2+q_2^2+q_3^2\,. \tag{4.87}$$

Due to the Ward identity, the tensor structures in Eq. (4.85) vanish linearly with q_2. We can thus write them as $\tau^{\nu\rho}_{\mathcal{U},i}(q_2,p_1,p_2)=\tau^{\nu\rho\sigma}_{\mathcal{U},i}(p_1,p_2)q_{2\sigma}+\mathcal{O}(q_2^2)$ with the new tensor structures

$$\{\tau^{\nu\rho\sigma}_{\mathcal{U},i}(p_1,p_2)\}=\{\epsilon^{\nu\rho\sigma\alpha}p_{1\alpha},\epsilon^{\nu\rho\sigma\alpha}p_{2\alpha},0,\epsilon^{\nu\sigma\alpha\beta}p_{1\alpha}p_{2\beta}p_1^\rho,\epsilon^{\nu\sigma\alpha\beta}p_{1\alpha}p_{2\beta}p_2^\rho\} \tag{4.88}$$

There are no linear dependencies between the four non-vanishing structures. Therefore, in this kinematic limit, Eq. (4.86) simplifies to

$$\mathcal{U}^{\nu\rho}(q_2,p_1,p_2)=\sum_{i=1}^{4}\tilde{\mathcal{U}}_i(q_3^2)\mathrm{i}\tilde{\tau}^{\nu\rho\sigma}_{\mathcal{U},i}(p_1,p_2)q_{2\sigma}+\mathcal{O}(q_2^2) \tag{4.89}$$

with

$$\{\tilde{\tau}^{\nu\rho\sigma}_{\mathcal{U},i}(p_1,p_2)\}=\{\tau^{\nu\rho\sigma}_{\mathcal{U},1}(p_1,p_2)\,,\ \tau^{\nu\rho\sigma}_{\mathcal{U},2}(p_1,p_2)\,,\ \tau^{\nu\rho\sigma}_{\mathcal{U},4}(p_1,p_2)\,,\ \tau^{\nu\rho\sigma}_{\mathcal{U},5}(p_1,p_2)\} \tag{4.90}$$

and

$$\tilde{\mathcal{U}}_i(q_3^2):=\tilde{\mathcal{U}}_i(q_3^2,m_\pi^2;0,q_3^2)\,, \tag{4.91}$$

where we have defined

$$\begin{aligned}\tilde{\mathcal{U}}_1(s,t;q_2^2,q_3^2)&:=\mathcal{U}_1(s,t;q_2^2,q_3^2)\,, &\qquad \tilde{\mathcal{U}}_2(s,t;q_2^2,q_3^2)&:=\mathcal{U}_2(s,t;q_2^2,q_3^2)\,,\\ \tilde{\mathcal{U}}_3(s,t;q_2^2,q_3^2)&:=\mathcal{U}_4(s,t;q_2^2,q_3^2)\,, &\qquad \tilde{\mathcal{U}}_4(s,t;q_2^2,q_3^2)&:=\mathcal{U}_5(s,t;q_2^2,q_3^2)\,.\end{aligned} \tag{4.92}$$

Crossing symmetry for the isospin $I=1$ pions implies

$$\begin{aligned}&\mathcal{U}_1(s,t;q_2^2,q_3^2)=-\mathcal{U}_2(s,u;q_2^2,q_3^2)\,, &\qquad &\mathcal{U}_3(s,t;q_2^2,q_3^2)=\mathcal{U}_3(s,u;q_2^2,q_3^2)\,,\\ &\mathcal{U}_4(s,t;q_2^2,q_3^2)=\mathcal{U}_5(s,u;q_2^2,q_3^2)\end{aligned} \tag{4.93}$$

and thus

$$\tilde{\mathcal{U}}_1(q_3^2)=-\tilde{\mathcal{U}}_2(q_3^2)\,,\qquad\qquad \tilde{\mathcal{U}}_3(q_3^2)=\tilde{\mathcal{U}}_4(q_3^2)\,. \tag{4.94}$$

Next, we insert the tensor decomposition Eq. (4.89) into the two-pion contribution to the discontinuity Eq. (4.83). We express the result in terms of the tensor structures $\tau_i^{\mu\nu\rho\sigma}(q_1)$ and read off

$$\begin{aligned}
\mathrm{Im}^{\pi^+\pi^-}\, \tilde{\mathcal{W}}_1(q^2) &= -\frac{1}{12}\int \widetilde{\mathrm{d}p_1}\widetilde{\mathrm{d}p_2}(2\pi)^4\delta^{(4)}(q+p_1+p_2) \\
&\quad\times F_\pi^V(q^2)\sigma_\pi^2(q^2)\left[2\tilde{\mathcal{U}}_1(q^2)^* + q^2\tilde{\mathcal{U}}_3(q^2)^*\right] , \\
\mathrm{Im}^{\pi^+\pi^-}\, \tilde{\mathcal{W}}_2(q^2) &= \frac{1}{6}\int \widetilde{\mathrm{d}p_1}\widetilde{\mathrm{d}p_2}(2\pi)^4\delta^{(4)}(q+p_1+p_2)F_\pi^V(q^2)\sigma_\pi^2(q^2)\tilde{\mathcal{U}}_1(q^2)^*
\end{aligned} \tag{4.95}$$

with $\sigma_\pi(q^2)=\sqrt{1-4m_\pi^2/q^2}$. Here, we made use of the pion-crossing relations and took into account the complex conjugation in Eq. (4.28). With the phase-space integral calculated in App. A.2, we find

$$\begin{aligned}
\mathrm{Im}^{\pi^+\pi^-}\, \tilde{\mathcal{W}}_1(q^2) &= -\frac{1}{96\pi}F_\pi^V(q^2)\sigma_\pi^3(q^2)\left[2\tilde{\mathcal{U}}_1(q^2)^* + q^2\tilde{\mathcal{U}}_3(q^2)^*\right] , \\
\mathrm{Im}^{\pi^+\pi^-}\, \tilde{\mathcal{W}}_2(q^2) &= \frac{1}{48\pi}F_\pi^V(q^2)\sigma_\pi^3(q^2)\tilde{\mathcal{U}}_1(q^2)^* .
\end{aligned} \tag{4.96}$$

4.2.4.2 Dispersion relations

The scalar functions $\tilde{\mathcal{U}}_i(q^2)$ are free of kinematic singularities and thus amenable to a dispersive treatment. The discontinuity can be calculated analogously to Eq. (4.28),

$$\mathrm{Im}\,\tilde{\mathcal{U}}_i(q^2) = \lim_{s\to q^2}\left[\mathrm{Im}_s\tilde{\mathcal{U}}_i(s,m_\pi^2;0,q^2+\mathrm{i}\epsilon) + \left(\mathrm{Im}_3\,\tilde{\mathcal{U}}_i(s+\mathrm{i}\epsilon,m_\pi^2;0,q^2)\right)^*\right] . \tag{4.97}$$

Again, there is a freedom in choosing which of the contributions should be complex conjugated.

We apply Eq. (2.24) to the two q_3^2-channel process $\gamma^*(-q_2,\lambda_2)\pi^+(p_1)\pi^-(p_2)\to a^*(q_3,\lambda_a)$ and the s-channel process $\pi^+(p_1)\pi^-(p_2)\to\gamma^*(q_2,\lambda_2)a^*(q_3,\lambda_a)$ with the two-pions in an isospin $I=1$ state

$$\begin{aligned}
&\mathrm{Im}_3\left(-\mathrm{i}\,\langle a^*(q_3,\lambda_a)|\gamma^*(-q_2,\lambda_2)[\pi^+(p_1)\pi^-(p_2)]_{I=1}\rangle\right) \\
&\quad=\sum_n\frac{1}{2S_n}\left(\prod_{i=1}^{N_n}\int\widetilde{\mathrm{d}p_i}\right)\langle\gamma^*(-q_2,\lambda_2)[\pi^+(p_1)\pi^-(p_2)]_{I=1}|n;\{p_i\}\rangle^*\,\langle a^*(q_3,\lambda_a)|n;\{p_i\}\rangle , \\
&\mathrm{Im}_s\left(-\mathrm{i}\,\langle\gamma^*(q_2,\lambda_2)a^*(q_3,\lambda_a)|\pi^+(p_1)\pi^-(p_2)\rangle_{I=1}\right) \\
&\quad=\sum_n\frac{1}{2S_n}\left(\prod_{i=1}^{n}\int\widetilde{\mathrm{d}p_i}\right)\,{}_{I=1}\langle\pi^+(p_1)\pi^-(p_2)|n;\{p_i\}\rangle^*\,\langle\gamma^*(q_2,\lambda_2)a^*(q_3,\lambda_A)|n;\{p_i\}\rangle .
\end{aligned} \tag{4.98}$$

As before, the $*$ denotes, in addition to complex conjugation, analytic continuation to the upper rim of the cut in all kinematic variables except for the one in which the discontinuity is calculated.

The discontinuity in q_3^2 includes pseudoscalar and axial poles, whereas the discontinuity in $s=(p_1+p_2)^2$ should be dominated at low energies by the two-pion intermediate state. We will discuss these intermediate states next.

4.2.4.3 Pseudoscalar-pole contribution

We single out the pseudoscalar poles in the q_3^2-discontinuity:

$$\begin{aligned}&\mathrm{Im}_3^P\left(-\mathrm{i}\left\langle a^*(q_3,\lambda_a)|\gamma^*(-q_2,\lambda_2)[\pi^+(p_1)\pi^-(p_2)]_{I=1}\right\rangle\right)\\&=\frac{1}{2}\int\widetilde{\mathrm{d}p}\left\langle\gamma^*(-q_2,\lambda_2)\pi^+(p_1)\pi^-(p_2)|P(p)\right\rangle^*\left\langle a^*(q_3,\lambda_a)|P(p)\right\rangle\,.\end{aligned}\tag{4.99}$$

The amplitude for $\gamma^{(*)}\to\pi^+\pi^-\pi^0$ has been studied dispersively in Refs. [11, 18, 171, 172] and the same tensor decomposition applies to $\gamma^{(*)}\to\pi^+\pi^-P$ [127]. We have dropped the isospin-projection label, as due to C-invariance only $I=1$ contributes. This lets us write

$$\begin{aligned}&\left\langle\gamma^*(-q_2,\lambda_2)\pi^+(p_1)\pi^-(p_2)|P(p)\right\rangle\\&=-\mathrm{i}e\epsilon_\nu^{\lambda_2}(-q_2)^*(2\pi)^4\delta^{(4)}(q_2-p_1-p_2+p)\left\langle\pi^+(p_1)\pi^-(p_2)|\,j_{\mathrm{em}}^\nu(0)\,|P(p)\right\rangle\\&=\mathrm{i}e\epsilon_\nu^{\lambda_2}(-q_2)^*(2\pi)^4\delta^{(4)}(q_2-p_1-p_2+p)\epsilon^{\nu\alpha\beta\gamma}p_{1\alpha}p_{2\beta}p_\gamma\\&\quad\times\mathcal{F}_P((p_1+p_2)^2,(q_2-p_2)^2,(q_2-p_1)^2;q_2^2)\,,\end{aligned}\tag{4.100}$$

where the function $\mathcal{F}_P$ is the only scalar amplitude for $\gamma^*\to\pi^+\pi^-P$ and defined through[2]

$$\begin{aligned}&\langle 0|\,j_{\mathrm{em}}^\mu(0)\,|\pi^+(p_+)\pi^-(p_-)P(p_0)\rangle\\&=\epsilon^{\mu\nu\rho\sigma}p_{+\nu}p_{-\rho}p_{0\sigma}\mathcal{F}_P\left((p_++p_-)^2,(p_-+p_0)^2,(p_++p_0)^2;q^2\right)\,.\end{aligned}\tag{4.101}$$

The other matrix element has been evaluated in Eq. (4.35). Plugging this in and keeping only linear terms in q_2, we find[3]

$$\begin{aligned}\mathrm{Im}_3^P\,\mathcal{U}^{\nu\rho}(q_2,p_1,p_2)&=2\pi\sum_a F_P^a\delta(q_3^2-m_P^2)\mathcal{F}_P(m_P^2,m_\pi^2,m_\pi^2;0)\\&\quad\times\left(\mathrm{i}\tilde{\tau}_{\mathcal{U},3}^{\nu\rho\sigma}(p_1,p_2)+\mathrm{i}\tilde{\tau}_{\mathcal{U},4}^{\nu\rho\sigma}(p_1,p_2)\right)q_{2\sigma}+\mathcal{O}(q_2^2)\end{aligned}\tag{4.102}$$

and thus

$$\begin{aligned}&\mathrm{Im}^P\,\tilde{\mathcal{U}}_1(s)=\mathrm{Im}^P\,\tilde{\mathcal{U}}_2(s)=0\,,\\&\mathrm{Im}^P\,\tilde{\mathcal{U}}_3(s)=\mathrm{Im}^P\,\tilde{\mathcal{U}}_4(s)=2\pi\sum_a F_P^a\delta(s-m_P^2)\mathcal{F}_P(m_P^2,m_\pi^2,m_\pi^2;0)\,.\end{aligned}\tag{4.103}$$

For $m_P^2>4m_\pi^2$, the kinematic point at which the function $\mathcal{F}_P$ is needed corresponds to the threshold of the process $\gamma P\to\pi^+\pi^-$. The partial-wave expansion for this process reads [18]

$$\mathcal{F}_P(s,t,u;0)=\sum_{l\text{ odd}}^\infty f_P^l(s,0)P_l'(z)\,,\tag{4.104}$$

[2] Notice the opposite sign compared to the definition in Refs. [11, 18] for $P=\pi^0$. We have checked from a tree-level χPT calculation that our definition leads to a positive normalization.

[3] Again, the analytic continuation implied by the $*$ in the unitarity relation removes the complex conjugation from the function $\mathcal{F}_P$. This only works up to cuts in the $\pi^+\pi^-\gamma^*$-channel, which are, however, of higher order in α and thus neglected. The same applies to the axial pole below.

where z is the cosine of the s-channel scattering angle and P_l' are the derivatives of the Legendre polynomials. Since at threshold

$$f_P^l(s,0) \sim (s-m_P^2)^{l-1}\,, \tag{4.105}$$

only the P-wave amplitude can contribute and we have

$$\mathcal{F}_P(m_P^2,m_\pi^2,m_\pi^2;0) = f_P^1(m_P^2,0)\,. \tag{4.106}$$

This is consistent with the virtual photon coupling only to P-wave two-pion states. If $m_P^2 < 4m_\pi^2$, the same result holds as can be seen by analytic continuation in m_P^2. In the chiral limit (and for the η' also in the large-N_c limit), the value of $f_P^1(m_P^2,0)$ is fixed by the chiral anomaly [18, 171, 173–175]

$$f_P^1(0,0) = \mathcal{F}_P(0,0,0;0) = \frac{N_P}{4\pi^2 F_\pi^3} \tag{4.107}$$

with $N_{\pi^0}=1$, $N_\eta = 1/\sqrt{3}$ and $N_{\eta'} = \sqrt{2/3}$.

4.2.4.4 Axial-pole contribution

We next consider the axial mesons in the sum over intermediate states in the unitarity relation in the axial-vector virtuality

$$\begin{aligned}&\mathrm{Im}_3^A\left(-\mathrm{i}\left\langle a^*(q_3,\lambda_a)|\gamma^*(-q_2,\lambda_2)[\pi^+(p_1)\pi^-(p_2)]_{I=1}\right\rangle\right)\\ &\quad= \frac{1}{2}\int \widetilde{\mathrm{d}p}\sum_{\lambda_A}\left\langle \gamma^*(-q_2,\lambda_2)[\pi^+(p_1)\pi^-(p_2)]_{I=1}|A(p,\lambda_A)\right\rangle^*\left\langle a^*(q_3,\lambda_a)|A(p,\lambda_A)\right\rangle\,.\end{aligned} \tag{4.108}$$

The second matrix element has been evaluated in Eq. (4.44). For the first one, we start by reducing the photon:

$$\begin{aligned}&\left\langle \gamma^*(-q_2,\lambda_2)[\pi^+(p_1)\pi^-(p_2)]_{I=1}|A(p,\lambda_A)\right\rangle\\ &\quad= -\mathrm{i}e\epsilon_\nu^{\lambda_2}(-q_2)^*(2\pi)^4\delta^{(4)}(q_2-p_1-p_2+p)\,{}_{I=1}\!\left\langle \pi^+(p_1)\pi^-(p_2)\right|j_\mathrm{em}^\nu(0)\left|A(p,\lambda_A)\right\rangle\,.\end{aligned} \tag{4.109}$$

The tensor structures can be deduced from those of $\mathcal{U}^{\nu\rho}$, where the only difference is an axial current instead of the axial meson. Thus, as opposed to $\mathcal{U}^{\nu\rho}$, the matrix element ${}_{I=1}\left\langle \pi^+(p_1)\pi^-(p_2)\right|j^\nu(0)\left|A(p,\lambda_M)\right\rangle$ always appears contracted with a polarization sum (cf. Ref. [131]), which projects one linear combination to zero:

$$\left(g_{\alpha\rho}-\frac{q_{3\alpha}q_{3\rho}}{q_3^2}\right)\left(\tau_{\mathcal{U},3}^{\nu\rho}-\tau_{\mathcal{U},4}^{\nu\rho}-\tau_{\mathcal{U},5}^{\nu\rho}\right)=0\,. \tag{4.110}$$

Hence, we can drop the sum of $\tau_{\mathcal{U},4}^{\nu\rho}$ and $\tau_{\mathcal{U},5}^{\nu\rho}$ and keep only the difference:

$$\begin{aligned}&{}_{I=1}\!\left\langle \pi^+(p_1)\pi^-(p_2)\right|j_\mathrm{em}^\nu(0)\left|A(p,\lambda_A)\right\rangle\\ &\quad= -\mathrm{i}\sum_{i=1}^4 \epsilon_\alpha^{\lambda_A}(p)\tau_{A,i}^{\nu\alpha}(q_2,p_1,p_2)\mathcal{F}_{A,i}((p_1+p_2)^2,(q_2-p_2)^2,(q_2-p_1)^2;q_2^2)\end{aligned} \tag{4.111}$$

with

$$\tau_A^{\nu\alpha}(q_2,p_1,p_2) = \{\epsilon^{\nu\alpha\beta\gamma}q_{2\beta}p_{1\gamma}, \epsilon^{\nu\alpha\beta\gamma}q_{2\beta}p_{2\gamma}, q_2^\alpha\epsilon^{\nu\beta\gamma\delta}q_{2\beta}p_{1\gamma}p_{2\delta}, (p_1-p_2)^\alpha\epsilon^{\nu\beta\gamma\delta}q_{2\beta}p_{1\gamma}p_{2\delta}\}\,. \tag{4.112}$$

Due to the restriction to the isospin $I=1$ component of the $\pi\pi$ state, pion-crossing symmetry implies the relations

$$\begin{aligned}
&\mathcal{F}_{A,1}(s,t,u;q_2^2) = -\mathcal{F}_{A,2}(s,u,t;q_2^2)\,,\\
&\mathcal{F}_{A,3}(s,t,u;q_2^2) = \mathcal{F}_{A,3}(s,u,t;q_2^2)\,, \quad \mathcal{F}_{A,4}(s,t,u;q_2^2) = -\mathcal{F}_{A,4}(s,u,t;q_2^2)\,,
\end{aligned} \tag{4.113}$$

and in particular $\mathcal{F}_{A,4}(m_A^2,m_\pi^2,m_\pi^2;0)=0$ for the $g-2$ limit.

This leads to

$$\begin{aligned}
\mathrm{Im}_3^A\,\mathcal{U}^{\nu\rho}(q_2,p_1,p_2) &= -2\pi\delta(q_3^2-m_A^2)\sum_{a=3,8,0}C_aF_A^a m_A\left(g_\alpha{}^\rho - \frac{q_{3\alpha}q_3^\rho}{m_A^2}\right)\\
&\quad\times\sum_{i=1}^4 \mathrm{i}\tau_{A,i}^{\nu\alpha}(q_2,p_1,p_2)\mathcal{F}_{A,i}((p_1+p_2)^2,(q_2-p_2)^2,(q_2-p_1)^2;q_2^2)\,.
\end{aligned} \tag{4.114}$$

Projecting onto the scalar functions $\tilde{\mathcal{U}}_i(q^2)$ in $g-2$ kinematics gives

$$\begin{aligned}
\mathrm{Im}^A\,\tilde{\mathcal{U}}_1(s) &= -\,\mathrm{Im}^A\,\tilde{\mathcal{U}}_2(s) = -2\pi\delta(s-m_A^2)\sum_{a=3,8,0}C_aF_A^a m_A\mathcal{F}_{A,1}(m_A^2,m_\pi^2,m_\pi^2;0)\,,\\
\mathrm{Im}^A\,\tilde{\mathcal{U}}_3(s) &= \mathrm{Im}^A\,\tilde{\mathcal{U}}_4(s) = 4\pi\delta(s-m_A^2)\sum_{a=3,8,0}C_a\frac{F_A^a}{m_A}\mathcal{F}_{A,1}(m_A^2,m_\pi^2,m_\pi^2;0)\,.
\end{aligned} \tag{4.115}$$

The function $\mathcal{F}_{A,3}$, which multiplies a structure quadratic in q_2, drops out in $g-2$ kinematics and, similar to $\mathcal{F}_P$, the function $\mathcal{F}_{A,1}$ is needed only at one particular kinematic point.

In analogy to the pseudoscalar case, we want to express $\mathcal{F}_{A,1}(m_A^2,m_\pi^2,m_\pi^2;0)$ in terms of helicity partial waves. We immediately set $q_2^2=0$ and work in the center-of-mass frame of the pion pair

$$\begin{aligned}
p &= \left(\frac{s+m_A^2}{2\sqrt{s}},0,0,\frac{s-m_A^2}{2\sqrt{s}}\right)\,,\\
q_2 &= \left(\frac{s-m_A^2}{2\sqrt{s}},0,0,-\frac{s-m_A^2}{2\sqrt{s}}\right)\,,\\
p_{1/2} &= \left(\frac{\sqrt{s}}{2},\pm\frac{\sqrt{s}\sigma_\pi(s)}{2}\sin\theta\cos\phi,\pm\frac{\sqrt{s}\sigma_\pi(s)}{2}\sin\theta\sin\phi,\pm\frac{\sqrt{s}\sigma_\pi(s)}{2}\cos\theta\right)\,.
\end{aligned} \tag{4.116}$$

The polarization vectors take the form

$$\begin{aligned}
\epsilon^\pm(p) &= \mp\frac{1}{\sqrt{2}}(0,1,\pm\mathrm{i},0)\,,\\
\epsilon^0(p) &= \left(\frac{s-m_A^2}{2\sqrt{s}m_A},0,0,\frac{s+m_A^2}{2\sqrt{s}m_A}\right)\,,\\
\epsilon^\pm(q_2) &= \mp\frac{1}{\sqrt{2}}(0,1,\mp\mathrm{i},0)\,.
\end{aligned} \tag{4.117}$$

We define helicity amplitudes for $A(p)\gamma(q_2) \to \pi^+(p_1)\pi^-(p_2)$ as

$$H_{\lambda_2\lambda_A} = \epsilon_\nu^{\lambda_2}(q_2)\ {}_{I=1}\langle\pi^+(p_1)\pi^-(p_2)|\, j^\nu_{\text{em}}(0)\, |A(p,\lambda_A)\rangle\ . \tag{4.118}$$

For $q_2^2 = 0$ there is one redundancy in the set of tensor structures and we can thus write

$${}_{I=1}\langle\pi^+(p_1)\pi^-(p_2)|\, j^\nu_{\text{em}}(0)\, |A(p,\lambda_A)\rangle = -\mathrm{i}\sum_{i=1,2,4} \epsilon_\alpha^{\lambda_A}(p)\tau_{A,i}^{\nu\alpha}(q_2,p_1,p_2)\tilde{\mathcal{F}}_{A,i}(s,t,u)\,, \tag{4.119}$$

where $s=(p_1+p_2)^2$, $t=(q_2-p_2)^2$ and $u=(q_2-p_1)^2$. The relation between these scalar functions and the previous ones is given by

$$\begin{aligned}
\tilde{\mathcal{F}}_{A,1}(s,t,u) &= \mathcal{F}_{A,1}(s,t,u;0) + (m_\pi^2 - t)\mathcal{F}_{A,3}(s,t,u;0)\,,\\
\tilde{\mathcal{F}}_{A,2}(s,t,u) &= \mathcal{F}_{A,2}(s,t,u;0) - (m_\pi^2 - u)\mathcal{F}_{A,3}(s,t,u;0)\,,\\
\tilde{\mathcal{F}}_{A,4}(s,t,u) &= \mathcal{F}_{A,4}(s,t,u;0)\,.
\end{aligned} \tag{4.120}$$

We need the scalar functions at threshold, where $t=u=m_\pi^2$ and thus the contribution from $\mathcal{F}_{A,3}$ drops out, $\mathcal{F}_i(m_A^2,m_\pi^2,m_\pi^2;0) = \tilde{\mathcal{F}}_i(m_A^2,m_\pi^2,m_\pi^2)$ for $i=1,2,4$.

Expressing the three independent helicity amplitudes in terms of these scalar functions and inverting the system, we find

$$\begin{aligned}
\tilde{\mathcal{F}}_{A,1} &= \frac{2\mathrm{i}}{s-m_A^2}\Bigg[H_{++} + \frac{\sqrt{2}m_A(1-z\sigma_\pi(s))}{\sqrt{s}\sigma_\pi(s)\sqrt{1-z^2}}e^{\mathrm{i}\phi}H_{+0}\\
&\qquad + \frac{s\sigma_\pi(s)-(s+m_A^2)z+m_A^2\sigma_\pi(s)z^2}{s\sigma_\pi(s)(1-z^2)}e^{2\mathrm{i}\phi}H_{+-}\Bigg]\,,\\
\tilde{\mathcal{F}}_{A,2} &= \frac{2\mathrm{i}}{s-m_A^2}\Bigg[H_{++} - \frac{\sqrt{2}m_A(1+z\sigma_\pi(s))}{\sqrt{s}\sigma_\pi(s)\sqrt{1-z^2}}e^{\mathrm{i}\phi}H_{+0}\\
&\qquad + \frac{s\sigma_\pi(s)+(s+m_A^2)z+m_A^2\sigma_\pi(s)z^2}{s\sigma_\pi(s)(1-z^2)}e^{2\mathrm{i}\phi}H_{+-}\Bigg]\,,\\
\tilde{\mathcal{F}}_{A,4} &= -\frac{8\mathrm{i}}{s(s-m_A^2)\sigma_\pi^2(s)(1-z^2)}e^{2\mathrm{i}\phi}H_{+-}
\end{aligned} \tag{4.121}$$

with $z=\cos\theta = (t-u)/\sigma_\pi(s)/(s-m_A^2)$. Next, we insert the partial wave expansions for the helicity amplitudes, which take the form [176]

$$\begin{aligned}
H_{++} &= \sum_{l=0}^\infty D^l_{00}(\phi,\theta,-\phi)\tilde{h}^l_{++}(s) = \sum_{l=0}^\infty P_l(z)h^l_{++}(s)\,,\\
H_{+0} &= \sum_{l=1}^\infty D^l_{-1\,0}(\phi,\theta,-\phi)\tilde{h}^l_{+0}(s) = e^{-\mathrm{i}\phi}\sqrt{1-z^2}\sum_{l=1}^\infty P_l'(z)h^l_{+0}(s)\,,\\
H_{+-} &= \sum_{l=2}^\infty D^l_{-2\,0}(\phi,\theta,-\phi)\tilde{h}^l_{+-}(s) = e^{-2\mathrm{i}\phi}(1-z)^2\sum_{l=2}^\infty P_l''(z)h^l_{+-}(s)\,,
\end{aligned} \tag{4.122}$$

where

$$\begin{aligned}
h^l_{++}(s) &= \tilde{h}^l_{++}(s)\,, \\
h^l_{+0}(s) &= -\frac{\tilde{h}^l_{+0}(s)}{\sqrt{l(l+1)}}\,, \\
h^l_{+-}(s) &= \frac{\tilde{h}^l_{+-}(s)}{\sqrt{(l-1)l(l+1)(l+2)}}\,,
\end{aligned} \tag{4.123}$$

and lead to

$$\begin{aligned}
\tilde{\mathcal{F}}_{A,1} &= \frac{2\mathrm{i}}{s-m_A^2}\sum_{l\text{ odd}}\Bigg[P_l(z)h^l_{++}(s) + \frac{\sqrt{2}m_A(1-z\sigma_\pi(s))}{\sqrt{s}\sigma_\pi(s)}P_l'(z)h^l_{+0}(s) \\
&\qquad + \frac{s\sigma_\pi(s)-(s+m_A^2)z+m_A^2\sigma_\pi(s)z^2}{s\sigma_\pi(s)}P_l''(z)h^l_{+-}(s)\Bigg]\,, \\
\tilde{\mathcal{F}}_{A,2} &= \frac{2\mathrm{i}}{s-m_A^2}\sum_{l\text{ odd}}\Bigg[P_l(z)h^l_{++}(s) - \frac{\sqrt{2}m_A(1+z\sigma_\pi(s))}{\sqrt{s}\sigma_\pi(s)}P_l'(z)h^l_{+0}(s) \\
&\qquad + \frac{s\sigma_\pi(s)+(s+m_A^2)z+m_A^2\sigma_\pi(s)z^2}{s\sigma_\pi(s)}P_l''(z)h^l_{+-}(s)\Bigg]\,, \\
\tilde{\mathcal{F}}_{A,4} &= -\frac{8\mathrm{i}}{s(s-m_A^2)\sigma_\pi^2(s)}\sum_{l\text{ odd}}P_l''(z)h^l_{+-}(s)\,,
\end{aligned} \tag{4.124}$$

where we have used that the crossing relations for $I=1$ pions Eq. (4.113) forbid even partial waves.

Since the functions $\tilde{\mathcal{F}}_{A,i}$ are free of kinematic singularities, the poles at $s=m_A^2$ due to the explicit pre-factors and the factors of z have to be accompanied by zeros in the helicity partial-wave amplitudes $h^l_{ab}(s)$. This requires

$$h^l_{ab}(s) = (s-m_A^2)^l g^l_{ab}(s) \tag{4.125}$$

with $g^l_{ab}(s)$ regular at $s=m_A^2$, but for each l one linear combination of $g^l_{ab}(m_A^2)$ has to vanish.[4] For $l=1$, the constraint reads

$$g^1_{++}(m_A^2) = \sqrt{2}g^1_{+0}(m_A^2)\,. \tag{4.126}$$

At threshold in addition $t=u$ holds, so only terms of order z^0 can contribute and we find

$$\begin{aligned}
\mathcal{F}_{A,1/2}(m_A^2,m_\pi^2,m_\pi^2;0) &= \tilde{\mathcal{F}}_{A,1/2}(m_A^2,m_\pi^2,m_\pi^2) = \pm\frac{2\sqrt{2}\,\mathrm{i}g^1_{+0}(m_A^2)}{\sigma_\pi(m_A^2)}\,, \\
\mathcal{F}_{A,4}(m_A^2,m_\pi^2,m_\pi^2;0) &= \tilde{\mathcal{F}}_{A,4}(m_A^2,m_\pi^2,m_\pi^2) = 0\,,
\end{aligned} \tag{4.127}$$

which only gets a P-wave contribution as expected since the pion pair couples to an off-shell photon and agrees with the previous conclusion that $\mathcal{F}_{A,4}$ vanishes at threshold.

[4] $\tilde{\mathcal{F}}_{A,1}$ and $\tilde{\mathcal{F}}_{A,2}$ give the same linear combinations since they are related to each other by $z \leftrightarrow -z$.

4.2.4.5 Two-pion rescattering

The lowest-lying cut with respect to the variable s is due to a two-pion state. Again, this state has to have isospin $I=1$ and thus only charged pions contribute. Singling out this state in Eq. (4.98) gives

$$\begin{aligned}
&\mathrm{Im}_s^{\pi^+\pi^-}\left(-\mathrm{i}\,\langle\gamma^*(q_2,\lambda_2)a^*(q_3,\lambda_a)|\pi^+(p_1)\pi^-(p_2)\rangle_{I=1}\right) \\
&\quad=\frac{1}{2}\int\widetilde{\mathrm{d}k}_1\widetilde{\mathrm{d}k}_2\;{}_{I=1}\langle\pi^+(p_1)\pi^-(p_2)|\pi^+(k_1)\pi^-(k_2)\rangle^*_{I=1} \\
&\qquad\times\langle\gamma^*(q_2,\lambda_2)a^*(q_3,\lambda_a)|\pi^+(k_1)\pi^-(k_2)\rangle_{I=1} \\
&\quad=\frac{1}{4}\int\widetilde{\mathrm{d}k}_1\widetilde{\mathrm{d}k}_2\,\langle 1,0(p_1,p_2)|1,0(k_1,k_2)\rangle^*\,\langle\gamma^*(q_2,\lambda_2)a^*(q_3,\lambda_a)|\pi^+(k_1)\pi^-(k_2)\rangle_{I=1} \\
&\quad=\frac{1}{4}\int\widetilde{\mathrm{d}k}_1\widetilde{\mathrm{d}k}_2(-\mathrm{i})(2\pi)^4\delta^{(4)}(k_1+k_2-p_1-p_2)\mathcal{T}^{(1)}(k_1,k_2\to p_1,p_2)^* \\
&\qquad\times\,\mathrm{i}eg_A\epsilon_\nu^{\lambda_2}(q_2)^*\epsilon_\rho^{\lambda_a}(q_3)^*(2\pi)^4\delta^{(4)}(q_2+q_3-k_1-k_2)\mathcal{U}^{\nu\rho}(q_2,k_1,k_2)\,.
\end{aligned}\tag{4.128}$$

In the second line we used that $\pi\pi$ scattering preserves isospin, in the third line we made use of Eq. (4.80), and in the last line we inserted the definition of the $I=1$ $\pi\pi$-scattering amplitude and Eq. (4.81). The * on the matrix element implies complex conjugation of the $\pi\pi$-scattering amplitude. Analytic continuation is not an issue since cuts in crossed channels are outside the region needed below.

This implies

$$\begin{aligned}
\mathrm{Im}_s^{\pi^+\pi^-}\mathcal{U}^{\nu\rho}(q_2,p_1,p_2)=\frac{1}{4}\int&\widetilde{\mathrm{d}k}_1\widetilde{\mathrm{d}k}_2(2\pi)^4\delta^{(4)}(q_2+q_3-k_1-k_2) \\
&\times\mathcal{T}^{(1)}(k_1,k_2\to p_1,p_2)^*\mathcal{U}^{\nu\rho}(q_2,k_1,k_2)\,.
\end{aligned}\tag{4.129}$$

The $\pi\pi$-scattering amplitude can be expanded into partial waves and the phase of each partial wave is denoted by $\delta_l^1(s)$. For isospin $I=1$, only odd partial waves contribute:

$$\begin{aligned}
\mathcal{T}^{(1)}(k_1,k_2\to p_1,p_2)&=\mathcal{T}^{(1)}(s,\cos\theta') \\
&=\sum_{l\text{ odd}}(2l+1)P_l(\cos\theta')t_l^1(s) \\
&=\sum_{l\text{ odd}}(2l+1)P_l(\cos\theta')|t_l^1(s)|e^{\mathrm{i}\delta_l^1(s)}\,,
\end{aligned}\tag{4.130}$$

where θ' is the angle between $\vec{p}_1$ and $\vec{k}_1$ in the $\pi\pi$ center-of-mass frame.

The 4-dimensional δ-function allows us to immediately perform 4 of the 6 integrals

$$\begin{aligned}
&\mathrm{Im}_s^{\pi^+\pi^-}\mathcal{U}^{\nu\rho}(q_2,p_1,p_2) \\
&\quad=\frac{1}{4}\sum_{l\text{ odd}}(2l+1)|t_l^1(s)|e^{-\mathrm{i}\delta_l^1(s)}\int\mathrm{d}\tilde{k}_1\,\mathrm{d}\tilde{k}_2(2\pi)^4\delta^{(4)}(q_2+q_3-k_1-k_2) \\
&\qquad\times P_l(\cos\theta')\mathcal{U}^{\nu\rho}(q_2,k_1,k_2) \\
&\quad=\frac{1}{128\pi^2}\sum_{l\text{ odd}}(2l+1)|t_l^1(s)|e^{-\mathrm{i}\delta_l^1(s)}\sigma_\pi(s)\int\mathrm{d}\Omega' P_l(\cos\theta')\mathcal{U}^{\nu\rho}(q_2,k_1,k_2)\,,
\end{aligned}\tag{4.131}$$

where the complex conjugation reverses the sign in the exponential.

Next, we expand the right-hand side in q_2 to linear order. Since $\mathcal{U}^{\nu\rho}(q_2,k_1,k_2)$ vanishes linearly for $q_2 \to 0$, we can replace s by q_3^2 in the other terms. We find

$$\begin{aligned}
\mathrm{Im}_s^{\pi^+\pi^-}\, \mathcal{U}^{\nu\rho}(q_2,p_1,p_2) = \frac{\mathrm{i}}{128\pi^2} \sum_{l\text{ odd}} &(2l+1)|t_l^1(q_3^2)|e^{-\mathrm{i}\delta_l^1(q_3^2)}\sigma_\pi(q_3^2)q_{2\sigma}\int \mathrm{d}\Omega' P_l(\cos\theta') \\
&\times \left(\tilde{\mathcal{U}}_1(q_3^2)\epsilon^{\nu\rho\sigma\alpha}(k_1-k_2)_\alpha + \tilde{\mathcal{U}}_3(q_3^2)(k_1+k_2)^\rho\epsilon^{\nu\sigma\alpha\beta}k_{1\alpha}k_{2\beta}\right) \\
&+\mathcal{O}(q_2^2)\,,
\end{aligned} \tag{4.132}$$

where we used crossing symmetry for the pions. We project this onto the tensor structures of $\mathcal{U}^{\nu\rho}(q_2,p_1,p_2)$ in $g-2$ kinematics given in Eq. (4.90):

$$\begin{aligned}
\mathrm{Im}^{\pi^+\pi^-}\, \tilde{\mathcal{U}}_i(s) &= \frac{1}{128\pi^2}\sum_{l\text{ odd}} |t_l^1(s)|e^{-\mathrm{i}\delta_l^1(s)}\sigma_\pi(s)\tilde{\mathcal{U}}_i(s)(2l+1)\int \mathrm{d}\Omega' P_l(\cos\theta')\cos\theta' \\
&= \frac{1}{32\pi}|t_1^1(s)|e^{-\mathrm{i}\delta_1^1(s)}\sigma_\pi(s)\tilde{\mathcal{U}}_i(s)\,.
\end{aligned} \tag{4.133}$$

We observe that—as expected—only the P-wave $\pi\pi$-scattering amplitude contributes.

Neglecting inelastic effects, unitarity for $\pi\pi$ scattering implies

$$|t_1^1(s)| = \frac{32\pi}{\sigma_\pi(s)}\sin\delta_1^1(s) \tag{4.134}$$

and thus

$$\mathrm{Im}^{\pi^+\pi^-}\, \tilde{\mathcal{U}}_i(s) = \sin\delta_1^1(s)e^{-\mathrm{i}\delta_1^1(s)}\tilde{\mathcal{U}}_i(s)\,. \tag{4.135}$$

4.2.4.6 Solution of the dispersion relations

In the absence of contributions to the discontinuity of $\tilde{\mathcal{U}}_i$ other than the two-pion rescattering, Eq. (4.135) would represent a homogeneous Omnès problem solved by the Omnès function

$$\Omega_1^1(s) = \exp\left\{\frac{s}{\pi}\int_{4m_\pi^2}^\infty \mathrm{d}s' \frac{\delta_1^1(s')}{s'(s'-s)}\right\} \tag{4.136}$$

multiplied by an arbitrary polynomial [177]. The inhomogeneous problem arising if pseudoscalar and axial poles are included can be solved by considering

$$\begin{aligned}
\mathrm{Im}\left(\frac{\tilde{\mathcal{U}}_i(s)}{\Omega_1^1(s)}\right) &= \frac{1}{2\mathrm{i}}\left(\frac{\tilde{\mathcal{U}}_i(s+\mathrm{i}\epsilon)}{\Omega_1^1(s+\mathrm{i}\epsilon)} - \frac{\tilde{\mathcal{U}}_i(s-\mathrm{i}\epsilon)}{\Omega_1^1(s-\mathrm{i}\epsilon)}\right) \\
&= \frac{\tilde{\mathcal{U}}_i(s+\mathrm{i}\epsilon)e^{-\mathrm{i}\delta_1^1(s)} - \tilde{\mathcal{U}}_i(s-\mathrm{i}\epsilon)e^{\mathrm{i}\delta_1^1(s)}}{2\mathrm{i}|\Omega_1^1(s)|} \\
&= \frac{-\tilde{\mathcal{U}}_i(s)\sin\delta_1^1(s) + e^{\mathrm{i}\delta_1^1(s)}\Delta\tilde{\mathcal{U}}_i(s)}{|\Omega_1^1(s)|}\,.
\end{aligned} \tag{4.137}$$

Writing the discontinuity of $\tilde{\mathcal{U}}_i(s)$ as

$$\mathrm{Im}\tilde{\mathcal{U}}_i(s) = \mathrm{Im}^{\pi^+\pi^-}\tilde{\mathcal{U}}_i(s) + I_i(s) = \sin\delta_1^1(s)e^{-\mathrm{i}\delta_1^1(s)}\tilde{\mathcal{U}}_i(s) + I_i(s)\,, \tag{4.138}$$

this simplifies to

$$\mathrm{Im}\left(\frac{\tilde{\mathcal{U}}_i(s)}{\Omega_1^1(s)}\right) = \frac{e^{\mathrm{i}\delta_1^1(s)}I_i(s)}{|\Omega_1^1(s)|}\,, \tag{4.139}$$

which can be solved by a standard dispersion relation.

Before doing that, we have to discuss the asymptotic behavior of the $\tilde{\mathcal{U}}_i$. The mass dimension of $\tilde{\mathcal{U}}_3$ is two units lower than that of $\tilde{\mathcal{U}}_1$ and it is thus expected that it falls off faster asymptotically by one power of q^2. We assume $\tilde{\mathcal{U}}_1(q^2) = \mathcal{O}(1/q^2)$ and $\tilde{\mathcal{U}}_3(q^2) = \mathcal{O}(1/q^4)$. Since we use a phase-shift that approaches π, the Omnès function Eq. (4.136) behaves as $1/q^2$, which means that one subtraction is required for $\tilde{\mathcal{U}}_1$ whereas an unsubtracted dispersion relation holds for $\tilde{\mathcal{U}}_3$

$$\begin{aligned}
\tilde{\mathcal{U}}_1(q^2) &= \Omega_1^1(q^2)\left[\tilde{\mathcal{U}}_1(0) + \frac{q^2}{\pi}\int_{4m_\pi^2}^\infty \mathrm{d}s\frac{e^{\mathrm{i}\delta_1^1(s)}I_1(s)}{s|\Omega_1^1(s)|(s-q^2-\mathrm{i}\epsilon)}\right]\,,\\
\tilde{\mathcal{U}}_3(q^2) &= \Omega_1^1(q^2)\frac{1}{\pi}\int_{4m_\pi^2}^\infty \mathrm{d}s\frac{e^{\mathrm{i}\delta_1^1(s)}I_3(s)}{|\Omega_1^1(s)|(s-q^2-\mathrm{i}\epsilon)}\,.
\end{aligned} \tag{4.140}$$

The value of the subtraction constant $\tilde{\mathcal{U}}_1(0)$ will be determined from a tree-level χPT calculation in the next section.

The inhomogeneity $I_i(s)$ is due to pseudoscalar and axial poles. Eqs. (4.103) and (4.115) together with Eq. (4.97) imply

$$\begin{aligned}
I_1(s) &= -2\pi\sum_A\sum_a C_aF_A^a m_A\delta(s-m_A^2)\mathcal{F}_{A,1}(m_A^2,m_\pi^2,m_\pi^2;0)^*\,,\\
I_3(s) &= 2\pi\sum_P\sum_a C_aF_P^a\delta(s-m_P^2)\mathcal{F}_P(m_P^2,m_\pi^2,m_\pi^2;0)^*\\
&\quad+4\pi\sum_A\sum_a C_aF_A^a m_A^{-1}\delta(s-m_A^2)\mathcal{F}_{A,1}(m_A^2,m_\pi^2,m_\pi^2;0)^*\,,
\end{aligned} \tag{4.141}$$

where the sums run over all contributing pseudoscalar and axial mesons. Therefore, we obtain

$$\begin{aligned}
\tilde{\mathcal{U}}_1(q^2) &= -\Omega_1^1(q^2)\left[\tilde{\mathcal{U}}_1(0) + \frac{q^2}{\pi}\int\mathrm{d}s\sum_A\frac{e^{\mathrm{i}\delta_1^1(s)}2\pi\delta(s-m_A^2)\sum_a C_aF_A^a m_A\mathcal{F}_{A,1}^*}{s|\Omega_1^1(s)|(s-q^2-\mathrm{i}\epsilon)}\right]\\
&= \Omega_1^1(q^2)\left[\tilde{\mathcal{U}}_1(0) + 2\sum_A\frac{q^2\sum_a C_aF_A^a m_A\mathcal{F}_{A,1}^*}{m_A^2\Omega_1^1(m_A^2)^*(q^2-m_A^2)}\right]\,,\\
\tilde{\mathcal{U}}_3(q^2) &= \Omega_1^1(q^2)\left[-\frac{1}{\pi}\int\mathrm{d}s\sum_P\frac{e^{\mathrm{i}\delta_1^1(s)}(-2\pi)\delta(s-m_P^2)\sum_a C_aF_P^a\mathcal{F}_P^*}{|\Omega_1^1(s)|(s-q^2-\mathrm{i}\epsilon)}\right.\\
&\quad\left.+\frac{1}{\pi}\int\mathrm{d}s\sum_A\frac{e^{\mathrm{i}\delta_1^1(s)}4\pi\delta(s-m_A^2)\sum_a C_aF_A^a m_A^{-1}\mathcal{F}_{A,1}^*}{|\Omega_1^1(s)|(s-q^2-\mathrm{i}\epsilon)}\right]
\end{aligned}$$

$$= \Omega_1^1(q^2)\left[-2\sum_P \frac{\sum_a C_a F_P^a \mathcal{F}_P^*}{\Omega_1^1(m_P^2)^*(q^2-m_P^2)} - 4\sum_A \frac{\sum_a C_a F_A^a \mathcal{F}_{A,1}^*}{m_A\Omega_1^1(m_A^2)^*(q^2-m_A^2)}\right] \tag{4.142}$$

with the abbreviations $\mathcal{F}_P = \mathcal{F}_P(m_P^2, m_\pi^2, m_\pi^2; 0)$ and $\mathcal{F}_{A,1} = \mathcal{F}_{A,1}(m_A^2, m_\pi^2, m_\pi^2; 0)$.

Finally, we plug this into Eq. (4.96) to obtain the contribution of the two-pion intermediate state to the VVA correlator

$$\begin{aligned}
\mathrm{Im}^{\pi^+\pi^-}\tilde{\mathcal{W}}_1(q^2) &= -\frac{1}{48\pi}F_\pi^V(q^2)\sigma_\pi^3(q^2)\Omega_1^1(q^2)^*\tilde{\mathcal{U}}_1(0) \\
&\quad + \frac{1}{48\pi}\sum_P \frac{q^2F_\pi^V(q^2)\sigma_\pi^3(q^2)\Omega_1^1(q^2)^*}{q^2-m_P^2}\sum_a C_a F_P^a \frac{\mathcal{F}_P}{\Omega_1^1(m_P^2)}\,, \\
\mathrm{Im}^{\pi^+\pi^-}\tilde{\mathcal{W}}_2(q^2) &= \frac{1}{48\pi}F_\pi^V(q^2)\sigma_\pi^3(q^2)\Omega_1^1(q^2)^*\tilde{\mathcal{U}}_1(0) \\
&\quad + \frac{1}{24\pi}\sum_A \frac{F_\pi^V(q^2)\sigma_\pi^3(q^2)\Omega_1^1(q^2)^*}{q^2-m_A^2}\sum_a C_a F_A^a m_A \frac{\mathcal{F}_{A,1}}{\Omega_1^1(m_A^2)}
\end{aligned} \tag{4.143}$$

and thus, using Eq. (4.27),

$$\begin{aligned}
\tilde{\mathcal{W}}_1^{\pi^+\pi^-}(q^2) &= -\frac{1}{48\pi^2}\int_{4m_\pi^2}^\infty \mathrm{d}s\frac{F_\pi^V(s)\sigma_\pi^3(s)\Omega_1^1(s)^*\tilde{\mathcal{U}}_1(0)}{s-q^2-i\epsilon} \\
&\quad + \frac{1}{48\pi^2}\sum_P\int_{4m_\pi^2}^\infty \mathrm{d}s\frac{sF_\pi^V(s)\sigma_\pi^3(s)\Omega_1^1(s)^*}{(s-q^2-i\epsilon)(s-m_P^2-i\epsilon)}\sum_a C_a F_P^a\frac{\mathcal{F}_P}{\Omega_1^1(m_P^2)}\,, \\
\tilde{\mathcal{W}}_2^{\pi^+\pi^-}(q^2) &= \frac{1}{48\pi^2}\int_{4m_\pi^2}^\infty \mathrm{d}s\frac{F_\pi^V(s)\sigma_\pi^3(s)\Omega_1^1(s)^*\tilde{\mathcal{U}}_1(0)}{s-q^2-i\epsilon} \\
&\quad + \frac{1}{24\pi^2}\sum_A\int_{4m_\pi^2}^\infty \mathrm{d}s\frac{sF_\pi^V(s)\sigma_\pi^3(s)\Omega_1^1(s)^*}{(s-q^2-i\epsilon)(s-m_A^2-i\epsilon)}\sum_a C_a\frac{F_A^a\mathcal{F}_{A,1}}{m_A\Omega_1^1(m_A^2)}\,,
\end{aligned} \tag{4.144}$$

where we have included the iϵ again to specify the integration contour for $m_{P/A}^2 > 4m_\pi^2$. Interestingly, the axial-meson contributions to the first scalar function have exactly canceled between $\tilde{\mathcal{U}}_1$ and $\tilde{\mathcal{U}}_3$. This is only achieved if $\tilde{\mathcal{U}}_1$ is subtracted once more than $\tilde{\mathcal{U}}_3$.

4.2.4.7 Fixing the subtraction constant from χPT

We now calculate the functions $\tilde{\mathcal{U}}_i$ at leading order in χPT, which will allow us to fix the subtraction constant $\tilde{\mathcal{U}}_1(0)$. Since in the numerical study we focus on the isovector component, we do the same here. This allows us to restrict the Lagrangian to the $SU(2)$ case. We use the leading-order odd-parity Lagrangian coupled to external currents [174], which can be found e.g. in Ref. [178]. There are two diagrams: the $j_{\mathrm{em}}j_5\pi^+\pi^-$ contact interaction and the $j_{\mathrm{em}}\pi^+\pi^-\pi^0$ vertex with subsequent mixing of the neutral pion with the axial current. Each of them contributes to only one scalar function. In the soft-photon limit, we obtain

$$\tilde{\mathcal{U}}_1^{(3)}(q_3^2) = \frac{N_c}{24\pi^2F^2}\,, \qquad \tilde{\mathcal{U}}_3^{(3)}(q_3^2) = -\frac{N_c}{12\pi^2F^2(q_3^2-m_\pi^2)}\,. \tag{4.145}$$

At this order, we have

$$\Omega_1^1(q_3^2) = 1\,, \qquad \mathcal{F}_{\pi^0}(m_\pi^2, m_\pi^2, m_\pi^2; 0) = \frac{N_c}{12\pi^2 F^3}\,, \qquad F_\pi^3 = F \tag{4.146}$$

so that the pion-pole contribution to $\tilde{\mathcal{U}}_3^{(3)}$ in Eq. (4.142) is reproduced by the chiral expression. We thus conclude that the axial-pole and heavier pseudoscalar-pole contributions in $\tilde{\mathcal{U}}_3^{(3)}$ are of higher order in the chiral counting. The result for $\tilde{\mathcal{U}}_1^{(3)}(q_3^2)$ fixes the subtraction constant

$$\tilde{\mathcal{U}}_1^{(3)}(0) = \frac{N_c}{24\pi^2 F^2}\,. \tag{4.147}$$

4.2.5 Results and the constraint from the anomaly

We have considered four contributions to the discontinuities of the functions $\tilde{\mathcal{W}}_i(q^2)$, which are given in Eqs. (4.39), (4.47), (4.58) and (4.143). For the scalar functions themselves, this gives

$$\begin{aligned}
\tilde{\mathcal{W}}_1(q^2) &= 2\sum_P\sum_a C_a F_P^a \frac{F_{P\gamma^*\gamma^*}(m_P^2,0)}{q^2-m_P^2} + \sum_V \frac{m_V f_V \tilde{\mathcal{V}}_1(0,m_V^2)}{q^2-m_V^2} \\
&\quad - \frac{1}{48\pi^2}\int_{4m_\pi^2}^\infty \mathrm{d}s \frac{F_\pi^V(s)\sigma_\pi^3(s)\Omega_1^1(s)^*\tilde{\mathcal{U}}_1(0)}{s-q^2-\mathrm{i}\epsilon} \\
&\quad + \frac{1}{48\pi^2}\sum_P\int_{4m_\pi^2}^\infty \mathrm{d}s \frac{sF_\pi^V(s)\sigma_\pi^3(s)\Omega_1^1(s)^*}{(s-q^2-\mathrm{i}\epsilon)(s-m_P^2-\mathrm{i}\epsilon)}\sum_a C_a F_P^a \frac{\mathcal{F}_P}{\Omega_1^1(m_P^2)}\,, \\
\tilde{\mathcal{W}}_2(q^2) &= -2\sum_A\sum_a C_a \frac{F_A^a}{m_A}\frac{\mathcal{F}_2^A(m_A^2,0)}{q^2-m_A^2} + \sum_V \frac{m_V f_V \tilde{\mathcal{V}}_2(0,m_V^2)}{q^2-m_V^2} \\
&\quad + \frac{1}{48\pi^2}\int_{4m_\pi^2}^\infty \mathrm{d}s \frac{F_\pi^V(s)\sigma_\pi^3(s)\Omega_1^1(s)^*\tilde{\mathcal{U}}_1(0)}{s-q^2-\mathrm{i}\epsilon} \\
&\quad + \frac{1}{24\pi^2}\sum_A\int_{4m_\pi^2}^\infty \mathrm{d}s \frac{sF_\pi^V(s)\sigma_\pi^3(s)\Omega_1^1(s)^*}{(s-q^2-\mathrm{i}\epsilon)(s-m_A^2-\mathrm{i}\epsilon)}\sum_a C_a \frac{F_A^a\mathcal{F}_{A,1}}{m_A\Omega_1^1(m_A^2)}\,.
\end{aligned} \tag{4.148}$$

In order for the phases in the two-pion discontinuities to cancel, the phases of F_π^V, $\mathcal{F}_P$ and $\mathcal{F}_{A,1}$ all have to be given by δ_1^1. This is indeed true if only two-pion rescattering is taken into account in these quantities. In that case, the vector-form factor is given through $F_\pi^V(s) = \Omega_1^1(s)$, which we will assume in the following.

The scalar functions are expected to be real on the real axis apart from poles and cuts according to the considered intermediate states. This is, however, not obvious from the expressions above if $m_{P/A} > 2m_\pi$. In this case, both the TFFs and the 2π-contributions have additional imaginary parts

$$
\begin{aligned}
\operatorname{Im}\tilde{\mathcal{W}}_1(q^2) &= 2\sum_P\sum_a C_a F_P^a \frac{\operatorname{Im}F_{P\gamma^*\gamma^*}(m_P^2,0)}{q^2-m_P^2} \\
&\quad - \frac{1}{48\pi}\sum_P\sum_a C_a F_P^a \frac{m_P^2\sigma_\pi^3(m_P^2)\Omega_1^1(m_P^2)^*\mathcal{F}_P(m_P^2,m_\pi^2,m_\pi^2;0)}{q^2-m_P^2} \\
&\quad + (P\text{-pole}) + (2\pi\text{-cut})\,, \\
\operatorname{Im}\tilde{\mathcal{W}}_2(q^2) &= -2\sum_A\sum_a C_a \frac{F_A^a}{m_A}\frac{\operatorname{Im}\mathcal{F}_2^A(m_A^2,0)}{q^2-m_A^2} \\
&\quad - \frac{1}{24\pi}\sum_A\sum_a C_a F_A^a m_A \frac{\sigma_\pi^3(m_A^2)\Omega_1^1(m_A^2)^*\mathcal{F}_{A,1}(m_A^2,m_\pi^2,m_\pi^2;0)}{q^2-m_A^2} \\
&\quad + (A\text{-pole}) + (2\pi\text{-cut})\,.
\end{aligned}
\tag{4.149}
$$

We have checked that the first two lines in both expressions indeed cancel and only the physical poles and cuts remain if the imaginary part of the pseudoscalar and axial TFFs derived in Secs. 4.3.1 and 4.3.2 below are plugged in.

Thus, the optimal strategy is to dispersively determine the TFFs from a formalism similar to Secs. 4.3.1 and 4.3.2, in which $\mathcal{F}_P$ and $\mathcal{F}_{A,1}$ are needed as input. This guarantees the cancellation of unphysical imaginary parts in the VVA scalar functions. In the case of the axial TFFs, such an analysis is presently not available and for our numerical implementation in Sec. 4.6 we will have to resort to a VMD model [179], which does not explicitly include a two-pion cut. We can then use the consistency condition that the unphysical imaginary parts have to cancel to determine $\mathcal{F}_{A,1}(m_A^2,m_\pi^2,m_\pi^2;0)$ from the imaginary part of the TFF.

The anomaly constraint for $\tilde{\mathcal{W}}_1$ in Eq. (4.15) is saturated by the first term in Eq. (4.148), which implies that in the chiral limit and neglecting the gluon anomaly the other contributions have to drop out. This indeed happens for the two-pion contribution when setting m_P to 0 for the lightest multiplet and dropping heavier pseudoscalars since their decay constants vanish in this limit. The value of the subtraction constant in Eq. (4.147) and the chiral-limit result of $\mathcal{F}_P$ are crucial for this cancellation. The vector-meson contributions to $\tilde{\mathcal{W}}_1$ have poles at finite q^2, which are not allowed by the axial anomaly and cannot cancel against another contribution. Thus, their residues have to vanish in the chiral limit. The implications of the non-renormalization constraint Eq. (4.16) will be discussed in Sec. 4.5.1 together with SDCs.

4.3 Dispersion relations for fixed photon virtualities

In this section, we derive dispersion relations for the VVA correlator in the axial-current virtuality q_3^2 while keeping the photon virtualities q_1^2 and q_2^2 fixed. The limit $q_2\to 0$ needed for $g-2$ is performed only in the end. This approach is the analog of the CHPS formalism for HLbL introduced in Sec. 2.4.3.

In general kinematics, the VVA correlator $\mathcal{W}^{\mu\nu\rho}(q_1, q_2)$ can be decomposed into four scalar functions according to Eq. (4.6). These depend on q_1^2, q_2^2 and $q_3^2 = (q_1 + q_2)^2$ and a dispersion relation in q_3^2 with fixed q_1^2 and q_2^2 holds

$$\mathcal{W}_i(q_1^2, q_2^2, q_3^2) = \frac{1}{\pi} \int \mathrm{d}s \frac{\mathrm{Im}_3\, \mathcal{W}_i(q_1^2, q_2^2, s)}{s - q_3^2 - \mathrm{i}\epsilon} . \tag{4.150}$$

The imaginary parts are determined from the unitarity relation in Eq. (4.29).

In Sec. 4.2, we have discussed two contributions to $\mathrm{Im}_3\, \mathcal{W}_i(q_1^2, q_2^2, s)$, namely single pseudoscalar- and axial-meson states and we can immediately use here the results we obtained before. Projecting the pseudoscalar contribution Eq. (4.37) onto the tensor decomposition gives

$$\mathrm{Im}_3^P\, \mathcal{W}_0(q_1^2, q_2^2, q_3^2) = -2\pi\delta(q_3^2 - m_P^2) F_{P\gamma^*\gamma^*}(q_1^2, q_2^2) \sum_a C_a F_P^a \tag{4.151}$$

for the first scalar function, whereas the other three do not receive a contribution from this state. Plugging this into the dispersion relation, we obtain

$$\mathcal{W}_i^{P\text{-pole}}(q_1^2, q_2^2, q_3^2) = 2 \sum_a C_a F_P^a \frac{F_{P\gamma^*\gamma^*}(q_1^2, q_2^2)}{q_3^2 - m_P^2} \delta_{i0} . \tag{4.152}$$

In the $g - 2$ limit, using Eq. (4.12), this leads to

$$\tilde{\mathcal{W}}_1^{P\text{-pole}}(q^2) = 2 \sum_a C_a F_P^a \frac{F_{P\gamma^*\gamma^*}(q^2, 0)}{q^2 - m_P^2} . \tag{4.153}$$

Also the axial-meson-pole contribution can easily be determined from the expressions above. The contribution to $\mathrm{Im}_3\, \mathcal{W}^{\mu\nu\rho}(q_1, q_2)$ can be found in Eq. (4.46). The decomposition into the scalar functions gives

$$\begin{aligned}
\mathrm{Im}_3^A\, \mathcal{W}_0(q_1^2, q_2^2, q_3^2) &= \frac{\pi}{m_A^3} \delta(q_3^2 - m_A^2) \sum_a C_a F_A^a \Big[2(q_1^2 - q_2^2) \mathcal{F}_1^A(q_1^2, q_2^2) \\
&\qquad - (m_A^2 - 2q_1^2) \mathcal{F}_2^A(q_1^2, q_2^2) + (m_A^2 - 2q_2^2) \mathcal{F}_3^A(q_1^2, q_2^2) \Big] , \\
\mathrm{Im}_3^A\, \mathcal{W}_1(q_1^2, q_2^2, q_3^2) &= -2 \frac{\pi}{m_A} \delta(q_3^2 - m_A^2) \sum_a C_a F_A^a \mathcal{F}_1^A(q_1^2, q_2^2) , \\
\mathrm{Im}_3^A\, \mathcal{W}_2(q_1^2, q_2^2, q_3^2) &= \frac{\pi}{m_A} \delta(q_3^2 - m_A^2) \sum_a C_a F_A^a \left[\mathcal{F}_2^A(q_1^2, q_2^2) - \mathcal{F}_3^A(q_1^2, q_2^2) \right] , \\
\mathrm{Im}_3^A\, \mathcal{W}_3(q_1^2, q_2^2, q_3^2) &= \frac{\pi}{m_A} \delta(q_3^2 - m_A^2) \sum_a C_a F_A^a \left[\mathcal{F}_2^A(q_1^2, q_2^2) + \mathcal{F}_3^A(q_1^2, q_2^2) \right] ,
\end{aligned} \tag{4.154}$$

which leads to the following contributions to the scalar functions

$$\begin{aligned}
\mathcal{W}_0^{A\text{-pole}}(q_1^2,q_2^2,q_3^2) &= -\frac{1}{m_A^3}\sum_a C_a F_A^a \frac{1}{q_3^2-m_A^2}\Big[2(q_1^2-q_2^2)\mathcal{F}_1^A(q_1^2,q_2^2) \\
&\qquad - (m_A^2-2q_1^2)\mathcal{F}_2^A(q_1^2,q_2^2) + (m_A^2-2q_2^2)\mathcal{F}_3^A(q_1^2,q_2^2)\Big]\,, \\
\mathcal{W}_1^{A\text{-pole}}(q_1^2,q_2^2,q_3^2) &= \frac{2}{m_A}\sum_a C_a F_A^a \frac{\mathcal{F}_1^A(q_1^2,q_2^2)}{q_3^2-m_A^2}\,, \\
\mathcal{W}_2^{A\text{-pole}}(q_1^2,q_2^2,q_3^2) &= -\frac{1}{m_A}\sum_a C_a F_A^a \frac{\mathcal{F}_2^A(q_1^2,q_2^2)-\mathcal{F}_3^A(q_1^2,q_2^2)}{q_3^2-m_A^2}\,, \\
\mathcal{W}_3^{A\text{-pole}}(q_1^2,q_2^2,q_3^2) &= -\frac{1}{m_A}\sum_a C_a F_A^a \frac{\mathcal{F}_2^A(q_1^2,q_2^2)+\mathcal{F}_3^A(q_1^2,q_2^2)}{q_3^2-m_A^2}\,.
\end{aligned} \tag{4.155}$$

In $g-2$ kinematics, this reduces to

$$\begin{aligned}
\tilde{\mathcal{W}}_1^{A\text{-pole}}(q^2) &= -\frac{2}{m_A^3}\sum_a C_a F_A^a\left[\mathcal{F}_1^A(q^2,0)+\mathcal{F}_2^A(q^2,0)\right]\,, \\
\tilde{\mathcal{W}}_2^{A\text{-pole}}(q^2) &= -\frac{2}{m_A}\sum_a C_a F_A^a \frac{\mathcal{F}_2^A(q^2,0)}{q^2-m_A^2}\,.
\end{aligned} \tag{4.156}$$

The pole residues of the results obtained here agree with the corresponding ones in the formalism in $g-2$ kinematics, Eqs. (4.40) and (4.48). However, the results differ by a non-pole axial-meson contribution to $\tilde{\mathcal{W}}_1^{A\text{-pole}}$ as well as by the arguments of the TFFs. This shows that the notions of pseudoscalar or axial-vector pole contributions are different in the two approaches. There is a re-shuffling of contributions that also involves the cuts in the q_1^2 channel, which do not show up here. In order to better understand this, we need dispersive representations of the TFFs taking into account the same intermediate states as in Sec. 4.2. Our goal here is not to compete with the much more involved analyses in Refs. [18, 50, 120, 125–128], but instead to derive dispersive representations facilitating the comparison between the two dispersive approaches in Sec. 4.4.

4.3.1 Dispersive analysis of the pseudoscalar transition form factors

The pion transition form factor can be decomposed into components where either the first or the second photon is an isovector [18]

$$F_{\pi^0\gamma^*\gamma^*}(q_1^2,q_2^2) = F_{vs}^{\pi^0}(q_1^2,q_2^2) + F_{vs}^{\pi^0}(q_2^2,q_1^2)\,. \tag{4.157}$$

Similarly, for the η and η' TFFs the decomposition reads [127]

$$F_{\eta^{(\prime)}\gamma^*\gamma^*}(q_1^2,q_2^2) = F_{vv}^{\eta^{(\prime)}}(q_1^2,q_2^2) + F_{ss}^{\eta^{(\prime)}}(q_1^2,q_2^2)\,. \tag{4.158}$$

In both cases, the singly-virtual TFF takes the form

$$F_{P\gamma^*\gamma^*}(q_1^2,0) = F_v^P(q_1^2) + F_s^P(q_1^2)\,, \tag{4.159}$$

where we only specify the isospin component of the virtual photon. Explicitly, the definitions of the isovector and isoscalar form factors read

$$\langle\gamma(q_2,\lambda_2)|\, j_\mu^{v/s}(0)\,|P(q_1+q_2)\rangle = -e\epsilon^{\lambda_2\nu}(q_2)^*\epsilon_{\mu\nu\rho\sigma}q_1^\rho q_2^\sigma F^P_{v/s}(q_1^2) \tag{4.160}$$

with $j_\mu^{v/s}(x)$ the isovector and isoscalar components of the electromagnetic current

$$j^\mu_{\text{em}} = j^\mu_v + j^\mu_s\,, \qquad j^\mu_v = j^\mu_3\,, \qquad j^\mu_s = \frac{1}{\sqrt{3}}j^\mu_8\,, \qquad j^\mu_a = \bar\psi\frac{\lambda_a}{2}\gamma^\mu\psi\,. \tag{4.161}$$

and $q_2^2 = 0$. We want to study two-pion intermediate states in the isovector channel and narrow vector resonances in the isoscalar channel.

4.3.1.1 Two-pion intermediate state

The unitarity relation in the isovector photon reads

$$\begin{aligned}\operatorname{Im}\left[-\mathrm{i}\,\langle\gamma_v^*(q_1,\lambda_1)|P(p)\gamma(q_2,\lambda_2)\rangle\right] = \sum_n \frac{1}{2S_n}\left(\prod_{i=1}^{N_n}\int\widetilde{\mathrm{d}p_i}\right)\langle P(p)\gamma(q_2,\lambda_2)|n;\{p_i\}\rangle^*\\ \times\langle\gamma_v^*(q_1,\lambda_1)|n;\{p_i\}\rangle\,.\end{aligned} \tag{4.162}$$

Taking the two-pion contribution from the sum over intermediate states, we find

$$\begin{aligned}&\operatorname{Im}^{\pi^+\pi^-}\left[-\mathrm{i}\,\langle\gamma_v^*(q_1,\lambda_1)|P(p)\gamma(q_2,\lambda_2)\rangle\right]\\ &\quad=\frac{1}{2}\int\widetilde{\mathrm{d}p_1}\widetilde{\mathrm{d}p_2}\,\langle P(p)\gamma(q_2,\lambda_2)|\pi^+(p_1)\pi^-(p_2)\rangle^*_{I=1}\,\langle\gamma_v^*(q_1,\lambda_1)|\pi^+(p_1)\pi^-(p_2)\rangle_{I=1}\,,\end{aligned} \tag{4.163}$$

which leads to

$$\begin{aligned}\epsilon^{\mu\nu\rho\sigma}q_{1\rho}q_{2\sigma}\operatorname{Im}^{\pi^+\pi^-}F_v^P(q_1^2) = -\frac{1}{2}\int\widetilde{\mathrm{d}p_1}\widetilde{\mathrm{d}p_2}(2\pi)^4\delta^{(4)}(q_1-p_1-p_2)\epsilon^{\nu\alpha\beta\gamma}p_{1\alpha}p_{2\beta}(q_1-q_2)_\gamma\\ \times(p_1-p_2)^\mu\mathcal{F}_P(q_1^2,(q_2-p_1)^2,(q_2-p_2)^2;0)F_\pi^V(q_1^2)^*\,.\end{aligned} \tag{4.164}$$

Here we have moved the $*$ from $\mathcal{F}_P$, where it would involve analytic continuation, to F_π^V, which only depends on q_1^2 and therefore does not require analytic continuation. Contraction with $\epsilon_{\mu\nu\rho\sigma}q_1^\rho q_2^\sigma/(2(q_1\cdot q_2)^2)$ simplifies this expression to

$$\begin{aligned}&\operatorname{Im}^{\pi^+\pi^-}F_v^P(q_1^2)\\ &\quad=-\frac{1}{2}\int\widetilde{\mathrm{d}p_1}\widetilde{\mathrm{d}p_2}(2\pi)^4\delta^{(4)}(q_1-p_1-p_2)\left[m_\pi^2-\frac{1}{4}q_1^2(1-z^2\sigma_\pi^2(q_1^2))\right]F_\pi^V(q_1^2)^*\\ &\quad\times\mathcal{F}_P\left(q_1^2,m_\pi^2-\frac{1}{2}(q_1^2-m_P^2)(1-z\sigma_\pi(q_1^2)),m_\pi^2-\frac{1}{2}(q_1^2-m_P^2)(1+z\sigma_\pi(q_1^2));0\right)\,,\end{aligned} \tag{4.165}$$

where $z = ((q_2-p_1)^2-(q_2-p_2)^2)/(\sigma_\pi(q_1^2)(q_1^2-m_P^2))$ is the cosine of the scattering angle in the $\pi\pi$ center-of-mass frame.

We perform a partial-wave expansion (cf. Eq. (4.104))

$$\mathcal{F}_P(s,t,u;q^2) = \sum_{l\ \mathrm{odd}} f_P^l(s,q^2)P_l'(z)\,, \tag{4.166}$$

where the restriction to odd l is due to the two pions being in an isovector state. Thus,

$$\begin{aligned}&\mathrm{Im}^{\pi^+\pi^-}\,F_v^P(q_1^2)\\ &\quad= \frac{1}{8}\sum_{l\ \mathrm{odd}} f_P^l(q_1^2,0)F_\pi^V(q_1^2)^*\int \widetilde{\mathrm{d}p_1}\widetilde{\mathrm{d}p_2}(2\pi)^4\delta^{(4)}(q_1-p_1-p_2)q_1^2\sigma_\pi^2(q_1^2)(1-z^2)P_l'(z)\,.\end{aligned} \tag{4.167}$$

The integrals can be performed as explained in App. A.2 and lead to a projection onto the P-wave

$$\mathrm{Im}^{\pi^+\pi^-}\,F_v^P(q_1^2) = \frac{1}{96\pi}q_1^2\sigma_\pi^3(q_1^2)f_P^1(q_1^2,0)F_\pi^V(q_1^2)^*\,. \tag{4.168}$$

The dispersion relation then gives [18]

$$F_v^P(q_1^2) = \frac{1}{96\pi^2}\int_{4m_\pi^2}^\infty \mathrm{d}s\frac{s\sigma_\pi^3(s)f_P^1(s,0)F_\pi^V(s)^*}{s-q_1^2}\,. \tag{4.169}$$

For the pion TFF, the isospin decomposition Eq. (4.157) shows that the normalization is distributed equally between isovector and isoscalar components. Since we only include the two-pion intermediate state in the isovector channel, this provides a sum rule (up to small chiral corrections)

$$F_v^{\pi^0}(0) = \frac{1}{96\pi^2}\int_{4m_\pi^2}^\infty \mathrm{d}s\,\sigma_\pi^3(s)f_{\pi^0}^1(s,0)F_\pi^V(s)^* = \frac{1}{2}F_{\pi^0\gamma^*\gamma^*}(0,0) = \frac{1}{8\pi^2F_\pi}\,, \tag{4.170}$$

whereas in the case of $\eta^{(\prime)}$ the distribution of the normalization between isovector and isoscalar parts is not fixed through crossing symmetry.

4.3.1.2 Vector-meson poles

While the isovector vector mesons should be included in the two-pion intermediate state through the pion scattering phase shift, isoscalar vector mesons couple only to heavier intermediate states starting from three pions. However, the ω and ϕ mesons are very narrow so that employing a NWA is justified.

We start again with the unitarity relation, this time for the isoscalar part of the TFF

$$\begin{aligned}&\mathrm{Im}\left[-i\,\langle\gamma_s^*(q_1,\lambda_1)|P(p)\gamma(q_2,\lambda_2)\rangle\right]\\ &\quad= \sum_n \frac{1}{2S_n}\left(\prod_{i=1}^{N_n}\int\widetilde{\mathrm{d}p_i}\right)\langle P(p)\gamma(q_2,\lambda_2)|n;\{p_i\}\rangle^*\,\langle\gamma_s^*(q_1,\lambda_1)|n;\{p_i\}\rangle\end{aligned} \tag{4.171}$$

and single out a vector meson V from the sum over intermediate states

$$\begin{aligned}&\mathrm{Im}^V\left[-\mathrm{i}\,\langle\gamma_s^*(q_1,\lambda_1)|P(p)\gamma(q_2,\lambda_2)\rangle\right]\\&\quad=\sum_{\lambda_V}\frac{1}{2}\int\widetilde{\mathrm{d}p_V}\,\langle P(p)\gamma(q_2,\lambda_2)|V(p_V,\lambda_V)\rangle^*\,\langle\gamma_s^*(q_1,\lambda_1)|V(p_V,\lambda_V)\rangle\,.\end{aligned}\tag{4.172}$$

Plugging in the matrix elements and performing the polarization sum and the integral, we obtain

$$\mathrm{Im}^V\,F_s^P(q_1^2)=\pi\delta(q_1^2-m_V^2)m_Vf_VF_{VP}\,.\tag{4.173}$$

Thus, summing over all contributing vector mesons and neglecting other intermediate states in the isoscalar channel, we finally arrive at

$$F_s^P(q_1^2)=-\sum_V\frac{m_Vf_VF_{VP}}{q_1^2-m_V^2}\,.\tag{4.174}$$

For the pion, the anomaly again provides a constraint

$$F_s^{\pi^0}(0)=\sum_V\frac{f_VF_{V\pi^0}}{m_V}=\frac{1}{8\pi^2F_\pi}\,.\tag{4.175}$$

Conversely, for η and η' due to the different isospin decomposition only the sum of isovector and isoscalar normalizations is constrained

$$\begin{aligned}\sum_{P=\eta,\eta'}F_P^a\left(F_v^P(0)+F_s^P(0)\right)&=\sum_{P=\eta,\eta'}F_P^a\left(\frac{1}{96\pi^2}\int_{4m_\pi^2}^\infty\mathrm{d}s\,\sigma_\pi^3(s)f_P^1(s,0)F_\pi^V(s)^*+\sum_V\frac{f_VF_{VP}}{m_V}\right)\\&=\frac{3}{4\pi^2}\,\mathrm{Tr}(\mathcal{Q}^2\lambda^a)\,,\end{aligned}\tag{4.176}$$

where we have accounted for η-η' mixing.

Summing isovector and isoscalar contributions, the total singly-virtual pseudoscalar TFFs read

$$F_{P\gamma^*\gamma^*}(q_1^2,0)=\frac{1}{96\pi^2}\int_{4m_\pi^2}^\infty\mathrm{d}s\frac{s\sigma_\pi^3(s)f_P^1(s,0)F_\pi^V(s)^*}{s-q_1^2}-\sum_V\frac{m_Vf_VF_{VP}}{q_1^2-m_V^2}\,.\tag{4.177}$$

In the formalism of Ref. [18], isoscalar vector mesons are included through the q^2-dependent subtraction constant $a(q^2)$ in the Khuri–Treiman equations for the sub-process $\gamma^*\to3\pi$, where q^2 is the virtuality of the isoscalar photon. Neglecting the conformal polynomial and the vector meson widths, the subtraction constant becomes

$$a(q^2)=\alpha_A+\sum_V\frac{q^2}{m_V^2}\frac{c_V}{m_V^2-q^2}\,.\tag{4.178}$$

Since the solution to the Khuri–Treiman equations and thus the dispersively reconstructed pion TFF is linear in $a(q^2)$, also the pion TFF has poles at $q^2=m_V^2$. However, both the q^2 dependence in the numerator of $a(q^2)$ due to the subtraction and the non-trivial q^2 dependence introduced in the angular integral give also a non-pole contribution to the isoscalar part of the singly-virtual TFF.

4.3.2 Dispersive analysis of the axial-vector transition form factors

The isospin decomposition for the axial-meson TFFs is similar to that for the pseudoscalar TFFs in the previous section with the difference that the TFFs are not symmetric in their two arguments. Thus, we have

$$\begin{aligned}
\mathcal{F}_i^{a_1}(q_1^2,q_2^2) &= \mathcal{F}_{i,vs}^{a_1}(q_1^2,q_2^2) + \mathcal{F}_{i,sv}^{a_1}(q_1^2,q_2^2)\,, \\
\mathcal{F}_i^{f_1^{(\prime)}}(q_1^2,q_2^2) &= \mathcal{F}_{i,vv}^{f_1^{(\prime)}}(q_1^2,q_2^2) + \mathcal{F}_{i,ss}^{f_1^{(\prime)}}(q_1^2,q_2^2)\,,
\end{aligned} \tag{4.179}$$

where the crossing properties in Ref. [131] imply relations between the different functions. In the singly-virtual case, this again reduces to

$$\mathcal{F}_i^A(q_1^2,0) = \mathcal{F}_{i,v}^A(q_1^2) + \mathcal{F}_{i,s}^A(q_1^2)\,. \tag{4.180}$$

In the following, we will discuss two-pion and vector-meson intermediate states in these TFFs in analogy to the pseudoscalar TFFs in the previous section.

4.3.2.1 Two-pion intermediate state

We start with the unitarity relation for the isovector part of the TFFs

$$\begin{aligned}
&\mathrm{Im}\left[-\mathrm{i}\,\langle\gamma_v^*(q_1,\lambda_1)|A(p,\lambda_A)\gamma(q_2,\lambda_2)\rangle\right] \\
&\quad= \sum_n \frac{1}{2S_n}\left(\prod_{i=1}^{N_n}\int\widetilde{\mathrm{d}p_i}\right)\langle A(p,\lambda_A)\gamma(q_2,\lambda_2)|n;\{p_i\}\rangle^*\,\langle\gamma_v^*(q_1,\lambda_1)|n;\{p_i\}\rangle
\end{aligned} \tag{4.181}$$

and single out the two-pion contribution

$$\begin{aligned}
&\mathrm{Im}^{\pi^+\pi^-}\left[-\mathrm{i}\,\langle\gamma_v^*(q_1,\lambda_1)|A(p,\lambda_A)\gamma(q_2,\lambda_2)\rangle\right] \\
&\quad= \frac{1}{2}\int\widetilde{\mathrm{d}p_1}\widetilde{\mathrm{d}p_2}\,\langle A(p,\lambda_A)\gamma(q_2,\lambda_2)|\pi^+(p_1)\pi^-(p_2)\rangle^*\,\langle\gamma_v^*(q_1,\lambda_1)|\pi^+(p_1)\pi^-(p_2)\rangle\,.
\end{aligned} \tag{4.182}$$

We use Eqs. (4.43), (4.109) and (4.78) and account for the facts that $T_3^{\mu\nu\alpha}$ vanishes at $q_2^2=0$ and that there is one linear relation between the structures $\tau_{A,i}^{\nu\alpha}$, see Eq. (4.119). We then obtain

$$\begin{aligned}
\mathrm{Im}^{\pi^+\pi^-}\left[\sum_{i=1}^{2}T_i^{\mu\nu\alpha}(q_1,-q_2)\mathcal{F}_{i,v}^A(q_1^2)\right] &= -\frac{m_A^2}{2}F_\pi^V(q_1^2)^*\int\widetilde{\mathrm{d}p_1}\widetilde{\mathrm{d}p_2}(2\pi)^4\delta^{(4)}(q_1-p_1-p_2) \\
&\times\sum_{i=1,2,4}\tau_{A,i}^{\nu\alpha}(-q_2,-p_2,-p_1)(p_1-p_2)^\mu\tilde{\mathcal{F}}_{A,i}((p_1+p_2)^2,(q_2-p_1)^2,(q_2-p_2)^2)\,.
\end{aligned} \tag{4.183}$$

We project the right-hand side onto the two TFFs[5] and replace the functions $\tilde{\mathcal{F}}_{A,i}$ by the helicity partial-wave amplitudes via Eq. (4.124), where we take into account the different

[5]The right-hand-side also gives a contribution to the unphysical TFF, which has to be taken into account in the projection.

assignment of the momenta. This gives

$$\begin{aligned}
\mathrm{Im}^{\pi^+\pi^-}\,\mathcal{F}^A_{1,v}(s) &= \frac{m_A^2\sigma_\pi(s)F_\pi^V(s)^*}{(s-m_A^2)^2}\int \widetilde{\mathrm{d}p_1}\widetilde{\mathrm{d}p_2}(2\pi)^4\delta^{(4)}(q_1-p_1-p_2) \\
&\quad\times\sum_{l\text{ odd}}\left(szP_l(z)\mathrm{i}h^l_{++}(s)-\frac{m_A}{\sqrt{2}}\sqrt{s}(1-z^2)P_l'(z)\mathrm{i}h^l_{+0}(s)\right)\,, \\
\mathrm{Im}^{\pi^+\pi^-}\,\mathcal{F}^A_{2,v}(s) &= -\frac{m_A^2\sigma_\pi(s)F_\pi^V(s)^*}{(s-m_A^2)}\int \widetilde{\mathrm{d}p_1}\widetilde{\mathrm{d}p_2}(2\pi)^4\delta^{(4)}(q_1-p_1-p_2)\sum_{l\text{ odd}}zP_l(z)\mathrm{i}h^l_{++}(s)
\end{aligned} \tag{4.184}$$

with $s=(p_1+p_2)^2=q_1^2$.

The phase-space integrals can now be performed and lead to

$$\begin{aligned}
\mathrm{Im}^{\pi^+\pi^-}\,\mathcal{F}^A_{1,v}(s) &= \frac{m_A^2\sigma_\pi^2(s)F_\pi^V(s)^*}{24\pi(s-m_A^2)}\left(s\mathrm{i}g^1_{++}(s)-\sqrt{2}m_A\sqrt{s}\mathrm{i}g^1_{+0}(s)\right)\,, \\
\mathrm{Im}^{\pi^+\pi^-}\,\mathcal{F}^A_{2,v}(s) &= -\frac{m_A^2\sigma_\pi^2(s)F_\pi^V(s)^*}{24\pi}\mathrm{i}g^1_{++}(s)\,,
\end{aligned} \tag{4.185}$$

where we have used Eq. (4.125). Notice that the residue of the apparent pole of $\mathrm{Im}^{\pi^+\pi^-}\,\mathcal{F}^A_{1,v}(s)$ at $s=m_A^2$ vanishes due to Eq. (4.126).

Plugging this into the dispersion relation, we finally obtain

$$\begin{aligned}
\mathcal{F}^A_{1,v}(q_1^2) &= \frac{1}{24\pi^2}\int_{4m_\pi^2}^\infty \mathrm{d}s\frac{m_A^2\sigma_\pi^2(s)F_\pi^V(s)^*}{(s-m_A^2)(s-q_1^2)}\left(s\mathrm{i}g^1_{++}(s)-\sqrt{2}m_A\sqrt{s}\mathrm{i}g^1_{+0}(s)\right)\,, \\
\mathcal{F}^A_{2,v}(q_1^2) &= -\frac{1}{24\pi^2}\int_{4m_\pi^2}^\infty \mathrm{d}s\frac{m_A^2\sigma_\pi^2(s)F_\pi^V(s)^*}{s-q_1^2}\mathrm{i}g^1_{++}(s)\,.
\end{aligned} \tag{4.186}$$

4.3.2.2 Vector-meson poles

The unitarity relation for the isoscalar part of the TFFs reads

$$\begin{aligned}
&\mathrm{Im}\left[-\mathrm{i}\left\langle\gamma_s^*(q_1,\lambda_1)|A(p,\lambda_A)\gamma(q_2,\lambda_2)\right\rangle\right] \\
&\quad=\sum_n\frac{1}{2S_n}\left(\prod_{i=1}^n\int\widetilde{\mathrm{d}p_i}\right)\left\langle A(p,\lambda_A)\gamma(q_2,\lambda_2)|n;\{p_i\}\right\rangle^*\left\langle\gamma_s^*(q_1,\lambda_1)|n;\{p_i\}\right\rangle
\end{aligned} \tag{4.187}$$

and we again only consider contributions from single vector mesons

$$\begin{aligned}
&\mathrm{Im}^V\left[-\mathrm{i}\left\langle\gamma_s^*(q_1,\lambda_1)|A(p,\lambda_A)\gamma(q_2,\lambda_2)\right\rangle\right] \\
&\quad=\sum_{\lambda_V}\frac{1}{2}\int\widetilde{\mathrm{d}p_V}\left\langle A(p,\lambda_A)\gamma(q_2,\lambda_2)|V(p_V,\lambda_V)\right\rangle^*\left\langle\gamma_s^*(q_1,\lambda_1)|V(p_V,\lambda_V)\right\rangle\,.
\end{aligned} \tag{4.188}$$

The matrix elements are given by Eqs. (4.43), (4.72) and (4.50). Plugging these in, performing the integral and using

$$T_i^{\mu\nu\alpha}(-q_1,-q_2)=-T_i^{\mu\nu\alpha}(q_1,q_2)\,, \tag{4.189}$$

we obtain

$$\begin{aligned}
\mathrm{Im}^V\,\mathcal{F}^A_{1,s}(q_1^2) &= \pi\delta(q_1^2-m_V^2)m_A^2 m_V f_V\left(F^1_{VA}+\frac{1}{2}F^2_{VA}\right)\,,\\
\mathrm{Im}^V\,\mathcal{F}^A_{2,s}(q_1^2) &= \pi\delta(q_1^2-m_V^2)m_A^2 m_V^{-1} f_V F^3_{VA}\,.
\end{aligned}\tag{4.190}$$

The dispersion relations then give

$$\begin{aligned}
\mathcal{F}^A_{1,s}(q_1^2) &= -\sum_V \frac{m_A^2 m_V f_V}{q_1^2-m_V^2}\left(F^1_{VA}+\frac{1}{2}F^2_{VA}\right)\,,\\
\mathcal{F}^A_{2,s}(q_1^2) &= -\sum_V \frac{m_A^2 f_V}{m_V(q_1^2-m_V^2)}F^3_{VA}\,.
\end{aligned}\tag{4.191}$$

In summary, we thus obtain for the axial TFFs

$$\begin{aligned}
\mathcal{F}^A_1(q_1^2) &= \frac{1}{24\pi^2}\int_{4m_\pi^2}^\infty \mathrm{d}s\frac{m_A^2\sigma_\pi^2(s)F_\pi^V(s)^*}{(s-m_A^2)(s-q_1^2)}\left(sig^1_{++}(s)-\sqrt{2}m_A\sqrt{s}ig^1_{+0}(s)\right)\\
&\quad-\sum_V \frac{m_A^2 m_V f_V}{q_1^2-m_V^2}\left(F^1_{VA}+\frac{1}{2}F^2_{VA}\right)\,,\\
\mathcal{F}^A_2(q_1^2) &= -\frac{1}{24\pi^2}\int_{4m_\pi^2}^\infty \mathrm{d}s\frac{m_A^2\sigma_\pi^2(s)F_\pi^V(s)^*}{s-q_1^2}ig^1_{++}(s)-\sum_V\frac{m_A^2 f_V}{m_V(q_1^2-m_V^2)}F^3_{VA}\,.
\end{aligned}\tag{4.192}$$

4.4 Comparison of the two dispersive approaches to VVA

In the previous two sections, we have worked out two representations for the VVA correlator in the limit where one of the photons is soft. In Sec. 4.2, we set the soft-photon momentum to zero at the beginning. In this limit, the imaginary part needed for the dispersion relation resulted from a sum of two cuts in general kinematics, which become indistinguishable in the limit of vanishing photon momentum. For that reason, we had to not only consider pseudoscalar- and axial-meson intermediate states in the axial-current channel, but also two-pion and vector-meson intermediate states in the vector-current channel.

In the formalism discussed in Sec. 4.3, we instead derived dispersion relations in general kinematics and took the limit only at the end. In this way, we only had to deal with one cut, which considerably simplified the unitarity constraints. However, the results contain virtuality-dependent pseudoscalar and axial TFFs, whose dispersive reconstruction reintroduced the complications due to two-pion and vector-meson intermediate states.

As the two approaches rely on different types of dispersion relations, it is clear that the contributions from individual intermediate states do not agree. However, in order for the results to be consistent, the infinite sum over all contributions has to be the same, which means that the difference in one contribution has to be compensated by others, i.e. there is a reshuffling between different intermediate states. Since we cannot evaluate dispersively an infinite sum over intermediate states, we have to employ a truncation. We chose to include the same states in both approaches, i.e. single-pseudoscalar, -axial and -vector as well as two-pion states. Since there can be a reshuffling between included and neglected contributions, the truncated results are not guaranteed to agree.

Consistency then demands that the difference between the results of the two approaches is such that it can be accounted for by neglected intermediate states in either of the two approaches. We will check this explicitly below. If the pattern of convergence in the two formalisms turns out to be similar, the difference between the results can also be seen as an estimate of the unknown effects due to these higher intermediate states.

In the dispersion relations for fixed photon virtualities, there are only pseudoscalar and axial-vector poles. The result of the dispersion relations in $g-2$ kinematics can also be separated into these two classes of contributions, with the poles being either in the direct process or some sub-process, and two-pion contributions with the subtraction constant in the sub-process. In the following, we will compare contributions involving pseudoscalar poles, axial-vector poles and the subtraction constant separately.

4.4.1 Contributions with a pseudoscalar pole

The pseudoscalar pole in the dispersion relations for fixed photon virtualities Eq. (4.153) contains the TFF evaluated at q^2. It can be separated into a pure pole and a part regular at $q^2 \to m_P^2$

$$\tilde{\mathcal{W}}_1^{P\text{-pole}}(q^2) = 2\sum_a C_a F_P^a \left(\frac{F_{P\gamma^*\gamma^*}(m_P, 0)}{q^2 - m_P^2} + \frac{F_{P\gamma^*\gamma^*}(q^2, 0) - F_{P\gamma^*\gamma^*}(m_P^2, 0)}{q^2 - m_P^2} \right) . \tag{4.193}$$

In the dispersion relations in $g-2$ kinematics, pseudoscalar poles contribute to the main process, Eq. (4.40), and this precisely reproduces the pure pole part of the previous equation. The non-pole part has to be compared against the pseudoscalar poles in the sub-process $V \to a^*\gamma$ appearing in the vector-meson pole contribution as well as in the $\gamma P \to \pi^+\pi^-$ sub-process of the two-pion contribution. To this end, we employ the TFF representation in Eq. (4.177) for the non-pole part, which leads to

$$\begin{aligned}\tilde{\mathcal{W}}_1^{P\text{ reg}} &= \sum_a C_a F_P^a \frac{1}{48\pi^2} \int_{4m_\pi^2}^\infty \mathrm{d}s \frac{s\sigma_\pi^3(s) F_\pi^V(s)^* f_P^1(s,0)}{(s-m_P^2)(s-q^2)} \\ &\quad - 2\sum_a C_a F_P^a \sum_V \frac{m_V f_V F_{VP}}{(q^2 - m_V^2)(m_V^2 - m_P^2)} . \end{aligned} \tag{4.194}$$

The second line of this equation agrees with Eq. (4.60) summed over all vector mesons with the pseudoscalar pole inserted in the sub-process as given in Eq. (4.70). The first line should be compared with the two-pion contribution with a pseudoscalar pole in the sub-process, given in the second line of Eq. (4.144). The difference between the two expressions is

$$\begin{aligned}\Delta\tilde{\mathcal{W}}_1^P &= \sum_a C_a F_P^a \frac{1}{48\pi^2}\int_{4m_\pi^2}^\infty \mathrm{d}s \frac{s\sigma_\pi^3(s)}{(s-m_P^2)(s-q^2)} \\ &\quad\times\left(F_\pi^V(s)^* f_P^1(s,0) - \frac{F_\pi^V(s)\Omega_1^1(s)^* f_P^1(m_P^2,0)}{\Omega_1^1(m_P^2)}\right) \\ &= \sum_a C_a F_P^a \frac{1}{48\pi^2}\int_{4m_\pi^2}^\infty \mathrm{d}s \frac{s\sigma_\pi^3(s)|\Omega_1^1(s)|^2}{s-q^2}\frac{\frac{f_P^1(s,0)}{\Omega_1^1(s)} - \frac{f_P^1(m_P^2,0)}{\Omega_1^1(m_P^2)}}{s-m_P^2}\,,\end{aligned} \tag{4.195}$$

where we have used that $F_\pi^V(s) = \Omega_1^1(s)$ in our approximations. Although this expression does not vanish, the pole of the integrand at $s = m_P^2$, corresponding to a pseudoscalar pole in the sub-process, cancels.

The remainder still has a two-pion cut. While it might seem surprising that the difference corresponds to an intermediate state that has been included in both approaches wherever it contributes, the reason is easy to understand: in the framework of Sec. 4.3, heavier intermediate states in the q_3^2 channel have been neglected. In the sub-processes that would be needed to account for such contributions, a two-pion intermediate state can contribute. In the $g-2$ limit, this contribution would have both a singularity due to the considered intermediate state and a two-pion cut due to the discontinuity in the sub-process. Thus, the dispersive formalism that keeps the photon virtualities fixed does not capture all two-pion singularities of the functions $\tilde{\mathcal{W}}_i$ correctly. We will present a toy-example illustrating this in Sec. 4.4.4.

4.4.2 Contributions with an axial-vector pole

In the CHPS-like formalism, axial-vector poles contribute to both scalar VVA functions. The axial contribution to $\tilde{\mathcal{W}}_1(q^2)$ does not contain a pole at $q^2 = m_A^2$, which is consistent with the result that in the dispersion relations in the $g-2$ limit, there is no axial-vector pole contribution to this scalar function. Plugging in the TFFs from Eqs. (4.186) and (4.191) gives

$$\begin{aligned}\tilde{\mathcal{W}}_1^{A\text{-pole}}(q_1^2) &= -2\frac{1}{m_A^3}\sum_a C_a F_A^a\left(\mathcal{F}_1^A(q_1^2,0) + \mathcal{F}_2^A(q_1^2,0)\right) \\ &= -\frac{1}{12\pi^2}\sum_a C_a F_A^a \int_{4m_\pi^2}^\infty \mathrm{d}s \frac{\sigma_\pi^2(s) F_\pi^V(s)^*}{(s-q_1^2)(s-m_A^2)}\left(m_A i g_{++}^1(s) - \sqrt{2}\sqrt{s}\, i g_{+0}^1(s)\right) \\ &\quad + \frac{2}{m_A}\sum_a C_a F_A^a \sum_V \frac{m_V f_V}{q_1^2 - m_V^2}\left(F_{VA}^1 + \frac{1}{2}F_{VA}^2 + \frac{1}{m_V^2}F_{VA}^3\right).\end{aligned} \tag{4.196}$$

The part with a vector-meson pole is reproduced in the other formalism by the vector-meson pole in VVA with an axial-vector pole in the sub-process. The integrand of the two-pion part does not have a pole at $s = m_A^2$ due to Eq. (4.126). This is consistent with the two-pion contribution to this scalar function in Eq. (4.148) not containing an axial contribution. Similarly to the pseudoscalar case, we cannot demand that also the non-pole parts agree.

The second scalar function contains an axial-vector pole, which can be split up in analogy to the pseudoscalar pole in the previous section as

$$\tilde{\mathcal{W}}_2^{A\text{-pole}}(q^2) = -\frac{2}{m_A}\sum_a C_a F_A^a \frac{\mathcal{F}_2^A(m_A^2,0)}{q^2-m_A^2} - \frac{2}{m_A}\sum_a C_a F_A^a \frac{\mathcal{F}_2^A(q^2,0)-\mathcal{F}_2^A(m_A^2,0)}{q^2-m_A^2}\,. \tag{4.197}$$

The first term agrees with the axial-vector pole in the formalism in $g-2$ kinematics. For the second term, we again employ the TFF representation derived in Eqs. (4.186) and (4.191). This leads to

$$\begin{aligned}\tilde{\mathcal{W}}_2^{A\text{ reg}}(q^2) = {}&\frac{m_A}{12\pi^2}\sum_a C_a F_A^a \int_{4m_\pi^2}^\infty \mathrm{d}s \frac{\sigma_\pi^2(s)F_\pi^V(s)^*\mathrm{i}g_{++}^1(s)}{(s-m_A^2)(s-q^2)}\\ &-2m_A\sum_a C_a F_A^a \frac{f_V F_{VA}^3}{m_V(m_A^2-m_V^2)(q^2-m_V^2)}\end{aligned} \tag{4.198}$$

and again the second term is reproduced in the other formalism by the vector-meson pole in VVA with an axial-vector pole in the sub-process. The other part has to be compared with the last line of Eq. (4.148). The difference of the two expressions is

$$\begin{aligned}\Delta\tilde{\mathcal{W}}_2^A(q_1^2) = {}&\frac{m_A}{12\pi^2}\sum_a C_a F_A^a \int_{4m_\pi^2}^\infty \mathrm{d}s \frac{\sigma_\pi^2(s)\Omega_1^1(s)^*}{(s-m_A^2)(s-q_1^2)}\\ &\times\left(\mathrm{i}g_{++}^1(s)-\sqrt{2}\frac{s\sigma_\pi(s)}{m_A^2\sigma_\pi(m_A^2)}\frac{\Omega_1^1(s)}{\Omega_1^1(m_A^2)}\mathrm{i}g_{+0}^1(m_A^2)\right)\,,\end{aligned} \tag{4.199}$$

where the integrand does not have a pole at $s=m_A^2$ due to Eq. (4.125). Thus, again, the two formalisms agree up to terms that can be accounted for by neglected contributions.

4.4.3 Contributions with the subtraction constant

In the dispersive approach in $g-2$ kinematics, there are also two-pion contributions with the subtraction constant $\tilde{\mathcal{U}}_1(0)$ in the sub-process, see Eq. (4.144). These only have a two-pion cut with a non-singular discontinuity. Thus, again, we cannot demand that they are also captured in the other approach. Only if the infinite tower of intermediate states in the q_3^2-channel is included, the two-pion cut of the scalar functions in the $g-2$ limit will be fully included. Since this is not possible in practice, SDCs can be used to approximate the neglected contributions. This will be studied in Sec. 4.5.1.

4.4.4 Toy example

In this section, we discuss a toy example to better understand the differences between the two formalisms. We consider a contribution of the form of the diagram in Fig. 4.5, where the resonance represented by the double line could e.g. be the charged ρ meson. We assume

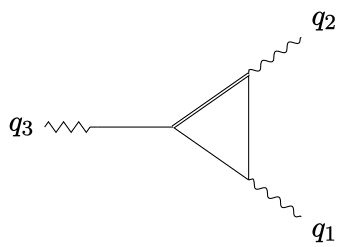

Figure 4.5: Toy-model diagram illustrating the different truncation schemes of the two dispersive approaches to VVA. The double line denotes a two-pion resonance, e.g. the ρ^+.

Feynman rules such that the diagram contributes to the longitudinal VVA function as

$$\mathcal{W}_0(q_1^2, q_2^2, q_3^2) = \frac{F_\pi \mathcal{F}_R \lambda_R F_\pi^V}{q_3^2 - m_\pi^2} C_{00}(q_1^2, q_2^2, q_3^2; m_\pi^2, m_\pi^2, M^2) \tag{4.200}$$

with the resonance mass M and coupling constants F_π, $\mathcal{F}_R$, λ_R and F_π^V for the respective vertices. The loop function is defined through

$$\begin{aligned} \frac{1}{\mathrm{i}}\mu^{2\epsilon}\int \frac{\mathrm{d}^D k}{(2\pi)^D} \frac{k^\mu k^\nu}{(k^2 - m_\pi^2)((q_1 - k)^2 - m_\pi^2)((q_3 + k)^2 - M^2)} &= g^{\mu\nu} C_{00}(q_1^2, q_2^2, q_3^2; m_\pi^2, m_\pi^2, M^2) \\ &\quad + (\text{terms} \sim q_i^\mu q_j^\nu)\,. \end{aligned} \tag{4.201}$$

In $g-2$ kinematics, this becomes

$$\tilde{\mathcal{W}}_1(q^2) = \frac{F_\pi \mathcal{F}_R \lambda_R F_\pi^V}{q^2 - m_\pi^2} C_{00}(q^2, 0, q^2; m_\pi^2, m_\pi^2, M^2)\,. \tag{4.202}$$

In the dispersive framework in $g-2$ kinematics, we have three contributions to the discontinuity

$$\begin{aligned} \mathrm{Im}^{\pi^0}\, \tilde{\mathcal{W}}_1(s) &= -\pi\delta(s - m_\pi^2) F_\pi \mathcal{F}_R \lambda_R F_\pi^V C_{00}(m_\pi^2, 0, m_\pi^2; m_\pi^2, m_\pi^2, M^2)\,, \\ \mathrm{Im}^{\pi^+\pi^-}\, \tilde{\mathcal{W}}_1(s) &= \frac{1}{192\pi} \frac{s F_\pi \mathcal{F}_R \lambda_R F_\pi^V \sigma_\pi^3(s)}{(s - m_\pi^2)(M^2 - m_\pi^2)} \theta(s - 4m_\pi^2)\,, \\ \mathrm{Im}^{R\pi}\, \tilde{\mathcal{W}}_1(s) &= -\frac{1}{192\pi} \frac{F_\pi \mathcal{F}_R \lambda_R F_\pi^V \lambda^{3/2}(s, m_\pi^2, M^2)}{s^2(s - m_\pi^2)(M^2 - m_\pi^2)} \theta(s - (m_\pi + M)^2)\,. \end{aligned} \tag{4.203}$$

Neglecting the pion-resonance cut would amount to modifications of the discontinuity at $s > (m_\pi + M)^2$ only. We have checked that the full function is recovered if we plug the sum of the three discontinuities into a dispersion relation. The full function contains a UV divergence that is included in the pion-pole contribution so that no subtraction is required.

Next, we want to analyze this diagram in the dispersive formalism with fixed photon virtualities, where it only has a pion pole and a pion-resonance cut. The corresponding discontinuities reads

$$
\begin{aligned}
\mathrm{Im}_3^{\pi^0}\,\mathcal{W}_0(q_1^2,q_2^2,q_3^2) &= -\pi\delta(q_3^2-m_\pi^2)F_\pi\mathcal{F}_R\lambda_R F_\pi^V C_{00}(q_1^2,q_2^2,m_\pi^2;m_\pi^2,m_\pi^2,M^2)\,,\\
\mathrm{Im}_3^{R\pi}\,\mathcal{W}_0(q_1^2,q_2^2,q_3^2) &= \frac{F_\pi\mathcal{F}_R\lambda_R F_\pi^V}{q_3^2-m_\pi^2}\,\mathrm{Im}_3^{R\pi}\,C_{00}(q_1^2,q_2^2,q_3^2;m_\pi^2,m_\pi^2,M^2)\theta(q_3^2-(m_\pi+M)^2)\,,
\end{aligned}
\tag{4.204}
$$

where the resonance-pion cut of the loop function shows up. The full function can be recovered from the dispersion relation Eq. (4.150) if the sum of both cuts is plugged in. Using only the pion-pole, we obtain

$$
\mathcal{W}_0^{\pi^0\text{-pole}}(q_1^2,q_2^2,q_3^2) = \frac{F_\pi\mathcal{F}_R\lambda_R F_\pi^V}{q_3^2-m_\pi^2}C_{00}(q_1^2,q_2^2,m_\pi^2;m_\pi^2,m_\pi^2,M^2)\,,
\tag{4.205}
$$

which in the $g-2$ limit becomes

$$
\tilde{\mathcal{W}}_1^{\pi^0\text{-pole}}(q^2) = \frac{F_\pi\mathcal{F}_R\lambda_R F_\pi^V}{q^2-m_\pi^2}C_{00}(q^2,0,m_\pi^2;m_\pi^2,m_\pi^2,M^2)\,.
\tag{4.206}
$$

Notice that compared to the result for the full diagram Eq. (4.200), the third argument of the loop function is replaced by m_π^2. It has a pion pole and a two-pion cut

$$
\begin{aligned}
\mathrm{Im}^{\pi^0}\,\tilde{\mathcal{W}}_1^{\pi^0\text{-pole}}(s) &= -\pi\delta(s-m_\pi^2)F_\pi\mathcal{F}_R\lambda_R F_\pi^V C_{00}(m_\pi^2,0,m_\pi^2;m_\pi^2,m_\pi^2,M^2)\,,\\
\mathrm{Im}^{\pi^+\pi^-}\,\tilde{\mathcal{W}}_1^{\pi^0\text{-pole}}(s) &= \frac{F_\pi\mathcal{F}_R\lambda_R F_\pi^V}{s-m_\pi^2}\,\mathrm{Im}_s^{\pi^+\pi^-}\,C_{00}(s,0,m_\pi^2;m_\pi^2,m_\pi^2,M^2)\theta(s-4m_\pi^2)\\
&= F_\pi\mathcal{F}_R\lambda_R F_\pi^V\left[\frac{1}{64\pi}\frac{s(s+2M^2-3m_\pi^2)\sigma_\pi(s)}{(s-m_\pi^2)^3}\right.\\
&\qquad\left.+\frac{1}{32\pi}\frac{m_\pi^6+M^2s(M^2+s-3m_\pi^2)}{(s-m_\pi^2)^4}L\right]\theta(s-4m_\pi^2)
\end{aligned}
\tag{4.207}
$$

with

$$
L = \log\left[\frac{3m_\pi^2-2M^2-s+\sigma_\pi(s)(s-m_\pi^2)}{3m_\pi^2-2M^2-s-\sigma_\pi(s)(s-m_\pi^2)}\right]\,.
\tag{4.208}
$$

The pion-pole residue is correctly reproduced, see Eq. (4.203), but the two-pion discontinuity not. The resonance-pion cut in this formalism gives precisely the missing contribution to the two-pion cut after taking the $g-2$ limit.

In summary, neglecting cuts in the formalism in $g-2$ kinematics leads to missing contributions to the discontinuity only above the respective threshold. Conversely, in the formalism with fixed photon virtualities, cuts in $g-2$ kinematics can emerge from any cut in q_3^2 in general kinematics. In this formalism, taking into account all cuts below s_0 does therefore not guarantee that the discontinuity of $\tilde{\mathcal{W}}_i(s)$ is correctly reproduced for $s<s_0$.

4.5 Constraints from the OPE

In neither of the two dispersive approaches to VVA presented above it is possible to model-independently include all intermediate states. Thus, the strategy is to include those contributions explicitly for which we are able to derive dispersive expressions and for which data exist to constrain the required input and to use SDCs to constrain the contribution from the infinite tower of remaining states. We will thus now review the relevant SDCs and explain how we implement them into our two approaches.

4.5.1 Review of OPE constraints

The OPE for the VVA correlator has been discussed in Refs. [6, 59, 167, 180]. Here, we review the results relevant for our analysis. We are interested in the behavior of the operator

$$\hat{T}_{\mu\nu}(q) = \mathrm{i}\int \mathrm{d}^4x\, e^{\mathrm{i}q\cdot x} T\{j_\mu(x) j_\nu^5(0)\} \tag{4.209}$$

for large space-like q. The matrix element of this operator between the vacuum and a photon state is related to the VVA correlator

$$\langle 0|\, \hat{T}^{\mu\rho}(q_1)\, |\gamma(-q_2, \lambda_2)\rangle = \mathrm{i}e\epsilon_\nu^{\lambda_2}(-q_2) W^{\mu\nu\rho}(q_1, q_2)\,, \tag{4.210}$$

where we restricted ourselves to $q_2^2 = 0$. The OPE can be written as [6]

$$\hat{T}_{\mu\nu}(q) = \sum_i \left\{-c_1^i(q^2) q_\nu q_\alpha g_{\mu\beta} + c_2^i(q^2)\left(-q^2 g_{\mu\alpha} g_{\nu\beta} + q_\mu q_\alpha g_{\nu\beta} - q_\nu q_\alpha g_{\mu\beta}\right)\right\} O_i^{\alpha\beta}(0) \tag{4.211}$$

with antisymmetric local operators $O_i^{\alpha\beta}$ and the matrix elements have the form

$$\langle 0|\, O_i^{\alpha\beta}(0)\, |\gamma(-q_2, \lambda_2)\rangle = \mathrm{i}e\epsilon^{\alpha\beta\gamma\delta} q_{2\gamma} \epsilon_\delta^{\lambda_2}(-q_2)\kappa_i\,, \tag{4.212}$$

where κ_i are numbers. Comparison with Eq. (4.11) then gives

$$\tilde{\mathcal{W}}_{1/2}(q^2) = \sum_i c_{1/2}^i(q^2)\kappa_i\,. \tag{4.213}$$

At large q^2, operators with higher dimensions are suppressed by the associated higher power of q^{-2} in the coefficient.

At mass dimension $d = 2$, there is only one operator that has a non-vanishing matrix element between these states

$$O_F^{\alpha\beta} = -e\epsilon^{\alpha\beta\gamma\delta}\partial_\gamma A_\delta\,, \tag{4.214}$$

where the prefactor is chosen such that $\kappa_F = 1$. The Wilson coefficient is

$$c_1^F(q_1^2) = -2c_2^F(q_1^2) = \sum_q \frac{N_c \mathcal{Q}_q^4}{2\pi^2 q_1^2}\left[\mathrm{Tr}(\mathcal{Q}^2\mathcal{Q}_5) + \frac{2\,\mathrm{Tr}(\mathcal{Q}^2\mathcal{Q}_5\mathcal{M}^2)}{q_1^2}\log\left(-\frac{q_1^2}{\mu^2}\right) + \mathcal{O}\left(\frac{\mathcal{M}^4}{q_1^4}\right)\right] \tag{4.215}$$

with $\mathcal{M} = \mathrm{diag}(m_u, m_d, m_s)$ the quark-mass matrix. Translated to the VVA correlator, the first term in the bracket gives the massless fermion loop and the second one has to be counted as $d = 4$.

At dimension $d = 3$, there is one operator for each quark flavor

$$O_q^{\alpha\beta} = \epsilon^{\alpha\beta\gamma\delta} \bar{q} \sigma_{\gamma\delta} q \,. \tag{4.216}$$

The Wilson coefficient, however, contains an explicit power of the quark mass

$$c_1^q(q_1^2) = -2c_2^q(q_1^2) = -\frac{2\mathcal{Q}_5^q \mathcal{Q}^q m_q}{q_1^4} \,, \tag{4.217}$$

which effectively increases the mass dimension of the operator to 4. Here, $\mathcal{Q}^q$ and $\mathcal{Q}_5^q$ are the respective entries of the charge matrices. Neglecting non-perturbative QCD effects, the matrix elements of these operators are given to logarithmic accuracy by

$$\kappa_q^{\mathrm{pert}} = -\frac{\mathcal{Q}_q N_c m_q}{2\pi^2} \ln \frac{\mu^2}{m_q^2} \,. \tag{4.218}$$

This combines with the quark-mass correction in Eq. (4.215) to give the term of order m_q^2 in the perturbative quark loop. Since the same results also hold for the leptonic contributions to the VVA correlator, this shows the consistency of the OPE with perturbation theory.

For quarks, however, the matrix elements are non-perturbative and the condensates κ_q are given by

$$\kappa_q = -\frac{2\mathcal{Q}^q X_q}{e} \,, \tag{4.219}$$

where X_q are so-called tensor coefficients related to the magnetic susceptibility and are known from lattice QCD in the $\overline{\mathrm{MS}}$-scheme at $\mu = 2\,\mathrm{GeV}$ [181] (see also Ref. [20])

$$X_u = (40.7 \pm 1.3)\,\mathrm{MeV} \,, \quad X_d = (39.4 \pm 1.4)\,\mathrm{MeV} \,, \quad X_s = (53.0 \pm 7.2)\,\mathrm{MeV} \,. \tag{4.220}$$

Ref. [6] uses (see also Ref. [167])

$$\kappa_q^{[6]} = \frac{N_c \mathcal{Q}^q \langle \bar{q} q \rangle}{2\pi^2 F_\pi^2} \,, \tag{4.221}$$

which with $\langle \bar{q} q \rangle = -(270\,\mathrm{MeV})^3$ and $F_\pi = 92\,\mathrm{MeV}$ gives

$$X_u^{[6]} = X_d^{[6]} = X_s^{[6]} = 53.5\,\mathrm{MeV} \,. \tag{4.222}$$

These estimates are comparable to the lattice QCD values, but somewhat larger.

At mass dimension $d = 4$ there is no new operator. The flavor decomposition proceeds according to

$$\sum_q c_1^q(q^2)\kappa_q = \frac{4\,\mathrm{Tr}(\mathcal{Q}_5 \mathcal{Q}^2 \mathcal{M} X)}{e q^4} = \sum_a \frac{4 C_a \,\mathrm{Tr}(\mathcal{Q}^2 m X \lambda^a)}{e q^4} \tag{4.223}$$

and similarly for the $d = 2$ term. Thus, we obtain to order q^{-4}

$$\begin{aligned}
\tilde{\mathcal{W}}_1^3(q^2) &= \frac{1}{4\pi^2 q^2} + \frac{2}{9eq^4}(4m_u X_u - m_d X_d) + \mathcal{O}(q^{-6}) \\
&= \frac{1}{4\pi^2 q^2} + \frac{4.9^{+2.3}_{-1.4} \times 10^{-3}\,\text{GeV}^2}{4\pi^2 q^4} + \mathcal{O}(q^{-6})\,, \\
\tilde{\mathcal{W}}_1^8(q^2) &= \frac{1}{4\sqrt{3}\pi^2 q^2} + \frac{2}{9\sqrt{3}eq^4}(4m_u X_u + m_d X_d - 2m_s X_s) + \mathcal{O}(q^{-6}) \\
&= \frac{1}{4\sqrt{3}\pi^2 q^2} - \frac{0.27^{+0.05}_{-0.04}\,\text{GeV}^2}{4\sqrt{3}\pi^2 q^4} + \mathcal{O}(q_1^{-6})\,, \\
\tilde{\mathcal{W}}_1^0(q^2) &= \frac{1}{\sqrt{6}\pi^2 q^2} + \frac{\sqrt{8}}{9\sqrt{3}eq^4}(4m_u X_u + m_d X_d + m_s X_s) + \mathcal{O}(q^{-6}) \\
&= \frac{1}{\sqrt{6}\pi^2 q^2} + \frac{0.079^{+0.013}_{-0.010}\,\text{GeV}^2}{\sqrt{6}\pi^2 q^4} + \mathcal{O}(q^{-6})\,.
\end{aligned} \tag{4.224}$$

and $\tilde{\mathcal{W}}_2^a(q^2) = -\tilde{\mathcal{W}}_1^a(q^2)/2 + \mathcal{O}(q^{-6})$, where we neglected terms involving two or more powers of the quark mass. Here, we have used the quark masses from Ref. [69] in the $\overline{\text{MS}}$ scheme at $\mu = 2\,\text{GeV}$ consistent with the tensor coefficients given above. The numerator of the q^{-4} term in $\tilde{\mathcal{W}}_1^3$ differs substantially from $m_\pi^2 \approx 18.2 \times 10^{-3}\,\text{GeV}^2$ used in Ref. [6]. This can be understood from the fact that that result relies on the Gell-Mann–Oakes–Renner relation in the isospin limit, which involves the combination $(m_u + m_d)/2$, whereas here we need the much smaller combination $(4m_u - m_d)/3$. Similar effects are even more drastic in the case of $\tilde{\mathcal{W}}_1^8$, where the hierarchy $m_s \gg m_{u/d}$ leads to a negative coefficient as opposed to $+m_\eta^2$ used in Ref. [6].

There are many operators at $d = 5$ and $d = 6$, which produce terms of order q^{-6} and higher. In the chiral limit, these provide the first non-perturbative corrections and, in agreement with the non-renormalization of the anomaly, contribute only to $\tilde{\mathcal{W}}_2$. Ref. [6] estimates in the chiral limit

$$\tilde{\mathcal{W}}_2(q^2) = -\frac{N_c \operatorname{Tr}(\mathcal{Q}_5 \mathcal{Q}^2)}{4\pi^2 q^2}\left[1 - \frac{(0.71\,\text{GeV})^4}{q^4} + \mathcal{O}\left(\frac{1}{q^6}\right)\right]\,. \tag{4.225}$$

In the following two sections, we explain how the SDCs in Eq. (4.224) can be incorporated into the two dispersive formalisms. This is required for our numerical study of the isovector scalar functions in Sec. 4.6, where we will compare the results of the two approaches.

4.5.2 Implementation of SDCs into dispersion relations in $g - 2$ kinematics

Each contribution to the two scalar functions in Eq. (4.148) behaves as q^{-2} asymptotically, in accordance with the OPE constraints. However, the parameters fixed from low-energy input make the coefficients of the leading and sub-leading terms in the high-energy expansion disagree with Eq. (4.224). To amend this, we add one additional pole contribution to each flavor channel of each scalar function

$$\tilde{\mathcal{W}}_{1,2}^{(a)\text{eff}} = \frac{n_{1,2}^{(a)\text{eff}}}{q^2 - \left(m_{1,2}^{(a)\text{eff}}\right)^2} . \tag{4.226}$$

This effective pole can be understood as resumming the effects of all heavier intermediate states that are not included explicitly. In each case, the two parameters $n_{1,2}^{(a)\text{eff}}$ and $m_{1,2}^{(a)\text{eff}}$ can be fixed by matching the two terms in the expansion in Eq. (4.224).

To do this, we need the asymptotic expansions of the dispersion integrals in the two-pion contributions to Eq. (4.148). The first integral reads

$$I_1^{\mathcal{U}(0)}(q_1^2) = \int_{4m_\pi^2}^\infty \mathrm{d}s \frac{F_\pi^V(s)\sigma_\pi^3(s)\Omega_1^1(s)^*}{s-q^2} . \tag{4.227}$$

We split this integral at some scale s_0 with $\{\Lambda_{\text{QCD}}^2, m^2\} \ll s_0 \ll q^2$. We can then take q^2 to be much larger than any other energy scale in the low-energy part and can thus Taylor expand the integrand. In the high-energy part, any hadron mass squared can be neglected against s and both the Omnès function and the VFF can be replaced by their asymptotic expressions. Assuming $F_\pi^V(s) = \Omega_1^1(s)$ and the asymptotic form $\Omega_1^1(s) = a/s + \mathcal{O}(1/s^2)$, we obtain

$$\begin{aligned}
I_1^{\mathcal{U}(0)}(q^2) &= -\int_{4m_\pi^2}^{s_0} \mathrm{d}s |\Omega_1^1(s)|^2 \sigma_\pi^3(s) \left[\frac{1}{q^2} + \frac{s}{q^4} + \mathcal{O}\left(\frac{s^2}{q^6}\right)\right] \\
&\quad + \int_{s_0}^\infty \mathrm{d}s \frac{1}{s-q^2}\left[\frac{|a|^2}{s^2} + \mathcal{O}\left(\frac{\Lambda_{\text{QCD}}^4}{s^3}\right)\right] \\
&= \frac{1}{q^2}\left[-\int_{4m_\pi^2}^{s_0} \mathrm{d}s |\Omega_1^1(s)|^2 \sigma_\pi^3(s) - \frac{|a|^2}{s_0} + \mathcal{O}\left(\frac{\Lambda_{\text{QCD}}^4}{s_0^2}\right)\right] - \frac{\log\left(-\frac{q^2}{\mu^2}\right)}{q^4}|a|^2 \\
&\quad + \frac{1}{q^4}\left[-\int_{4m_\pi^2}^{s_0} \mathrm{d}s s |\Omega_1^1(s)|^2 \sigma_\pi^3(s) + |a|^2 \log\left(\frac{s_0}{\mu^2}\right) + \mathcal{O}\left(\frac{\Lambda_{\text{QCD}}^4}{s_0}\right)\right] + \mathcal{O}\left(\frac{\Lambda_{\text{QCD}}^4}{q^6}\right) .
\end{aligned} \tag{4.228}$$

Since s_0 is arbitrary, the dependence on this has to cancel for each order. We have also checked that higher orders in the asymptotic expansion of the Omnès function do not modify the result at the given order. The other integrals can be expanded in the same way.

The expansion of each of these integrals contains a term scaling as $\log(-q^2/\mu^2)/q^4$. Such terms are indeed expected from the OPE calculation, see Eq. (4.215), but we have neglected them in Eq. (4.224) since they are quadratic in the quark mass. We do not put constraints on the coefficients of these terms, but include in the uncertainty estimate a variation of the arbitrary scale μ within a factor 3 around 1 GeV.

4.5.3 Implementation of SDCs into dispersion relations for fixed photon virtualities

In the results from dispersion relations for fixed photon virtualities, Eqs. (4.153) and (4.156), the contributions from each intermediate state behaves as q^{-4}. Similarly to HLbL, the infinite tower of intermediate states has to behave differently in order to fulfill the OPE constraints. Thus, it is impossible to model the tower of heavier intermediate states with one or any finite number of effective poles. Instead, one has to resort to hadronic models as discussed in Sec. 3.1.4.

Instead, we here follow the approach of Ch. 3 and Ref. [45] to smoothly interpolate between the dispersively described low-energy region and the asymptotic region where SDCs are valid. Since in this case we are dealing with functions of only one variable, only the step from Sec. 3.3 is required. We use the interpolants

$$\begin{aligned}\tilde{\mathcal{W}}_1^{3,\text{int}}(q^2) &= \frac{1}{4\pi^2 q^2} + \frac{4.9^{+2.3}_{-1.4} \times 10^{-3}\,\text{GeV}^2}{4\pi^2 q^4} + \frac{c_1^1}{4\pi^2 q^6} + \frac{c_1^2}{4\pi^2 q^8}\,,\\ \tilde{\mathcal{W}}_2^{3,\text{int}}(q^2) &= -\frac{1}{8\pi^2 q^2} - \frac{4.9^{+2.3}_{-1.4} \times 10^{-3}\,\text{GeV}^2}{8\pi^2 q^4} - \frac{c_2^1}{8\pi^2 q^6} - \frac{c_2^2}{8\pi^2 q^8}\,.\end{aligned} \tag{4.229}$$

for the isovector functions above a matching point $Q^2 = -q^2 = m^2$. This follows from Eq. (3.21) by adding further sub-leading terms. The coefficients c_i^j are fixed such that the functions and their first derivatives are continuous at the matching point. Below this point, the dispersive representation is used. We will not provide an uncertainty estimation in our numerical study in this case and thus do not consider alternative interpolants. Using two free parameters and matching at $m^2 = 0.5\,\text{GeV}^2$ turned out to be reasonable choices for HLbL, so we will adopt them here.

4.6 Numerical implementation in isovector channel

In this section, we provide numerical implementations for both dispersive representations in the isovector channel. We compare the results against each other as well as the models introduced in Sec. 4.1.4 and provide results for a_μ^{VVA}.

4.6.1 Phase and Omnès function

For the isovector P-wave phase shift, we use the results of Ref. [182] based on Roy equations [183]. We guide it to the asymptotic value π by using the function

$$\delta_{\text{asymp}} = \pi + \frac{a}{s+b} \tag{4.230}$$

above $s = 1\,\text{GeV}^2$ with the parameters a and b chosen such that the function and its first derivative are continuous at the matching point. We have checked that the exact form of

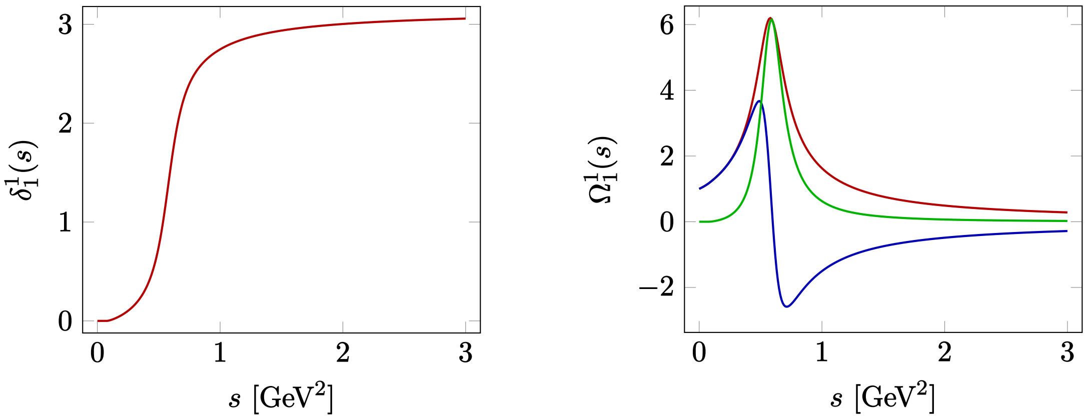

Figure 4.6: Left: $I = 1$ P-wave phase shift from Ref. [182] guided to π asymptotically, right: Omnès function obtained from this phase shift. Red corresponds to the absolute value, blue to the real part and green to the imaginary part.

the asymptotic matching and the matching point only have a minor effect on our results for VVA. The phase shift is displayed on the left-hand side of Fig. 4.6. We then plug this into Eq. (4.136) to calculate the Omnès function. The result is shown on the right-hand side of Fig. 4.6. It is dominated by a strong peak from the ρ-resonance.

4.6.2 Pion TFF and $\gamma \to 3\pi$

For the space-like pion TFF needed in the formalism with fixed photon virtualities, we use the dispersive representation of Ref. [18, 50]. In the formalism in $g-2$ kinematics, we need the singly-virtual pion TFF evaluated at the time-like value m_π^2. Due to the smallness of m_π^2, the simple VMD-model

$$F_{\pi^0\gamma^*\gamma^*}(q^2, 0) = F_{\pi^0\gamma^*\gamma^*}(q^2, 0)\frac{-m_\rho^2}{q^2 - m_\rho^2} \tag{4.231}$$

is sufficient. We vary the ρ-meson mass in this equation within its width. For the normalization, we employ the experimentally measured value [184], which is in excellent agreement with the leading-order χPT expression

$$F_{\pi^0\gamma^*\gamma^*}(0, 0) = \frac{1}{4\pi^2 F_\pi}\,. \tag{4.232}$$

In addition, we need the value $\mathcal{F}_{\pi^0}(m_\pi^2, m_\pi^2, m_\pi^2; 0) = f_{\pi^0}(m_\pi^2, 0)$. To this end, we solve the Khuri–Treiman equations [185] for $\mathcal{F}_{\pi^0}(s, t, u; 0)$ [18, 186] iteratively with the $\pi\pi$-phase input discussed above. We obtain

$$\frac{\mathcal{F}_{\pi^0}(m_\pi^2, m_\pi^2, m_\pi^2; 0)}{\Omega_1^1(m_\pi^2)} \approx \frac{1.07}{4\pi^2 F_\pi^3}\,, \tag{4.233}$$

where quark-mass effects in the normalization [18, 171, 175] are taken into account and are responsible for the largest part of the difference to the chiral limit expression in Eq. (4.146).

4.6.3 a_1 TFF and $\gamma a_1 \to 2\pi$

For $\tilde{\mathcal{W}}_2^3(q^2)$ in the approach in $g-2$ kinematics, we need $\mathcal{F}_2^{a_1}(m_{a_1}^2, 0)$. We employ the minimal VMD model for the f_1 TFFs of Ref. [179] together with flavor symmetry. This model with the numerical input from the first fit in Tab. 8 of that reference gives

$$\mathcal{F}_2^{f_1}(m_{f_1}^2, 0) = -1.29 - 0.16\mathrm{i}\,. \tag{4.234}$$

From flavor symmetry, we deduce

$$\mathcal{F}_2^{f^a}(q_1^2, q_2^2) \propto \mathrm{Tr}(\mathcal{Q}^2 \lambda^a) \tag{4.235}$$

and the mixing pattern is parameterized as

$$\begin{pmatrix} a_1 \\ f_1 \\ f_1' \end{pmatrix} = \begin{pmatrix} 1 & 0 & 0 \\ 0 & \cos\theta_A & \sin\theta_A \\ 0 & -\cos\theta_A & \cos\theta_A \end{pmatrix} \begin{pmatrix} f^3 \\ f^0 \\ f^8 \end{pmatrix} \tag{4.236}$$

with $\theta_A \approx 62°$. This allows to relate the a_1 TFF to the f_1 TFF

$$\mathcal{F}_2^{a_1}(q_1^2, q_2^2) \approx \frac{\mathrm{Tr}(\mathcal{Q}^2\lambda^3)}{\cos\theta_A \,\mathrm{Tr}(\mathcal{Q}^2\lambda^0) + \sin\theta_A \,\mathrm{Tr}(\mathcal{Q}^2\lambda^8)} \mathcal{F}_2^{f_1}(q_1^2, q_2^2)\,. \tag{4.237}$$

We note that this assumes equal masses for ρ, ω and ϕ, since the isoscalar f_1 couples to $\rho\rho$ states, whereas the isovector a_1 couples to $\rho\omega$ states. Thus, it is unclear at which mass the TFF should be evaluated. For the two choices, we obtain

$$\mathcal{F}_2^{a_1}(m_{a_1}^2, 0) = -0.89 + 0.01\mathrm{i}\,, \quad \mathcal{F}_2^{a_1}(m_{f_1}^2, 0) = -1.01 - 0.12\mathrm{i}\,. \tag{4.238}$$

Including also the other fits in Tab. 8 of Ref. [179] as well as the extended VMD model with the fits in Tab. 9 of that reference, we find that all results are within the range

$$\mathcal{F}_2^{a_1}(m_{a_1}^2, 0) = (-0.71 \pm 0.34) - (0.04 \pm 0.09)\mathrm{i}\,. \tag{4.239}$$

The imaginary parts are very sensitive to the exact mass plugged in. Therefore, determining $\mathcal{F}_{a_1,1}(m_{a_1}^2, m_\pi^2, m_\pi^2; 0)$ from the cancellation of imaginary parts as explained in Sec. 4.2.5 leads to a broad range

$$\mathcal{F}_{a_1,1}(m_{a_1}^2, m_\pi^2, m_\pi^2; 0) \in (-9.5, 24.7)\,. \tag{4.240}$$

Below, we will examine the numerical effect of this.

The real part of the TFF will be varied within the range given in Eq. (4.239). We assume that the uncertainty induced by the use of $SU(3)$ symmetry is captured by the evaluation at $m_{a_1}^2$ and $m_{f_1}^2$. We note that the result from the hQCD model reviewed in Sec. 4.1.4, $\mathcal{F}_2^{a_1}(m_{a_1}^2, 0) = -0.35$, is slightly outside the interval in Eq. (4.239).

For the space-like a_1 TFFs required for the dispersion relations with fixed photon virtualities, we use the parameterization [164, 165]

$$\mathcal{F}_1^{a_1}(q^2,0) = 0\,, \qquad \mathcal{F}_2^{a_1}(q^2,0) = \mathcal{F}_2^{a_1}(0,0)\left(1-\frac{q^2}{\Lambda^2}\right)^{-2}\,. \tag{4.241}$$

The parameter Λ has been found to be around 1 GeV for $f_1(1285)$ and $f_1'(1420)$ [164, 165] and we assume the same to be true for the a_1. For the normalization, we consider the so-called equivalent two-photon decay width

$$\tilde{\Gamma}_{a_1\to\gamma\gamma} = \lim_{q^2\to 0}\frac{m_{a_1}^2}{q^2}\frac{1}{2}\Gamma(a_1\to\gamma_L^*\gamma_T)\,, \tag{4.242}$$

where q^2 is virtuality of the longitudinal off-shell photon. Ref. [131] has estimated it from $SU(3)$ symmetry and the measurements for $f_1(1285)$ and $f_1'(1420)$ [164, 165]

$$\tilde{\Gamma}_{a_1\to\gamma\gamma} = (2.0\pm 0.7)\,\text{keV}\,. \tag{4.243}$$

The relation to the form factor [131]

$$\tilde{\Gamma}_{a_1\to\gamma\gamma} = \frac{\pi\alpha^2 m_{a_1}}{12}|\mathcal{F}_2^{a_1}(0,0)|^2 \tag{4.244}$$

leads to

$$\mathcal{F}_2^{a_1}(0,0) = 0.34\pm 0.06\,. \tag{4.245}$$

4.6.4 Input for the vector mesons

For the vector-meson poles in the dispersive framework in $g-2$ kinematics, we need the parameters $\tilde{\mathcal{V}}_i^{V,(3)}(0,m_V^2)$. According to Sec. 4.2.3.2, these can be written as

$$\begin{aligned}
\tilde{\mathcal{V}}_1^{V,(3)}(0,m_V^2) &= -F_\pi\frac{F_{V\pi}}{m_V^2-m_\pi^2} + \frac{F_{a_1}}{m_{a_1}}\left(F_{Va_1}^1 + \frac{1}{2}F_{Va_1}^2 + \frac{F_{Va_1}^3}{m_V^2}\right)\,,\\
\tilde{\mathcal{V}}_2^{V,(3)}(0,m_V^2) &= \frac{F_{a_1}m_{a_1}}{m_V^2}\frac{F_{Va_1}^3}{m_V^2-m_{a_1}^2}\,,
\end{aligned} \tag{4.246}$$

where we have again taken into account π^0 and a_1 poles. The coupling constants in this equation are related to decay widths via

$$\begin{aligned}
\Gamma_{V\to P\gamma} &= \frac{\alpha(F_{VP})^2}{24}\left(\frac{m_V^2-m_P^2}{m_V}\right)^3\,,\\
\Gamma_{A\to V\gamma} &= \frac{\alpha(m_A^2-m_V^2)^3}{24m_A^5m_V^2}\Bigg[m_V^2(m_A^2-m_V^2)^2\left(F_{VA}^1+\frac{1}{2}F_{VA}^2\right)^2 + (m_A^2+m_V^2)(F_{VA}^3)^2\\
&\qquad -2m_V^2(m_A^2-m_V^2)\left(F_{VA}^1+\frac{1}{2}F_{VA}^2\right)F_{VA}^3\Bigg]\,.
\end{aligned} \tag{4.247}$$

Both Eqs. (4.246) and (4.247) depend only on the linear combinations $\tilde{F}^1_{VA} = F^1_{VA} + F^2_{VA}/2$ and $\tilde{F}^2_{VA} = F^3_{VA}$.

In principle there is an infinite tower of isoscalar vector resonances. Of course it is impossible to fix the corresponding infinite number of parameters from experimental input. However, we expect it to be sufficient to only include the lightest one explicitly, the ω-meson, for the following reasons. First, the parameters of the ϕ-meson are related to those of the ω through the approximate $U(3)$-symmetry relation

$$\frac{F_{\phi\pi}}{F_{\omega\pi}} = \frac{\tilde{F}^i_{\phi a_1}}{\tilde{F}^i_{\omega a_1}} = \frac{\cot\theta_V - \sqrt{2}}{\tan\theta_V + \sqrt{2}}. \tag{4.248}$$

The vector-meson mixing angle θ_V is close to the ideal mixing angle $\theta_V^{\text{ideal}} = \tan^{-1}(1/\sqrt{2})$, which implies $F_{\phi\pi} \ll F_{\omega\pi}$, $\tilde{F}^i_{\phi a_1} \ll \tilde{F}^i_{\omega a_1}$ and thus $\tilde{\mathcal{V}}_i^{\phi,(3)}(0, m_\phi^2) \ll \tilde{\mathcal{V}}_i^{\omega,(3)}(0, m_\omega^2)$. Second, the masses of all heavier vector mesons are significantly larger than 1 GeV and there are other intermediate states in this mass range that we do not include explicitly like $\pi(1300)$. The sum of all these contributions thus has to be described through the effective poles that match the dispersive expressions to the SDCs.

For the pseudoscalar parameters, the experimental measurements of the width $\Gamma_{\omega\to\pi\gamma}$ can be used together with Eq. (4.247) to determine $F_{\omega\pi}$. However, the decay $a_1 \to \omega\gamma$ has not been measured yet. We could use the measurement of $\Gamma_{f_1\to\rho\gamma}$ together with a $U(3)$ relation, but even that would only fix the combination appearing in Eq. (4.247). In principle, the decay $\Gamma_{f_1\to\phi\gamma}$ probes another combination due to $m_\phi \neq m_\rho$, but in the $U(3)$ limit the masses become degenerate so that then $U(3)$ symmetry cannot be used any more.

For these reasons, we take a simpler approach: first, the ω-pole contribution to $\tilde{\mathcal{W}}_1^{(3)}$ has to vanish in chiral limit due to the anomaly. Since we are in the isovector channel, we expect chiral corrections to be below 5 %. We thus take $m_\omega f_\omega \tilde{\mathcal{V}}_1^{\omega,(3)} = 0$ as our central value and vary it between ± 5 % of the residue of the pion pole. For $\tilde{\mathcal{W}}_2^{(3)}$, a similar argument does not hold. Thus, in the absence of more reliable input, we fix the residue from the holographic model, taking into account that the vector-meson pole in this model includes in addition to the ω-pole also the ρ-resoance, which is part of the dispersive 2π contribution. We assign a conservative 50 % uncertainty to the value in Ref. 4.1. Fixing the parameters in this way implies strong correlations between the vector-meson residues and other quantities such as the ones entering the two-pion contribution to $\tilde{\mathcal{W}}_2$. We take these into account in our error estimation.

4.6.5 Results for dispersion relations in $g-2$ kinematics

We are now ready to put all pieces together and obtain representations for the functions $\tilde{\mathcal{W}}_i$—based on the dispersion relations in $g-2$ kinematics in this section and then based on the dispersion relations for fixed photon virtualities in the next one. Afterwards, we will compare the results of the two approaches. Starting from Eq. (4.148), we include the pion and a_1 poles, which are assumed to be pure isovector states, the ω-meson pole in the q_3^2-channel as well as the two-pion intermediate state with π^0 and a_1 poles in the sub-process. Furthermore, we add effective pole-terms as described in Sec. 4.5.2. The scalar functions then take the form

$$\begin{aligned}\tilde{\mathcal{W}}_1^3(q_1^2) &= F_\pi \frac{F_{\pi^0\gamma^*\gamma^*}(m_\pi^2, 0)}{q_1^2 - m_\pi^2} + \frac{m_\omega f_\omega \tilde{\mathcal{V}}_1^{\omega,(3)}(0, m_\omega^2)}{q_1^2 - m_\omega^2} - \frac{1}{48\pi^2}\int_{4m_\pi^2}^\infty \mathrm{d}s \frac{|\Omega_1^1(s)|^2 \sigma_\pi^3(s) \tilde{\mathcal{U}}_1^{(3)}(0)}{s - q_1^2 - \mathrm{i}\epsilon} \\ &+ \frac{1}{96\pi^2}\int_{4m_\pi^2}^\infty \mathrm{d}s \frac{s|\Omega_1^1(s)|^2\sigma_\pi^3(s)}{(s - q_1^2 - \mathrm{i}\epsilon)(s - m_\pi^2 - \mathrm{i}\epsilon)} F_\pi \frac{\mathcal{F}_{\pi^0}}{\Omega_1^1(m_\pi^2)} + \frac{n_1^{(3)\mathrm{eff}}}{q_1^2 - \left(m_1^{(3)\mathrm{eff}}\right)^2}, \\ \tilde{\mathcal{W}}_2^3(q_1^2) &= -\frac{F_{a_1}}{m_{a_1}} \frac{\mathcal{F}_2^{a_1}(m_{a_1}^2, 0)}{q_1^2 - m_{a_1}^2} + \frac{m_\omega f_\omega \tilde{\mathcal{V}}_2^{\omega,(3)}(0, m_\omega^2)}{q_1^2 - m_\omega^2} + \frac{1}{48\pi^2}\int_{4m_\pi^2}^\infty \mathrm{d}s \frac{|\Omega_1^1(s)|^2 \sigma_\pi^3(s) \tilde{\mathcal{U}}_1^{(3)}(0)}{s - q_1^2 - \mathrm{i}\epsilon} \\ &+ \frac{1}{48\pi^2}\int_{4m_\pi^2}^\infty \mathrm{d}s \frac{s|\Omega_1^1(s)|^2\sigma_\pi^3(s)}{(s - q_1^2 - \mathrm{i}\epsilon)(s - m_{a_1}^2 - \mathrm{i}\epsilon)} \frac{F_{a_1}\mathcal{F}_{a_1,1}}{m_{a_1}\Omega_1^1(m_{a_1}^2)} + \frac{n_2^{(3)\mathrm{eff}}}{q_1^2 - \left(m_2^{(3)\mathrm{eff}}\right)^2}. \end{aligned} \tag{4.249}$$

Solving the systems of equations for the effective-pole parameters gives

$$\begin{aligned} n_1^{(3)\mathrm{eff}} &= 0.0025 \pm 0.0021, & m_1^{(3)\mathrm{eff}} &= 0.83^{+0.13}_{-0.09}\,\mathrm{GeV} \\ n_2^{(3)\mathrm{eff}} &= -0.07 \pm 0.05, & m_2^{(3)\mathrm{eff}} &= 1.35^{+0.31}_{-0.14}\,\mathrm{GeV}, \end{aligned} \tag{4.250}$$

where we have taken into account uncertainties from all input parameters. For the uncertainties of the results in $\tilde{\mathcal{W}}_1$, the most important ones are the allowed size of the ω-pole residue compared to the one of the pion pole, the value of the subtraction constant in $\mathcal{U}_1$, to which we assign a 5 % uncertainty due to higher order corrections in $SU(2)$ χPT, and parameters that enter the pion-pole residue, i.e. F_π, the pion TFF normalization $F_{\pi\gamma^*\gamma^*}(0,0)$ and the mass in the VMD model for the pion TFF in Eq. (4.231), which we vary within the width of the ρ meson. In the case of $\tilde{\mathcal{W}}_2$, the uncertainty is completely dominated by the value of the a_1 TFF at $m_{a_1}^2$ and the holographic input for the vector-meson residue.

For the longitudinal scalar function, we obtain a small effective-pole residue that is almost compatible with zero. For comparison, the residue of the pion pole is 0.026. This is in accordance with every contribution beyond the pion pole vanishing in the chiral limit. The mass of the effective pole is slightly smaller than the masses of intermediate states that have not been included explicitly. We note, however, that in our procedure the effective pole mass can be considerably reduced compared to the mass scale of neglected contributions if those involve partial cancellations. This is because we fix both parameters of the effective pole from asymptotic constraints as opposed to using low-energy input as e.g. Ref. [18] for the pion TFF. Since the effective-pole mass is still much larger than the dominant scale in the isovector component of $\tilde{\mathcal{W}}_1$, m_π, we do not expect that our result for $m_1^{(3)\mathrm{eff}}$ invalidates our conclusion.

In the transversal case, the residue of the effective pole is not suppressed compared to e.g. the a_1-pole residue of 0.10 ± 0.05 and the mass of the pole is in the expected range. The large residue of the effective pole can be understood from a comparison with the holographic model.

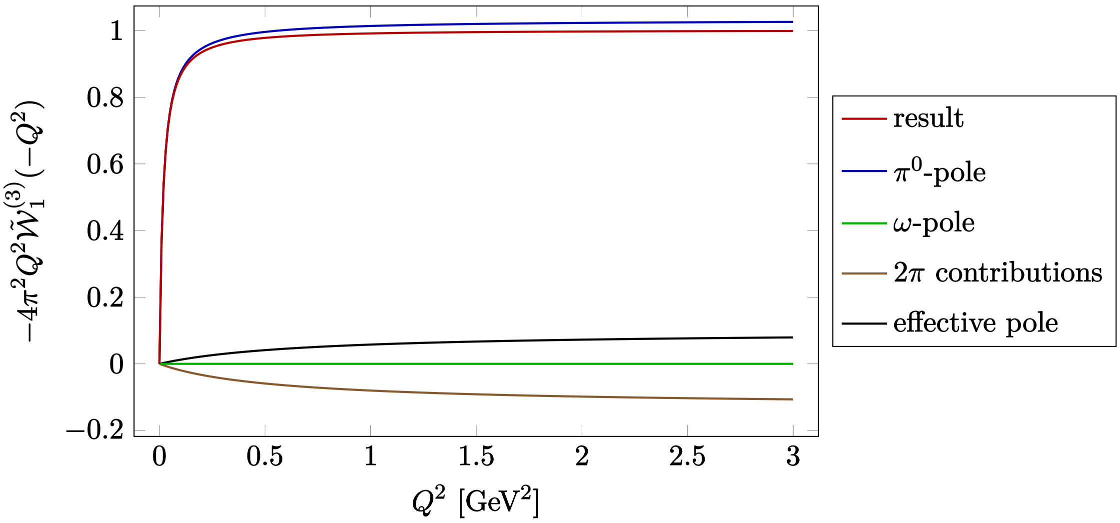

Figure 4.7: Individual contributions to $\tilde{\mathcal{W}}_1^{(3)}$ in the dispersive framework in $g-2$ kinematics.

In that case, the effective pole has to approximate the whole infinite towers of axial-vector and vector poles. In Tab. 4.1, it can be seen that the residues of these poles increase with the radial excitation so that any truncation of the infinite sums will lead to a large error at high energies that has to be compensated by an effective pole with a large residue.

The contributions to the two functions from individual intermediate states can be found in Figs. 4.7 and 4.8 for our central result. Also there, the very different behavior of the two functions can be seen: while the longitudinal function is completely dominated by the pion pole, the transversal one involves a large cancellation between individual terms, mainly the a_1 and the effective poles, in such a way that the sum is much smaller than the individual contributions.

Plugging these functions into the integrals Eq. (4.17), together with the electron loop in Eq. (4.20), we obtain the first-family electroweak contribution

$$a_{\mu,g-2}^{\mathrm{VVA},L}[u,d,e] = -0.89^{+0.03}_{-0.02} \times 10^{-11}\,, \qquad a_{\mu,g-2}^{\mathrm{VVA},T}[u,d,e] = -1.17^{+0.26}_{-0.19} \times 10^{-11} \tag{4.251}$$

such that the sum becomes

$$a_{\mu,g-2}^{\mathrm{VVA}}[u,d,e] = -2.07^{+0.27}_{-0.19} \times 10^{-11}\,. \tag{4.252}$$

The uncertainty of $a_{\mu,g-2}^{\mathrm{VVA},T,3}$ is completely dominated by the error of the holographic input for the ω-pole residue and the much smaller uncertainty of $a_{\mu,g-2}^{\mathrm{VVA},L,3}$ is dominated by the errors of the quantities that enter the pion-pole residue, i.e. F_π, the pion TFF normalization and the mass in the VMD model for the pion TFF in Eq. (4.231). A comparison with results from the literature is deferred to Sec. 4.6.7.

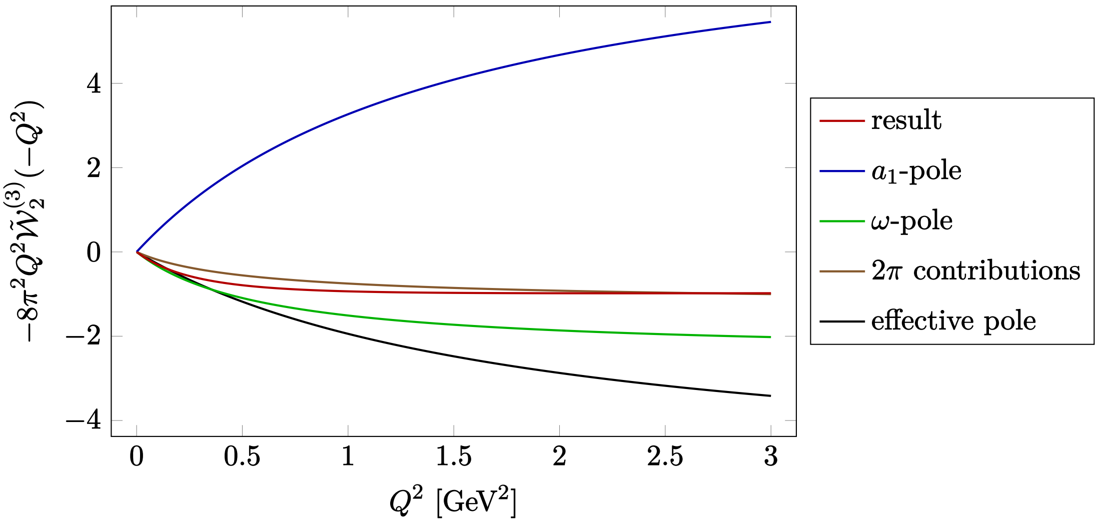

Figure 4.8: Individual contributions to $\tilde{\mathcal{W}}_2^{(3)}$ in the dispersive framework in $g-2$ kinematics.

4.6.6 Results for dispersion relations with fixed photon virtualities

We now provide an implementation of the approach of Sec. 4.3 matched to the SDCs as described in Sec. 4.5.3. Since a dispersive description of the a_1 TFF that is useful for numerical studies is still missing, we refrain from giving an uncertainty estimation and just show central results based on the simple parameterization given in Sec. 4.6.3.

Below the matching point, we use representations with only π^0- and a_1-poles

$$\begin{aligned}\tilde{\mathcal{W}}_1^3(q^2) &= F_\pi \frac{F_{\pi^0\gamma^*\gamma^*}(q^2,0)}{q^2-m_\pi^2} - \frac{F_{a_1}}{m_{a_1}^3}\left[\mathcal{F}_1^{a_1}(q^2,0)+\mathcal{F}_2^{a_1}(q^2,0)\right], \\ \tilde{\mathcal{W}}_2^3(q^2) &= -\frac{F_{a_1}}{m_{a_1}}\frac{\mathcal{F}_2^{a_1}(q^2,0)}{q^2-m_{a_1}^2}. \end{aligned} \tag{4.253}$$

Matching this to the asymptotic functions Eq. (4.229) allows us to determine the parameters of the latter

$$\begin{aligned} c_1^1 &= -0.176\,\text{GeV}^4, & c_1^2 &= -0.064\,\text{GeV}^6, \\ c_2^1 &= -0.431\,\text{GeV}^4, & c_2^2 &= -0.143\,\text{GeV}^6. \end{aligned} \tag{4.254}$$

The transition from the dispersively described low-energy region to the asymptotic form and the approach of the asymptotic limit can be seen in Figs. 4.9 and 4.10. For the electroweak contribution to a_μ, this implies

$$a_{\mu,FPV}^{\text{VVA},L}[u,d,e] = -1.10\times10^{-11}, \qquad a_{\mu,FPV}^{\text{VVA},T}[u,d,e] = -1.39\times10^{-11} \tag{4.255}$$

with the sum

$$a_{\mu,FPV}^{\text{VVA}}[u,d,e] = -2.49\times10^{-11}. \tag{4.256}$$

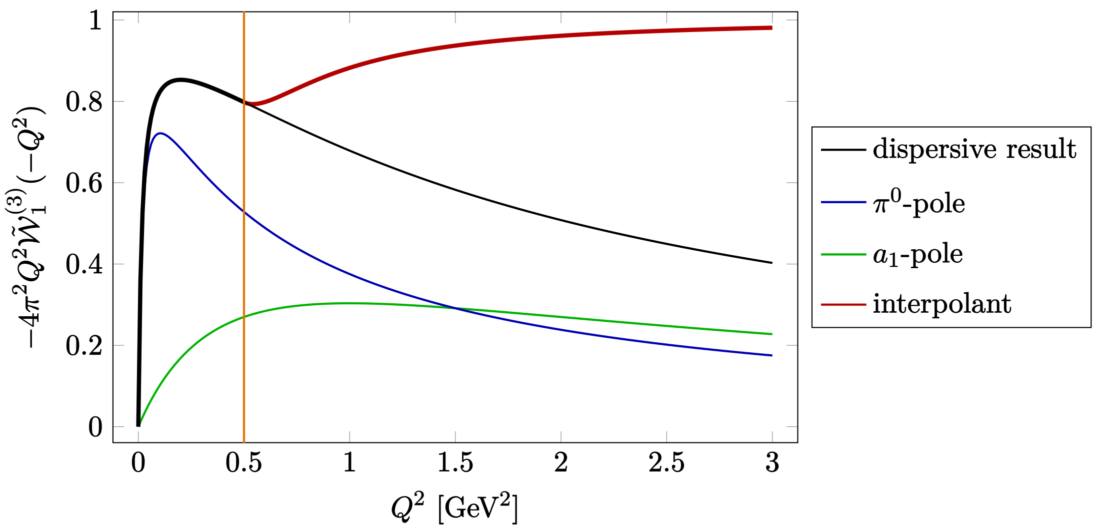

Figure 4.9: Results for $\tilde{\mathcal{W}}_1^{(3)}$ in the dispersive framework with fixed photon virtualities and the matching to the SDCs. The dispersive result is used below the matching point at $Q^2 = 0.5\,\text{GeV}^2$ (vertical orange line) and the interpolant above as indicated by the thick line.

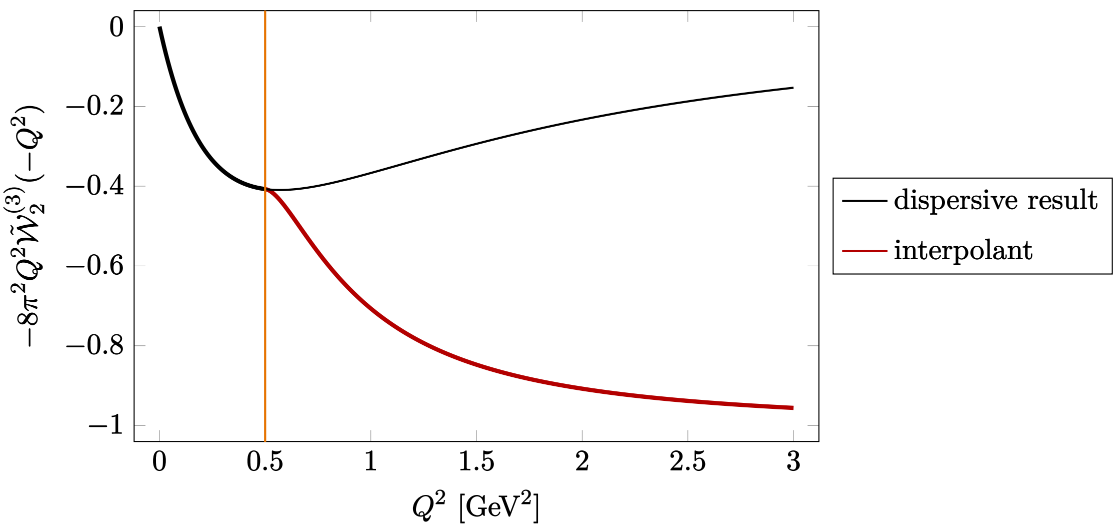

Figure 4.10: Results for $\tilde{\mathcal{W}}_2^{(3)}$ in the dispersive framework with fixed photon virtualities and the matching to the SDCs. The dispersive result is used below the matching point at $Q^2 = 0.5\,\text{GeV}^2$ (vertical orange line) and the interpolant above as indicated by the thick line.

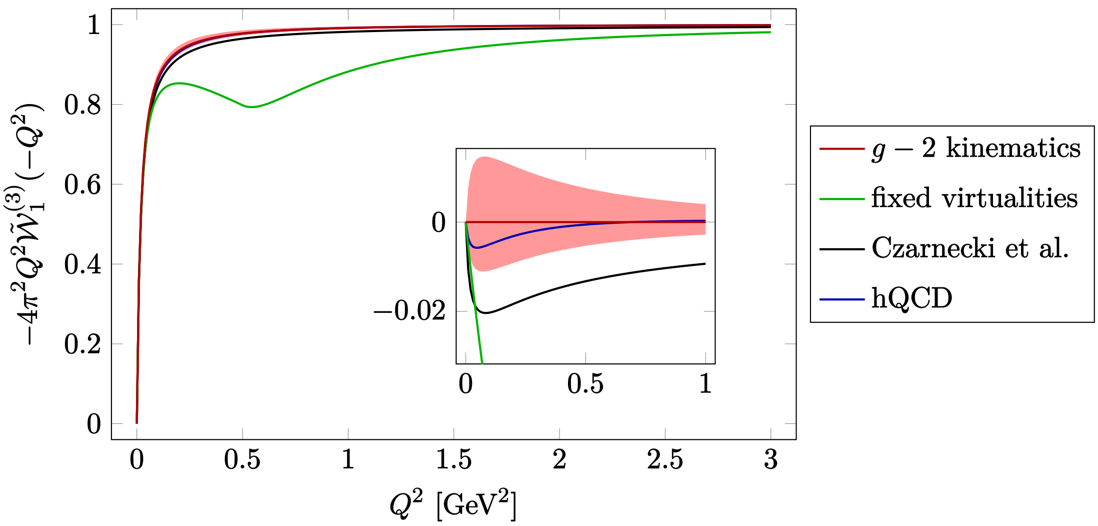

Figure 4.11: Comparison of the two dispersive approaches to VVA with the two models introduced in Sec. 4.1.4 for $\tilde{\mathcal{W}}_1$. The band corresponds to the uncertainty of the result based on dispersion relations in $g-2$ kinematics. The small insert shows the difference to the central result for the dispersion relations in $g-2$ kinematics in the low-Q^2 region. Notice the different scale in the insert.

4.6.7 Comparison

In Figs. 4.11 and 4.12, we compare the two dispersive representations against the two models introduced in Sec. 4.1.4 for the two scalar functions. In $\tilde{\mathcal{W}}_1$, the two models are very close to the dispersive representation in $g-2$ kinematics over the whole plotted Q^2 range. However, due to the small uncertainty band, there are some deviations with the model of Ref. [6] as can be seen in the insert. This can be understood as a consequence of the model consisting only of a pion pole with the residue being adjusted to the SDC. With the leading-order expression for the pion TFF normalization, the model agrees with our dispersively-defined pion pole up to a shift of the argument from m_π^2 to 0. This shift slightly reduces the residue, which influences the scalar function at small Q^2. At larger Q^2, the heavier intermediate states in our representation become relevant such that both functions fulfill the same SDCs. However, also our uncertainty band gets narrower so that the model curve stays outside the band. The pion-pole residue in the holographic model is closer to our value, which explains why this model stays within our uncertainty band for all Q^2.

Conversely, the dispersive representation in fixed photon kinematics differs substantially from all other curves, especially around the matching point of $Q^2 = 0.5\,\text{GeV}^2$. This is due to the effect that each individual intermediate state drops off too fast for large Q^2 and only the infinite tower has the correct asymptotic behavior. A truncated representation as we use it

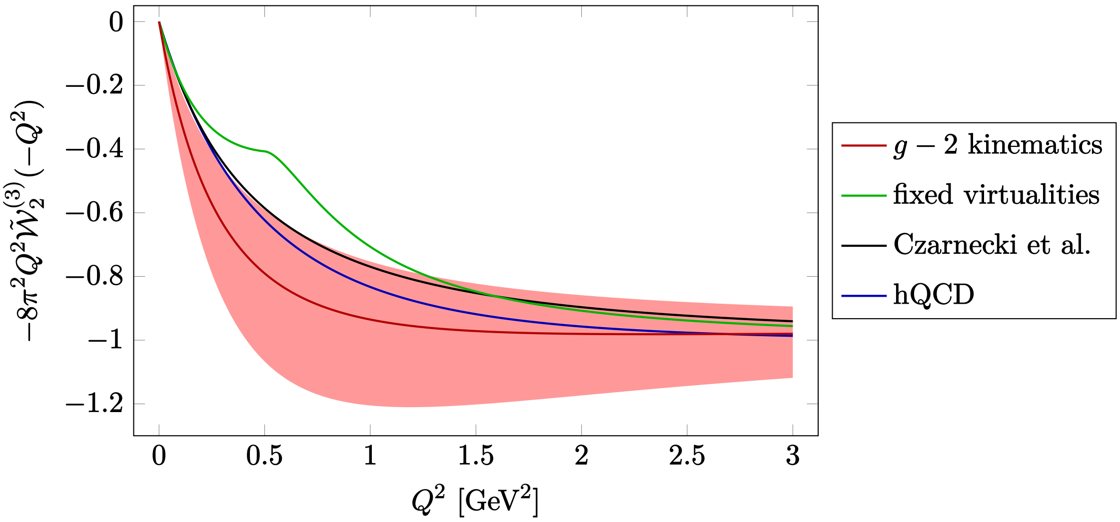

Figure 4.12: Comparison of the two dispersive approaches to VVA with the two models introduced in Sec. 4.1.4 for $\tilde{\mathcal{W}}_2$. The band corresponds to the uncertainty of the result based on dispersion relations in $g-2$ kinematics.

below the matching point thus underestimates the full function and in the present case this sets in already at $Q^2 = 0$.

For the transversal function, the uncertainty band of our result in $g-2$ kinematics is very broad and includes both model calculations with a slight exception at small Q^2. Even the possibility that the curve slightly exceeds the asymptotic value $-1/(8\pi)^2 = 0.0127$ before approaching it cannot be excluded from our calculation. However, the result from fixed-virtuality dispersion relations again drops out of the uncertainty band below the matching point before the transition to the asymptotic form guides it back into the uncertainty band and eventually to the asymptotic value.

It is striking in Fig. 4.12 that the curve from dispersion relations in $g-2$ kinematics differs from both models and the fixed-virtualities dispersion relations already by the slope at the origin, i.e. the value for $\tilde{\mathcal{W}}_2^{(3)}(0)$ is larger, although largely compatible within uncertainties. Indeed, we obtain

$$\begin{aligned} \tilde{\mathcal{W}}^{(3)}_{2,g-2}(0) &= 0.049^{+0.019}_{-0.016}\,\mathrm{GeV}^{-2} & \tilde{\mathcal{W}}^{(3)}_{2,\mathrm{FPV}}(0) &= 0.031\,\mathrm{GeV}^{-2}\,, \\ \tilde{\mathcal{W}}^{(3)}_{2,\mathrm{CMV}}(0) &= 0.029\,\mathrm{GeV}^{-2} & \tilde{\mathcal{W}}^{(3)}_{2,\mathrm{hQCD}}(0) &= 0.028\,\mathrm{GeV}^{-2}\,. \end{aligned} \tag{4.257}$$

The corresponding values for the longitudinal component are

$$\begin{aligned} \tilde{\mathcal{W}}^{(3)}_{1,g-2}(0) &= -1.433^{+0.024}_{-0.031}\,\mathrm{GeV}^{-2} & \tilde{\mathcal{W}}^{(3)}_{1,\mathrm{FPV}}(0) &= -1.419\,\mathrm{GeV}^{-2}\,, \\ \tilde{\mathcal{W}}^{(3)}_{1,\mathrm{CMV}}(0) &= -1.390\,\mathrm{GeV}^{-2} & \tilde{\mathcal{W}}^{(3)}_{1,\mathrm{hQCD}}(0) &= -1.418\,\mathrm{GeV}^{-2}\,. \end{aligned} \tag{4.258}$$

These numbers can be compared against the one-loop χPT expressions given in Ref. [94]. Evaluated at the origin and adapted to our definition of the scalar functions, these read

$$\tilde{\mathcal{W}}^{(3)}_{1,\chi\mathrm{PT}}(0) = \frac{64}{3}C^W_7 - \frac{16}{3}C^W_{22}(\mu) + \frac{1}{384\pi^4 F_\pi^2}\left(\log\frac{m_\pi^2}{\mu^2} + \log\frac{m_K^2}{\mu^2} + 2\right) - \frac{1}{4\pi^2 m_\pi^2}\,,$$
$$\tilde{\mathcal{W}}^{(3)}_{2,\chi\mathrm{PT}}(0) = \frac{16}{3}C^W_{22}(\mu) - \frac{1}{384\pi^4 F_\pi^2}\left(\log\frac{m_\pi^2}{\mu^2} + \log\frac{m_K^2}{\mu^2} + 2\right)\,. \tag{4.259}$$

These expressions depend on two low-energy constants, which have been introduced in Ref. [178]. They can be fixed from the normalization and slope parameter of the π^0 TFF. With this replacement, the expressions simplify to

$$\tilde{\mathcal{W}}^{(3)}_{1,\chi\mathrm{PT}}(0) = -\frac{(1+a_\pi)F_\pi F_{\pi\gamma^*\gamma^*}(0,0)}{m_\pi^2}\,,$$
$$\tilde{\mathcal{W}}^{(3)}_{2,\chi\mathrm{PT}}(0) = \frac{a_\pi F_\pi F_{\pi\gamma^*\gamma^*}(0,0)}{m_\pi^2}\,, \tag{4.260}$$

where we have used the definition

$$a_\pi = \frac{m_\pi^2}{F_{\pi\gamma^*\gamma^*}(0,0)}\frac{\partial}{\partial q^2}F_{\pi\gamma^*\gamma^*}(q^2,0)\,. \tag{4.261}$$

Using the experimental value for the normalization [184] and the dispersive value for the slope [18], this leads to

$$\tilde{\mathcal{W}}^{(3)}_{1,\chi\mathrm{PT}}(0) = (-1.43 \pm 0.08)\,\mathrm{GeV}^{-2}\,, \qquad \tilde{\mathcal{W}}^{(3)}_{2,\chi\mathrm{PT}}(0) = (0.044 \pm 0.003)\,\mathrm{GeV}^{-2}\,, \tag{4.262}$$

where we have propagated the uncertainties of the input parameters and added a 5 % uncertainty due to neglected higher orders in χPT.[6]

In the case of the longitudinal function, the uncertainty on the normalization from χPT is too large to discriminate between the different numbers in Eq. (4.258). However, for the transversal function the χPT result clearly prefers the value from the dispersion relations in $g-2$ kinematics over the other dispersive approach or the two considered models. Due to the small uncertainty of the χPT number for the normalization compared to the dispersive one, this additional constraint might even be used to shrink the uncertainty band in Fig. 4.12 and thus also reduce the uncertainty of $a_{\mu,g-2}^{\mathrm{VVA}}[u,d,e]$ in Eq. (4.252).

The results for $a_\mu^{\mathrm{VVA}}[u,d,e]$ in the fixed-photon-virtuality approach, Eq. (4.256) is outside the uncertainty range of the result based on dispersion relations in the $g-2$ limit, Eq. (4.252), but as no uncertainties on the former have been considered, the significance of this discrepancy cannot be assessed. The model results in Eqs. (4.22) and (4.25) lie between the central values

[6] Although we have started from $SU(3)$ χPT, Eq. (4.260) only contains $SU(2)$ quantities. Thus, we expect the same expressions to arise if the calculation were done in $SU(2)$ χPT so that higher-order corrections should be small.

of our two dispersive approaches and within the uncertainty range in Eq. (4.252). Thus, we generally agree with the commonly used result from Ref. [6]. The uncertainty on the electroweak contribution to a_μ is negligible compared to the ones on HVP, HLbL or the experimental measurement.

4.7 Conclusions

In this chapter, we introduced the novel dispersive formalism for hadronic matrix elements involving soft photons using the VVA correlator as an example. We showed how the imaginary part of the matrix element in the soft-photon limit, $q_2 \to 0$, can be obtained from a sum of two cuts in general kinematics. Based on this, we calculated the effects of single pseudoscalar, single axial-vector, single vector and two-pion intermediate states on VVA. In all cases, we dispersively reconstructed also the required sub-processes taking into account the same intermediate states. This reflects the strategy we will follow for HLbL in the next chapter.

For comparison, we also derived dispersion relations in the axial-vector current invariant mass keeping the photon virtualities fixed. This is done in analogy to the CHPS formalism to HLbL. In this case, only pseudoscalar and axial-vector poles contribute, whereas the effects of vector poles and two-pion intermediate states are hidden in the TFFs. By deriving dispersive representations for the TFFs, taking into account the same intermediate states as in the new formalism, we were able to perform a detailed comparison between the two dispersive frameworks for VVA. We found that the two-pion discontinuity of the scalar functions in the soft-photon limit is not correctly reproduced in the CHPS-like formalism due to neglected contributions with a two-pion cut in the sub-process and we presented a toy-example to illustrate this. Conversely, in the new formalism, the discontinuity is correct up to the lowest threshold of an intermediate state that has not been taken into account.

We concluded the chapter with a numerical evaluation of the VVA correlator in the soft-photon limit, taking into account the SDCs from an OPE calculation. In the case of the new dispersive formalism, a single effective pole in each scalar function suffices to fulfill these SDCs, whereas in the CHPS-like formalism each pole-contribution falls off too fast asymptotically and we thus employed a matching procedure similar to what we introduced for HLbL in Ch. 3.

For the longitudinal component, the numerical result obtained from the new dispersive formalism is very close to hadronic models and the uncertainties are small. In contrast, the results based on dispersion relations with fixed photon virtualities differ substantially around the matching point. A similar picture is also obtained for the transversal component, but with larger differences between the different representations and much larger uncertainties. Therefore, for VVA the dispersion relations in $g-2$ clearly lead to a more realistic description of the scalar functions in the space-like regime. It remains to be seen whether this applies also to HLbL.

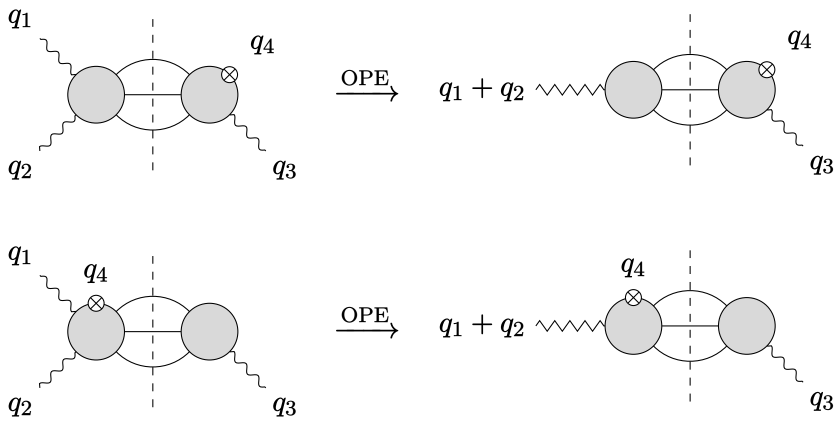

Figure 4.13: Connection between HLbL in the new approach evaluated in the MV regime with the dispersive approach to VVA. The three lines in the intermediate state represent an arbitrary N-particle state and the arrow stands for the OPE expansion Eq. (3.3) that relates a two-photon state to an axial-vector current. The momenta are assigned according to the standard convention for HLbL, which differs from the convention for VVA used in this chapter.

The picture obtained for the scalar functions is also reflected in our results for the electroweak contribution to a_μ due to the VVA correlator. It agrees with previous model estimates within uncertainties. The uncertainty on our dispersive result in $g-2$ kinematics is dominated by missing information on the ω-pole residues, to which a measurement of the decay $a_1 \to \omega\gamma$ would provide valuable constraints. We argued that the χPT-result for the normalization might help to significantly reduce the uncertainties.

The numerical study can be extended to the isoscalar parts of the VVA correlator. This would allow us to calculate the strange-quark contribution to the electroweak diagram, which has to be combined with perturbative charm and muon loops. The third family can be treated fully perturbatively, so that this would complete the calculation of a_μ contributions of the form of the diagram on the right-hand side of Fig. 2.2.

Let us close this chapter by pointing out an interesting application of these results in the context of HLbL. In Sec. 3.1.1, we showed that in the asymmetric asymptotic regimes of HLbL, e.g. $q_1^2 \sim q_2^2 \gg \{q_3^2, \Lambda_{\text{QCD}}^2\}$, an OPE can be used whose leading term relates HLbL to the VVA correlator. The relation between HLbL in the MV region and the VVA correlator can be established for each intermediate-state contribution separately if the dispersion relation is written in the small variable (here q_3^2) keeping the other ones fixed (here q_1^2 and q_2^2) and OPE results are used for the form factors appearing in the HLbL reconstruction. This is illustrated diagrammatically in Fig. 4.13 and shown analytically in Refs. [187, 188], see also

Ref. [21]. Thus, exactly those intermediate states that are numerically important in VVA are also required in HLbL in that regime to fulfill the SDC and obtain a numerically precise representation of the scalar functions. A similar relation also holds in the CHPS formalism, where one only has the s-cut illustrated in the first line of Fig. 4.13. However, as we have shown in this chapter, in the new formalism a finite number of intermediate states is sufficient to obtain a satisfactory numerical description of VVA. Conversely, an infinite tower, possibly mimicked by interpolants, is required in the CHPS approach to compensate for the fact that each individual exclusive intermediate state falls off too fast asymptotically to saturate the SDC. We expect this to prove useful in an implementation of SDCs into HLbL in the formalism introduced in the next chapter.

5 Dispersion Relations for Hadronic Light-by-Light Scattering in Triangle Kinematics

After having introduced the new dispersive formalism in the case of the VVA correlator in the previous chapter, we are now ready to apply it to HLbL. We have argued before that achieving control over the contributions from intermediate states with masses between 1 and 2 GeV is crucial to reduce the theory error of HLbL to the size of the projected precision of the final experimental results at Fermilab [3, 24]. A model-independent evaluation of these effects is not available yet, also due to the fact that it is not known how to unambiguously include contributions from intermediate states of spin two or larger within the standard dispersive representation of HLbL in general four-point kinematics [17, 38, 39].

In this chapter, we explain this issue in detail and show that the novel approach, i.e. dispersion relations directly in the soft-photon limit (triangle kinematics), is free of ambiguities due to redundancies in the tensor decomposition. Compared to the CHPS approach, contributions from different intermediate states get reshuffled, unitarity relations become more involved, and the dispersive reconstructions of additional hadronic sub-processes are required. Here, we explicitly derive analytic expressions for the single-particle intermediate-state contributions to HLbL in triangle kinematics, including tensor resonances. We show that for an inclusion of two-pion rescattering the sub-processes $\gamma^*\gamma^* \to \gamma\pi\pi$ and $\pi\pi \to \gamma\pi\pi$ are required, whose tensor decompositions in the soft-photon limit are also free of kinematic singularities.

Sec. 5.1 is devoted to the issue of kinematic singularities in the CHPS approach and how dispersion relations in $g-2$ kinematics avoid them. We also explain how the discontinuity in triangle kinematics can be obtained from two different cuts in four-point kinematics. Then, in Sec. 5.2, we focus on the unitarity relations and the sub-processes required for a reconstruction of pseudoscalar poles, narrow-width resonances and two-pion rescattering. Furthermore, we explain the reshuffling of contributions with respect to the CHPS formalism and derive results for single-particle contributions in terms of TFFs. In Sec. 5.3, we concentrate on singularities in the soft-photon limit, which cancel between the two cuts. We provide a method to split a soft-singular amplitude into a simple singular piece and a non-singular piece that can be studied dispersively in the soft-photon limit. The content of this chapter has been published in Ref. [60] with the exception of Sec. 5.3.

5.1 Motivation and general idea

5.1.1 Kinematic singularities in the CHPS approach

The framework worked out in Refs. [17, 39] and reviewed in Sec. 2.4.3 consists of dispersion relations for the HLbL tensor in general four-point kinematics, which can be derived from the Mandelstam double-spectral representation. The photon virtualities are treated as fixed external variables, while dispersion relations are written in terms of the Mandelstam variables. In particular, in Ref. [17] a basis of scalar functions $\check{\Pi}_i$ was derived that is suitable for dispersion relations in the singly-on-shell limit $q_4^2 = 0$. For $t = q_2^2$, the scalar functions are free from kinematic singularities in the Mandelstam variables s and u, enabling fixed-t dispersion relations. The representation is also manifestly free from contributions of unphysical helicity amplitudes. After writing the dispersion relation, the limit $q_4 \to 0$ is taken to arrive at the kinematics relevant for $g-2$.

One of the major difficulties in this approach is the fact that the BTT tensor decomposition does not directly provide a tensor basis free from kinematic singularities, but rather a redundant set of structures. Although the singly-on-shell basis functions $\check{\Pi}_i$ derived in Ref. [17] are free from singularities in the Mandelstam variables, the redundancies in the tensor basis result in spurious kinematic singularities in the photon virtualities. The residues of these apparent singularities vanish due to a set of sum rules: these follow directly from the fact that the tensor decomposition involves structures of different mass dimension and they guarantee that the result of the dispersion relation for the entire HLbL tensor is independent of the choice of tensor basis. At the same time, they imply that the apparent kinematic singularities drop out for contributions that satisfy the sum rules. This is guaranteed to happen only for the entire HLbL contribution, i.e., the sum over all intermediate states in the unitarity relation. In contrast, individual intermediate states do not necessarily satisfy the sum rules. These sum-rule violations make the contributions of individual states depend on the chosen basis [3, 46, 51] and suffer from kinematic singularities [46].

The basis dependence affects all single-particle intermediate states in the unitarity relation apart from the pseudoscalar contributions as these do not contribute to the sum rules. The sum rules are exactly fulfilled by the pion box [17]. Scalar intermediate states or two-particle S-wave contributions are in general basis dependent, but they are not affected by spurious singularities, see Ref. [51]. In the basis of Ref. [17], axial-vector contributions are affected by singularities, but there exists an alternative basis, where this problem is absent, as discussed in Ref. [46]. By making use just of the minimal set of sum rules that are necessary to render the entire HLbL contribution basis independent, it is impossible to fully remove the spurious kinematic singularities from the contribution of tensor-meson resonances or two-particle D- and higher partial waves. Whether this can be achieved by making use of additional sum rules remains to be studied.

As long as no representation is available that is manifestly free of any kinematic singularities, the spurious singularities need to be subtracted as described in Ref. [17]. The same subtraction scheme needs to be applied in all contributions that are affected by the singularities. In the sum over all intermediate states, the subtraction again vanishes due to the sum rules. The subtraction scheme introduces an ambiguity in the contribution of individual intermediate states that is in addition to the general basis dependence. Due to these ambiguities, one cannot expect to obtain a meaningful result for these contributions unless the sum of included states fulfills the sum rules. This is one of the reasons why to date no evaluation of the tensor-resonance contributions within the dispersive framework is available [3].

5.1.2 Dispersion relations in triangle kinematics

Instead of fixing the photon virtualities, writing dispersion relations in the Mandelstam variables and finally taking the limit $q_4 \to 0$, here we propose to take a different approach: we first take the limit $q_4 \to 0$ and then write dispersion relations for the functions $\hat{\Pi}_i(q_1^2, q_2^2, q_3^2)$ entering the master formula, exploiting the analytic structure in the variables q_i^2. This alternative set of dispersion relations has been briefly discussed in Ref. [21]. As explained there, these new dispersion relations have the disadvantage that the original cuts in the Mandelstam variables and in the photon virtualities are no longer separated.

However, this approach has an important advantage over the dispersion relations for the four-point function: all the redundancies of the BTT set disappear in the $g-2$ limit. The functions $\hat{\Pi}_i(q_1^2, q_2^2, q_3^2)$ in the $g-2$ kinematic limit are free from any kinematic singularities. Working directly with them removes the problem of spurious divergences. Hence, this alternative is a promising approach for the model-independent evaluation of the contributions of D- and higher partial waves, or narrow tensor-meson resonances such as the $f_2(1270)$ [189].

A potential pitfall is the fact that for the new dispersion relations in triangle kinematics, we need to reconstruct additional hadronic sub-processes, in particular $\gamma^*\gamma^* \to \gamma\pi\pi$ as well as $\pi\pi \to \gamma\pi\pi$. These sub-processes require their own tensor decomposition, which could potentially re-introduce the problem of redundancies and kinematic singularities. In the following, we derive the BTT tensor decompositions for these sub-processes and we show that in the limit of $g-2$ kinematics, all but a single redundancy in $\gamma^*\gamma^* \to \gamma\pi\pi$ disappear, which under the assumption of a uniform asymptotic behavior of the tensor amplitude can be traded for one kinematic constraint. This enables dispersion relations for scalar functions free of kinematic singularities.

In the case of dispersion relations in triangle kinematics, the objects under consideration are the functions $\hat{\Pi}_i$ in Eq. (2.48), which in $g-2$ kinematics depend on the three photon virtualities, $\hat{\Pi}_i(q_1^2, q_2^2, q_3^2)$. For the contribution to a_μ, only a restricted domain of the three virtualities belongs to the physical region, as determined by the master formula Eq. (2.51), but analytic continuation allows us to treat the three virtualities as independent variables and to continue the function beyond the physical region. We start by writing a dispersion relation for $\hat{\Pi}_i(q_1^2, q_2^2, q_3^2)$ in q_3^2, while keeping the other two virtualities $q_{1,2}^2$ fixed:

$$\hat{\Pi}_i(q_1^2, q_2^2, q_3^2) = \frac{1}{\pi} \int_{s_0}^{\infty} \mathrm{d}s' \frac{1}{s' - q_3^2 - \mathrm{i}\epsilon} \operatorname{Im} \hat{\Pi}_i(q_1^2, q_2^2, s') , \tag{5.1}$$

where the imaginary part is obtained from

$$\operatorname{Im} \hat{\Pi}_i(q_1^2, q_2^2, s') = \frac{\hat{\Pi}_i(q_1^2, q_2^2, s' + \mathrm{i}\epsilon) - \hat{\Pi}_i(q_1^2, q_2^2, s' - \mathrm{i}\epsilon)}{2\mathrm{i}} \tag{5.2}$$

and the lowest threshold is $s_0 = m_{\pi^0}^2$. We now demonstrate how to obtain this imaginary part by taking the appropriate limits of imaginary parts in four-point kinematics.

In Ref. [17], a basis of 27 scalar functions $\check{\Pi}_i$ for HLbL scattering was derived, which applies to four-point kinematics at fixed $t = q_2^2$ and in the limit $q_4^2 = 0$. The 19 functions $\hat{\Pi}_i$ relevant for a_μ can be obtained from a subset of the $\check{\Pi}_i$ functions,

$$\check{\Pi}_i = \hat{\Pi}_{g_i} + (s - q_3^2)\overline{\Delta}_i + (s - q_3^2)^2 \overline{\overline{\Delta}}_i , \tag{5.3}$$

i.e., by denoting the arguments as $\check{\Pi}_i(s; q_1^2, q_2^2, q_3^2)$, the limit of $g-2$ kinematics is given by

$$\hat{\Pi}_{g_i}(q_1^2, q_2^2, q_3^2) = \check{\Pi}_i(q_3^2; q_1^2, q_2^2, q_3^2) . \tag{5.4}$$

The imaginary part Eq. (5.2) can be written as (cf. Eq. (4.28))

$$\begin{aligned}
\operatorname{Im} \hat{\Pi}_{g_i}(q_1^2, q_2^2, s') &= \lim_{q_3^2 \to s'} \frac{\check{\Pi}_i(s' + \mathrm{i}\epsilon; q_1^2, q_2^2, q_3^2 + \mathrm{i}\epsilon) - \check{\Pi}_i(s' - \mathrm{i}\epsilon; q_1^2, q_2^2, q_3^2 - \mathrm{i}\epsilon)}{2\mathrm{i}} \\
&= \lim_{q_3^2 \to s'} \bigg[\frac{\check{\Pi}_i(s' + \mathrm{i}\epsilon; q_1^2, q_2^2, q_3^2 + \mathrm{i}\epsilon) - \check{\Pi}_i(s' - \mathrm{i}\epsilon; q_1^2, q_2^2, q_3^2 + \mathrm{i}\epsilon)}{2\mathrm{i}} \\
&\qquad + \frac{\check{\Pi}_i(s' - \mathrm{i}\epsilon; q_1^2, q_2^2, q_3^2 + \mathrm{i}\epsilon) - \check{\Pi}_i(s' - \mathrm{i}\epsilon; q_1^2, q_2^2, q_3^2 - \mathrm{i}\epsilon)}{2\mathrm{i}} \bigg] \\
&= \lim_{q_3^2 \to s'} \bigg[\frac{\check{\Pi}_i(s' + \mathrm{i}\epsilon; q_1^2, q_2^2, q_3^2 + \mathrm{i}\epsilon) - \check{\Pi}_i(s' - \mathrm{i}\epsilon; q_1^2, q_2^2, q_3^2 + \mathrm{i}\epsilon)}{2\mathrm{i}} \\
&\qquad + \left(\frac{\check{\Pi}_i(s' + \mathrm{i}\epsilon; q_1^2, q_2^2, q_3^2 + \mathrm{i}\epsilon) - \check{\Pi}_i(s' + \mathrm{i}\epsilon; q_1^2, q_2^2, q_3^2 - \mathrm{i}\epsilon)}{2\mathrm{i}} \right)^* \bigg] \\
&=: \lim_{q_3^2 \to s'} \Big[\operatorname{Im}_s \check{\Pi}_i(s'; q_1^2, q_2^2, q_3^2 + \mathrm{i}\epsilon) + \Big(\operatorname{Im}_3 \check{\Pi}_i(s' + \mathrm{i}\epsilon; q_1^2, q_2^2, q_3^2) \Big)^* \Big]
\end{aligned} \tag{5.5}$$

Here, we denote by Im_s the s-channel discontinuity in four-point kinematics, analytically continued in the third photon virtuality to $q_3^2 + \mathrm{i}\epsilon$, while Im_3 denotes the discontinuity in the variable q_3^2, again in four-point kinematics and now analytically continued in the Mandelstam variable to $s' + \mathrm{i}\epsilon$.

Before taking the limit $q_3^2 \to s'$, the expression contains kinematic singularities of the form $1/(q_1^2 + q_3^2)$ and $1/\lambda(q_1^2, q_2^2, q_3^2)$, which are present in the quantities $\overline{\Delta}_i$ and $\overline{\overline{\Delta}}_i$ [17], with λ

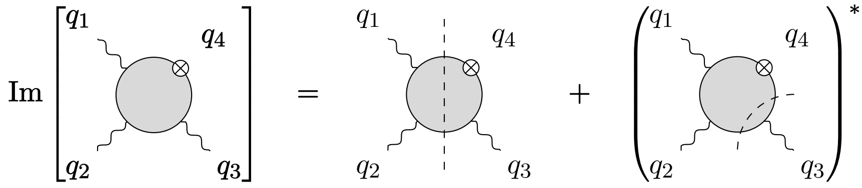

Figure 5.1: Unitarity cuts contributing to the discontinuity of HLbL with respect to q_3^2 in triangle kinematics.

denoting the Källén triangle function $\lambda(a,b,c) = a^2 + b^2 + c^2 - 2(ab + ac + bc)$. In the original s-channel dispersion relations [17], the residue of these kinematic singularities vanishes due to the presence of sum rules for the scalar functions $\check{\Pi}_i$. Since individual partial waves or single narrow resonances violate the sum rules, the residues of the kinematic singularities had to be subtracted "by hand." The basis $\check{\Pi}_i$ was then chosen in a way that leads to a simple form of kinematic singularities and at the same time optimizes the convergence of the partial-wave-expanded pion box. The alternative basis of $\tilde{\Pi}_i$ functions discussed in Ref. [46] contains singularities that are products of $1/q_i^2$ and $1/(q_1^2 + q_3^2)$.

We note that the limit of each of the two discontinuities in Eq. (5.5) may be singular: if the soft photon is emitted from an external leg of the sub-process, the limit $q_4 \to 0$ puts an internal propagator on-shell. With the additional derivative in Eq. (2.46), this potentially leads to a double-pole in $1/(s' - q_3^2)$. However, analogous poles exist in both discontinuities $\mathrm{Im}_s \check{\Pi}_i$ and $\mathrm{Im}_3 \check{\Pi}_i$ and they are guaranteed to cancel in the sum of the two discontinuities because the HLbL tensor is free of such singularities. This will be discussed in more detail in Sec. 5.3. Due to this absence of poles in the sum of the two discontinuities, the contributions from $\overline{\Delta}_i$ and $\overline{\overline{\Delta}}_i$ vanish in the limit $q_3^2 \to s'$, so that $\mathrm{Im}\, \hat{\Pi}_{g_i}$ does not contain any kinematic singularities. For this reason, the contribution of a single partial wave or a narrow resonance to a_μ can be defined without relying on a sum rule that is violated by this particular contribution alone.

Writing a dispersion relation in q_3^2 and fixing $q_{1,2}^2$ in Eq. (5.1) is an arbitrary choice: crossing symmetry requires that dispersion relations in any of the other virtualities lead to the same result. In the final dispersive representation this symmetrization needs to be taken into account, in a way that avoids any double counting.

5.2 Dispersion relations for HLbL in triangle kinematics

5.2.1 Unitarity relations

According to Eq. (5.5), the relevant imaginary part that is needed in the new dispersion relations can be obtained from the sum of the discontinuities in the s-channel and the q_3^2-channel in four-point kinematics, illustrated in Fig. 5.1. Unitarity of the S-matrix provides

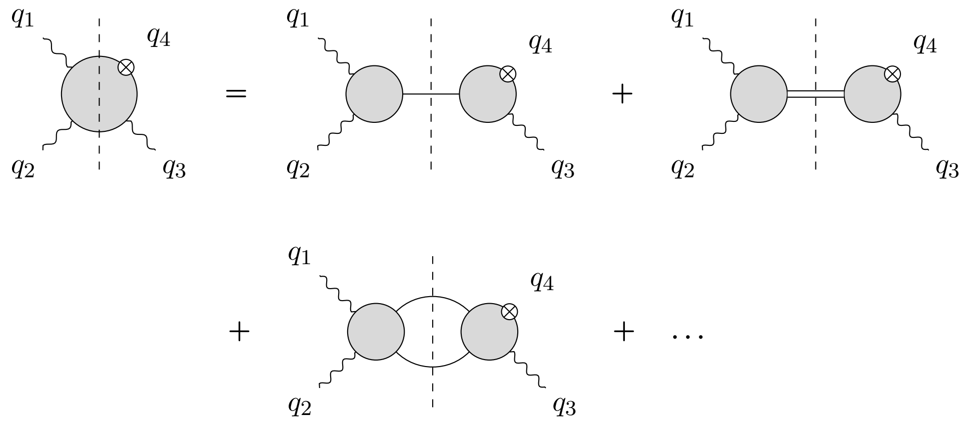

Figure 5.2: Contribution of different intermediate states to the s-channel discontinuity in HLbL.

these discontinuities in the form of two different relations. The first one is the s-channel unitarity relation in Eq. (2.55). Similarly, the discontinuity in the virtuality q_3^2 can be obtained from the unitarity relation, where the fourth photon is crossed to the initial state:[1]

$$\begin{aligned}&\mathrm{Im}_3\left(-\mathrm{i}\left\langle\gamma^*(-q_3,\lambda_3)|\gamma^*(q_1,\lambda_1)\gamma^*(q_2,\lambda_2)\gamma^*(-q_4,\lambda_4)\right\rangle\right)\\&\quad=\sum_n\frac{1}{2S_n}\left(\prod_{i=1}^{N_n}\int\widetilde{\mathrm{d}p_i}\right)\left\langle n;\{p_i\}|\gamma^*(-q_3,\lambda_3)\right\rangle^*\left\langle n;\{p_i\}|\gamma^*(q_1,\lambda_1)\gamma^*(q_2,\lambda_2)\gamma^*(-q_4,\lambda_4)\right\rangle\ .\end{aligned}\tag{5.6}$$

The general strategy of the dispersive evaluation of the HLbL contribution to a_μ amounts to summing up individual contributions to the unitarity relations in Eqs. (2.55) and (5.6). Of course, in practice it is not possible to resum the whole tower of intermediate states and one needs to truncate the sum. The remainder is assumed to be small at low energies, where the lightest intermediate states dominate, but it becomes more important at higher energies and in the end it needs to be taken into account by a proper matching to asymptotic constraints [3, 15, 20, 21, 40–49].

The contributions of the lightest intermediate states to the unitarity relations in the s- and q_3^2-channels are illustrated in terms of unitarity diagrams in Figs. 5.2 and 5.3. In order to evaluate the discontinuities, input for the sub-processes is required. In the case of the s-channel discontinuities, the input is identical to the one in the familiar dispersion relations, although evaluated for a different kinematic configuration: the evaluation of the single-pseudoscalar intermediate states requires the pion, η and η' TFFs as input. For two-pion intermediate

[1] For consistency with Ref. [60], we have crossed the two matrix elements on the right-hand side with respect to the general relation in Eq. (2.24).

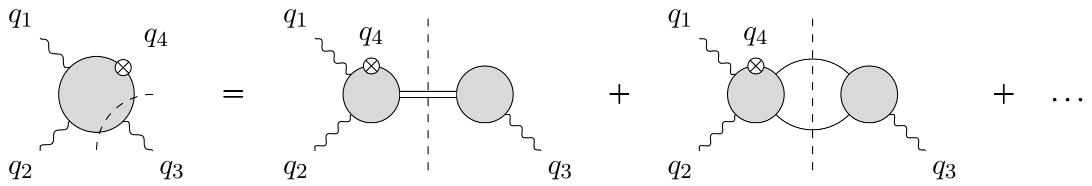

Figure 5.3: Contribution of different intermediate states to the q_3^2-channel discontinuity in HLbL.

states, the helicity partial waves for $\gamma^*\gamma^* \to \pi\pi$ are the required input. The formalism for the full inclusion of three-particle intermediate states in the s-channel is currently not available. This contribution contains axial-vector resonances, which are expected to be numerically relevant [3, 15, 41–44, 55, 56, 151]. In a first step, these effects can be described in a NWA, replacing the three-pion intermediate state by a narrow resonance, indicated by a double line in Fig. 5.2. The required input in this approximation are the axial-vector TFFs. The effect of two-pion intermediate states gets enhanced close to scalar or tensor resonances. In this case, the two-pion unitarization can be compared to a NWA, which is used to include scalar and tensor resonances in different isospin channels [51]. Again, the respective TFFs are required as input.

The input for the discontinuities in the q_3^2-channel are given by the pion VFF and $\gamma^*\gamma^* \to \gamma\pi\pi$ in the case of two-pion intermediate states. In the case of three-pion intermediate states, the sub-processes are $\gamma^* \to 3\pi$ and $\gamma^*\gamma^* \to 3\pi\gamma$, with potentially non-negligible effects due to the narrow vector resonances ω and ϕ, illustrated by the double lines in Fig. 5.3.[2] Therefore, compared to the CHPS approach, the dispersion relations in triangle kinematics require the processes $\gamma^*\gamma^* \to \gamma\pi\pi$ and $\gamma^*\gamma^* \to \gamma V$ as new inputs, where V denotes a vector resonance. We note that the intermediate states discussed here are exactly the ones we have included in our VVA reconstruction in Ch. 4.

The new inputs required for the dispersion relations in triangle kinematics should be reconstructed again dispersively. For $\gamma^*\gamma^* \to \gamma V$, much can be taken over directly from HLbL: in particular, this sub-process will be linked to the isoscalar vector resonances in the pion TFF reshuffled from the pion pole in the established dispersion relations [18]. We discuss the tensor decomposition and kinematics in Sect. 5.2.3.

The second new input is the sub-process $\gamma^*\gamma^* \to \gamma\pi\pi$ needed for the two-pion intermediate state in the q_3^2-channel cut. The different unitarity cuts for $\gamma^*\gamma^* \to \gamma\pi\pi$ are shown in Fig. 5.4. The soft limit is understood after taking the derivative with respect to q_4 in Eq. (2.46). Only terms that are singular or finite in this limit are required. The singular terms can be expressed

[2] In the case of the pion pole in the dispersion relations in four-point kinematics, the three-pion cut is included in the dispersive treatment of the pion TFF [18, 50, 120].

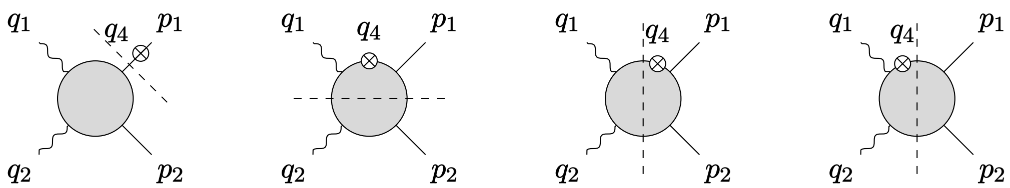

Figure 5.4: Unitarity cuts for $\gamma^*\gamma^* \to \gamma\pi\pi$ for a soft external on-shell photon. The first diagram denotes the soft divergence, the second one denotes the left-hand cut. The last two diagrams are the two s-channel cuts. Crossed diagrams are not shown.

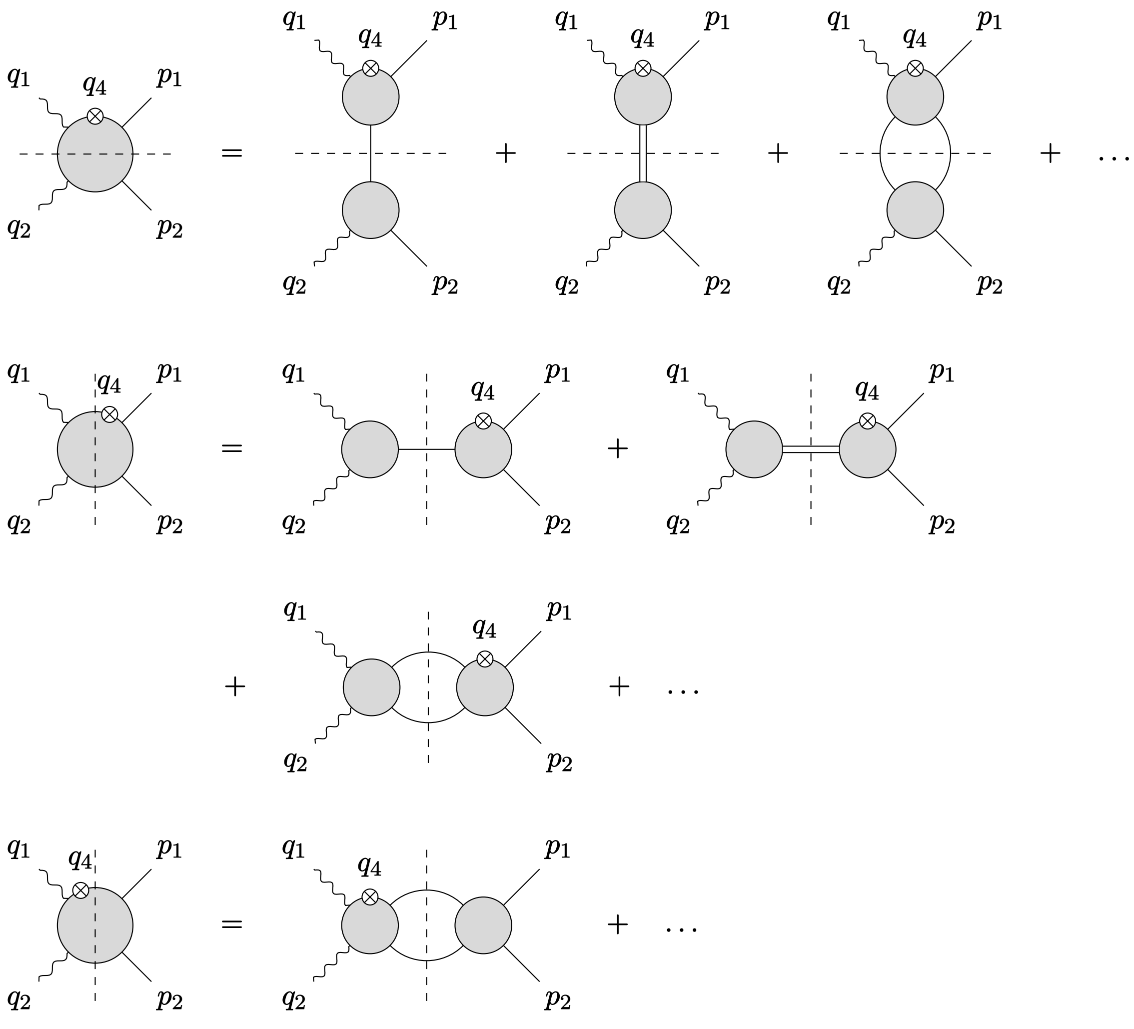

Figure 5.5: The contribution of different intermediate states to the discontinuities in $\gamma^*\gamma^* \to \gamma\pi\pi$. The last diagram denotes $\pi\pi$ rescattering: the process $\gamma^*\gamma^* \to \gamma\pi\pi$ itself reappears as a sub-process.

in terms of $\gamma^*\gamma^* \to \pi\pi$ via dispersion relations, see Sec. 5.3. The finite remainder is not directly determined by $\gamma^*\gamma^* \to \pi\pi$ and needs its own dispersion relation. The relevant intermediate states of the different unitarity cuts are illustrated in Fig. 5.5: if the photon virtualities are kept fixed, the original five-particle process reduces to four-point kinematics in the $g-2$ limit. The complexity again increases with the multiplicity of the intermediate states. The formalism for a fully dispersive reconstruction of the three-pion intermediate state is not available, but resonant contributions to the three-particle channel can be estimated in a NWA. Therefore, the main unknown sub-process is $\pi\pi \to \gamma\pi\pi$ for a soft photon. This sub-process will be the subject of Ch. 6. Possible input could also be provided by lattice QCD [190–192].

Any dispersion relation allows one to split up the entire HLbL contribution into a sum over intermediate states in the unitarity relation. However, the notion of the contribution of an individual intermediate state, obtained by inserting one term of the unitarity sum into the dispersion integral, depends on the dispersion relation under consideration as we have seen in the simpler case of VVA in Ch. 4. This is true for basis changes in the existing approach, as explained in Sec. 5.1.1, but also if one uses dispersion relations in a different kinematic variable. Only the result for the sum over all intermediate states is unique. In particular, this means that, e.g., the pion pole as defined in the CHPS approach [18, 39] does not coincide with the pion pole in triangle kinematics, as discussed in Ref. [21]. When comparing the two approaches, one finds that a reshuffling happens between the contributions of different intermediate states. Since each dispersive approach requires some truncation of the unitarity sum, the correspondence is not exact, but the remainder needs to be covered by the uncertainties in the matching to an inclusive asymptotic contribution. We compare the two dispersion relations in Tab. 5.1: the splitting by intermediate states in the established approach corresponds to columns, while the rows correspond to the contributions in the new dispersion relations in triangle kinematics. Therefore, if asymptotic constraints are included for the sub-processes, the established dispersion relations perform a resummation of columns, while the new approach would correspond to a resummation of rows. Crosses in the table denote the absence of a contribution. This sketch illustrates that the most promising strategy will be to combine the two approaches, which however requires some care in avoiding any double-counting. A detailed analysis of the reshuffling and the matching to asymptotic constraints in the case of VVA has been performed in Sec. 4.4. A similar analysis for the more complicated case of HLbL is left for future work.

In Secs. 5.2.2 and 5.2.3, we consider single-particle intermediate states in triangle kinematics, while two-pion intermediate states will be discussed in Sec. 5.2.4.

5.2.2 Single-particle intermediate states in the s-channel

As shown in Fig. 5.2 and Tab. 5.1, the s-channel cut receives single-particle contributions from pseudoscalar poles, as well as from resonances in the NWA. The q_3^2-channel discontinuity

	DR in four-point kinematics					
triangle-DR	π^0, η, η'	2π	S	A	T	...
π^0, η, η'	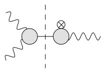	×	×	×	×	×
2π	× 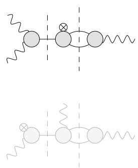	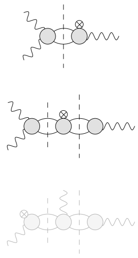	× 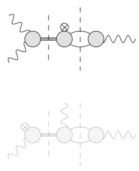	× 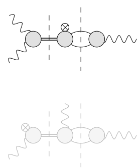	× 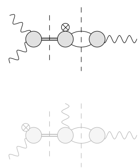	× 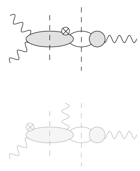
V	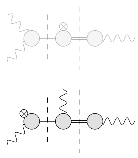	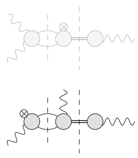	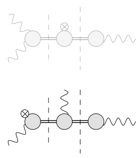	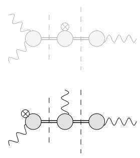	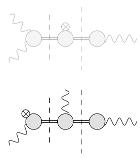	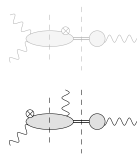
S	×	×	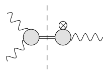	×	×	×
A	×	×	×	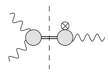	×	×
T	×	×	×	×	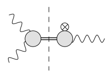	×
...	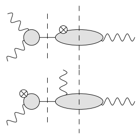	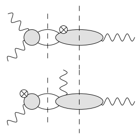	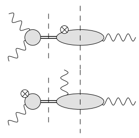	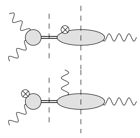	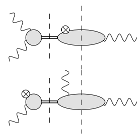	...

Table 5.1: Comparison of different unitarity contributions in the CHPS approach and the proposed dispersion relations in triangle kinematics. The longer dashed line is the primary cut in triangle-kinematics dispersion relations. Cuts through gray blobs denote even higher intermediate states that need to be covered via the implementation of asymptotic constraints. Depending on the dispersion relation for the sub-processes, the diagrams shown in light-gray only contribute to normalizations. Some scalar and tensor resonances correspond to a NWA of two-pion contributions. Table taken from Ref. [60].

receives single-particle contributions only in the NWA due to vector-meson resonances, which will be the topic of Sec. 5.2.3.

In Sec. 5.2.2.1, we work out the explicit expression for the pion-pole contribution in triangle kinematics and compare the result to the pion pole in the established dispersion relations in four-point kinematics. Similar results follow immediately for the other pseudoscalars η and η'. In Secs. 5.2.2.2–5.2.2.4, we derive analogous expressions for resonance contributions in the NWA.

5.2.2.1 Pion pole

The contribution of a single neutral pion in the s-channel unitarity relation is given in Eq. (2.59). This expression can be evaluated for fixed-t kinematics and via projection onto the tensor structures one arrives at the single-pion discontinuity of the functions $\check{\Pi}_i$:

$$\begin{aligned} \mathrm{Im}_s^\pi\, \check{\Pi}_1(s'; q_1^2, q_2^2, q_3^2) &= -\pi\delta(s' - m_\pi^2) F_{\pi^0\gamma^*\gamma^*}(q_1^2, q_2^2) F_{\pi^0\gamma^*\gamma^*}(q_3^2, 0)\,, \\ \mathrm{Im}_s^\pi\, \check{\Pi}_i(s'; q_1^2, q_2^2, q_3^2) &= 0\,, \quad i \neq 1\,. \end{aligned} \tag{5.7}$$

Since there is no one-pion intermediate state in the q_3^2-channel, the one-pion discontinuity of the $\hat{\Pi}_i$ functions follows by taking the limit in Eq. (5.5):

$$\begin{aligned} \mathrm{Im}^\pi\, \hat{\Pi}_1(q_1^2, q_2^2, s') &= -\pi\delta(s' - m_\pi^2) F_{\pi^0\gamma^*\gamma^*}(q_1^2, q_2^2) F_{\pi^0\gamma^*\gamma^*}(m_\pi^2, 0)\,, \\ \mathrm{Im}^\pi\, \hat{\Pi}_i(q_1^2, q_2^2, s') &= 0\,, \quad i \in \{2,3,4,5,6,7,8,9,10,11,13,14,16,17,39,50,51,54\}\,. \end{aligned} \tag{5.8}$$

Inserting this imaginary part into the dispersion relation Eq. (5.1) leads to a pion-pole contribution just in $\hat{\Pi}_1$ and no pole contribution in any other function. However, due to crossing symmetry it is clear that $\hat{\Pi}_{2,3}$ contain pion poles in the q_2^2- and q_1^2-channels, respectively. Those contributions can be reconstructed in the dispersion relation in q_3^2 from higher intermediate states due to cuts through the pion TFF, starting with a two-pion cut. Anticipating that a double counting must be avoided when including higher intermediate states, we impose crossing symmetry to arrive at the final result for the pion-pole contribution in triangle kinematics:

$$\begin{aligned} \hat{\Pi}_1^\pi(q_1^2, q_2^2, q_3^2) &= \frac{F_{\pi^0\gamma^*\gamma^*}(q_1^2, q_2^2) F_{\pi^0\gamma^*\gamma^*}(m_\pi^2, 0)}{q_3^2 - m_\pi^2}\,, \\ \hat{\Pi}_i^\pi(q_1^2, q_2^2, q_3^2) &= 0\,, \quad i \in \{4,7,17,39,54\}\,, \end{aligned} \tag{5.9}$$

written in terms of the six representatives in Eq. (2.49), while the remaining 13 functions follow from the crossing relations Eq. (2.50).

The result for the pion pole in Eq. (5.9) differs from the expression for the pion pole that follows from the dispersion relations in four-point kinematics [39] given in Eq. (2.63). This mismatch led to some confusion in the literature [93, 94], although the reason for it was already explained in Ref. [21]: the different expressions Eq. (5.9) and Eq. (2.63) do not put the validity of either dispersion relation into question. Both, the dispersion relations in four-point kinematics and the ones in triangle kinematics can be used to describe the hadronic light-by-light contribution to a_μ. They reconstruct the same function if the tower of intermediate states in the unitarity relation is resummed. However, since the limit $q_4 \to 0$ changes the meaning of the kinematic invariants, writing dispersion relations before or after taking this limit does not lead to the same expressions. In particular, the contributions of one particular intermediate state do not need to agree in the two formalisms. As discussed in Ref. [21], the difference between Eqs. (5.9) and (2.63) is regular at $q_3^2 = m_\pi^2$:

$$\hat{\Pi}_1^{\pi^0\text{-pole}}(q_1^2, q_2^2, q_3^2) - \hat{\Pi}_1^{\pi}(q_1^2, q_2^2, q_3^2) = F_{\pi^0\gamma^*\gamma^*}(q_1^2, q_2^2) \frac{F_{\pi^0\gamma^*\gamma^*}(q_3^2, 0) - F_{\pi^0\gamma^*\gamma^*}(m_\pi^2, 0)}{q_3^2 - m_\pi^2} . \tag{5.10}$$

As shown in Tab. 5.1, this quantity can be identified with contributions from higher intermediate states in the dispersion relation in triangle kinematics [46], which needs to be considered when combining the two approaches. Eq. (5.9) corresponds to the first row of the table (for the case of a π^0) and consists only of the upper left entry, while Eq. (2.63) contains the first column.

5.2.2.2 Scalar resonances

In complete analogy to the single-pseudoscalar contribution in the s-channel, we can consider single-particle scalar, axial-vector, and tensor intermediate states, describing the contribution of resonances in the NWA. We start with scalars in this section.

The contribution of a scalar resonance to the s-channel unitarity relation is given by

$$\begin{aligned} &\mathrm{Im}_s^S \left(-i \langle \gamma^*(-q_3, \lambda_3)\gamma^*(q_4, \lambda_4)|\gamma^*(q_1, \lambda_1)\gamma^*(q_2, \lambda_2)\rangle\right) \\ &\quad = \frac{1}{2} \int \widetilde{\mathrm{d}p} \, \langle S(p)|\gamma^*(-q_3, \lambda_3)\gamma(q_4, \lambda_4)\rangle^* \, \langle S(p)|\gamma^*(q_1, \lambda_1)\gamma^*(q_2, \lambda_2)\rangle \, . \end{aligned} \tag{5.11}$$

The matrix element $\langle S(p)|\gamma^*(q_1, \lambda_1)\gamma^*(q_2, \lambda_2)\rangle$ has been decomposed in terms of the scalar TFFs $\mathcal{F}_1^S$ and $\mathcal{F}_2^S$ in Ref. [131]. For fixed-t kinematics, one obtains the following discontinuity of the functions $\check{\Pi}_i$ [51]:

$$\begin{aligned} \mathrm{Im}_s^S \check{\Pi}_4(s'; q_1^2, q_2^2, q_3^2) &= -\pi\delta(s' - m_S^2) \left(\frac{\mathcal{F}_1^S(q_1^2, q_2^2)}{m_S^2} - \frac{(s' + q_1^2 + q_2^2)}{2m_S^4} \mathcal{F}_2^S(q_1^2, q_2^2) \right) \mathcal{F}_1^S(q_3^2, 0) \, , \\ \mathrm{Im}_s^S \check{\Pi}_{15}(s'; q_1^2, q_2^2, q_3^2) &= -\pi\delta(s' - m_S^2) \frac{\mathcal{F}_2^S(q_1^2, q_2^2)\mathcal{F}_1^S(q_3^2, 0)}{m_S^4} \, , \\ \mathrm{Im}_s^S \check{\Pi}_i(s'; q_1^2, q_2^2, q_3^2) &= 0 \, , \quad i \notin \{4, 15\} \, . \end{aligned} \tag{5.12}$$

The discontinuity of the $\hat{\Pi}_i$ functions follows as:

$$\begin{aligned}
\operatorname{Im}^S \hat{\Pi}_4(q_1^2,q_2^2,s') &= -\pi\delta(s'-m_S^2)\left(\frac{\mathcal{F}_1^S(q_1^2,q_2^2)}{m_S^2} - \frac{(m_S^2+q_1^2+q_2^2)}{2m_S^4}\mathcal{F}_2^S(q_1^2,q_2^2)\right)\mathcal{F}_1^S(m_S^2,0)\,, \\
\operatorname{Im}^S \hat{\Pi}_{17}(q_1^2,q_2^2,s') &= -\pi\delta(s'-m_S^2)\frac{\mathcal{F}_2^S(q_1^2,q_2^2)\mathcal{F}_1^S(m_S^2,0)}{m_S^4}\,, \\
\operatorname{Im}^S \hat{\Pi}_i(q_1^2,q_2^2,s') &= 0\,, \quad i\notin\{4,17\}\,.
\end{aligned} \tag{5.13}$$

Inserting this imaginary part into the dispersion relation Eq. (5.1) leads to

$$\begin{aligned}
\hat{\Pi}_4^S(q_1^2,q_2^2,q_3^2) &= \frac{\mathcal{F}_1^S(m_S^2,0)}{q_3^2-m_S^2}\left(\frac{\mathcal{F}_1^S(q_1^2,q_2^2)}{m_S^2} - \frac{(m_S^2+q_1^2+q_2^2)}{2m_S^4}\mathcal{F}_2^S(q_1^2,q_2^2)\right)\,, \\
\hat{\Pi}_{17}^S(q_1^2,q_2^2,q_3^2) &= \frac{\mathcal{F}_1^S(m_S^2,0)}{q_3^2-m_S^2}\frac{\mathcal{F}_2^S(q_1^2,q_2^2)}{m_S^4}\,, \\
\hat{\Pi}_i^S(q_1^2,q_2^2,q_3^2) &= 0\,, \quad i\in\{1,7,39,54\}\,,
\end{aligned} \tag{5.14}$$

while the other functions follow from the crossing relations in Eq. (2.50). The result Eq. (5.14) can be obtained from the scalar contribution in four-point kinematics [51] by keeping only the pure pole in q_3^2. It differs from it by a piece regular at $q_3^2 = m_S^2$, which corresponds to the entries in the "S" column of Tab. 5.1 that do not belong to the "S" row.

5.2.2.3 Axial-vector resonances

Next, we consider the contribution of an axial-vector resonance to the s-channel:

$$\begin{aligned}
&\operatorname{Im}_s^A\left(-i\langle\gamma^*(-q_3,\lambda_3)\gamma^*(q_4,\lambda_4)|\gamma^*(q_1,\lambda_1)\gamma^*(q_2,\lambda_2)\rangle\right) \\
&\quad = \frac{1}{2}\sum_{\lambda_A}\int\widetilde{dp}\,\langle A(p,\lambda_A)|\gamma^*(-q_3,\lambda_3)\gamma(q_4,\lambda_4)\rangle^*\,\langle A(p,\lambda_A)|\gamma^*(q_1,\lambda_1)\gamma^*(q_2,\lambda_2)\rangle\,.
\end{aligned} \tag{5.15}$$

The matrix element of the sub-process can be decomposed into Lorentz structures according to Ref. [131] defining the axial-vector TFFs $\mathcal{F}_i^A$. For fixed-t kinematics, the discontinuity of the functions $\check{\Pi}_i$ in the basis of [17] is rather complicated and contains kinematic singularities proportional to $s'-q_3^2$, which drop out when we take the limit $q_3^2\to s'$. This leads to

$$\begin{aligned}
\operatorname{Im}^A \hat{\Pi}_5(q_1^2,q_2^2,s') &= \pi\delta(s'-m_A^2)\frac{m_A^2-q_1^2-q_2^2}{2m_A^4}\mathcal{F}_2^A(m_A^2,0)\left(2\mathcal{F}_1^A(q_1^2,q_2^2)+\mathcal{F}_3^A(q_1^2,q_2^2)\right)\,, \\
\operatorname{Im}^A \hat{\Pi}_6(q_1^2,q_2^2,s') &= -\pi\delta(s'-m_A^2)\frac{m_A^2-q_1^2-q_2^2}{2m_A^4}\mathcal{F}_2^A(m_A^2,0)\left(2\mathcal{F}_1^A(q_1^2,q_2^2)+\mathcal{F}_2^A(q_1^2,q_2^2)\right)\,, \\
\operatorname{Im}^A \hat{\Pi}_9(q_1^2,q_2^2,s') &= -\operatorname{Im}^A \hat{\Pi}_{13}(q_1^2,q_2^2,s') \\
&= -\pi\delta(s'-m_A^2)\frac{\mathcal{F}_2^A(m_A^2,0)}{m_A^4}\left(2\mathcal{F}_1^A(q_1^2,q_2^2)+\mathcal{F}_2^A(q_1^2,q_2^2)+\mathcal{F}_3^A(q_1^2,q_2^2)\right)\,,
\end{aligned}$$

$$
\begin{aligned}
\mathrm{Im}^A\,\hat{\Pi}_{10}(q_1^2,q_2^2,s') &= \pi\delta(s'-m_A^2)\frac{\mathcal{F}_2^A(m_A^2,0)}{m_A^4}\left(2\mathcal{F}_1^A(q_1^2,q_2^2)+\mathcal{F}_3^A(q_1^2,q_2^2)\right)\,,\\
\mathrm{Im}^A\,\hat{\Pi}_{11}(q_1^2,q_2^2,s') &= \mathrm{Im}^A\,\hat{\Pi}_{54}(q_1^2,q_2^2,s') = -\,\mathrm{Im}^A\,\hat{\Pi}_{16}(q_1^2,q_2^2,s')\\
&= -\pi\delta(s'-m_A^2)\frac{\mathcal{F}_2^A(m_A^2,0)}{2m_A^4}\left(4\mathcal{F}_1^A(q_1^2,q_2^2)+\mathcal{F}_2^A(q_1^2,q_2^2)+\mathcal{F}_3^A(q_1^2,q_2^2)\right)\,,\\
\mathrm{Im}^A\,\hat{\Pi}_{14}(q_1^2,q_2^2,s') &= -\pi\delta(s'-m_A^2)\frac{\mathcal{F}_2^A(m_A^2,0)}{m_A^4}\left(2\mathcal{F}_1^A(q_1^2,q_2^2)+\mathcal{F}_2^A(q_1^2,q_2^2)\right)\,,\\
\mathrm{Im}^A\,\hat{\Pi}_{17}(q_1^2,q_2^2,s') &= \mathrm{Im}^A\,\hat{\Pi}_{39}(q_1^2,q_2^2,s') = \mathrm{Im}^A\,\hat{\Pi}_{50}(q_1^2,q_2^2,s') = \mathrm{Im}^A\,\hat{\Pi}_{51}(q_1^2,q_2^2,s')\\
&= \pi\delta(s'-m_A^2)\frac{\mathcal{F}_2^A(m_A^2,0)}{2m_A^4}\left(\mathcal{F}_2^A(q_1^2,q_2^2)-\mathcal{F}_3^A(q_1^2,q_2^2)\right)\,,\\
\mathrm{Im}^A\,\hat{\Pi}_i(q_1^2,q_2^2,s') &= 0\,,\quad i\in\{1,2,3,4,7,8\}\,.
\end{aligned}
\tag{5.16}
$$

If only the six representative functions (2.49) are used to write dispersion relations in q_3^2, one obtains

$$
\begin{aligned}
\hat{\Pi}_{17}^{A,3}(q_1^2,q_2^2,q_3^2) &= \hat{\Pi}_{39}^{A,3}(q_1^2,q_2^2,q_3^2) = \frac{\mathcal{F}_2^A(m_A^2,0)}{q_3^2-m_A^2}\frac{\mathcal{F}_3^A(q_1^2,q_2^2)-\mathcal{F}_2^A(q_1^2,q_2^2)}{2m_A^4}\,,\\
\hat{\Pi}_{54}^{A,3}(q_1^2,q_2^2,q_3^2) &= \frac{\mathcal{F}_2^A(m_A^2,0)}{q_3^2-m_A^2}\frac{4\mathcal{F}_1^A(q_1^2,q_2^2)+\mathcal{F}_2^A(q_1^2,q_2^2)+\mathcal{F}_3^A(q_1^2,q_2^2)}{2m_A^4}\,,\\
\hat{\Pi}_i^{A,3}(q_1^2,q_2^2,q_3^2) &= 0\,,\quad i\in\{1,4,7\}\,,
\end{aligned}
\tag{5.17}
$$

while the other functions follow from the crossing relations Eq. (2.50). However, dispersion relations in q_3^2 for the crossed functions generate additional poles, which need to be taken into account in addition to Eq. (5.17). We write the full axial-meson contribution as $\hat{\Pi}_i^A = \hat{\Pi}_i^{A,1}+\hat{\Pi}_i^{A,2}+\hat{\Pi}_i^{A,3}$, where the additional contributions are obtained using crossing symmetry:

$$
\begin{aligned}
\hat{\Pi}_1^{A,1}(q_1^2,q_2^2,q_3^2) &= 0\,,\\
\hat{\Pi}_4^{A,1}(q_1^2,q_2^2,q_3^2) &= -\left(m_A^2-q_2^2-q_3^2\right)\frac{\mathcal{F}_2^A(m_A^2,0)}{q_1^2-m_A^2}\frac{2\mathcal{F}_1^A(q_2^2,q_3^2)+\mathcal{F}_3^A(q_2^2,q_3^2)}{2m_A^4}\,,\\
\hat{\Pi}_7^{A,1}(q_1^2,q_2^2,q_3^2) &= \frac{\mathcal{F}_2^A(m_A^2,0)}{q_1^2-m_A^2}\frac{2\mathcal{F}_1^A(q_2^2,q_3^2)+\mathcal{F}_2^A(q_2^2,q_3^2)+\mathcal{F}_3^A(q_2^2,q_3^2)}{m_A^4}\,,\\
\hat{\Pi}_{17}^{A,1}(q_1^2,q_2^2,q_3^2) &= -\frac{\mathcal{F}_2^A(m_A^2,0)}{q_1^2-m_A^2}\frac{4\mathcal{F}_1^A(q_2^2,q_3^2)+\mathcal{F}_2^A(q_2^2,q_3^2)+\mathcal{F}_3^A(q_2^2,q_3^2)}{2m_A^4}\,,\\
\hat{\Pi}_{39}^{A,1}(q_1^2,q_2^2,q_3^2) &= \hat{\Pi}_{54}^{A,1}(q_1^2,q_2^2,q_3^2) = \frac{\mathcal{F}_2^A(m_A^2,0)}{q_1^2-m_A^2}\frac{\mathcal{F}_3^A(q_2^2,q_3^2)-\mathcal{F}_2^A(q_2^2,q_3^2)}{2m_A^4}\,,
\end{aligned}
\tag{5.18}
$$

as well as

$$
\begin{aligned}
\hat{\Pi}_1^{A,2}(q_1^2,q_2^2,q_3^2) &= 0\,,\\
\hat{\Pi}_4^{A,2}(q_1^2,q_2^2,q_3^2) &= -\left(m_A^2-q_1^2-q_3^2\right)\frac{\mathcal{F}_2^A(m_A^2,0)}{q_2^2-m_A^2}\frac{2\mathcal{F}_1^A(q_1^2,q_3^2)+\mathcal{F}_3^A(q_1^2,q_3^2)}{2m_A^4}\,,
\end{aligned}
$$

$$\begin{aligned}
\hat{\Pi}_7^{A,2}(q_1^2,q_2^2,q_3^2) &= -\frac{\mathcal{F}_2^A(m_A^2,0)}{q_2^2-m_A^2}\frac{2\mathcal{F}_1^A(q_1^2,q_3^2)+\mathcal{F}_3^A(q_1^2,q_3^2)}{m_A^4}\,,\\
\hat{\Pi}_{17}^{A,2}(q_1^2,q_2^2,q_3^2) &= -\frac{\mathcal{F}_2^A(m_A^2,0)}{q_2^2-m_A^2}\frac{4\mathcal{F}_1^A(q_1^2,q_3^2)+\mathcal{F}_2^A(q_1^2,q_3^2)+\mathcal{F}_3^A(q_1^2,q_3^2)}{2m_A^4}\,,\\
\hat{\Pi}_{39}^{A,2}(q_1^2,q_2^2,q_3^2) &= -\hat{\Pi}_{54}^{A,2}(q_1^2,q_2^2,q_3^2) = \frac{\mathcal{F}_2^A(m_A^2,0)}{q_2^2-m_A^2}\frac{\mathcal{F}_3^A(q_1^2,q_3^2)-\mathcal{F}_2^A(q_1^2,q_3^2)}{2m_A^4}\,.
\end{aligned}\tag{5.19}$$

We note that these additional contributions to the six representative functions (2.49) do not contain a single-particle intermediate state in the q_3^2-channel, but higher cuts in q_3^2 due to the singularity structure of the TFFs that depend on q_3^2. This needs to be considered when taking into account higher cuts in q_3^2, in order to avoid a double counting, in analogy to the pion-pole contribution.

5.2.2.4 Tensor resonances

We finally consider the contribution of a tensor resonance to the s-channel:

$$\begin{aligned}
&\mathrm{Im}_s^T\left(-\mathrm{i}\,\langle\gamma^*(-q_3,\lambda_3)\gamma^*(q_4,\lambda_4)|\gamma^*(q_1,\lambda_1)\gamma^*(q_2,\lambda_2)\rangle\right)\\
&\quad=\frac{1}{2}\sum_{\lambda_T}\int\widetilde{\mathrm{d}p}\,\langle T(p,\lambda_T)|\gamma^*(-q_3,\lambda_3)\gamma(q_4,\lambda_4)\rangle^*\,\langle T(p,\lambda_T)|\gamma^*(q_1,\lambda_1)\gamma^*(q_2,\lambda_2)\rangle\,.
\end{aligned}\tag{5.20}$$

Again, a Lorentz decomposition of the sub-process in terms of TFFs is given in Ref. [131]. The polarization sum is

$$s^T_{\alpha\beta\alpha'\beta'}(p) := \sum_{\lambda_T}\epsilon^{\lambda_T}_{\alpha\beta}(p)\epsilon^{\lambda_T}_{\alpha'\beta'}{}^*(p) = \frac{1}{2}\left(s_{\alpha\beta'}s_{\alpha'\beta}+s_{\alpha\alpha'}s_{\beta\beta'}\right)-\frac{1}{3}s_{\alpha\beta}s_{\alpha'\beta'}\,,\tag{5.21}$$

where

$$s_{\alpha\alpha'} := -\left(g_{\alpha\alpha'}-\frac{p_\alpha p_{\alpha'}}{m_T^2}\right).\tag{5.22}$$

The projection onto the functions $\hat{\Pi}_i$ leads to the following imaginary parts:

$$\mathrm{Im}^T\,\hat{\Pi}_i(q_1^2,q_2^2,q_3^2) = \pi\delta(s'-m_T^2)\sum_{j=1}^5 t_{i,j}(q_1^2,q_2^2)\frac{\mathcal{F}_j^T(q_1^2,q_2^2)}{m_T^6}\left(\mathcal{F}_1^T(m_T^2,0)+\mathcal{F}_5^T(m_T^2,0)\right),\tag{5.23}$$

where

$$\begin{aligned}
t_{4,1}(q_1^2,q_2^2) &= \frac{8m_T^4}{3}\,,\\
t_{4,2}(q_1^2,q_2^2) &= \frac{2}{3}\left(m_T^4+(q_1^2+q_2^2)m_T^2-2(q_1^2-q_2^2)^2\right)\,,\\
t_{4,3}(q_1^2,q_2^2) &= \frac{2}{3}\left(m_T^4-(q_1^2+q_2^2)m_T^2-2(q_1^2-q_2^2)^2\right)\,,
\end{aligned}$$

$$
\begin{aligned}
t_{4,4}(q_1^2,q_2^2) &= t_{4,5}(q_2^2,q_1^2) = -\frac{4}{3}\left(m_T^4 - q_2^2 m_T^2 - (q_1^2-q_2^2)^2\right)\,, \\
t_{5,1}(q_1^2,q_2^2) &= t_{6,1}(q_1^2,q_2^2) = -m_T^2(m_T^2-q_1^2-q_2^2)\,, \\
t_{5,3}(q_1^2,q_2^2) &= -t_{5,5}(q_1^2,q_2^2) = t_{6,3}(q_2^2,q_1^2) = -t_{6,4}(q_2^2,q_1^2) = (m_T^2+q_2^2)(m_T^2-q_1^2-q_2^2)\,, \\
t_{5,4}(q_1^2,q_2^2) &= t_{6,5}(q_1^2,q_2^2) = \frac{1}{2}(m_T^2-q_1^2-q_2^2)^2\,, \\
t_{7,4}(q_1^2,q_2^2) &= t_{7,5}(q_1^2,q_2^2) = -t_{7,2}(q_1^2,q_2^2) = -t_{7,3}(q_1^2,q_2^2) \\
&= t_{8,4}(q_2^2,q_1^2) = t_{8,5}(q_2^2,q_1^2) = -t_{8,2}(q_2^2,q_1^2) = -t_{8,3}(q_2^2,q_1^2) = 2(m_T^2-q_1^2+q_2^2)\,, \\
t_{9,3}(q_1^2,q_2^2) &= t_{10,1}(q_1^2,q_2^2) = t_{13,3}(q_1^2,q_2^2) = t_{14,1}(q_1^2,q_2^2) \\
&= t_{50,1}(q_1^2,q_2^2) = t_{51,1}(q_1^2,q_2^2) = -t_{39,1}(q_1^2,q_2^2) = -2m_T^2\,, \\
t_{9,5}(q_1^2,q_2^2) &= t_{10,4}(q_1^2,q_2^2) = t_{13,4}(q_1^2,q_2^2) = t_{14,5}(q_1^2,q_2^2) \\
&= -t_{9,4}(q_1^2,q_2^2) = -t_{13,5}(q_1^2,q_2^2) = m_T^2-q_1^2-q_2^2\,, \\
t_{10,3}(q_1^2,q_2^2) &= -t_{10,5}(q_1^2,q_2^2) = t_{14,3}(q_2^2,q_1^2) = -t_{14,4}(q_2^2,q_1^2) = 2(m_T^2+q_2^2)\,, \\
t_{11,3}(q_1^2,q_2^2) &= t_{54,3}(q_1^2,q_2^2) = t_{16,3}(q_2^2,q_1^2) = q_1^2-q_2^2\,, \\
t_{11,4}(q_1^2,q_2^2) &= t_{54,4}(q_1^2,q_2^2) = -t_{16,4}(q_1^2,q_2^2) = t_{16,5}(q_2^2,q_1^2) \\
&= -t_{11,5}(q_2^2,q_1^2) = -t_{54,5}(q_2^2,q_1^2) = \frac{1}{2}(m_T^2-q_1^2+q_2^2)\,, \\
t_{17,1}(q_1^2,q_2^2) &= -\frac{10m_T^2}{3}\,, \\
t_{17,3}(q_1^2,q_2^2) &= \frac{1}{3}(2m_T^2+5(q_1^2+q_2^2))\,, \\
t_{17,4}(q_1^2,q_2^2) &= t_{17,5}(q_2^2,q_1^2) = \frac{1}{6}(7m_T^2-7q_1^2-13q_2^2)\,, \\
t_{39,3}(q_1^2,q_2^2) &= 2m_T^2-q_1^2-q_2^2\,, \\
t_{39,4}(q_1^2,q_2^2) &= t_{39,5}(q_2^2,q_1^2) = \frac{1}{2}(-3m_T^2+3q_1^2+q_2^2)\,, \\
t_{50,3}(q_1^2,q_2^2) &= t_{51,3}(q_1^2,q_2^2) = q_1^2+q_2^2\,, \\
t_{50,4}(q_1^2,q_2^2) &= t_{51,4}(q_1^2,q_2^2) = t_{50,5}(q_2^2,q_1^2) = t_{51,5}(q_2^2,q_1^2) = \frac{1}{2}(m_T^2-q_1^2-3q_2^2)
\end{aligned}
\tag{5.24}
$$

and all other $t_{i,j}$ vanish. Using the dispersion relations in q_3^2, Eq. (5.1), we obtain the pole contributions to the six representative functions in Eq. (2.49) due to a single-tensor meson intermediate state

$$
\begin{aligned}
\hat{\Pi}_i^{T,3}(q_1^2,q_2^2,q_3^2) &= -\sum_{j=1}^{5} t_{i,j}(q_1^2,q_2^2)\frac{\mathcal{F}_j^T(q_1^2,q_2^2)}{m_T^6}\frac{\mathcal{F}_1^T(m_T^2,0)+\mathcal{F}_5^T(m_T^2,0)}{q_3^2-m_T^2}\,,\ i\in\{4,7,17,39,54\}\,, \\
\hat{\Pi}_1^{T,3}(q_1^2,q_2^2,q_3^2) &= 0\,.
\end{aligned}
\tag{5.25}
$$

The contribution from the q_3^2-dispersion relations for the crossed functions can be expressed in terms of the six representative functions as

$$\begin{aligned}
\hat{\Pi}_1^{T,1}(q_1^2,q_2^2,q_3^2) &= 0\,,\\
\hat{\Pi}_4^{T,1}(q_1^2,q_2^2,q_3^2) &= -\sum_{j=1}^{5} t_{5,j}(q_2^2,q_3^2)\frac{\mathcal{F}_j^T(q_2^2,q_3^2)}{m_T^6}\frac{\mathcal{F}_1^T(m_T^2,0)+\mathcal{F}_5^T(m_T^2,0)}{q_1^2-m_T^2}\,,\\
\hat{\Pi}_7^{T,1}(q_1^2,q_2^2,q_3^2) &= -\sum_{j=1}^{5} t_{9,j}(q_2^2,q_3^2)\frac{\mathcal{F}_j^T(q_2^2,q_3^2)}{m_T^6}\frac{\mathcal{F}_1^T(m_T^2,0)+\mathcal{F}_5^T(m_T^2,0)}{q_1^2-m_T^2}\,,\\
\hat{\Pi}_{17}^{T,1}(q_1^2,q_2^2,q_3^2) &= -\sum_{j=1}^{5} t_{16,j}(q_2^2,q_3^2)\frac{\mathcal{F}_j^T(q_2^2,q_3^2)}{m_T^6}\frac{\mathcal{F}_1^T(m_T^2,0)+\mathcal{F}_5^T(m_T^2,0)}{q_1^2-m_T^2}\,,\\
\hat{\Pi}_{39}^{T,1}(q_1^2,q_2^2,q_3^2) &= -\sum_{j=1}^{5} t_{39,j}(q_2^2,q_3^2)\frac{\mathcal{F}_j^T(q_2^2,q_3^2)}{m_T^6}\frac{\mathcal{F}_1^T(m_T^2,0)+\mathcal{F}_5^T(m_T^2,0)}{q_1^2-m_T^2}\,,\\
\hat{\Pi}_{54}^{T,1}(q_1^2,q_2^2,q_3^2) &= -\sum_{j=1}^{5} t_{50,j}(q_2^2,q_3^2)\frac{\mathcal{F}_j^T(q_2^2,q_3^2)}{m_T^6}\frac{\mathcal{F}_1^T(m_T^2,0)+\mathcal{F}_5^T(m_T^2,0)}{q_1^2-m_T^2}
\end{aligned}\tag{5.26}$$

and

$$\begin{aligned}
\hat{\Pi}_1^{T,2}(q_1^2,q_2^2,q_3^2) &= 0\,,\\
\hat{\Pi}_4^{T,2}(q_1^2,q_2^2,q_3^2) &= -\sum_{j=1}^{5} t_{5,j}(q_1^2,q_3^2)\frac{\mathcal{F}_j^T(q_1^2,q_3^2)}{m_T^6}\frac{\mathcal{F}_1^T(m_T^2,0)+\mathcal{F}_5^T(m_T^2,0)}{q_2^2-m_T^2}\,,\\
\hat{\Pi}_7^{T,2}(q_1^2,q_2^2,q_3^2) &= -\sum_{j=1}^{5} t_{10,j}(q_1^2,q_3^2)\frac{\mathcal{F}_j^T(q_1^2,q_3^2)}{m_T^6}\frac{\mathcal{F}_1^T(m_T^2,0)+\mathcal{F}_5^T(m_T^2,0)}{q_2^2-m_T^2}\,,\\
\hat{\Pi}_{17}^{T,2}(q_1^2,q_2^2,q_3^2) &= -\sum_{j=1}^{5} t_{16,j}(q_1^2,q_3^2)\frac{\mathcal{F}_j^T(q_1^2,q_3^2)}{m_T^6}\frac{\mathcal{F}_1^T(m_T^2,0)+\mathcal{F}_5^T(m_T^2,0)}{q_2^2-m_T^2}\,,\\
\hat{\Pi}_{39}^{T,2}(q_1^2,q_2^2,q_3^2) &= -\sum_{j=1}^{5} t_{39,j}(q_1^2,q_3^2)\frac{\mathcal{F}_j^T(q_1^2,q_3^2)}{m_T^6}\frac{\mathcal{F}_1^T(m_T^2,0)+\mathcal{F}_5^T(m_T^2,0)}{q_2^2-m_T^2}\,,\\
\hat{\Pi}_{54}^{T,2}(q_1^2,q_2^2,q_3^2) &= \sum_{j=1}^{5} t_{50,j}(q_1^2,q_3^2)\frac{\mathcal{F}_j^T(q_1^2,q_3^2)}{m_T^6}\frac{\mathcal{F}_1^T(m_T^2,0)+\mathcal{F}_5^T(m_T^2,0)}{q_2^2-m_T^2}
\end{aligned}\tag{5.27}$$

and the full tensor-meson contribution is given by $\hat{\Pi}_i^T = \hat{\Pi}_i^{T,1} + \hat{\Pi}_i^{T,2} + \hat{\Pi}_i^{T,3}$. The same comment regarding double counting with higher cuts in q_3^2 applies as for the other resonances.

To the best of our knowledge, there is no alternative basis of $\check{\Pi}_i$ functions that would allow dispersion relations in four-point kinematics for the tensor-meson contributions that are manifestly free from spurious kinematic singularities if no additional sum rules compared to the ones of Ref. [17] are invoked. The modified basis discussed in Ref. [46] reduces the spurious kinematic singularities in the tensor-meson contribution to simple poles of the type $1/q_1^2$ for fixed-t kinematics.

5.2.3 Vector resonances in the q_3^2 channel

In the q_3^2-channel, single-particle intermediate states only appear in the NWA, in particular the isoscalar vector-meson resonances ω and ϕ (the prominent isovector ρ resonance is best described in terms of two-pion P-wave rescattering). The unitarity relation reads

$$\begin{aligned}&\mathrm{Im}_3\left[-\mathrm{i}\,\langle\gamma^*(-q_3,\lambda_3)|\gamma^*(q_1,\lambda_1)\gamma^*(q_2,\lambda_2)\gamma^*(-q_4,\lambda_4)\rangle\right]\\&\quad=\frac{1}{2}\sum_{\lambda_V}\int\widetilde{\mathrm{d}p}\,\langle V(p,\lambda_V)|\gamma^*(-q_3,\lambda_3)\rangle^*\,\langle V(p,\lambda_V)|\gamma^*(q_1,\lambda_1)\gamma^*(q_2,\lambda_2)\gamma(-q_4,\lambda_4)\rangle\,.\end{aligned}\tag{5.28}$$

The matrix element of the first sub-process is given in Eq. (4.50) in terms of the vector-meson decay constant f_V. For the matrix element of the second sub-process $\gamma^*\gamma^*\gamma\to V$, we define

$$\begin{aligned}\langle V(p,\lambda_V)|\gamma^*(q_1,\lambda_1)\gamma^*(q_2,\lambda_2)\gamma(-q_4,\lambda_4)\rangle&=\mathrm{i}(2\pi)^4\delta^{(4)}(q_1+q_2-q_4-p)e^3\\&\quad\times\epsilon_\mu^{\lambda_1}(q_1)\epsilon_\nu^{\lambda_2}(q_2)\epsilon_\sigma^{\lambda_4}(-q_4)\epsilon_\lambda^{\lambda_V}(p)^*\,\Pi_V^{\mu\nu\lambda\sigma}\,,\end{aligned}\tag{5.29}$$

where

$$\epsilon_\lambda^{\lambda_V}(p)^*\,\Pi_V^{\mu\nu\lambda\sigma}(q_1,q_2,p)=\int\mathrm{d}^4x\,\mathrm{d}^4y e^{-i(q_1\cdot x+q_2\cdot y)}\,\langle V(p,\lambda_V)|\,\mathrm{T}\{j_\mathrm{em}^\mu(x)j_\mathrm{em}^\nu(y)j_\mathrm{em}^\sigma(0)\}\,|0\rangle\,,\tag{5.30}$$

and we perform the BTT tensor decomposition (reviewed in Sec. 2.4.1 for the case of HLbL) for $\Pi_V^{\mu\nu\lambda\sigma}(q_1,q_2,p)$. We first impose transversality for the three photons by making use of gauge projectors

$$I_{12}^{\mu\nu}=g^{\mu\nu}-\frac{q_2^\mu q_1^\nu}{q_1\cdot q_2}\,,\qquad\qquad I_4^{\sigma\sigma'}=g^{\sigma\sigma'}-\frac{q_4^\sigma q_4^{\sigma'}}{q_4^2}\,,\tag{5.31}$$

and we remove kinematic singularities in the projected tensor structures according to the BTT recipe. This leads to a highly redundant generating set of 72 tensor structures. For the dispersion relations in triangle kinematics, we can immediately take the derivative with respect to the external photon momentum and put $q_4\to 0$. After this step, only 26 linear combinations of tensor structures are non-vanishing. In a final step, we note that in any observable (in particular in a_μ) the tensor $\Pi_V^{\mu\nu\lambda\sigma}$ appears contracted with the vector-meson polarization sum

$$\sum_{\lambda_V}\epsilon_\lambda^{\lambda_V}(p)\epsilon_{\lambda'}^{\lambda_V}(p)^*=-\left(g_{\lambda\lambda'}-\frac{p_\lambda p_{\lambda'}}{m_V^2}\right)\,.\tag{5.32}$$

This implies that out of the 26 derivative tensor structures, only 19 linear combinations enter a_μ, which can be chosen to be identical to the HLbL tensor structures

$$\hat{T}_i^{\mu\nu\lambda\sigma;\rho}:=\left(\frac{\partial}{\partial q_{4\rho}}\hat{T}_{g_i}^{\mu\nu\lambda\sigma}(q_1,q_2,q_4-q_1-q_2)\right)\bigg|_{q_4=0}\,.\tag{5.33}$$

The contraction with the polarization sum has the same effect as imposing the QED Ward identity, with the difference that factors of m_V^2 in the denominator should not be regarded as kinematic singularities. Choosing the HLbL structures instead of the ones that naturally come out of the BTT construction with a vector meson only amounts to a basis change that does not introduce kinematic singularities but involves factors of $1/m_V^2$. The ideal basis for a dispersive reconstruction of the scalar functions depends on the asymptotic behavior, which will require a dedicated analysis. Here, we decompose the tensor as

$$\frac{\partial}{\partial q_{4\rho}} \Pi_V^{\mu\nu\lambda\sigma}(q_1, q_2, p)\bigg|_{q_4=0} = \sum_{i=1}^{19} \hat{T}_i^{\mu\nu\lambda\sigma;\rho}(q_1, q_2) \mathcal{F}_i^V(q_1^2, q_2^2), \tag{5.34}$$

dropping directly the unphysical contributions that vanish upon contraction with the polarization sum. Hence, the unitarity relation leads to

$$\mathrm{Im}^V \hat{\Pi}_{g_i}(q_1^2, q_2^2, s') = \pi\delta(s' - m_V^2) m_V f_V \mathcal{F}_i^V(q_1^2, q_2^2), \tag{5.35}$$

and therefore

$$\hat{\Pi}_{g_i}^{V,3}(q_1^2, q_2^2, q_3^2) = -\mathcal{F}_i^V(q_1^2, q_2^2) \frac{m_V f_V}{q_3^2 - m_V^2}. \tag{5.36}$$

Analogous expressions hold for the contributions in the two crossed channels. Again, when writing a representation that is manifestly crossing symmetric, a double counting must be avoided. E.g., the crossed pion-pole contributions already contain the vector-resonance contribution that corresponds to the pion pole in $\mathcal{F}_i^V$ in the q_1^2- and q_2^2-channels.

5.2.4 Two-pion intermediate states and sub-processes

Two-pion intermediate states can appear in both s- and q_3^2-channels as can be seen in Figs. 5.2 and 5.3. The s-channel contribution is also needed in the established formalism and has been discussed in depth in Refs. [17, 39]. The contribution to the unitarity relation in Eq. (2.55) reads

$$\begin{aligned}
&\mathrm{Im}_s^{\pi^+\pi^-} \left(-i \langle \gamma^*(-q_3, \lambda_3)\gamma^*(q_4, \lambda_4)|\gamma^*(q_1, \lambda_1)\gamma^*(q_2, \lambda_2)\rangle\right) \\
&\quad = \frac{1}{2}\int \widetilde{\mathrm{d}p_1}\widetilde{\mathrm{d}p_2} \langle \gamma^*(q_1, \lambda_1)\gamma^*(q_2, \lambda_2)|\pi^+(p_1)\pi^-(p_2)\rangle^* \langle \gamma^*(-q_3, \lambda_3)\gamma^*(q_4, \lambda_4)|\pi^+(p_1)\pi^-(p_2)\rangle
\end{aligned} \tag{5.37}$$

for the charged one and

$$\begin{aligned}
&\mathrm{Im}_s^{\pi^0\pi^0} \left(-i \langle \gamma^*(-q_3, \lambda_3)\gamma^*(q_4, \lambda_4)|\gamma^*(q_1, \lambda_1)\gamma^*(q_2, \lambda_2)\rangle\right) \\
&\quad = \frac{1}{4}\int \widetilde{\mathrm{d}p_1}\widetilde{\mathrm{d}p_2} \langle \gamma^*(q_1, \lambda_1)\gamma^*(q_2, \lambda_2)|\pi^0(p_1)\pi^0(p_2)\rangle^* \langle \gamma^*(-q_3, \lambda_3)\gamma^*(q_4, \lambda_4)|\pi^0(p_1)\pi^0(p_2)\rangle
\end{aligned} \tag{5.38}$$

for the neutral one. With the definitions of the HLbL tensor in Eq. (2.39) and the $\gamma^*\gamma^* \to \pi\pi$ amplitude [39]

$$W^{\mu\nu}_{ab}(p^1, p^2, q) = \mathrm{i} \int \mathrm{d}^4x e^{-\mathrm{i}q\cdot x} \langle \pi^a(p^1)\pi^b(p^2)| \, \mathrm{T}\{j^\mu_{\mathrm{em}}(x) j^\nu_{\mathrm{em}}(0)\} \, |0\rangle \ , \tag{5.39}$$

where a and b denote the pion charges, this becomes

$$\begin{aligned}
&\mathrm{Im}^{\pi^+\pi^-}_s \, \Pi^{\mu\nu\lambda\sigma}(q_1, q_2, q_3) \\
&\quad = \frac{1}{2} \int \widetilde{\mathrm{d}p_1} \widetilde{\mathrm{d}p_2} (2\pi)^4 \delta^{(4)}(p_1 + p_2 - q_1 - q_2) W_{+-}(p_1, p_2, -q_3)^* W_{+-}(p_1, p_2, q_1) \, , \\
&\mathrm{Im}^{\pi^0\pi^0}_s \, \Pi^{\mu\nu\lambda\sigma}(q_1, q_2, q_3) \\
&\quad = \frac{1}{4} \int \widetilde{\mathrm{d}p_1} \widetilde{\mathrm{d}p_2} (2\pi)^4 \delta^{(4)}(p_1 + p_2 - q_1 - q_2) W_{00}(p_1, p_2, -q_3)^* W_{00}(p_1, p_2, q_1) \, .
\end{aligned} \tag{5.40}$$

We next consider two-pion intermediate states in the q_3^2-channel. C-symmetry of the strong interaction implies that the two-pion state is odd under charge conjugation and hence pure isospin $I = 1$, i.e., only charged pions contribute. The contribution to the imaginary part is given by

$$\begin{aligned}
&\mathrm{Im}^{\pi^+\pi^-}_3 \left(-\mathrm{i} \langle \gamma^*(-q_3, \lambda_3) | \gamma^*(q_1, \lambda_1) \gamma^*(q_2, \lambda_2) \gamma^*(-q_4, \lambda_4) \rangle \right) \\
&\quad = \frac{1}{2} \int \widetilde{\mathrm{d}p_1} \widetilde{\mathrm{d}p_2} \, \langle \gamma^*(q_1, \lambda_1) \gamma^*(q_2, \lambda_2) \gamma^*(-q_4, \lambda_4) | \pi^+(p_1) \pi^-(p_2) \rangle^* \\
&\qquad \times \langle \gamma^*(-q_3, \lambda_3) | \pi^+(p_1) \pi^-(p_2) \rangle \ .
\end{aligned} \tag{5.41}$$

While the matrix element of $\gamma^* \to \pi\pi$ is related to the well-known pion VFF, see Eq. (4.78), $\gamma^*\gamma^* \to \gamma\pi\pi$ has not appeared before and is largely unknown. It will thus have to be reconstructed dispersively. We define the amplitude via

$$\begin{aligned}
&\langle \pi^+(p_1) \pi^-(p_2) | \gamma^*(q_1, \lambda_1) \gamma^*(q_2, \lambda_2) \gamma^*(-q_4, \lambda_4) \rangle \\
&\quad = \mathrm{i} e^3 \epsilon^{\lambda_1}_\mu(q_1) \epsilon^{\lambda_2}_\nu(q_2) \epsilon^{\lambda_4}_\sigma(-q_4) \int \mathrm{d}^4x \, \mathrm{d}^4y \, \mathrm{d}^4z e^{-\mathrm{i}(q_1\cdot x + q_2 \cdot y - q_4 \cdot z)} \\
&\qquad \times \langle \pi^+(p_1) \pi^-(p_2) | \, \mathrm{T}\{ j^\mu_{\mathrm{em}}(x) j^\nu_{\mathrm{em}}(y) j^\sigma_{\mathrm{em}}(z) \} \, |0\rangle \\
&\quad = \mathrm{i} e^3 (2\pi)^4 \delta^{(4)}(p_1 + p_2 - q_1 - q_2 + q_4) \epsilon^{\lambda_1}_\mu(q_1) \epsilon^{\lambda_2}_\nu(q_2) \epsilon^{\lambda_4}_\sigma(-q_4) \\
&\qquad \times \int \mathrm{d}^4x \, \mathrm{d}^4y e^{-\mathrm{i}(q_1 \cdot x + q_2 \cdot y)} \langle \pi^+(p_1) \pi^-(p_2) | \, \mathrm{T}\{ j^\mu_{\mathrm{em}}(x) j^\nu_{\mathrm{em}}(y) j^\sigma_{\mathrm{em}}(0) \} \, |0\rangle \\
&\quad =: \mathrm{i} e^3 (2\pi)^4 \delta^{(4)}(p_1 + p_2 - q_1 - q_2 + q_4) \epsilon^{\lambda_1}_\mu(q_1) \epsilon^{\lambda_2}_\nu(q_2) \epsilon^{\lambda_4}_\sigma(-q_4) \mathcal{M}^{\mu\nu\sigma}(p_1, p_2, q_1, q_2) \, ,
\end{aligned} \tag{5.42}$$

which leads to

$$\begin{aligned}
&\mathrm{Im}^{\pi^+\pi^-}_3 \, \Pi^{\mu\nu\lambda\sigma}(q_1, q_2, q_3) \\
&\quad = \frac{1}{2} \int \widetilde{\mathrm{d}p_1} \, \widetilde{\mathrm{d}p_2} (2\pi)^4 \delta^{(4)}(p_1 + p_2 + q_3)(p_1 - p_2)^\lambda F^V_\pi(q_3^2) \mathcal{M}^{\mu\nu\sigma}(p_1, p_2, q_1, q_2) \, .
\end{aligned} \tag{5.43}$$

The BTT decomposition of $\mathcal{M}^{\mu\nu\sigma}(p_1,p_2,q_1,q_2)$ has been derived in Ref. [60]. In general kinematics, a highly redundant set of 74 tensors structures generates the space of Lorentz structures fulfilling the Ward identity in all kinematic limits. There are 27 independent helicity amplitudes, 38 Tarrach redundancies and 9 additional relations between the structures in 4 dimensions due to the Schouten identity. For the part of the matrix element that is non-singular in the soft-photon limit, the derivative and limit $q_4 \to 0$ in Eq. (2.46) can be performed. Thus, for this part a reduced set of Lorentz structures suffices to generate the space. This is in analogy to the 54 BTT structures for HLbL reducing to 19 in the $g-2$ limit. Using also the crossing properties of $\mathcal{M}^{\mu\nu\sigma}(p_1,p_2,q_1,q_2)$ allows one to remove all but a single redundancy in this limit. As explained in Ref. [60], this can be traded for a kinematic constraint. Since the implementation of this constraint does not require sum rules beyond the ones that guarantee basis independence, it is harmless. In addition, the spurious singularities in the basis functions, whose residues vanish due to the sum rules, are never integrated over. Thus, a dispersive reconstruction of the regular part of $\mathcal{M}^{\mu\nu\sigma}(p_1,p_2,q_1,q_2)$ without introducing kinematic singularities is possible. For this, a definition of the soft-singular contribution is required, which can be obtained by the methods introduced in Sec. 5.3. Afterwards, the unitarity relations and dispersion relations for the non-singular contribution can be derived in analogy to the formalism for $\pi\pi \to \gamma\pi\pi$ in the soft-photon limit derived in Ch. 6.

As mentioned above, the unitarity relations for $\mathcal{M}^{\mu\nu\sigma}(p_1,p_2,q_1,q_2)$ illustrated in Fig. 5.5 involve $\pi\pi \to \gamma\pi\pi$ as the main missing sub-process. A dispersive reconstruction in the soft-photon limit of this five-particle process will be provided in Ch. 6. Importantly, in a solution of the two-pion rescattering only $\pi\pi$ scattering and $\pi\pi \to \gamma\pi\pi$ itself appear as sub-processes, which thus allows for an iterative solution for $\pi\pi \to \gamma\pi\pi$ with $\pi\pi$-scattering phase shifts as input. Furthermore, a tensor decomposition free of redundancies and kinematic singularities for $\pi\pi \to \gamma\pi\pi$ in the soft-photon limit exists, see Sec. 6.2 and Ref. [60].

5.3 Soft-photon singularities

5.3.1 Split into singular and regular parts

The new dispersive formalism requires the soft-photon limit to be taken in the unitarity relations. As already mentioned, the sub-processes that appear in Figs. 5.2 and 5.3 are in general singular in this limit, but in such a way that the singularities cancel when the two cuts are added and the limit in Eq. (5.5) exists. This is guaranteed because the HLbL tensor is free of soft-photon singularities.

In this section, we denote the soft-photon momentum by q. A matrix element involving charged external particles and the soft photon in general scales as $1/q$ due to an internal propagator that goes on-shell in the limit $q \to 0$. Conversely, matrix elements that do not involve charged external particles (as HLbL) are non-singular and, since they fulfill the Ward identity, they have to scale as q. Thus, the first two terms in the small-q expansion have to cancel between the cuts. With the derivative in Eq. (2.46), the scaling with q is reduced by one power in both cases so that the individual cuts contain up to double poles in q, but the sum is regular at $q = 0$.

We call processes involving the soft photon as an external particle radiative and processes not involving it non-radiative. Each soft-singular contribution to the unitarity relations for HLbL always combines a radiative process on one side of the cut with a non-radiative one on the other side. For the radiative process with invariant amplitude $\mathcal{M}$, we define $\mathcal{M}^\mu$ through

$$\mathcal{M} = \epsilon_\mu^\lambda(q)\mathcal{M}^\mu \,, \tag{5.44}$$

where we assumed the photon to be in the initial state. We also perform a Lorentz decomposition for general q

$$\mathcal{M}^\mu = \sum_i T_i^\mu \mathcal{M}_i \,, \tag{5.45}$$

where the scalar functions $\mathcal{M}_i$ are free of kinematic singularities and zeros and depend only on Lorentz-invariant quantities, but in general, this decomposition contains redundancies. The tensor structures can be obtained e.g. from the BTT construction, see Sec. 2.4.1. They are non-singular and fulfill the Ward identity and are thus at least of order q, which implies that the scalar functions have singularities of up to order q^{-2}. All singular terms have to cancel and the terms of order q^0 are the ones relevant for HLbL.

It will prove convenient to split the scalar functions into singular and non-singular pieces

$$\mathcal{M}_i = \mathcal{M}_i^{\text{sing}} + \mathcal{M}_i^{\text{non-sing}} \,. \tag{5.46}$$

This should be done such that $\mathcal{M}_i^{\text{sing}}$ contains all terms that are singular in the limit $q \to 0$. There is of course a freedom to move non-singular terms between $\mathcal{M}_i^{\text{sing}}$ and $\mathcal{M}_i^{\text{non-sing}}$, but this ambiguity cancels once the two terms are added again. $\mathcal{M}_i^{\text{sing}}$ should be chosen as simple as possible such that the demonstration of the cancellation of singularities is not unnecessarily complicated. $\mathcal{M}_i^{\text{non-sing}}$ is only needed at $q = 0$. By defining this splitting at the level of the scalar functions, the corresponding splitting of the amplitude is automatically gauge invariant.

It is important to note that the limit $q \to 0$ of a term of the form

$$\frac{p \cdot q}{p' \cdot q} \,, \tag{5.47}$$

where $p^{(\prime)}$ are some momenta of other external particles, depends on the direction of q and is thus singular despite formally being of order q^0. It thus has to be included in $\mathcal{M}_i^{\text{sing}}$.

According to Low's theorem [193], both the terms of order q^{-1} and q^0 in $\mathcal{M}^\mu$ are fully determined by the non-radiative process obtained by removing the soft photon. This corresponds to all terms of order q^{-2} and q^{-1} in $\mathcal{M}_i$. We can thus demonstrate the cancellation of these terms without the need for a dispersive treatment of the radiative process. A convenient recipe to

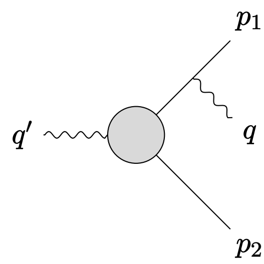

Figure 5.6: Feynman diagram for the external amplitude for $\gamma^*\gamma^* \to \pi^+\pi^-$. The crossed diagram is not shown.

obtain these singular terms will be presented in Sec. 5.3.2 below. However, this recipe is based on an expansion in q and thus not guaranteed to include also the singular terms of order q^0 and higher. Thus, we will afterwards explain how we can use dispersion relations and unitarity to obtain all singular terms of the radiative process from the corresponding non-radiative one.

5.3.2 Adler–Dothan recipe

In Ref. [194], a recipe has been given to calculate the terms of order q^{-1} and q^0 of the amplitude of a radiative process. It involves the following steps:

1. Calculate the so-called external amplitude by attaching the soft photon to any of the charged external particles and (if that particle is a scalar) use scalar QED for the respective vertex. Assume the soft photon to be on-shell.

2. Expand the non-radiative amplitude, which the result depends on, around a common kinematic point.

3. Drop all terms from the external amplitude that are independent of q.

4. Add terms independent of q such that the result fulfills the Ward identity up to neglected higher orders.

To illustrate the use of this recipe in practice, let us consider the process $\gamma^*(q,\lambda)\gamma^*(q',\lambda') \to \pi^+(p^+)\pi^-(p^-)$ in the limit $q \to 0$. This is relatively simple, but still relevant as a sub-process for HLbL, see Fig. 5.2. The matrix element is defined in Eq. (5.39). The external amplitude can be calculated from the diagram in Fig. 5.6 as well as the crossed one and reads

$$\begin{aligned} W^{\mu\nu}_{+-,\text{ext}}(p^+,p^-,q) = &-\frac{1}{2p^+\cdot q}(2p^+-q)^\mu(p^+-p^--q)^\nu F^V_\pi(q'^2,(p^+-q)^2,m_\pi^2) \\ &-\frac{1}{2p^-\cdot q}(2p^--q)^\mu(p^--p^+-q)^\nu F^V_\pi(q'^2,m_\pi^2,(p^--q)^2)\,, \end{aligned} \tag{5.48}$$

where $F_\pi^V(q^2,p_1^2,p_2^2)$ is the pion VFF for the photon virtuality q^2 and the pion invariant masses p_i^2. Due to the soft emission, one of the pions is slightly off-shell, but only the on-shell VFF $F_\pi^V(q^2) = F_\pi^V(q^2,m_\pi^2,m_\pi^2)$ is physical and can contribute to observables.

The non-radiative amplitude in this case is given by the pion VFF and we choose the common kinematic point to expand around as on-shell kinematics

$$
\begin{aligned}
F_\pi^V(q'^2,(p^+-q)^2,m_\pi^2) &= F_\pi^V(q'^2) - 2\frac{\partial}{\partial p^2}F_\pi^V(q'^2,p^2,m_\pi^2)\Big|_{p^2=m_\pi^2} p^+\cdot q + \mathcal{O}(q^2)\,, \\
F_\pi^V(q'^2,m_\pi^2,(p^--q)^2) &= F_\pi^V(q'^2) - 2\frac{\partial}{\partial p^2}F_\pi^V(q'^2,m_\pi^2,p^2)\Big|_{p^2=m_\pi^2} p^-\cdot q + \mathcal{O}(q^2)\,.
\end{aligned} \tag{5.49}
$$

We plug this in and drop all terms independent of q. This removes the unphysical derivatives of the VFF with respect to the pion invariant mass

$$
\begin{aligned}
W^{\mu\nu}_{+-,\text{ext'}}(p^+,p^-,q) = &-\frac{1}{2p^+\cdot q}(2p^+-q)^\mu(p^+-p^--q)^\nu F_\pi^V(q'^2) \\
&-\frac{1}{2p^-\cdot q}(2p^--q)^\mu(p^--p^+-q)^\nu F_\pi^V(q'^2)\,.
\end{aligned} \tag{5.50}
$$

If we contract this with q^μ, we obtain $2q^\nu F_\pi^V(q'^2)$, so the Ward identity is not yet fulfilled. This is easily corrected by subtracting $2g^{\mu\nu}F_\pi^V(q'^2)$ and we obtain the result

$$
\begin{aligned}
W^{\mu\nu}_{+-}(p^+,p^-,q) = &-(p^+-p^-)^\nu\left(\frac{p_+^\mu}{p^+\cdot q}-\frac{p_-^\mu}{p^-\cdot q}\right)F_\pi^V(q'^2) \\
&-2\left(g^{\mu\nu}-\frac{(p^+-p^-)^\nu q^\mu+2p_+^\mu q^\nu}{4(p^+\cdot q)}-\frac{(p^--p^+)^\nu q^\mu+2p_-^\mu q^\nu}{4(p^-\cdot q)}\right)F_\pi^V(q'^2) \\
&+\mathcal{O}(q)\,.
\end{aligned} \tag{5.51}
$$

We have applied this recipe also to the more complicated sub-process $\gamma^*\gamma^*\gamma \to \pi^+\pi^-$. This allowed us to demonstrate the cancellation of terms of order $1/q^2$ and $1/q$ in the imaginary parts of the HLbL scalar functions $\check{\Pi}_i$. However, as mentioned before, this procedure gives correct results for the first two orders in a formal expansion for small q, but generally fails to reproduce also higher-order singular terms. It is thus not suited for a definition of $\mathcal{M}_i^{\text{sing}}$ in Eq. (5.46) since then the limit $q\to 0$ of $\mathcal{M}_i^{\text{non-sing}}$ would still not exist. In the next section, we show that unitarity and dispersion relations enable the calculation of all singular terms and thus provide an adequate definition of $\mathcal{M}_i^{\text{sing}}$. We will apply it to the same example and compare the results.

5.3.3 Dispersive definition of singular pieces

We consider again a general process with charged external particles and a soft photon of momentum q in the initial state. Feynman diagrams for this process can be divided into two classes: external diagrams, where the soft photon is attached to an external charged particle, and internal diagrams, where the soft photon is attached to an internal propagator, independent of whether it belongs to a closed loop or not. The sum of all internal diagrams, which is not gauge invariant, has a finite limit $q \to 0$. Each external diagram contains a propagator with denominator $(q \pm p_i)^2 - m^2$, where p_i is the momentum of the charged particle the photon is attached to and m its mass. The sign depends on whether this particle is incoming or outgoing. This leads to single poles at $q = 0$ since $p_i^2 = m^2$ and these are the only singularities at $q = 0$ in the amplitude $\mathcal{M}^\mu$.

The tensor decomposition in Eq. (5.45) is assumed to be free of kinematic singularities and zeros, which implies that the scalar functions $\mathcal{M}_i$ can be chosen to only have the singularities already present in $\mathcal{M}^\mu$, i.e. single poles at $(q \pm p_i)^2 - m^2 = 0$ for any charged-particle momentum p_i. The terms of order q^{-2} in the scalar functions must be products of such single poles with different i. In a dispersive language, these poles can only be due to single-particle intermediate states of mass m in the $(q \pm p_i)^2$ channels. Assuming a non-degenerate spectrum, the intermediate and external particles thus have to be the same. The sub-processes needed in the unitarity relations for a radiative process in the $(q \pm p_i)^2$-channel are always the corresponding non-radiative process and the coupling of the charged particle to the soft photon. The latter is very simple in the soft limit so that the only required input will be the non-radiative process, similar to the Adler–Dothan recipe considered in the previous section.

Let us apply also this procedure to the process $\gamma^*(q, \lambda)\gamma^*(q', \lambda') \to \pi^+(p^+)\pi^-(p^-)$. According to the previous argument, the singular terms can only be due to pion-pole contributions, see Fig. 5.6 with a cut through the internal pion. These have been studied in Ref. [39] and we will review the main steps and results here.

We start by writing down the unitarity relations in the channels that allow for a single-pion intermediate state

$$\begin{aligned}
&\mathrm{Im}_+ \left(-\mathrm{i}\, \langle \pi^-(p^-)\gamma^*(-q', \lambda')|\pi^-(-p^+)\gamma^*(q, \lambda)\rangle\right) \\
&\quad = \sum_n \frac{1}{2S_n} \left(\prod_{i=1}^{N_n} \int \widetilde{\mathrm{d}p_i}\right) \langle \pi^-(-p^+)\gamma^*(q, \lambda)|n, \{p_i\}\rangle^* \, \langle \pi^-(p^-)\gamma^*(-q', \lambda')|n, \{p_i\}\rangle \ , \\
&\mathrm{Im}_- \left(-\mathrm{i}\, \langle \pi^+(p^+)\gamma^*(-q', \lambda')|\pi^+(-p^-)\gamma^*(q, \lambda)\rangle\right) \\
&\quad = \sum_n \frac{1}{2S_n} \left(\prod_{i=1}^{N_n} \int \widetilde{\mathrm{d}p_i}\right) \langle \pi^+(-p^-)\gamma^*(q, \lambda)|n, \{p_i\}\rangle^* \, \langle \pi^+(p^+)\gamma^*(-q', \lambda')|n, \{p_i\}\rangle \ . \qquad (5.52)
\end{aligned}$$

Singling out a one-pion state in each relation, plugging in expressions for the matrix elements and performing the trivial phase-space integral, we obtain

$$\begin{aligned}
\mathrm{Im}_+^\pi \, W_{+-}^{\mu\nu}(p^+, p^-, q) &= \pi\delta((p^+ - q)^2 - m_\pi^2)(2p^+ - q)^\mu (2p^- - q')^\nu F_\pi^V(q^2) F_\pi^V(q'^2) \, , \\
\mathrm{Im}_-^\pi \, W_{+-}^{\mu\nu}(p^+, p^-, q) &= \pi\delta((p^- - q)^2 - m_\pi^2)(2p^- - q)^\mu (2p^+ - q')^\nu F_\pi^V(q^2) F_\pi^V(q'^2) \, . \qquad (5.53)
\end{aligned}$$

These expressions fulfill the Ward identities only due to the δ-functions [39].

For this process, a Lorentz basis free of kinematic singularities has been derived in Ref. [39]:

$$W^{\mu\nu}_{+-}(p^+,p^-,q) = \sum_{i=1}^{5} T_i^{\mu\nu} A_i \,, \tag{5.54}$$

where

$$\begin{aligned}
T_1^{\mu\nu} &= q\cdot q' g^{\mu\nu} - q'^\mu q^\nu \,, \\
T_2^{\mu\nu} &= q^2 q'^2 g^{\mu\nu} + q\cdot q' q^\mu q'^\nu - q^2 q'^\mu q'^\nu - q'^2 q^\mu q^\nu \,, \\
T_3^{\mu\nu} &= 2p\cdot q \left[-q^2 q'^\mu p^\nu + q'^2 p^\mu q^\nu + q\cdot q'(q^\mu p^\nu - p^\mu q'^\nu) \right] \\
&\quad + 2(p\cdot q)^2 \left[q^\mu q^\nu + q'^\mu q'^\nu - (q^2+q'^2) g^{\mu\nu} \right] \,, \\
T_4^{\mu\nu} &= q\cdot q' p^\mu p^\nu - (p\cdot q)^2 g^{\mu\nu} + p\cdot q(p^\mu q^\nu - q'^\mu p^\nu) \,, \\
T_5^{\mu\nu} &= q^2 q'^2 p^\mu p^\nu + p\cdot q(q^2 p^\mu q'^\nu - q'^2 q^\mu p^\nu) - (p\cdot q)^2 q^\mu q'^\nu
\end{aligned} \tag{5.55}$$

with $p = p^- - p^+$. Projecting the imaginary parts onto these tensor structures, one arrives at

$$\begin{aligned}
\mathrm{Im}_+^\pi A_1 &= -\pi\delta((p^+-q)^2 - m_\pi^2) F_\pi^V(q^2) F_\pi^V(q'^2) \,, \\
\mathrm{Im}_-^\pi A_1 &= -\pi\delta((p^--q)^2 - m_\pi^2) F_\pi^V(q^2) F_\pi^V(q'^2) \,, \\
\mathrm{Im}_+^\pi A_4 &= -\pi\delta((p^+-q)^2 - m_\pi^2) \frac{1}{q\cdot q'} F_\pi^V(q^2) F_\pi^V(q'^2) \,, \\
\mathrm{Im}_-^\pi A_4 &= -\pi\delta((p^--q)^2 - m_\pi^2) \frac{1}{q\cdot q'} F_\pi^V(q^2) F_\pi^V(q'^2) \,,
\end{aligned} \tag{5.56}$$

whereas the scalar functions $A_{2,3,5}$ do not have a pion pole.

Now one writes a dispersion relation for the A_i in $(p^+ - q)^2$ with q^2, q'^2 and $q\cdot q'$ fixed.

$$A_i = \frac{1}{\pi} \int \mathrm{d}t \frac{\mathrm{Im}^\pi A_i(t)}{t - (p^+ - q)^2} \,. \tag{5.57}$$

Due to $(p^- - q)^2 = 2m_\pi^2 - 2q\cdot q' - (p^+ - q)^2$, the π^--pole appears on the negative real axis in this integral and since $(p^+ - q)^2$ above the cut implies $(p^- - q)^2$ below the cut, a sign is picked up in this term. This leads to

$$\begin{aligned}
A_1^{\pi\text{-pole}} &= \int \mathrm{d}t \frac{-\delta(t - m_\pi^2) + \delta(m_\pi^2 - 2q\cdot q' - t)}{t - (p^+ - q)^2} F_\pi^V(q^2) F_\pi^V(q'^2) \\
&= \left(\frac{1}{(p^+-q)^2 - m_\pi^2} + \frac{1}{(p^- - q)^2 - m_\pi^2} \right) F_\pi^V(q^2) F_\pi^V(q'^2) \,, \\
A_4^{\pi\text{-pole}} &= \int \mathrm{d}t \frac{-\delta(t - m_\pi^2) + \delta(m_\pi^2 - 2q\cdot q' - t)}{t - (p^+ - q)^2} \frac{1}{q\cdot q'} F_\pi^V(q^2) F_\pi^V(q'^2) \\
&= \left(\frac{1}{(p^+-q)^2 - m_\pi^2} + \frac{1}{(p^- - q)^2 - m_\pi^2} \right) \frac{1}{q\cdot q'} F_\pi^V(q^2) F_\pi^V(q'^2) \\
&= \frac{2}{[(p^+-q)^2 - m_\pi^2]\,[(p^- - q)^2 - m_\pi^2]} F_\pi^V(q^2) F_\pi^V(q'^2) \,.
\end{aligned} \tag{5.58}$$

The scalar function A_4 scales as q^{-2} due to a product of single poles, whereas A_1 only diverges as q^{-1} in the soft-photon limit.

If these scalar functions are multiplied by the respective tensor structures and q^2 is set to zero, one obtains

$$\begin{aligned}&\left(W_{+-}^{\pi\text{-pole}}(p^+,p^-,q)\right)^{\mu\nu}\\&\quad=-\left[\frac{(2p^+-q)^\mu(p^+-p^--q)^\nu}{2p^+\cdot q}+\frac{(2p^--q)^\mu(p^--p^+-q)^\nu}{2p^-\cdot q}+2g^{\mu\nu}\right]F_\pi^V(q'^2)\,.\end{aligned}\tag{5.59}$$

It is easy to see that this agrees with Eq. (5.51) up to neglected higher orders. However, as opposed to the Adler–Dothan recipe, this result is guaranteed to contain all terms that are singular as $q\to 0$. Thus, we can use it in Eq. (5.46) as the singular term and are guaranteed that the limit $q\to 0$ can be taken for the remaining non-singular term. Another more complicated example for the application of the two recipes will be provided in Sec. 6.4.2.

5.4 Conclusions

In this chapter, we introduced a novel dispersive framework for HLbL, which directly applies in the kinematic limit relevant for a_μ. We showed in detail how this allows us to overcome issues with kinematic singularities that affect intermediate states of spin two and higher present in the established dispersive approach in four-point kinematics. Similarly to what we have seen for VVA in the previous chapter, a reshuffling of intermediate-state contributions takes place and further sub-processes enter the two-pion unitarity relations. These can be dispersively reconstructed without introducing kinematic singularities nor ambiguities. Our results pave the way for a first complete data-driven evaluation of all contributions to HLbL that are described in terms of exclusive hadronic intermediate states and that are required to reach an accuracy matching the final precision goal of the E989 experiment at Fermilab.

We stress that the goal of our new dispersive formalism is not to replace the established one but rather to extend and complement it. The dispersive reconstruction of the sub-processes needed to solve two-pion unitarity in triangle kinematics will allow us to obtain numerical results for two-pion contributions to HLbL beyond the S-wave, including the $f_2(1270)$ resonance in the D-wave. Once a description of all relevant sub-processes is available, a detailed analysis of the reshuffling of intermediate-state contributions with respect to the established approach will be possible yielding more robust estimates of suppressed effects. Therefore, while the new formalism offers a path towards a dispersive treatment of higher-spin resonances, we expect that the detailed comparison of the two approaches will be very useful even for contributions that can be included in the established approach, such as those due to scalar and axial-vector mesons. Moreover, as mentioned already in the previous chapter, the new approach provides new perspectives on the matching onto asymptotic constraints [21,187,188]. A suitable combination of the two dispersive approaches to HLbL will enable a precise data-driven determination of this contribution with reliable uncertainties, compatible with all theoretical and experimental constraints.

The dispersive reconstruction of two-pion rescattering in the new approach requires input for the new sub-processes $\gamma^*\gamma^* \to \gamma\pi\pi$ and $\pi\pi \to \gamma\pi\pi$ in the limit of a soft on-shell photon. These processes have not been studied dispersively before. Therefore, in the next chapter we apply the new formalism to $\pi\pi \to \gamma\pi\pi$. This analysis also serves to exemplify several of the concepts introduced here, e.g. the dispersive definition of a separation into singular and regular pieces, the cancellation of soft singularities between the two cuts and the dispersive reconstruction of the regular piece in the soft-photon limit.

6 Dispersive Reconstruction of the Sub-Process $\pi\pi \to \gamma\pi\pi$

In the previous chapter, we introduced a novel dispersive approach to HLbL, in which the dispersion relations are written in the limit of vanishing q_4. While many of the relevant sub-processes have already been studied in the context of the CHPS formalism, we saw that $\gamma^*\gamma^* \to \gamma\pi\pi$ and $\pi\pi \to \gamma\pi\pi$ play a central role in the new dispersive approach and have not been analyzed in detail before.

For the dispersive reconstruction of $\gamma^*\gamma^* \to \gamma\pi\pi$, the process $\pi\pi \to \gamma\pi\pi$ is needed as input, which makes it the natural next step to focus on. This process is also interesting for other reasons. As opposed to the case of the VVA correlator (cf. Ch. 4), in $\pi\pi \to \gamma\pi\pi$ we have to deal with the cancellation of soft-photon singularities. However, the tensor structure here is very simple, as we will see, and the required sub-process to define the singular contribution is the very well-known $\pi\pi$-scattering. Thus, the method needed for dealing with these singularities can be developed for this process without having to deal with additional complications.

Here, we are dealing with a five-particle process, which reduces to four-point kinematics in the limit where the photon momentum q vanishes. In contrast to that, VVA is a three-point correlator reducing to two-point kinematics and HLbL a four-particle process reducing to three-point kinematics in the soft-photon limit. We will see that this makes the calculation of $\pi\pi \to \gamma\pi\pi$ much more challenging and, again, the techniques developed in this study will later be useful in the dispersive reconstruction of $\gamma^*\gamma^* \to \gamma\pi\pi$.

We begin the chapter by discussing the kinematics, the Lorentz decomposition and constraints from isospin and crossing symmetry on the process $\gamma^*\gamma^* \to \gamma\pi\pi$. Then, we examine how the amplitude can be split into a pole and a non-pole part. We analyze the limit $q \to 0$ in the non-pole contribution and explicitly derive a representation for the pole contribution in terms of $\pi\pi$-scattering amplitudes. Afterwards, we derive the imaginary parts of the non-pole parts due to $\pi\pi$ rescattering and check them against a one-loop calculation in χPT. In order to obtain the amplitudes from the imaginary parts, we derive reconstruction theorems for this process as well as the corresponding inhomogeneous Omnès solution. Finally, we present a preliminary numerical implementation, in which we fix the subtraction constants from the χPT expressions. The Lorentz decomposition for the channel $\pi^0\pi^0 \to \gamma\pi^+\pi^-$ has been presented in Ref. [60].

6.1 Kinematics and matrix element

We consider $\pi\pi$ scattering with the emission of an additional soft photon of momentum q and polarization λ, $\pi\pi \to \gamma^*\pi\pi$. We define the process via the matrix element

$$\begin{aligned}
&\langle \pi^c(-p_3)\pi^d(-p_4)\gamma^*(-q,\lambda)|\pi^a(p_1)\pi^b(p_2)\rangle \\
&= -\mathrm{i}e\epsilon_\mu^{\lambda^*}(-q)\int \mathrm{d}^4x e^{-\mathrm{i}q\cdot x}\left\langle \pi^c(-p_3)\pi^d(-p_4)\right| j^\mu_{\mathrm{em}}(x)\left|\pi^a(p_1)\pi^b(p_2)\right\rangle \\
&= -\mathrm{i}e(2\pi)^4\delta^{(4)}(p_1+p_2+p_3+p_4+q)\epsilon_\mu^{\lambda^*}(-q)\left\langle \pi^c(-p_3)\pi^d(-p_4)\right| j^\mu_{\mathrm{em}}(0)\left|\pi^a(p_1)\pi^b(p_2)\right\rangle \\
&=: -\mathrm{i}e(2\pi)^4\delta^{(4)}(p_1+p_2+p_3+p_4+q)\epsilon_\mu^{\lambda^*}(-q)\mathcal{M}^\mu_{ab\to cd}(p_1,p_2,p_3,p_4)
\end{aligned} \tag{6.1}$$

with a,b,c,d denoting the pion charges or, equivalently, their third components of isospin. We are interested in the limit $q \to 0$.

The full five-particle process depends on ten invariant scalar products, which can be chosen as

$$p_1\cdot p_2\,,\quad p_1\cdot p_3\,,\quad p_1\cdot p_4\,,\quad p_2\cdot p_3\,,\quad p_2\cdot p_4\,,\quad p_3\cdot p_4\,,\quad p_1\cdot q\,,\quad p_2\cdot q\,,\quad p_3\cdot q\,,\quad p_4\cdot q\,. \tag{6.2}$$

Since the pions are on-shell ($p_i^2 = m_\pi^2$), four scalar products are fixed, which leaves six free variables. The scalar products can be expressed in terms of a subset of the following invariants:

$$\begin{aligned}
&s = (p_1+p_2)^2\,, \qquad t = (p_1+p_3)^2\,, \qquad u = (p_1+p_4)^2\,, \\
&\tilde{s} = (p_3+p_4)^2\,, \qquad \tilde{t} = (p_2+p_4)^2\,, \qquad \tilde{u} = (p_2+p_3)^2\,, \\
&w_1 = (p_1+q)^2\,, \qquad w_2 = (p_2+q)^2\,, \qquad w_3 = (p_3+q)^2\,, \qquad w_4 = (p_4+q)^2\,, \qquad q^2\,.
\end{aligned} \tag{6.3}$$

6.2 Lorentz decomposition

In a first step, we consider the decomposition of the matrix element into gauge invariant Lorentz structures. To this end, we apply the BTT [112,113] recipe introduced in Sec. 2.4.1 to the matrix element $\mathcal{M}^\mu(p_1,p_2,p_3,p_4)$ with charge indices suppressed for notational convenience. One starts with four independent four-vectors and applies gauge projectors, which leave three independent structures. However, these structures become degenerate in certain kinematic limits, requiring the introduction of three redundant Tarrach structures. This is equivalent to including the crossed Lorentz structures. The decomposition then reads

$$\mathcal{M}^\mu(p_1,p_2,p_3,p_4) = \sum_{i=1}^{6} T_i^\mu \mathcal{M}_i\,, \tag{6.4}$$

where

$$T_1^\mu = p_1^\mu(p_2\cdot q) - p_2^\mu(p_1\cdot q) \tag{6.5}$$

and the remaining structures are related by crossing:

$$T_2^\mu = \mathcal{C}_{23} T_1^\mu\,, \quad T_3^\mu = \mathcal{C}_{24} T_1^\mu\,, \quad T_4^\mu = -\mathcal{C}_{13} T_1^\mu\,, \quad T_5^\mu = -\mathcal{C}_{14} T_1^\mu\,, \quad T_6^\mu = \mathcal{C}_{13}\mathcal{C}_{24} T_1^\mu\,. \tag{6.6}$$

Here, we define the crossing operators $\mathcal{C}_{ij}$ to exchange momenta and isospin indices of the pions i and j. There is one internal crossing symmetry,

$$T_1^\mu = -\mathcal{C}_{12} T_1^\mu\,. \tag{6.7}$$

Crossing symmetry of the full amplitude implies crossing relations for the scalar functions $\mathcal{M}_i$. We will only need them in the limit $q \to 0$, for which case they are worked out in Sec. 6.3.

Gauge invariance is manifestly fulfilled by the Lorentz structures,

$$q_\mu T_i^\mu = 0\,, \tag{6.8}$$

and at the same time the scalar functions $\mathcal{M}_i$ are free of kinematic singularities. The three Tarrach redundancies read

$$\begin{aligned}
&(p_3 \cdot q) T_1^\mu - (p_2 \cdot q) T_2^\mu + (p_1 \cdot q) T_4^\mu = 0\,,\\
&(p_4 \cdot q) T_1^\mu - (p_2 \cdot q) T_3^\mu + (p_1 \cdot q) T_5^\mu = 0\,,\\
&(p_4 \cdot q) T_2^\mu - (p_3 \cdot q) T_3^\mu + (p_1 \cdot q) T_6^\mu = 0\,.
\end{aligned} \tag{6.9}$$

Eliminating redundant structures introduces kinematic singularities into the scalar coefficient functions.

Finally, we perform a basis change

$$\mathcal{M}^\mu(p_1,p_2,p_3,p_4) = \sum_{i=1}^{6} T_i^\mu \mathcal{M}_i = \sum_{i=1}^{6} \hat{T}_i^\mu \hat{\mathcal{M}}_i\,, \tag{6.10}$$

where

$$\begin{aligned}
&\hat{T}_1^\mu = T_4^\mu\,, && \hat{T}_2^\mu = -T_2^\mu\,, && \hat{T}_3^\mu = T_1^\mu\,,\\
&\hat{T}_4^\mu = T_1^\mu + T_2^\mu + T_3^\mu\,, && \hat{T}_5^\mu = -T_1^\mu + T_4^\mu + T_5^\mu\,, && \hat{T}_6^\mu = -T_2^\mu - T_4^\mu + T_6^\mu\,,
\end{aligned} \tag{6.11}$$

explicitly

$$\begin{aligned}
&\hat{T}_1^\mu = p_2^\mu (p_3 \cdot q) - p_3^\mu (p_2 \cdot q)\,, && \hat{T}_2^\mu = p_3^\mu (p_1 \cdot q) - p_1^\mu (p_3 \cdot q)\,, && \hat{T}_3^\mu = p_1^\mu (p_2 \cdot q) - p_2^\mu (p_1 \cdot q)\,,\\
&\hat{T}_4^\mu = q^\mu (p_1 \cdot q) - p_1^\mu q^2\,, && \hat{T}_5^\mu = q^\mu (p_2 \cdot q) - p_2^\mu q^2\,, && \hat{T}_6^\mu = q^\mu (p_3 \cdot q) - p_3^\mu q^2\,.
\end{aligned} \tag{6.12}$$

The Tarrach redundancies Eq. (6.9) imply that the shifts

$$\begin{aligned}
&\hat{\mathcal{M}}_1 \mapsto \hat{\mathcal{M}}_1 + (p_1 \cdot q)\Delta_1\,, && \hat{\mathcal{M}}_2 \mapsto \hat{\mathcal{M}}_2 + (p_2 \cdot q)\Delta_1 + q^2 \Delta_3\,,\\
&\hat{\mathcal{M}}_3 \mapsto \hat{\mathcal{M}}_3 + (p_3 \cdot q)\Delta_1 + q^2 \Delta_2\,, && \hat{\mathcal{M}}_4 \mapsto \hat{\mathcal{M}}_4 + (p_2 \cdot q)\Delta_2 - (p_3 \cdot q)\Delta_3\,,\\
&\hat{\mathcal{M}}_5 \mapsto \hat{\mathcal{M}}_5 - (p_1 \cdot q)\Delta_2\,, && \hat{\mathcal{M}}_6 \mapsto \hat{\mathcal{M}}_6 + (p_1 \cdot q)\Delta_3
\end{aligned} \tag{6.13}$$

with arbitrary non-singular Δ_i leave the amplitude unchanged.

6.3 Isospin symmetry and Crossing relations

Since the photon is C-odd, at least two pions need to be charged, otherwise the amplitude vanishes due to C-invariance of the strong interaction. The possible channels in the charge basis are

$$\begin{aligned}
\text{mixed:} \quad & s:\ \pi^0\pi^0 \to \gamma\pi^+\pi^- \,, \qquad t:\ \pi^0\pi^- \to \gamma\pi^0\pi^- \,, \qquad u:\ \pi^0\pi^+ \to \gamma\pi^0\pi^+ \,, \\
\text{fully charged:} \quad & s,t:\ \pi^+\pi^- \to \gamma\pi^+\pi^- \,, \quad u:\ \pi^+\pi^+ \to \gamma\pi^+\pi^+ \,.
\end{aligned} \tag{6.14}$$

The isospin basis is defined through the relation of one-pion states

$$|\pi^\pm\rangle = |1,\pm1\rangle \,, \qquad\qquad |\pi^0\rangle = |1,\pm0\rangle \,. \tag{6.15}$$

For two-pion states, we have to perform a Clebsch–Gordan decomposition, which leads e.g. to

$$\begin{aligned}
|\pi^0\pi^0\rangle &= -\frac{1}{\sqrt{3}}\,|0,0\rangle + \sqrt{\frac{2}{3}}\,|2,0\rangle \,, \\
|\pi^+\pi^-\rangle &= \frac{1}{\sqrt{3}}\,|0,0\rangle + \frac{1}{\sqrt{2}}\,|1,0\rangle + \frac{1}{\sqrt{6}}\,|2,0\rangle \,, \\
|\pi^\pm\pi^0\rangle &= \pm\frac{1}{\sqrt{2}}\,|1,\pm1\rangle + \frac{1}{\sqrt{2}}\,|2,\pm1\rangle \,.
\end{aligned} \tag{6.16}$$

Plugging these decompositions into the matrix elements and taking into account how the states and the current transform under $\mathcal{C}$, we arrive at a decomposition of the matrix elements showing that only the isovector component of the photon contributes

$$\begin{aligned}
\langle\pi^+\pi^-|\,j^\mu_{\text{em}}\,|\pi^0\pi^0\rangle &= \frac{1}{\sqrt{3}}\,\langle 1,0|\,j^\mu_v\,|2,0\rangle - \frac{1}{\sqrt{6}}\,\langle 1,0|\,j^\mu_v\,|0,0\rangle \,, \\
\langle\pi^0\pi^0|\,j^\mu_{\text{em}}\,|\pi^+\pi^-\rangle &= \frac{1}{\sqrt{3}}\,\langle 2,0|\,j^\mu_v\,|1,0\rangle - \frac{1}{\sqrt{6}}\,\langle 0,0|\,j^\mu_v\,|1,0\rangle \,, \\
\langle\pi^0\pi^+|\,j^\mu_{\text{em}}\,|\pi^0\pi^+\rangle &= \frac{1}{2}\left[\langle 2,1|\,j^\mu_v\,|2,1\rangle - \langle 1,1|\,j^\mu_v\,|2,1\rangle - \langle 2,1|\,j^\mu_v\,|1,1\rangle + \langle 1,1|\,j^\mu_v\,|1,1\rangle\right] , \\
\langle\pi^0\pi^+|\,j^\mu_{\text{em}}\,|\pi^+\pi^0\rangle &= \frac{1}{2}\left[\langle 2,1|\,j^\mu_v\,|2,1\rangle - \langle 1,1|\,j^\mu_v\,|2,1\rangle + \langle 2,1|\,j^\mu_v\,|1,1\rangle - \langle 1,1|\,j^\mu_v\,|1,1\rangle\right] , \\
\langle\pi^+\pi^0|\,j^\mu_{\text{em}}\,|\pi^0\pi^+\rangle &= \frac{1}{2}\left[\langle 2,1|\,j^\mu_v\,|2,1\rangle + \langle 1,1|\,j^\mu_v\,|2,1\rangle - \langle 2,1|\,j^\mu_v\,|1,1\rangle - \langle 1,1|\,j^\mu_v\,|1,1\rangle\right] , \\
\langle\pi^+\pi^0|\,j^\mu_{\text{em}}\,|\pi^+\pi^0\rangle &= \frac{1}{2}\left[\langle 2,1|\,j^\mu_v\,|2,1\rangle + \langle 1,1|\,j^\mu_v\,|2,1\rangle + \langle 2,1|\,j^\mu_v\,|1,1\rangle + \langle 1,1|\,j^\mu_v\,|1,1\rangle\right] , \\
\langle\pi^+\pi^-|\,j^\mu_{\text{em}}\,|\pi^+\pi^-\rangle &= \frac{1}{\sqrt{12}}\,\langle 1,0|\,j^\mu_v\,|2,0\rangle + \frac{1}{\sqrt{12}}\,\langle 2,0|\,j^\mu_v\,|1,0\rangle \\
&\quad + \frac{1}{\sqrt{6}}\,\langle 0,0|\,j^\mu_v\,|1,0\rangle + \frac{1}{\sqrt{6}}\,\langle 1,0|\,j^\mu_v\,|0,0\rangle \,, \\
\langle\pi^+\pi^+|\,j^\mu_{\text{em}}\,|\pi^+\pi^+\rangle &= \langle 2,2|\,j^\mu_v\,|2,2\rangle \,,
\end{aligned} \tag{6.17}$$

where the electromagnetic current is split into isovector and isoscalar components according to Eq. (4.161).

Next, we use the Wigner–Eckart theorem to factor out the m_i-dependence from the matrix elements. Since the isovector current has $i = 1$ and $m_i = 0$, in this case it reads

$$\langle i, m_i | \, j_v^\mu \, | i', m_i' \rangle = C_{1i'}(i, m_i; 0, m_i') \, \langle i || j_v^\mu || i' \rangle \; . \tag{6.18}$$

Here, $C_{i'i''}(i, m_i; m_i', m_i'')$ is the Clebsch–Gordan coefficient coupling isospins (i', m_i') and (i'', m_i'') to (i, m_i) and $\langle i || j_v^\mu || i' \rangle$ is a reduced matrix element, which is independent of the quantum numbers $m_i^{(\prime)}$. Plugging this in, we obtain

$$\begin{aligned}
\langle \pi^+\pi^- | \, j_{\rm em}^\mu \, | \pi^0\pi^0 \rangle &= -\sqrt{\frac{2}{15}} \, \langle 1 || j_v^\mu || 2 \rangle - \frac{1}{\sqrt{6}} \, \langle 1 || j_v^\mu || 0 \rangle \; , \\
\langle \pi^0\pi^0 | \, j_{\rm em}^\mu \, | \pi^+\pi^- \rangle &= \frac{\sqrt{2}}{3} \, \langle 2 || j_v^\mu || 1 \rangle + \frac{1}{3\sqrt{2}} \, \langle 0 || j_v^\mu || 1 \rangle \; , \\
\langle \pi^0\pi^+ | \, j_{\rm em}^\mu \, | \pi^0\pi^+ \rangle &= -\frac{1}{2\sqrt{6}} \, \langle 2 || j_v^\mu || 2 \rangle + \frac{\sqrt{3}}{2\sqrt{10}} \, \langle 1 || j_v^\mu || 2 \rangle - \frac{1}{2\sqrt{2}} \, \langle 2 || j_v^\mu || 1 \rangle - \frac{1}{2\sqrt{2}} \, \langle 1 || j_v^\mu || 1 \rangle \; , \\
\langle \pi^0\pi^+ | \, j_{\rm em}^\mu \, | \pi^+\pi^0 \rangle &= -\frac{1}{2\sqrt{6}} \, \langle 2 || j_v^\mu || 2 \rangle + \frac{\sqrt{3}}{2\sqrt{10}} \, \langle 1 || j_v^\mu || 2 \rangle + \frac{1}{2\sqrt{2}} \, \langle 2 || j_v^\mu || 1 \rangle + \frac{1}{2\sqrt{2}} \, \langle 1 || j_v^\mu || 1 \rangle \; , \\
\langle \pi^+\pi^0 | \, j_{\rm em}^\mu \, | \pi^0\pi^+ \rangle &= -\frac{1}{2\sqrt{6}} \, \langle 2 || j_v^\mu || 2 \rangle - \frac{\sqrt{3}}{2\sqrt{10}} \, \langle 1 || j_v^\mu || 2 \rangle - \frac{1}{2\sqrt{2}} \, \langle 2 || j_v^\mu || 1 \rangle + \frac{1}{2\sqrt{2}} \, \langle 1 || j_v^\mu || 1 \rangle \; , \\
\langle \pi^+\pi^0 | \, j_{\rm em}^\mu \, | \pi^+\pi^0 \rangle &= -\frac{1}{2\sqrt{6}} \, \langle 2 || j_v^\mu || 2 \rangle - \frac{\sqrt{3}}{2\sqrt{10}} \, \langle 1 || j_v^\mu || 2 \rangle + \frac{1}{2\sqrt{2}} \, \langle 2 || j_v^\mu || 1 \rangle - \frac{1}{2\sqrt{2}} \, \langle 1 || j_v^\mu || 1 \rangle \; , \\
\langle \pi^+\pi^- | \, j_{\rm em}^\mu \, | \pi^+\pi^- \rangle &= -\frac{1}{\sqrt{30}} \, \langle 1 || j_v^\mu || 2 \rangle + \frac{1}{3\sqrt{2}} \, \langle 2 || j_v^\mu || 1 \rangle - \frac{1}{3\sqrt{2}} \, \langle 0 || j_v^\mu || 1 \rangle + \frac{1}{\sqrt{6}} \, \langle 1 || j_v^\mu || 0 \rangle \; , \\
\langle \pi^+\pi^+ | \, j_{\rm em}^\mu \, | \pi^+\pi^+ \rangle &= -\sqrt{\frac{2}{3}} \, \langle 2 || j_v^\mu || 2 \rangle \; .
\end{aligned} \tag{6.19}$$

We simplify the expressions by absorbing the pre-factors into the reduced matrix elements and define

$$\begin{aligned}
\mathcal{M}^\mu_{(10)} &= -\frac{1}{\sqrt{6}} \, \langle 1 || j_v^\mu || 0 \rangle \; , \quad & \mathcal{M}^\mu_{(01)} &= \frac{1}{3\sqrt{2}} \, \langle 0 || j_v^\mu || 1 \rangle \; , \quad & \mathcal{M}^\mu_{(12)} &= \frac{\sqrt{3}}{2\sqrt{10}} \, \langle 1 || j_v^\mu || 2 \rangle \; , \\
\mathcal{M}^\mu_{(21)} &= -\frac{1}{2\sqrt{2}} \, \langle 2 || j_v^\mu || 1 \rangle \; , \quad & \mathcal{M}^\mu_{(11)} &= -\frac{1}{2\sqrt{2}} \, \langle 1 || j_v^\mu || 1 \rangle \; , \quad & \mathcal{M}^\mu_{(22)} &= -\frac{1}{2\sqrt{6}} \, \langle 2 || j_v^\mu || 2 \rangle \; ,
\end{aligned} \tag{6.20}$$

so that

$$\begin{aligned}
\langle \pi^+\pi^- | \, j_{\rm em}^\mu \, | \pi^0\pi^0 \rangle &= \mathcal{M}^\mu_{(10)} - \frac{4}{3} \mathcal{M}^\mu_{(12)} \, , \\
\langle \pi^0\pi^0 | \, j_{\rm em}^\mu \, | \pi^+\pi^- \rangle &= \mathcal{M}^\mu_{(01)} - \frac{4}{3} \mathcal{M}^\mu_{(21)} \, , \\
\langle \pi^0\pi^+ | \, j_{\rm em}^\mu \, | \pi^0\pi^+ \rangle &= \mathcal{M}^\mu_{(22)} + \mathcal{M}^\mu_{(12)} + \mathcal{M}^\mu_{(21)} + \mathcal{M}^\mu_{(11)} \, , \\
\langle \pi^+\pi^0 | \, j_{\rm em}^\mu \, | \pi^0\pi^+ \rangle &= \mathcal{M}^\mu_{(22)} - \mathcal{M}^\mu_{(12)} + \mathcal{M}^\mu_{(21)} - \mathcal{M}^\mu_{(11)} \, , \\
\langle \pi^0\pi^+ | \, j_{\rm em}^\mu \, | \pi^+\pi^0 \rangle &= \mathcal{M}^\mu_{(22)} + \mathcal{M}^\mu_{(12)} - \mathcal{M}^\mu_{(21)} - \mathcal{M}^\mu_{(11)} \, , \\
\langle \pi^+\pi^0 | \, j_{\rm em}^\mu \, | \pi^+\pi^0 \rangle &= \mathcal{M}^\mu_{(22)} - \mathcal{M}^\mu_{(12)} - \mathcal{M}^\mu_{(21)} + \mathcal{M}^\mu_{(11)} \, .
\end{aligned} \tag{6.21}$$

By inverting the system, we obtain the isospin amplitudes in terms of the mixed-charge amplitudes

$$\begin{aligned}
\mathcal{M}^{\mu}_{(10)} &= \frac{1}{3}\Big(- \langle \pi^+\pi^0 |\, j^{\mu}_{\text{em}} \,| \pi^+\pi^0 \rangle - \langle \pi^+\pi^0 |\, j^{\mu}_{\text{em}} \,| \pi^0\pi^+ \rangle \\
&\quad + \langle \pi^0\pi^+ |\, j^{\mu}_{\text{em}} \,| \pi^0\pi^+ \rangle + \langle \pi^0\pi^+ |\, j^{\mu}_{\text{em}} \,| \pi^+\pi^0 \rangle \Big) + \langle \pi^+\pi^- |\, j^{\mu}_{\text{em}} \,| \pi^0\pi^0 \rangle \ , \\
\mathcal{M}^{\mu}_{(01)} &= \frac{1}{3}\Big(- \langle \pi^+\pi^0 |\, j^{\mu}_{\text{em}} \,| \pi^+\pi^0 \rangle + \langle \pi^+\pi^0 |\, j^{\mu}_{\text{em}} \,| \pi^0\pi^+ \rangle \\
&\quad + \langle \pi^0\pi^+ |\, j^{\mu}_{\text{em}} \,| \pi^0\pi^+ \rangle - \langle \pi^0\pi^+ |\, j^{\mu}_{\text{em}} \,| \pi^+\pi^0 \rangle \Big) + \langle \pi^0\pi^0 |\, j^{\mu}_{\text{em}} \,| \pi^+\pi^- \rangle \ , \\
\mathcal{M}^{\mu}_{(12)} &= \frac{1}{4}\Big(- \langle \pi^+\pi^0 |\, j^{\mu}_{\text{em}} \,| \pi^+\pi^0 \rangle - \langle \pi^+\pi^0 |\, j^{\mu}_{\text{em}} \,| \pi^0\pi^+ \rangle \\
&\quad + \langle \pi^0\pi^+ |\, j^{\mu}_{\text{em}} \,| \pi^0\pi^+ \rangle + \langle \pi^0\pi^+ |\, j^{\mu}_{\text{em}} \,| \pi^+\pi^0 \rangle \Big) , \\
\mathcal{M}^{\mu}_{(21)} &= \frac{1}{4}\Big(- \langle \pi^+\pi^0 |\, j^{\mu}_{\text{em}} \,| \pi^+\pi^0 \rangle + \langle \pi^+\pi^0 |\, j^{\mu}_{\text{em}} \,| \pi^0\pi^+ \rangle \\
&\quad + \langle \pi^0\pi^+ |\, j^{\mu}_{\text{em}} \,| \pi^0\pi^+ \rangle - \langle \pi^0\pi^+ |\, j^{\mu}_{\text{em}} \,| \pi^+\pi^0 \rangle \Big) , \\
\mathcal{M}^{\mu}_{(11)} &= \frac{1}{4}\Big(\langle \pi^+\pi^0 |\, j^{\mu}_{\text{em}} \,| \pi^+\pi^0 \rangle - \langle \pi^+\pi^0 |\, j^{\mu}_{\text{em}} \,| \pi^0\pi^+ \rangle \\
&\quad + \langle \pi^0\pi^+ |\, j^{\mu}_{\text{em}} \,| \pi^0\pi^+ \rangle - \langle \pi^0\pi^+ |\, j^{\mu}_{\text{em}} \,| \pi^+\pi^0 \rangle \Big) , \\
\mathcal{M}^{\mu}_{(22)} &= \frac{1}{4}\Big(\langle \pi^+\pi^0 |\, j^{\mu}_{\text{em}} \,| \pi^+\pi^0 \rangle + \langle \pi^+\pi^0 |\, j^{\mu}_{\text{em}} \,| \pi^0\pi^+ \rangle \\
&\quad + \langle \pi^0\pi^+ |\, j^{\mu}_{\text{em}} \,| \pi^0\pi^+ \rangle + \langle \pi^0\pi^+ |\, j^{\mu}_{\text{em}} \,| \pi^+\pi^0 \rangle \Big) .
\end{aligned} \tag{6.22}$$

The fully charged channels can also be decomposed into the same reduced matrix elements, e.g.

$$\begin{aligned}
\langle \pi^+\pi^- |\, j^{\mu}_{\text{em}} \,| \pi^+\pi^- \rangle &= -\frac{1}{\sqrt{30}} \langle 1 || j^{\mu}_{v} || 2 \rangle + \frac{1}{3\sqrt{2}} \langle 2 || j^{\mu}_{v} || 1 \rangle - \frac{1}{3\sqrt{2}} \langle 0 || j^{\mu}_{v} || 1 \rangle + \frac{1}{\sqrt{6}} \langle 1 || j^{\mu}_{v} || 0 \rangle \\
&= -\frac{2}{3}\mathcal{M}^{\mu}_{(12)} - \frac{2}{3}\mathcal{M}^{\mu}_{(21)} - \mathcal{M}^{\mu}_{(01)} - \mathcal{M}^{\mu}_{(10)} \\
&= \langle \pi^+\pi^0 |\, j^{\mu}_{\text{em}} \,| \pi^+\pi^0 \rangle - \langle \pi^0\pi^+ |\, j^{\mu}_{\text{em}} \,| \pi^0\pi^+ \rangle \\
&\quad - \langle \pi^0\pi^0 |\, j^{\mu}_{\text{em}} \,| \pi^+\pi^- \rangle - \langle \pi^+\pi^- |\, j^{\mu}_{\text{em}} \,| \pi^0\pi^0 \rangle \ ,
\end{aligned} \tag{6.23}$$

i.e. in the isospin limit they can be expressed in terms of the mixed ones [195]. For this reason, we will from now on focus on the mixed channels.

The crossing relations of these amplitudes are obtained from the ones in the charge basis, taking into account the Condon–Shortley phase for the crossing of a charged pion

$$\begin{aligned}
C_{12}\mathcal{M}^{\mu}_{(ii')} &= (-1)^{i'}\mathcal{M}^{\mu}_{(ii')} , \quad C_{34}\mathcal{M}^{\mu}_{(ii')} = (-1)^{i}\mathcal{M}^{\mu}_{(ii')} , \\
C_{13}\mathcal{M}^{\mu}_{(10)} &= \frac{1}{3}\left(\mathcal{M}^{\mu}_{(10)} - \mathcal{M}^{\mu}_{(01)} - \mathcal{M}^{\mu}_{(11)}\right) + \frac{5}{9}\left(\mathcal{M}^{\mu}_{(12)} - \mathcal{M}^{\mu}_{(21)}\right) + \frac{5}{3}\mathcal{M}^{\mu}_{(22)} , \\
C_{13}\mathcal{M}^{\mu}_{(01)} &= \frac{1}{3}\left(-\mathcal{M}^{\mu}_{(10)} + \mathcal{M}^{\mu}_{(01)} - \mathcal{M}^{\mu}_{(11)}\right) + \frac{5}{9}\left(-\mathcal{M}^{\mu}_{(12)} + \mathcal{M}^{\mu}_{(21)}\right) + \frac{5}{3}\mathcal{M}^{\mu}_{(22)} ,
\end{aligned}$$

$$
\begin{aligned}
C_{13}\mathcal{M}^\mu_{(12)} &= \frac{1}{4}\left(\mathcal{M}^\mu_{(10)} - \mathcal{M}^\mu_{(01)}\right) + \frac{1}{3}\left(-\mathcal{M}^\mu_{(12)} + \mathcal{M}^\mu_{(21)}\right) + \frac{1}{2}\left(\mathcal{M}^\mu_{(11)} + \mathcal{M}^\mu_{(22)}\right) , \\
C_{13}\mathcal{M}^\mu_{(21)} &= \frac{1}{4}\left(-\mathcal{M}^\mu_{(10)} + \mathcal{M}^\mu_{(01)}\right) + \frac{1}{3}\left(\mathcal{M}^\mu_{(12)} - \mathcal{M}^\mu_{(21)}\right) + \frac{1}{2}\left(\mathcal{M}^\mu_{(11)} + \mathcal{M}^\mu_{(22)}\right) , \\
C_{13}\mathcal{M}^\mu_{(11)} &= \frac{1}{4}\left(-\mathcal{M}^\mu_{(10)} - \mathcal{M}^\mu_{(01)}\right) + \frac{5}{6}\left(\mathcal{M}^\mu_{(12)} + \mathcal{M}^\mu_{(21)}\right) , \\
C_{13}\mathcal{M}^\mu_{(22)} &= \frac{1}{4}\left(\mathcal{M}^\mu_{(10)} + \mathcal{M}^\mu_{(01)}\right) + \frac{1}{6}\left(\mathcal{M}^\mu_{(12)} + \mathcal{M}^\mu_{(21)}\right)
\end{aligned} \tag{6.24}
$$

and the remaining permutations are compositions of these.

6.4 Soft-photon limit

For the application within the new dispersive formalism to HLbL, only the soft-photon limit $q \to 0$ of this process is needed. In this limit, the scalar coefficient functions $\mathcal{M}_i$ contain double and single poles, which are determined by $\pi\pi$ scattering alone. We assume a gauge-invariant separation

$$
\hat{\mathcal{M}}_i = \hat{\mathcal{M}}_i^{\text{poles}} + \hat{\mathcal{M}}_i^{\text{non-pole}} , \tag{6.25}
$$

which will later be defined by specifying $\hat{\mathcal{M}}_i^{\text{poles}}$. We will study these two terms separately and start with the non-pole one.

6.4.1 The limit $q \to 0$ for the non-pole piece

We are only interested in the leading non-pole term, i.e. in the limit $\lim_{q\to 0} \hat{\mathcal{M}}_i^{\text{non-pole}}$. Defining

$$
\mathcal{M}^\mu_{\text{reg}}(p_1,p_2,p_3,p_4) = \sum_{i=1}^{6} \hat{T}_i^\mu \hat{\mathcal{M}}_i^{\text{non-pole}} , \tag{6.26}
$$

we obtain the desired contribution by taking the following derivative:

$$
\begin{aligned}
\frac{\partial}{\partial q_\nu}\mathcal{M}^\mu_{\text{reg}}(p_1,p_2,p_3,p_4)\bigg|_{q=0} &= \sum_{i=1}^{6}\left(\frac{\partial}{\partial q_\nu}\hat{T}_i^\mu\right)\bigg|_{q=0} \hat{\mathcal{M}}_i^{\text{non-pole}}(q=0) \\
&= \sum_{i,j,k=1}^{3} \epsilon_{ijk} p_i^\mu p_j^\nu \hat{\mathcal{M}}_k^{\text{non-pole}}(q=0) ,
\end{aligned} \tag{6.27}
$$

where ϵ_{ijk} is the antisymmetric tensor with $\epsilon_{123} = 1$.

The first three coefficient functions $\hat{\mathcal{M}}_i$ contain a Tarrach redundancy of the form

$$
\hat{\mathcal{M}}_i \mapsto \hat{\mathcal{M}}_i + (p_i \cdot q)\Delta , \quad i = 1,2,3 , \tag{6.28}
$$

with arbitrary non-singular Δ, which drops out in the limit $q \to 0$. However, the three non-vanishing $\hat{\mathcal{M}}_i^{\text{non-pole}}(q=0)$ are not independent due to crossing symmetry. To see this, we first note that for $\bar{T}_k^\mu = \sum_{i,j=1}^3 \epsilon_{ijk} p_i^\mu p_j^\nu$, we have

$$\begin{aligned} &\mathcal{C}_{12}\bar{T}_1^{\mu\nu} = -\bar{T}_2^{\mu\nu}\,, && \mathcal{C}_{12}\bar{T}_3^{\mu\nu} = -\bar{T}_3^{\mu\nu}\,, \\ &\mathcal{C}_{34}\bar{T}_1^{\mu\nu} = -\bar{T}_1^{\mu\nu} + \bar{T}_3^{\mu\nu}\,, && \mathcal{C}_{34}\bar{T}_2^{\mu\nu} = -\bar{T}_2^{\mu\nu} + \bar{T}_3^{\mu\nu}\,, \qquad \mathcal{C}_{34}\bar{T}_3^{\mu\nu} = \bar{T}_3^{\mu\nu}\,. \end{aligned} \tag{6.29}$$

The arguments of the scalar functions in the limit $q \to 0$ can be chosen as $s = (p_1 + p_2)^2$ and $t - u = (p_1 + p_3)^2 - (p_1 + p_4)^2$ and the combined operation $\mathcal{C}_{12}\mathcal{C}_{34}$, which leaves these arguments invariant, implies for the process $\pi^0\pi^0 \to \pi^+\pi^-$

$$\hat{\mathcal{M}}_1^{\text{non-pole}}(s, t-u, q=0) = -\hat{\mathcal{M}}_2^{\text{non-pole}}(s, t-u, q=0)\,. \tag{6.30}$$

Thus, we can use a decomposition with only two scalar functions

$$\frac{\partial}{\partial q_\nu}\mathcal{M}^\mu_{\text{reg}}(p_1,p_2,p_3,p_4)\bigg|_{q=0} = (p_3^\mu p_4^\nu - p_4^\mu p_3^\nu)\bar{\mathcal{M}}_1 + (p_1^\mu p_2^\nu - p_2^\mu p_1^\nu)\bar{\mathcal{M}}_2 \tag{6.31}$$

with

$$\bar{\mathcal{M}}_1(s, t-u) = \hat{\mathcal{M}}_1^{\text{non-pole}}(s, t-u, q=0)\,, \quad \bar{\mathcal{M}}_2(s, t-u) = \hat{\mathcal{M}}_3^{\text{non-pole}}(s, t-u, q=0)\,. \tag{6.32}$$

The individual crossing operations further imply that $\bar{\mathcal{M}}_1$ is symmetric and $\bar{\mathcal{M}}_2$ antisymmetric under $t \leftrightarrow u$.

Similarly, the crossing relations Eq. (6.24) for the isospin amplitudes imply that these can be decomposed according to

$$\begin{aligned} \frac{\partial}{\partial q_\nu}\mathcal{M}^\mu_{(10)}\bigg|_{q=0} &= (p_3^\mu p_4^\nu - p_4^\mu p_3^\nu)\mathcal{M}_{(10)} - (p_1^\mu p_2^\nu - p_2^\mu p_1^\nu)\mathcal{M}_{(01)}\,, \\ \frac{\partial}{\partial q_\nu}\mathcal{M}^\mu_{(01)}\bigg|_{q=0} &= (p_3^\mu p_4^\nu - p_4^\mu p_3^\nu)\mathcal{M}_{(01)} - (p_1^\mu p_2^\nu - p_2^\mu p_1^\nu)\mathcal{M}_{(10)}\,, \\ \frac{\partial}{\partial q_\nu}\mathcal{M}^\mu_{(12)}\bigg|_{q=0} &= (p_3^\mu p_4^\nu - p_4^\mu p_3^\nu)\mathcal{M}_{(12)} - (p_1^\mu p_2^\nu - p_2^\mu p_1^\nu)\mathcal{M}_{(21)}\,, \\ \frac{\partial}{\partial q_\nu}\mathcal{M}^\mu_{(21)}\bigg|_{q=0} &= (p_3^\mu p_4^\nu - p_4^\mu p_3^\nu)\mathcal{M}_{(21)} - (p_1^\mu p_2^\nu - p_2^\mu p_1^\nu)\mathcal{M}_{(12)}\,, \\ \frac{\partial}{\partial q_\nu}\mathcal{M}^\mu_{(11)}\bigg|_{q=0} &= [(p_3 - p_4)^\mu (p_1 - p_2)^\nu - (p_1 - p_2)^\mu (p_3 - p_4)^\nu]\mathcal{M}_{(11)}\,, \\ \frac{\partial}{\partial q_\nu}\mathcal{M}^\mu_{(22)}\bigg|_{q=0} &= [(p_3 - p_4)^\mu (p_1 - p_2)^\nu - (p_1 - p_2)^\mu (p_3 - p_4)^\nu]\mathcal{M}_{(22)}\,. \end{aligned} \tag{6.33}$$

The six scalar functions appearing in these decompositions are in one-to-one correspondence to $\bar{\mathcal{M}}_{1/2}$ in s-, t- and u-channels as can be seen by plugging the charge-basis decomposition into the right-hand side of Eq. (6.22) and projecting the result onto the isospin-basis tensor structures

$$\begin{aligned}
\mathcal{M}^{(10)}(s,t-u) &= \frac{1}{3}\Big(3\bar{\mathcal{M}}_1(s,t-u) - \bar{\mathcal{M}}_1(t,u-s) - \bar{\mathcal{M}}_1(u,t-s) \\
&\qquad - \bar{\mathcal{M}}_2(t,u-s) - \bar{\mathcal{M}}_2(u,t-s)\Big)\,, \\
\mathcal{M}^{(01)}(s,t-u) &= \frac{1}{3}\Big(- \bar{\mathcal{M}}_1(t,u-s) + \bar{\mathcal{M}}_1(u,t-s) \\
&\qquad - 3\bar{\mathcal{M}}_2(s,t-u) - \bar{\mathcal{M}}_2(t,u-s) + \bar{\mathcal{M}}_2(u,t-s)\Big)\,, \\
\mathcal{M}^{(12)}(s,t-u) &= \frac{1}{4}\Big(- \bar{\mathcal{M}}_1(t,u-s) - \bar{\mathcal{M}}_1(u,t-s) - \bar{\mathcal{M}}_2(t,u-s) - \bar{\mathcal{M}}_2(u,t-s)\Big)\,, \\
\mathcal{M}^{(21)}(s,t-u) &= \frac{1}{4}\Big(- \bar{\mathcal{M}}_1(t,u-s) + \bar{\mathcal{M}}_1(u,t-s) - \bar{\mathcal{M}}_2(t,u-s) + \bar{\mathcal{M}}_2(u,t-s)\Big)\,, \\
\mathcal{M}^{(11)}(s,t-u) &= \frac{1}{8}\Big(- \bar{\mathcal{M}}_1(t,u-s) - \bar{\mathcal{M}}_1(u,t-s) + \bar{\mathcal{M}}_2(t,u-s) + \bar{\mathcal{M}}_2(u,t-s)\Big)\,, \\
\mathcal{M}^{(22)}(s,t-u) &= \frac{1}{8}\Big(- \bar{\mathcal{M}}_1(t,u-s) + \bar{\mathcal{M}}_1(u,t-s) + \bar{\mathcal{M}}_2(t,u-s) - \bar{\mathcal{M}}_2(u,t-s)\Big)\,. \qquad (6.34)
\end{aligned}$$

Crossing symmetry furthermore leads to

$$\begin{aligned}
\mathcal{M}^{(10)}(s,u-t) &= \mathcal{M}^{(10)}(s,t-u)\,, \\
\mathcal{M}^{(01)}(s,u-t) &= -\mathcal{M}^{(01)}(s,t-u)\,, \\
\mathcal{M}^{(12)}(s,u-t) &= \mathcal{M}^{(12)}(s,t-u)\,, \\
\mathcal{M}^{(21)}(s,u-t) &= -\mathcal{M}^{(21)}(s,t-u)\,, \\
\mathcal{M}^{(11)}(s,u-t) &= \mathcal{M}^{(11)}(s,t-u)\,, \\
\mathcal{M}^{(22)}(s,u-t) &= -\mathcal{M}^{(22)}(s,t-u)\,, \qquad (6.35)
\end{aligned}$$

and

$$\begin{aligned}
\mathcal{M}^{(10)}(t,s-u) &= -\frac{1}{3}\left(\mathcal{M}^{(10)} + \mathcal{M}^{(01)}\right) - \frac{2}{3}\mathcal{M}^{(11)} - \frac{5}{9}\left(\mathcal{M}^{(12)} + \mathcal{M}^{(21)}\right) - \frac{10}{3}\mathcal{M}^{(22)}\,, \\
\mathcal{M}^{(01)}(t,s-u) &= -\frac{1}{3}\left(\mathcal{M}^{(10)} + \mathcal{M}^{(01)}\right) + \frac{2}{3}\mathcal{M}^{(11)} - \frac{5}{9}\left(\mathcal{M}^{(12)} + \mathcal{M}^{(21)}\right) + \frac{10}{3}\mathcal{M}^{(22)}\,, \\
\mathcal{M}^{(12)}(t,s-u) &= -\frac{1}{4}\left(\mathcal{M}^{(10)} + \mathcal{M}^{(01)}\right) + \mathcal{M}^{(11)} + \frac{1}{3}\left(\mathcal{M}^{(12)} + \mathcal{M}^{(21)}\right) - \mathcal{M}^{(22)}\,, \\
\mathcal{M}^{(21)}(t,s-u) &= -\frac{1}{4}\left(\mathcal{M}^{(10)} + \mathcal{M}^{(01)}\right) - \mathcal{M}^{(11)} + \frac{1}{3}\left(\mathcal{M}^{(12)} + \mathcal{M}^{(21)}\right) + \mathcal{M}^{(22)}\,, \\
\mathcal{M}^{(11)}(t,s-u) &= -\frac{1}{8}\left(\mathcal{M}^{(10)} - \mathcal{M}^{(01)}\right) + \frac{5}{12}\left(\mathcal{M}^{(12)} - \mathcal{M}^{(21)}\right)\,, \\
\mathcal{M}^{(22)}(t,s-u) &= -\frac{1}{8}\left(\mathcal{M}^{(10)} - \mathcal{M}^{(01)}\right) - \frac{1}{12}\left(\mathcal{M}^{(12)} - \mathcal{M}^{(21)}\right)\,, \qquad (6.36)
\end{aligned}$$

where the scalar functions on the right-hand side are evaluated at $(s,t-u)$.

6.4.2 Definition of the pole piece

As photons only couple to charged pions, it is easier to perform this calculation in the charge rather than the isospin basis. We concentrate on $\pi^0\pi^0 \to \pi^+\pi^-\gamma^*$. The other mixed channels are related to this by crossing and the fully-charged channel can be deduced using the isospin relation Eq. (6.23). The corresponding expressions in the isospin basis can be obtained through Eq. (6.22) from the ones in the charge basis.

Applying the Adler–Dothan recipe [194] explained in Sec. 5.3.2 to this amplitude, we obtain

$$\begin{aligned}\mathcal{M}^\mu_{\text{AD}} &= \mathcal{T}(s,t'-u')\left[\frac{(2p_3+q)^\mu}{2(p_3\cdot q)+q^2} - \frac{(2p_4+q)^\mu}{2(p_4\cdot q)+q^2}\right] \\ &\quad + \frac{\partial\mathcal{T}(s,x)}{\partial x}\bigg|_{x=t'-u'}\left[\frac{q\cdot(p_1-p_2)(2p_3+q)^\mu}{2p_3\cdot q+q^2} + \frac{q\cdot(p_1-p_2)(2p_4+q)^\mu}{2p_4\cdot q+q^2} - 2(p_1-p_2)^\mu\right] \\ &\quad + \mathcal{O}(q^1)\,, \end{aligned} \tag{6.37}$$

where $\mathcal{T}$ is the $\pi\pi$ scattering amplitude for the considered charge channel and we have performed the expansion around $t'-u' = \frac{1}{2}(t+\tilde{t}-u-\tilde{u})$. This is exactly gauge invariant by construction.

As discussed before, this result is not sufficient for the separation into pole and non-pole terms due to possible singularities at higher orders in the expansion. We thus formulate a new dispersive definition of the pole term similar to what has been done in Sec. 5.3.3. In a dispersive language, all terms that become singular in the limit $q \to 0$ are due to pion poles in the w_3 and w_4 channels.

The w_3-unitarity relation reads

$$\begin{aligned}&\mathrm{Im}_{w_3}\left[-i\left\langle\pi^+(-p_3)\gamma(-q,\lambda)|\pi^0(p_1)\pi^0(p_2)\pi^+(p_4)\right\rangle\right] \\ &\quad = \sum_n \frac{1}{2S_n}\left(\prod_{i=1}^n \int \widetilde{dp_i}\right)\left\langle\pi^0(p_1)\pi^0(p_2)\pi^+(p_4)|n;\{p_i\}\right\rangle^* \left\langle\pi^+(-p_3)\gamma(-q,\lambda)|n;\{p_i\}\right\rangle\,.\end{aligned} \tag{6.38}$$

Singling out a one-pion state from the sum and expressing the matrix elements in terms of the amplitudes $\mathcal{M}^\mu$ and $\mathcal{T}$, leads to

$$\mathrm{Im}^\pi_{w_3}\mathcal{M}^\mu = -\pi\mathcal{T}(s,\tilde{t}-u)F^V_\pi(q^2)\delta(w_3-m_\pi^2)(q+2p_3)^\mu\,. \tag{6.39}$$

and similarly in the w_4 channel

$$\mathrm{Im}^\pi_{w_4}\mathcal{M}^\mu = \pi\mathcal{T}(s,t-\tilde{u})F^V_\pi(q^2)\delta(w_4-m_\pi^2)(q+2p_4)^\mu\,. \tag{6.40}$$

These imaginary parts are gauge invariant only due to the δ-functions.

We next rewrite these expressions in terms of the BTT functions with poles only in $w_3 - m_\pi^2$ and $w_4 - m_\pi^2$. For the first scalar function, we obtain

$$\begin{aligned}\mathrm{Im}^\pi_{w_3}\hat{\mathcal{M}}_1 &= -\pi\mathcal{T}(s,\tilde{t}-u)F^V_\pi(q^2)\delta(w_3-m_\pi^2)\frac{4}{w_4-m_\pi^2} + (p_1\cdot q)\delta(w_3-m_\pi^2)\frac{\Delta_1^{w_3}}{w_4-m_\pi^2}\,, \\ \mathrm{Im}^\pi_{w_4}\hat{\mathcal{M}}_1 &= -\pi\mathcal{T}(s,t-\tilde{u})F^V_\pi(q^2)\delta(w_4-m_\pi^2)\frac{4}{w_3-m_\pi^2} + (p_1\cdot q)\delta(w_4-m_\pi^2)\frac{\Delta_1^{w_4}}{w_3-m_\pi^2}\,.\end{aligned} \tag{6.41}$$

Here, we have included the Tarrach redundancies Eq. (6.13) explicitly. Although these parameterize the redundancy in the BTT decomposition of the imaginary part, we will see that the dispersively calculated real parts are not independent of them.

We determine the real parts from dispersion relations in w_3 for s, $t'-u'$, q^2, w_1 and w_2 fixed. The imaginary part then gets contributions from both unitarity relations. In terms of the fixed and dispersed variables, it is given by

$$\begin{aligned}\mathrm{Im}_{w_3}^{\pi\text{-poles}}\hat{\mathcal{M}}_1 &= \frac{F_\pi^V(q^2)\delta(w_3-m_\pi^2)}{2q^2-w_1-w_2+2m_\pi^2}\left(-4\pi\mathcal{T}(s,\tilde{t}-u)+\frac{1}{2}(w_1-m_\pi^2-q^2)\Delta_1^{w_3}\right)\\ &\quad-\frac{F_\pi^V(q^2)\delta(w_3-2q^2+w_1+w_2-3m_\pi^2)}{2q^2-w_1-w_2+2m_\pi^2}\\ &\quad\times\left(-4\pi\mathcal{T}(s,t-\tilde{u})+\frac{1}{2}(w_1-m_\pi^2-q^2)\Delta_1^{w_4}\right)\,,\end{aligned} \tag{6.42}$$

where $\tilde{t}-u=t'-u'+(w_1-w_2)/2$ and $t-\tilde{u}=t'-u'-(w_1-w_2)/2$. Here we have taken into account that the w_4-pole is located on the negative real w_3 axis, which changes its sign, cf. Eq. (5.58). The dispersion relation gives

$$\begin{aligned}\hat{\mathcal{M}}_1^{\pi\text{-poles}} &= -F_\pi^V(q^2)\frac{-4\mathcal{T}(s,\tilde{t}-u)+\frac{1}{2\pi}(w_1-m_\pi^2-q^2)\Delta_1^{w_3}}{(2q^2-w_1-w_2+2m_\pi^2)(w_3-m_\pi^2)}\\ &\quad+F_\pi^V(q^2)\frac{-4\mathcal{T}(s,t-\tilde{u})+\frac{1}{2\pi}(w_1-m_\pi^2-q^2)\Delta_1^{w_4}}{(2q^2-w_1-w_2+2m_\pi^2)(w_3+w_1+w_2-2q^2-3m_\pi^2)}\,.\end{aligned} \tag{6.43}$$

where $\Delta_1^{w_3}$ and $\Delta_1^{w_4}$ must be independent of w_3.

Repeating the same steps for the other $\hat{\mathcal{M}}_i$ and contracting the scalar functions with the tensor structures, we see that the result is independent of $\Delta_2^{w_3}$ and $\Delta_2^{w_4}$ and only depends on the combinations $\Delta_1=\Delta_1^{w_3}-\Delta_1^{w_4}$ and $\Delta_3=\Delta_3^{w_3}-\Delta_3^{w_4}$. The full amplitude must not contain a pole at $2q^2-w_1-w_2+2m_\pi^2=0$. The only way to achieve this without introducing other unphysical singularities is by choosing

$$\begin{aligned}\Delta_1 &= 16\pi F_\pi^V(q^2)\frac{\mathcal{T}(s,\tilde{t}-u)-\mathcal{T}(s,t-\tilde{u})}{w_1-w_2}+(w_1+w_2-2q^2-2m_\pi^2)A_1\,,\\ \Delta_3 &= 0\,.\end{aligned} \tag{6.44}$$

We notice that this is non-singular for $w_1=w_2$. We have added an arbitrary non-singular function A_1 that leads to a piece in the amplitude that is regular at $q\to 0$. The resulting amplitude $\mathcal{M}_\mu^{\pi\text{-poles}}$ has the same crossing symmetries as the full $\mathcal{M}_\mu$ if A_1 is antisymmetric under $p_1\leftrightarrow p_2$ and symmetric under $p_3\leftrightarrow p_4$. A contribution to Δ_3 similar to A_1 would break this symmetry and is therefore omitted. The function A_1 does not contain a pion pole and no other singularities should be contained in the pion-pole contribution. This means that A_1 has to be an analytic function in w_3 and if the BTT functions fall off asymptotically to allow for an unsubtracted dispersion relation, A_1 has to vanish.

The remaining ambiguities can be used to remove the unphysical poles also from the BTT functions. We obtain

$$\begin{aligned}
\hat{\mathcal{M}}_1^{\pi\text{-poles}} &= \frac{4F_\pi^V(q^2)(\mathcal{T} - 2(2m_\pi^2 + w_1 - w_2 - 2w_4)\Delta\mathcal{T})}{(w_3 - m_\pi^2)(w_4 - m_\pi^2)} \,, \\
\hat{\mathcal{M}}_2^{\pi\text{-poles}} &= -\frac{4F_\pi^V(q^2)(\mathcal{T} + 2(2m_\pi^2 - w_1 + w_2 - 2w_4)\Delta\mathcal{T})}{(w_3 - m_\pi^2)(w_4 - m_\pi^2)} \,, \\
\hat{\mathcal{M}}_3^{\pi\text{-poles}} &= 0 \,, \\
\hat{\mathcal{M}}_4^{\pi\text{-poles}} &= -\frac{2F_\pi^V(q^2)(\mathcal{T} + (2m_\pi^2 - w_1 + w_2 - 2w_4)\Delta\mathcal{T})}{(w_3 - m_\pi^2)(w_4 - m_\pi^2)} \,, \\
\hat{\mathcal{M}}_5^{\pi\text{-poles}} &= -\frac{2F_\pi^V(q^2)(\mathcal{T} - (2m_\pi^2 + w_1 - w_2 - 2w_4)\Delta\mathcal{T})}{(w_3 - m_\pi^2)(w_4 - m_\pi^2)} \,, \\
\hat{\mathcal{M}}_6^{\pi\text{-poles}} &= 0
\end{aligned} \tag{6.45}$$

with

$$\mathcal{T} = \frac{\mathcal{T}(s, \tilde{t} - u) + \mathcal{T}(s, t - \tilde{u})}{2} \,, \qquad \Delta\mathcal{T} = \frac{\mathcal{T}(s, \tilde{t} - u) - \mathcal{T}(s, t - \tilde{u})}{w_1 - w_2} \,. \tag{6.46}$$

The final amplitude has a simple form

$$\mathcal{M}_\mu^{\pi\text{-poles}} = F_\pi^V(q^2)\left(\frac{(2p_3 + q)^\mu}{w_3 - m_\pi^2}\mathcal{T}(s, \tilde{t} - u) - \frac{(2p_4 + q)^\mu}{w_4 - m_\pi^2}\mathcal{T}(s, t - \tilde{u}) - 2(p_1 - p_2)^\mu \Delta\mathcal{T}\right) \,. \tag{6.47}$$

We have repeated the calculation with a dispersion relation in w_3 with s, $t' - u'$, w_1, w_2 and $p_3 \cdot q$ fixed. The result is the same up to shifts in the arguments of the pion VFFs by $w_3 - m_\pi^2$ or $w_4 - m_\pi^2$ for the two poles, respectively. The difference between the results from the two dispersion relations therefore does not contain pion poles in w_3 or w_4. We are free to add such non-singular terms to $\mathcal{M}_\mu^{\pi\text{-poles}}$, which we will make use of in the next section.

Eq. (6.47) agrees with the Adler–Dothan result Eq. (6.37) up to neglected higher-order terms in the latter, but in contrast to this includes all singular terms to all orders in q. Thus, we can use $\hat{\mathcal{M}}_i^{\pi\text{-poles}}$ as $\hat{\mathcal{M}}_i^{\text{poles}}$ in Eq. (6.25) with a well-defined limit $q \to 0$ of $\hat{\mathcal{M}}_i^{\text{non-poles}}$.

6.4.3 Translation to isospin basis and modified pole definition

For the unitarity relations and the dispersive reconstruction of two-pion rescattering, the isospin basis will prove to be much more convenient. We thus decompose Eq. (6.47) into isospin components using Eq. (6.22). The results can be written as

$$\begin{aligned}
\mathcal{M}_{(i'i''),\mu}^{\pi\text{-poles}} = \sum_{i=0}^{2} \Big[& b_1^{ii'i''} \mathcal{M}_\mu^{\text{pole},(i)}(p_1, p_2, p_3, p_4) + b_2^{ii'i''} \mathcal{M}_\mu^{\text{pole},(i)}(p_1, p_3, p_4, p_2) \\
& + b_3^{ii'i''} \mathcal{M}_\mu^{\text{pole},(i)}(p_1, p_4, p_3, p_2) + b_4^{ii'i''} \mathcal{M}_\mu^{\text{pole},(i)}(p_2, p_3, p_4, p_1) \\
& + b_5^{ii'i''} \mathcal{M}_\mu^{\text{pole},(i)}(p_2, p_4, p_3, p_1) + b_6^{ii'i''} \mathcal{M}_\mu^{\text{pole},(i)}(p_3, p_4, p_1, p_2) \Big]
\end{aligned} \tag{6.48}$$

with

$$
\begin{aligned}
&\mathcal{M}_\mu^{\text{pole},(i)}(p_1,p_2,p_3,p_4) \\
&\quad = F_\pi^V(q^2)\bigg(\frac{(2p_3+q)^\mu}{w_3-m_\pi^2}\mathcal{T}^{(i)}(s,\tilde{t}-u) - \frac{(2p_4+q)^\mu}{w_4-m_\pi^2}\mathcal{T}^{(i)}(s,t-\tilde{u}) \\
&\qquad - 2(p_1-p_2)^\mu \Delta\mathcal{T}^{(i)}(p_1,p_2,p_3,p_4)\bigg)
\end{aligned}
\tag{6.49}
$$

and the non-vanishing coefficients

$$
\begin{aligned}
&b_1^{010} = -b_6^{001} = -\frac{1}{3}\,, \\
&b_2^{110} = b_2^{101} = b_3^{110} = -b_3^{101} = -b_4^{110} = b_4^{101} = -b_5^{110} = -b_5^{101} = -\frac{1}{6}\,, \\
&b_2^{112} = b_2^{121} = b_2^{111} = b_2^{122} = b_3^{112} = -b_3^{121} = b_3^{111} = -b_3^{122} \\
&\quad = -b_4^{112} = b_4^{121} = b_4^{111} = -b_4^{122} = -b_5^{112} = -b_5^{121} = b_5^{111} = b_5^{122} = -\frac{1}{8}\,, \\
&b_1^{210} = -b_6^{201} = \frac{1}{3}\,, \\
&b_2^{210} = b_2^{201} = -b_3^{201} = b_3^{201} = b_4^{201} = -b_4^{201} = -b_5^{201} = -b_5^{201} = -\frac{1}{6}\,, \\
&b_2^{212} = b_2^{221} = b_2^{211} = b_2^{222} = -b_3^{212} = b_3^{221} = -b_3^{211} = b_3^{222} \\
&\quad = b_4^{212} = -b_4^{221} = -b_4^{211} = b_4^{222} = -b_5^{212} = -b_5^{221} = b_5^{211} = b_5^{222} = -\frac{1}{8}\,.
\end{aligned}
\tag{6.50}
$$

Here, the index i at the $\pi\pi$-scattering amplitudes always refers to the isospin in the channel that becomes the s-channel for $q \to 0$ and in translating it to this channel it is important to take into account that the arguments of the amplitudes in general do not fulfill $s+t+u = 4m_\pi^2$ away from $q = 0$.

We see that not all coefficients with $i \neq i'$ and $i \neq i''$ vanish, i.e. an isospin amplitude of $\pi\pi \to \gamma\pi\pi$ depends on different isospin amplitudes of $\pi\pi$ scattering. In order to avoid this unpleasant feature, we can use the freedom to add arbitrary non-singular terms to the pole definition. We start from the definition above and add non-singular terms to it, which we construct in the following way. Since we want to keep Lorentz covariance and gauge invariance, the general Lorentz structure is given by the decomposition in Eq. (6.33) contracted with q_ν. We are not interested in non-singular terms beyond linear order in q and it is thus not necessary to add the tensor structures quadratic in q from Eq. (6.10). Furthermore, the coefficient functions should be non-singular and of order q^0. The tensor structures have dimension 3 and $\mathcal{M}^{\pi\text{-poles}}_{(ii'),\mu}$ has dimension -1, so the coefficient functions must have dimension -4. We cannot have dimensionful quantities in the denominator as these would either lead to singularities in kinematic limits or in the chiral limit. Thus, we have to take derivatives of $\pi\pi$-scattering amplitudes. The amplitudes are dimensionless, so we need a second derivative to obtain

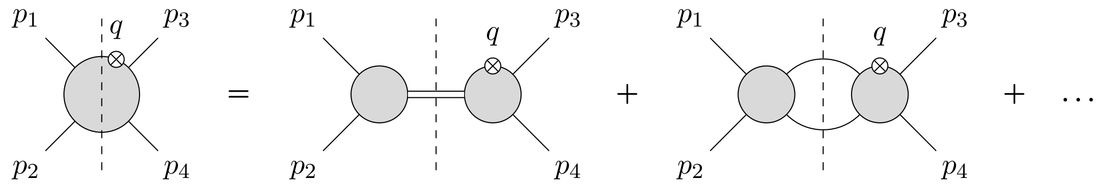

Figure 6.1: Intermediate states in the s-channel cut of $\pi\pi \to \gamma\pi\pi$. Crossed diagrams are not shown.

the right dimension. We only get up to second derivatives from the expansion of the pole contributions to order q^1, so we do not consider higher derivatives here. This leaves us with a result of the form Eq. (6.33), contracted with q_ν and $\mathcal{M}_{(i'i'')}$ replaced by

$$\Delta\mathcal{M}^{\pi\text{-poles}}_{(i'i'')} = \sum_{i=0}^{2} \left[c_1^{ii'i''} \frac{\partial^2}{\partial s^2} \mathcal{T}^{(i)}(s,x) + c_2^{ii'i''} \frac{\partial^2}{\partial s \partial x} \mathcal{T}^{(i)}(s,x) + c_3^{ii'i''} \frac{\partial^2}{\partial x^2} \mathcal{T}^{(i)}(s,x) \right]_{x=t-u} . \tag{6.51}$$

The 54 parameters $c_j^{ii'i''}$ are subject to two constraints: first, crossing symmetry reduces the number of free parameters to 9 and second, these are chosen to remove the dependence of $\mathcal{M}^{\pi\text{-poles}}_{(ii'),\mu}$ on a $\pi\pi$-scattering amplitude with isospin $j \neq i, i'$. This leaves only one free parameter. The modified pole definition still has a simple form in the charge basis. For the channel $\pi^0\pi^0 \to \gamma\pi^+\pi^-$, it only depends on the amplitude $\mathcal{T}$ for $\pi^0\pi^0 \to \pi^+\pi^-$

$$\begin{aligned} \mathcal{M}^{\pi\text{-poles}}_{\mu,\text{ mod}} = F_\pi^V(q^2) \Bigg(& \frac{(2p_3+q)^\mu}{w_3 - m_\pi^2} \mathcal{T}(s, \tilde{t} - u) - \frac{(2p_4+q)^\mu}{w_4 - m_\pi^2} \mathcal{T}(s, t - \tilde{u}) - 2(p_1 - p_2)^\mu \Delta\mathcal{T} \\ & + \frac{1}{2}(p_3^\mu (p_4 \cdot q) - p_4^\mu (p_3 \cdot q)) \left[(24d+5) \frac{\partial^2}{\partial x^2} \mathcal{T}(s,x) - (8d+3) \frac{\partial^2}{\partial s^2} \mathcal{T}(s,x) \right]_{x=t-u} \\ & + (p_1^\mu (p_2 \cdot q) - p_2^\mu (p_1 \cdot q))(8d-1) \left. \frac{\partial^2}{\partial s \partial x} \mathcal{T}(s,x) \right|_{x=t-u} \Bigg) . \end{aligned} \tag{6.52}$$

The remaining free parameter d will be fixed in the next section.

6.5 Unitarity relations

In this section, we derive the imaginary parts of the non-pole pieces. We expect these to have a much simpler form in the isospin basis compared to the the charge basis since $\pi\pi$-scattering conserves isospin and the isovector photon can change isospin by one unit at most.

The unitarity relations in the s- and $\tilde{s}$-channels are depicted in Figs. 6.1 and 6.2. We do not consider resonances in this work since they are assumed to be included in the $\pi\pi$-scattering

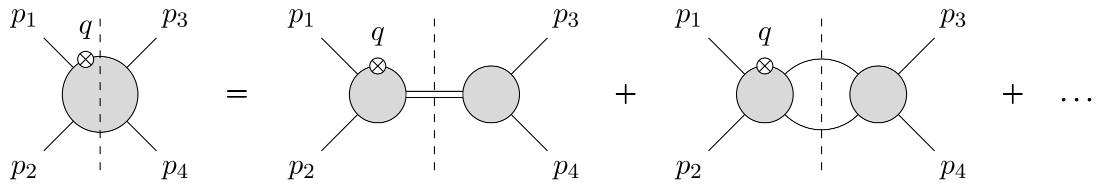

Figure 6.2: Intermediate states in the $\tilde{s}$-channel cut of $\pi\pi \to \gamma\pi\pi$. Crossed diagrams are not shown.

phase shifts. Singling out a two-pion intermediate state, we obtain

$$\begin{aligned}
\mathrm{Im}_s^{\pi\pi}\,\mathcal{M}^\mu_{(ii')}(p_1,p_2,p_3,p_4) &= \sum_l \frac{2l+1}{4} t_l^{i'}(s)^* \int \widetilde{\mathrm{d}q_1}\widetilde{\mathrm{d}q_2}(2\pi)^4\delta^{(4)}(q_1+q_2-p_1-p_2) \\
&\qquad \times P_l(z_s')\mathcal{M}^\mu_{(ii')}(q_1,q_2,p_3,p_4)\,, \\
\mathrm{Im}_{\tilde{s}}^{\pi\pi}\,\mathcal{M}^\mu_{(ii')}(p_1,p_2,p_3,p_4) &= \sum_l \frac{2l+1}{4} t_l^{i}(s)^* \int \widetilde{\mathrm{d}q_1}\widetilde{\mathrm{d}q_2}(2\pi)^4\delta^{(4)}(q_1+q_2+p_3+p_4) \\
&\qquad \times P_l(z_s'')\mathcal{M}^\mu_{(ii')}(p_1,p_2,-q_1,-q_2)\,.
\end{aligned} \tag{6.53}$$

As in VVA (cf. Eq. (4.28)) and HLbL (cf. Eq. (5.5)), $\mathrm{Im}_s^{\pi\pi}\,\mathcal{M}^{(ii')}(s,t-u)$ is given by the sum of these two discontinuities with one of them complex conjugated in the limit $q \to 0$. On the right-hand side of the last equations, $\mathcal{M}^\mu_{(ii')}$ is written as a sum of pole and regular contributions. We decompose the latter according to Eq. (6.33), plug it into the phase-space integral, perform the limit $q \to 0$ and project onto the scalar functions. We obtain, including both cuts,

$$\begin{aligned}
\mathrm{Im}_s\,\mathcal{M}^{(ii')}(s,t-u) &= \sum_l \frac{2l+1}{4} \int \widetilde{\mathrm{d}q_1}\widetilde{\mathrm{d}q_2}(2\pi)^4\delta^{(4)}(p_1+p_2-q_1-q_2)P_l(z_s') \\
&\quad \times \Bigg[t_l^{i'}(s)^* \left(\mathcal{M}^{(ii')}(s,t''-u'') - \frac{z_s''-z_s z_s'}{1-z_s^2}\mathcal{M}^{(i'i)}(s,t''-u'') \right) \\
&\qquad + t_l^i(s)\frac{z_s'-z_s z_s''}{1-z_s^2}\mathcal{M}^{(ii')}(s,t''-u'')^* \Bigg] + I^{(ii')}(s,t-u)
\end{aligned} \tag{6.54}$$

for $i \neq i'$ and

$$\begin{aligned}
\mathrm{Im}_s\,\mathcal{M}^{(ii)}(s,t-u) &= \sum_l \frac{2l+1}{4} \int \widetilde{\mathrm{d}q_1}\widetilde{\mathrm{d}q_2}(2\pi)^4\delta^{(4)}(p_1+p_2-q_1-q_2)P_l(z_s')\frac{z_s'-z_s z_s''}{1-z_s^2} \\
&\quad \times \left[t_l^i(s)^*\mathcal{M}^{(ii)}(s,t''-u'') + t_l^i(s)\mathcal{M}^{(ii)}(s,t''-u'')^* \right] + I^{(ii)}(s,t-u)
\end{aligned} \tag{6.55}$$

for the isospin-diagonal scalar functions. Here, $I^{(ii')}$ contains all inhomogeneous contributions from the pole pieces and

$$z_s = \frac{t-u}{s-4m_\pi^2}\,, \qquad z_s' = \frac{t'-u'}{s-4m_\pi^2}\,, \qquad z_s'' = \frac{t''-u''}{s-4m_\pi^2} \tag{6.56}$$

with

$$t' = (p_1-q_1)^2\,, \qquad u' = (p_2-q_1)^2\,, \qquad t'' = (p_3+q_1)^2\,, \qquad u'' = (p_4+q_1)^2\,. \tag{6.57}$$

In deriving these expressions, we have used the symmetry of the integrals under exchanging all primed and double-primed variables.

We then calculate the inhomogeneous contributions to the imaginary parts, $I^{(ii')}(s,t-u)$. To this end, we plug the modified pole definition Eq. (6.52), in the isospin basis, into the s-channel unitarity relation and insert partial-wave expansions for the $\pi\pi$-scattering amplitudes of the form[1]

$$\mathcal{T}^{(i)}(s,t-u) = \sum_l (2l+1) t_l^i(s) P_l\left(\frac{t-u}{s-4m_\pi^2}\right)\,. \tag{6.58}$$

We then split the integrands into two pieces: one that contains terms proportional to

$$\begin{aligned} \hat{I}^\mu_{ll'} = \int \widetilde{\mathrm{d}q_1}\widetilde{\mathrm{d}q_2}(2\pi)^4\delta^{(4)}(q_1+q_2-p_1-p_2)\frac{(2q_1+q)^\mu}{(q_1+q)^2-m_\pi^2} \\ \times P_l\left(\frac{(p_1-q_1)^2-(p_2-q_1)^2}{s-4m_\pi^2}\right) P_{l'}\left(\frac{(p_4+q_2)^2-(p_3+q_2)^2}{\tilde{s}-4m_\pi^2}\right) \end{aligned} \tag{6.59}$$

or the same with q_1 and q_2 interchanged and another one that does not contain singularities in $(q_1+q)^2-m_\pi^2$ nor in $(q_2+q)^2-m_\pi^2$. We express the latter through the invariants s, $t-\tilde{u}$, w_1, w_2, w_4, q^2, z_s', z_s'' with

$$z_s' = \frac{(p_1-q_1)^2-(p_2-q_1)^2}{s-4m_\pi^2}\,, \qquad z_s'' = \frac{(p_3+q_1)^2-(p_4+q+q_1)^2}{\sigma_\pi(s)\lambda^{1/2}(s,m_\pi^2,w_4)} \tag{6.60}$$

as well as the 4-vectors p_1^μ, p_2^μ, p_3^μ, q^μ, q_1^μ and expand the result for small q counting $w_i - m_\pi^2$ and q^μ as $\mathcal{O}(q^1)$ and q^2 as $\mathcal{O}(q^2)$. By expanding the angle-dependent factors in (derivatives of) Legendre polynomials, these terms can be expressed through only three integrals

$$\begin{aligned} I^0_{ll'} &= \int \widetilde{\mathrm{d}q_1}\widetilde{\mathrm{d}q_2}(2\pi)^4\delta^{(4)}(q_1+q_2-p_1-p_2)P_l(z_s')P_{l'}(z_s'')\,, \\ I^{1\mu}_{ll'} &= \int \widetilde{\mathrm{d}q_1}\widetilde{\mathrm{d}q_2}(2\pi)^4\delta^{(4)}(q_1+q_2-p_1-p_2)(q_1-q_2)_\mu P_l(z_s')P_{l'}'(z_s'')\,, \\ I^{2\mu\nu}_{ll'} &= \int \widetilde{\mathrm{d}q_1}\widetilde{\mathrm{d}q_2}(2\pi)^4\delta^{(4)}(q_1+q_2-p_1-p_2)(q_1-q_2)_\mu(q_1-q_2)_\nu P_l(z_s')P_{l'}''(z_s'')\,. \end{aligned} \tag{6.61}$$

The calculation of these integrals is described in App. A.

[1] It is crucial here to use s and $t-u$ as the independent variables since in general the arguments of the amplitudes do not fulfill $s+t+u=4m_\pi^2$ away from $q=0$.

The terms from the $\tilde{s}$-unitarity relation without singularities in $(q_1+q)^2-m_\pi^2$ nor in $(q_2+q)^2-m_\pi^2$ can be obtained from the s-cut by the crossing operation $\mathcal{C}_{13}\mathcal{C}_{24}$. For the terms with these singularities, we see that only the combination of integrals $\hat{I}^\mu_{ll'}+\mathcal{C}_{13}\mathcal{C}_{24}\hat{I}^\mu_{l'l}$ is required. Neglecting terms that are quadratic in q or higher, this combination is reduced to the integrals in Eq. (6.61) in App. A.4.

Finally, we add the different parts of the result and subtract the imaginary part of the pole term $\mathcal{M}^{\pi\text{-poles}}_{(i'i''),\mu,\text{ mod}}$ obtained from plugging the unitarity relations for $\pi\pi$-scattering into the definition in Eq. (6.52). The difference is non-singular and fulfills the Ward identity up to neglected higher-order terms.

To project this result onto the tensor structures, we express the invariants and momenta through p_2, p_3, p_4 and q, calculate the q-derivative and set $q=0$. It is crucial to keep the p_i^2 fixed when taking the derivatives, i.e. one has to replace one scalar product of p_2, p_3, p_4 and q through the others using that $p_3^2=m_\pi^2$. Only then it is guaranteed that another choice of independent momenta including q will lead to the same result. Then, we can project this onto the tensor decomposition in Eq. (6.33) to obtain the inhomogeneous contributions $I^{(ii')}$ to the imaginary parts of $\mathcal{M}^{(ii')}$ in Eqs. (6.54) and (6.55).

In general, the functions $I^{(10)}(s,t-u)$ and $I^{(12)}(s,t-u)$ behave as $(s-4m_\pi^2)^{-3/2}\theta(s-4m_\pi^2)$ close to threshold. This behavior makes standard dispersion relations invalid since the part of the integration contour surrounding the branch point can no longer be neglected and only the sum of this integral and the one along the cut is finite. While one could assume that the coefficient of this term is purely imaginary and thus can be subtracted from the scalar function before deriving a dispersion relation, this is more subtle for the next term in the expansion proportional to $(s-4m_\pi^2)^{-1}\theta(s-4m_\pi^2)$, which cannot be seen as originating from a usual branch point.

However, the free parameter in the modified pole definition Eq. (6.52), d, comes to our rescue: by choosing $d=-3/8$, both leading terms in the expansion at threshold can be removed. The leading term is then proportional to $(s-4m_\pi^2)^{-1/2}$, in which case a standard dispersion relation holds and the contour around the branch point does not contribute. With this choice and including S-, P- and D-waves in $\pi\pi$ scattering, the result simplifies to

$$
\begin{aligned}
I^{10} = \frac{1}{24\pi s^3\sigma_\pi^3(s)}\Big[&-20m_\pi^2 s t_2^{0\prime}(s)t_0^0(s)^* + 20m_\pi^2 s t_2^{0\prime}(s)t_2^0(s)^* + 5s^2 t_2^{0\prime}(s)t_0^0(s)^* \\
&+5\left(2m_\pi^2-s\right)t_2^0(s)(t_0^0(s)^*-t_2^0(s)^*) + 3s\left(4m_\pi^2-s\right)t_1^{1\prime}(s)(t_0^0(s)^*-t_1^1(s)^*) \\
&-6m_\pi^2 t_0^0(s)^* t_1^1(s) + 6m_\pi^2 t_1^1(s)t_1^1(s)^* - 5s^2 t_2^{0\prime}(s)t_2^0(s)^* + 3s t_0^0(s)^* t_1^1(s)\Big]\,, \\
I^{01} = \frac{5z_s}{8\pi s^3\sigma_\pi^3(s)}\Big[&s\left(s-4m_\pi^2\right)t_2^{0\prime}(s)(t_2^0(s)^*-t_1^1(s)^*) \\
&+t_2^0(s)\left(2m_\pi^2 t_2^0(s)+\left(s-2m_\pi^2\right)t_1^1(s)\right)\Big]\,,
\end{aligned}
$$

$$
\begin{aligned}
I^{12} &= \frac{1}{32\pi s^3 \sigma_\pi^3(s)} \Big[s\left(s-4m_\pi^2\right)\left(3t_1^{1\prime}(s)(t_1^1(s)^* - t_0^2(s)^*) + 5t_2^{2\prime}(s)(t_0^2(s)^* - t_2^2(s)^*)\right) \\
&\qquad + 3t_1^1(s)\left(2m_\pi^2 t_1^1(s)^* + \left(s-2m_\pi^2\right)t_0^2(s)^*\right) + 5\left(2m_\pi^2 - s\right)t_2^2(s)(t_0^2(s)^* - t_2^2(s)^*)\Big] , \\
I^{21} &= \frac{15 z_s}{32\pi s^3 \sigma_\pi^3(s)} \Big[s\left(4m_\pi^2 - s\right) t_2^{2\prime}(s)(t_1^1(s)^* - t_2^2(s)^*) \\
&\qquad + t_2^2(s)\left(\left(s-2m_\pi^2\right)t_1^1(s)^* + 2m_\pi^2 t_2^2(s)^*\right)\Big] , \\
I^{11} &= -\frac{3t_1^1(s)t_1^1(s)^*}{64\pi s^2 \sigma_\pi(s)} , \\
I^{22} &= -\frac{15 z_s t_2^2(s) t_2^2(s)^*}{64\pi s^2 \sigma_\pi(s)} .
\end{aligned}
\tag{6.62}
$$

We notice that these functions would vanish if we had considered only $\pi\pi$-scattering S-waves. If we had included S- and P-waves, only three of them would be non-vanishing and they would be independent of the angle z_s. Finally, including D-waves, terms up to first power in z_s contribute.

Assuming that the scalar functions depend on the cosine of the scattering angle polynomially, as expected from a partial-wave expansion, we can also examine the z_s-dependence of the homogeneous contributions to the imaginary parts. For this, we again truncate the $\pi\pi$ partial-wave expansion after D-waves. Then, the phase-space integrals in Eqs. (6.54) and (6.55) can be performed for $\mathcal{M}^{(ii')}$ set to a polynomial of the cosine of the angle. We observe that for the off-diagonal isospin functions we get results that are at most quadratic in z_s. In the case of the diagonal isospin functions, we even obtain results that are at most linear in z_s. Thus, a truncation of the $\pi\pi$ partial-wave expansion automatically truncates the partial-wave expansion (to be defined below) of the imaginary parts of $\mathcal{M}^{(ii')}$ without the need to make any assumptions about their real parts. This makes the problem ideally suited for a reconstruction theorem, for which only a truncation of the partial-wave expansion of the imaginary parts is required, whereas the real part is not truncated. In this way, we avoid additional approximations. Before turning to this, we now calculate the scalar functions in the limit $q \to 0$ at one loop in χPT. This allows us to check the imaginary parts we have obtained and will prove useful in the dispersive reconstruction below.

6.6 Calculation at one loop in Chiral Perturbation Theory

We have calculated the amplitude for $\pi^0\pi^0 \to \gamma^*\pi^+\pi^-$ to one loop in $SU(2)$ χPT. Again, other charge-basis channels and the isospin-basis expressions can be obtained from the relations in Sec. 6.3. This will serve as a check of the unitarity relations derived in the previous sections and the dispersive reconstruction explained in Sec. 6.7 below. In addition, we will use the results to fix the subtraction constants appearing in the dispersive formalism. The calculation

Figure 6.3: Tree level diagrams for the process $\pi\pi \to \gamma^*\pi\pi$ in χPT. Crossed diagrams are not shown.

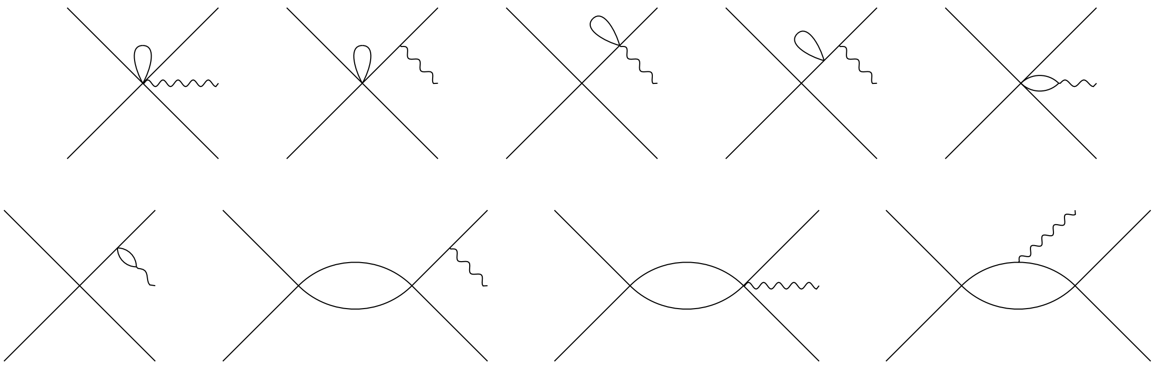

Figure 6.4: One-loop diagrams for the process $\pi\pi \to \gamma^*\pi\pi$ in χPT. Crossed diagrams are not shown.

of the amplitude has already been done in Ref. [196], but the subtraction of the poles, the q-derivative and the limit $q \to 0$ are new.

At tree level, there are two topologies that are shown in Fig. 6.6. The amplitude has the very simple form

$$\mathcal{M}_\mu^{\chi\text{PT, tree}} = -\frac{s - m_\pi^2}{F^2} \left[\frac{(2p_3 + q)_\mu}{w_3 - m_\pi^2} - \frac{(2p_4 + q)_\mu}{w_4 - m_\pi^2} \right] . \tag{6.63}$$

This exactly agrees with the dispersive pion poles in Eq. (6.52) for all values of d if the leading order expressions

$$F_\pi^{V,\chi\text{PT, tree}}(q^2) = 1 , \qquad \mathcal{T}^{\chi\text{PT, tree}}(s, t-u) = -\frac{s - m_\pi^2}{F^2} \tag{6.64}$$

are used. Thus, the non-pole scalar functions $\bar{\mathcal{M}}_i$ vanish at leading order in χPT.

At one loop, there are 9 topologies that are shown in Fig. 6.6 and in addition counterterm diagrams. The amplitude in general kinematics is very lengthy and we thus refer to Ref. [196] for the explicit expression. Also, a projection of the full amplitude onto the BTT structures is very complicated. Instead, we have checked that the pion poles are again reproduced by Eq. (6.52), i.e. that the difference

$$\mathcal{M}_\mu^{\chi\text{PT, 1 loop}} - \mathcal{M}_{\mu,\text{ mod}}^{\pi\text{-poles, }\chi\text{PT, 1 loop}} \tag{6.65}$$

does not contain poles at $w_{3,4} = m_\pi^2$. Here, $\mathcal{M}_{\mu,\,\text{mod}}^{\pi\text{-poles, }\chi\text{PT, 1 loop}}$ denotes Eq. (6.52) with either F_π^V or $\mathcal{T}$ taken at one loop and the other one at tree level. This allows us to take the q_ν derivative of the difference and then the limit $q \to 0$. We have checked that the result has the two independent tensor structures in Eq. (6.31) and the corresponding scalar functions read for $d = -3/8$

$$
\begin{aligned}
\bar{\mathcal{M}}_1 &= -\frac{4m_\pi^2(s-m_\pi^2)}{F^4 s(s-4m_\pi^2)}\bar{J}_{\pi\pi}(s) - \frac{2m_\pi^2(t-3m_\pi^2)}{F^4 t(t-4m_\pi^2)}\bar{J}_{\pi\pi}(t) - \frac{2m_\pi^2(u-3m_\pi^2)}{F^4 u(u-4m_\pi^2)}\bar{J}_{\pi\pi}(u) \\
&\quad + \frac{3m_\pi^2}{48\pi^2 F^4}\left(\frac{6}{s-4m_\pi^2} + \frac{1}{t-4m_\pi^2} + \frac{1}{u-4m_\pi^2}\right) + \frac{5}{24\pi^2 F^4}\,, \\
\bar{\mathcal{M}}_2 &= \frac{t^2-2tm_\pi^2-2m_\pi^4}{3F^4 t(t-4m_\pi^2)}\bar{J}_{\pi\pi}(t) - \frac{u^2-2um_\pi^2-2m_\pi^4}{3F^4 u(u-4m_\pi^2)}\bar{J}_{\pi\pi}(u) + \frac{m_\pi^2(t-u)}{16\pi^2 F^4(t-4m_\pi^2)(u-4m_\pi^2)}
\end{aligned}
\tag{6.66}
$$

with the loop function

$$
\bar{J}_{\pi\pi}(s) = \frac{1}{16\pi^2}\left(\sigma_\pi(s)\log\left(\frac{\sigma_\pi(s)-1}{\sigma_\pi(s)+1}\right) + 2\right) \tag{6.67}
$$

and the pion decay constant in the chiral limit F. These expressions are non-singular if one of the Mandelstam variables approaches zero and diverge at most as $(s-4m_\pi^2)^{1/2}$ at thresholds. Interestingly, both the full amplitude for $\pi\pi \to \gamma\pi\pi$ and the pole piece depend on four low-energy constants, but in the difference they all drop out. This would not be the case if we had taken another definition of the pole, e.g. the difference for the original pole definition Eq. (6.47) depends on one low-energy constant.

We now use this result to check the unitarity relations Eqs. (6.54) and (6.55). To obtain the one-loop imaginary part, the sub-processes in the unitarity relations have to be evaluated at tree level. As mentioned above, the functions $\mathcal{M}^{(ii')}$ vanish at tree level so that we only get contributions from the inhomogeneous pieces Eq. (6.62). There, we plug in the tree-level expressions

$$
t_0^0(s) = \frac{2s-m_\pi^2}{F^2}\,, \qquad t_1^1(s) = \frac{s-4m_\pi^2}{3F^2}\,, \qquad t_0^2(s) = -\frac{s-2m_\pi^2}{F^2}\,. \tag{6.68}
$$

We compare this against the imaginary parts of the isospin-basis χPT expressions generated by the logarithm in $\bar{J}_{\pi\pi}(s)$. We find agreement, which provides a check on both the unitarity relations and the χPT expressions.

6.7 Reconstruction theorems

As mentioned above, the problem is well-suited for a reconstruction theorem since the dependence of the imaginary parts on the scattering angle has the form of a low-order polynomial if we truncate the partial-wave expansion of the $\pi\pi$-scattering amplitudes so that no additional approximation is needed. The reconstruction theorem relates the scalar functions $\mathcal{M}^{(ii')}$ to a set of functions that only depend on one variable and fulfill simple dispersion relations without left-hand cuts. These dispersion relations are coupled through the homogeneous contributions to the imaginary parts. We will derive Omnès solutions for them, which leads to a system of coupled integral equations that will be solved by an iterative algorithm. We will close this section by presenting a preliminary determination of the subtraction constants appearing in these integral equations using the χPT expressions derived in the previous section.

6.7.1 Derivation of the reconstruction theorems

We start from a 3-times subtracted fixed-t dispersion relation

$$\begin{aligned}\mathcal{M}^{(ii')} &= a^{(ii')}(t) + b^{(ii')}(t)s + c^{(ii')}(t)s^2 \\ &\quad + \frac{s^3}{\pi}\int_{4m_\pi^2}^{\infty} \mathrm{d}s' \frac{\mathrm{Im}_s\,\mathcal{M}^{(ii')}(s',t)}{s'^3(s'-s)} + \frac{u^3}{\pi}\int_{4m_\pi^2}^{\infty} \mathrm{d}u' \frac{\mathrm{Im}_u\,\mathcal{M}^{(ii')}(s(t,u'),t)}{s'^3(u'-u)}\end{aligned} \tag{6.69}$$

with $u = 4m_\pi^2 - s - t$ and $s(t,u') = 4m_\pi^2 - t - u' = s + u + u'$. It is likely that the asymptotic behavior of $\mathcal{M}^{(ii')}(s,t)$ would actually allow for fewer subtractions, but only in this way will we be able to symmetrize the result in the end.

The partial-wave expansion of $\mathcal{M}^{(ii')}$ is subtle since this function arises from a kinematic limit of a five-particle process. However, as we have argued above, we do not impose a truncation of this partial-wave expansion and thus it is sufficient to assume expansions in Legendre-polynomials in all three channels

$$\mathcal{M}^{(ii')}(s,t) = \sum_j (2j+1) f_j^{(ii')}(s) P_j(z_s) = \sum_j (2j+1) g_j^{(ii')}(t) P_j(z_t) = \sum_j (2j+1) h_j^{(ii')}(u) P_j(z_u) \tag{6.70}$$

with the angles

$$z_s = \frac{t-u}{s-4m_\pi^2}\,, \qquad z_t = \frac{s-u}{t-4m_\pi^2}\,, \qquad z_u = \frac{s-t}{u-4m_\pi^2}\,. \tag{6.71}$$

As argued above, if we truncate the $\pi\pi$ partial waves after D-waves, $\mathrm{Im}_s\,\mathcal{M}^{(ii')}(s,t)$ is at most quadratic in z_s and therefore $f_j^{(ii')}(s) \in \mathbb{R}\ \forall\, j > 2$. Since the crossed-channel unitarity relations can easily be obtained from the s-channel ones through Eqs. (6.35) and (6.36), we also have $g_j^{(ii')}(t) \in \mathbb{R}\ \forall\, j > 2$ and $h_j^{(ii')}(u) \in \mathbb{R}\ \forall\, j > 2$.

When we plug in the partial-wave expansions for the imaginary parts in the respective channel, the s' integral involves the angle

$$z_s(s',t) = \frac{t-u(s',t)}{s'-4m_\pi^2} = \frac{2t+s'-4m_\pi^2}{s'-4m_\pi^2} = \frac{s'-s}{s'-4m_\pi^2} + \frac{t-u}{s'-4m_\pi^2}\,. \tag{6.72}$$

Thus,

$$\begin{aligned}\mathrm{Im}_s\,\mathcal{M}^{(ii')}(s',t) &= \mathrm{Im}\,f_0^{(ii')}(s') + 3\left(\frac{s'-s}{s'-4m_\pi^2} + \frac{t-u}{s'-4m_\pi^2}\right)\mathrm{Im}\,f_1^{(ii')}(s') \\ &+ \frac{5}{2}\left(3\left(\frac{s'-s}{s'-4m_\pi^2}\right)^2 + 6\frac{(s'-s)(t-u)}{(s'-4m_\pi^2)^2} + 3\left(\frac{t-u}{s'-4m_\pi^2}\right)^2 - 1\right)\mathrm{Im}\,f_2^{(ii')}(s')\end{aligned} \tag{6.73}$$

and we obtain

$$\begin{aligned}&\frac{s^3}{\pi}\int_{4m_\pi^2}^{\infty}\mathrm{d}s'\frac{\mathrm{Im}_s\,\mathcal{M}^{(ii')}(s',t)}{s'^3(s'-s)} \\ &= \frac{s^3}{\pi}\int_{4m_\pi^2}^{\infty}\mathrm{d}s'\left[\frac{\mathrm{Im}\,f_0^{(ii')}(s')}{s'^3(s'-s)} + 3\frac{\mathrm{Im}\,f_1^{(ii')}(s')}{s'^3(s'-4m_\pi^2)} + 3(t-u)\frac{\mathrm{Im}\,f_1^{(ii')}(s')}{s'^3(s'-s)(s'-4m_\pi^2)}\right. \\ &\qquad + \frac{15}{2}\frac{(s'-s)\,\mathrm{Im}\,f_2^{(ii')}(s')}{s'^3(s'-4m_\pi^2)^2} + 15(t-u)\frac{\mathrm{Im}\,f_2^{(ii')}(s')}{s'^3(s'-4m_\pi^2)^2} \\ &\qquad \left. + \frac{15}{2}(t-u)^2\frac{\mathrm{Im}\,f_2^{(ii')}(s')}{s'^3(s'-s)(s'-4m_\pi^2)^2} - \frac{5}{2}\frac{\mathrm{Im}\,f_2^{(ii')}(s')}{s'^3(s'-s)}\right].\end{aligned} \tag{6.74}$$

The second, fourth and fifth term in the square bracket have no non-trivial dependence on the Mandelstam variables in the integral and can thus be absorbed into a polynomial. We can therefore write

$$\begin{aligned}\frac{s^3}{\pi}\int_{4m_\pi^2}^{\infty}\mathrm{d}s'\frac{\mathrm{Im}_s\,\mathcal{M}^{(ii')}(s',t)}{s'^3(s'-s)} &= \frac{s^3}{\pi}\int_{4m_\pi^2}^{\infty}\mathrm{d}s'\left[\frac{\mathrm{Im}\,f_0^{(ii')}(s')}{s'^3(s'-s)} + 3(t-u)\frac{\mathrm{Im}\,f_1^{(ii')}(s')}{s'^3(s'-s)(s'-4m_\pi^2)}\right. \\ &\qquad \left. + \frac{15}{2}(t-u)^2\frac{\mathrm{Im}\,f_2^{(ii')}(s')}{s'^3(s'-s)(s'-4m_\pi^2)^2} - \frac{5}{2}\frac{\mathrm{Im}\,f_2^{(ii')}(s')}{s'^3(s'-s)}\right] \\ &+ A_s^{(ii')}s^3 + B_s^{(ii')}s^4 + C_s^{(ii')}s^3(t-u)\,.\end{aligned} \tag{6.75}$$

We note that in contrast to the t-dependent subtraction constants in the dispersion relation, A_i^s, B_i^s and C_i^s are pure numbers. A similar calculation can be performed for the u-channel integral and putting everything together we arrive at

$$\begin{aligned}\mathcal{M}^{(ii')}(s,t) &= a^{(ii')}(t) + b^{(ii')}(t)s + c^{(ii')}(t)s^2 + A_s^{(ii')}s^3 + B_s^{(ii')}s^4 + C_s^{(ii')}s^3(t-u) \\ &+ A_u^{(ii')}u^3 + B_u^{(ii')}u^4 + C_u^{(ii')}u^3(s-u) \\ &+ \frac{s^3}{\pi}\int_{4m_\pi^2}^{\infty}\mathrm{d}s'\left[\frac{\mathrm{Im}\,f_0^{(ii')}(s')}{s'^3(s'-s)} + 3(t-u)\frac{\mathrm{Im}\,f_1^{(ii')}(s')}{s'^3(s'-s)(s'-4m_\pi^2)}\right. \\ &\qquad \left. + \frac{15}{2}(t-u)^2\frac{\mathrm{Im}\,f_2^{(ii')}(s')}{s'^3(s'-s)(s'-4m_\pi^2)^2} - \frac{5}{2}\frac{\mathrm{Im}\,f_2^{(ii')}(s')}{s'^3(s'-s)}\right]\end{aligned}$$

$$+\frac{u^3}{\pi}\int_{4m_\pi^2}^{\infty}\mathrm{d}u'\left[\frac{\mathrm{Im}\,h_0^{(ii')}(u')}{u'^3(u'-u)}+3(s-t)\frac{\mathrm{Im}\,h_1^{(ii')}(u')}{u'^3(u'-u)(u'-4m_\pi^2)}\right.$$
$$\left.+\frac{15}{2}(s-t)^2\frac{\mathrm{Im}\,h_2^{(ii')}(u')}{u'^3(u'-u)(u'-4m_\pi^2)^2}-\frac{5}{2}\frac{\mathrm{Im}\,f_2^{(ii')}(u')}{u'^3(u'-u)}\right] \quad (6.76)$$

This result is not manifestly crossing symmetric under $t \leftrightarrow u$. In order to symmetrize it, we derive also fixed-u dispersion relations. The u-channel integrals appearing in the fixed-t dispersion relation must be part of the u-dependent subtraction constants in the fixed-u dispersion relation and vice versa. This would not be possible if we had started with fewer subtractions. Writing both these integrals explicitly gives a fully crossing-symmetric relation and the remaining parts from the subtraction constants must be polynomials

$$\mathcal{M}^{(ii')}(s,t)=P_4^{(ii')}(s,t-u)$$
$$+\frac{s^3}{\pi}\int_{4m_\pi^2}^{\infty}\mathrm{d}s'\left[\frac{\mathrm{Im}\,f_0^{(ii')}(s')}{s'^3(s'-s)}+3(t-u)\frac{\mathrm{Im}\,f_1^{(ii')}(s')}{s'^3(s'-s)(s'-4m_\pi^2)}\right.$$
$$\left.+\frac{15}{2}(t-u)^2\frac{\mathrm{Im}\,f_2^{(ii')}(s')}{s'^3(s'-s)(s'-4m_\pi^2)^2}-\frac{5}{2}\frac{\mathrm{Im}\,f_2^{(ii')}(s')}{s'^3(s'-s)}\right]$$
$$+\frac{t^3}{\pi}\int_{4m_\pi^2}^{\infty}\mathrm{d}t'\left[\frac{\mathrm{Im}\,g_0^{(ii')}(t')}{t'^3(t'-t)}+3(s-u)\frac{\mathrm{Im}\,g_1^{(ii')}(t')}{t'^3(t'-t)(t'-4m_\pi^2)}\right.$$
$$\left.+\frac{15}{2}(s-u)^2\frac{\mathrm{Im}\,g_2^{(ii')}(t')}{t'^3(t'-t)(t'-4m_\pi^2)^2}-\frac{5}{2}\frac{\mathrm{Im}\,g_2^{(ii')}(t')}{t'^3(t'-t)}\right]$$
$$+\frac{u^3}{\pi}\int_{4m_\pi^2}^{\infty}\mathrm{d}u'\left[\frac{\mathrm{Im}\,h_0^{(ii')}(u')}{u'^3(u'-u)}+3(s-t)\frac{\mathrm{Im}\,h_1^{(ii')}(u')}{u'^3(u'-u)(u'-4m_\pi^2)}\right.$$
$$\left.+\frac{15}{2}(s-t)^2\frac{\mathrm{Im}\,h_2^{(ii')}(u')}{u'^3(u'-u)(u'-4m_\pi^2)^2}-\frac{5}{2}\frac{\mathrm{Im}\,f_2^{(ii')}(u')}{u'^3(u'-u)}\right], \quad (6.77)$$

where $P_i^4(s,t-u)$ is an undetermined polynomial of order 4 in both arguments.

So far, we did not make use of the symmetry properties of $\mathcal{M}^{(ii')}$ and these can be used to simplify the result. First, the most general polynomials either symmetric or antisymmetric under exchange of t and u are

$$P_4^{(1i')}(s,t-u)=\bar{\alpha}^{(1i')}+\bar{\beta}^{(1i')}s+\bar{\gamma}^{(1i')}s^2+\bar{\delta}^{(1i')}(t-u)^2+\bar{\epsilon}^{(1i')}s^3$$
$$+\bar{\zeta}^{(1i')}s(t-u)^2+\bar{\eta}^{(1i')}s^4+\bar{\theta}^{(1i')}s^2(t-u)^2+\bar{\iota}^{(1i')}(t-u)^4\,,$$
$$P_4^{(ii')}(s,t-u)=\bar{\alpha}^{(ii')}(t-u)+\bar{\beta}^{(ii')}s(t-u)+\bar{\gamma}^{(ii')}s^2(t-u)$$
$$+\bar{\delta}^{(ii')}(t-u)^3+\bar{\epsilon}^{(ii')}s^3(t-u)+\bar{\zeta}^{(ii')}s(t-u)^3 \quad \text{for } i\neq 1\,, \quad (6.78)$$

respectively. Second, the s-channel partial wave $f_1^{(ii')}$ vanishes for the even scalar functions and $f_0^{(ii')}$ and $f_2^{(ii')}$ for the odd ones. Thus, the corresponding integrals can be dropped. Finally, the t- and u-channel partial waves are related through

$$h^i_j(t) = \pm g^i_j(t) \tag{6.79}$$

with $+$ for $i = 1$ and $-$ else.

Using all these results, we arrive at the reconstruction theorems

$$\begin{aligned}
\mathcal{M}^{(10)} &= F_0^{(10)}(s) + \frac{15}{2}(t-u)^2 F_2^{(10)}(s) + G_0^{(10)}(t) + G_0^{(10)}(u) + 3(s-u)G_1^{(10)}(t) \\
&\quad + 3(s-t)G_1^{(10)}(u) + \frac{15}{2}(s-u)^2 G_2^{(10)}(t) + \frac{15}{2}(s-t)^2 G_2^{(10)}(u)\,, \\
\mathcal{M}^{(01)} &= 3(t-u)F_1^{(01)}(s) + G_0^{(01)}(t) - G_0^{(01)}(u) + 3(s-u)G_1^{(01)}(t) - 3(s-t)G_1^{(01)}(u) \\
&\quad + \frac{15}{2}(s-u)^2 G_2^{(01)}(t) - \frac{15}{2}(s-t)^2 G_2^{(01)}(u)\,, \\
\mathcal{M}^{(12)} &= F_0^{(12)}(s) + \frac{15}{2}(t-u)^2 F_2^{(12)}(s) + G_0^{(12)}(t) + G_0^{(12)}(u) + 3(s-u)G_1^{(12)}(t) \\
&\quad + 3(s-t)G_1^{(12)}(u) + \frac{15}{2}(s-u)^2 G_2^{(12)}(t) + \frac{15}{2}(s-t)^2 G_2^{(12)}(u)\,, \\
\mathcal{M}^{(21)} &= 3(t-u)F_1^{(21)}(s) + G_0^{(21)}(t) - G_0^{(21)}(u) + 3(s-u)G_1^{(21)}(t) - 3(s-t)G_1^{(21)}(u) \\
&\quad + \frac{15}{2}(s-u)^2 G_2^{(21)}(t) - \frac{15}{2}(s-t)^2 G_2^{(21)}(u)\,, \\
\mathcal{M}^{(11)} &= F_0^{(11)}(s) + \frac{15}{2}(t-u)^2 F_2^{(11)}(s) + G_0^{(11)}(t) + G_0^{(11)}(u) + 3(s-u)G_1^{(11)}(t) \\
&\quad + 3(s-t)G_1^{(11)}(u) + \frac{15}{2}(s-u)^2 G_2^{(11)}(t) + \frac{15}{2}(s-t)^2 G_2^{(11)}(u)\,, \\
\mathcal{M}^{(22)} &= 3(t-u)F_1^{(22)}(s) + G_0^{(22)}(t) - G_0^{(22)}(u) + 3(s-u)G_1^{(22)}(t) - 3(s-t)G_1^{(22)}(u) \\
&\quad + \frac{15}{2}(s-u)^2 G_2^{(22)}(t) - \frac{15}{2}(s-t)^2 G_2^{(22)}(u)
\end{aligned} \tag{6.80}$$

with

$$\begin{aligned}
F_0^{(ii')}(s) &= P^4_{F_0^{(ii')}}(s) + \frac{s^3}{\pi}\int_{4m_\pi^2}^{\infty} \mathrm{d}s' \frac{\operatorname{Im} f_0^{(ii')}(s') - \frac{5}{2}\operatorname{Im} f_2^{(ii')}(s')}{s'^3(s'-s)}\,, \\
F_1^{(ii')}(s) &= P^3_{F_1^{(ii')}}(s) + \frac{s^3}{\pi}\int_{4m_\pi^2}^{\infty} \mathrm{d}s' \frac{\operatorname{Im} f_1^{(ii')}(s')}{s'^3(s'-s)(s'-4m_\pi^2)}\,, \\
F_2^{(ii')}(s) &= P^2_{F_2^{(ii')}}(s) + \frac{s^3}{\pi}\int_{4m_\pi^2}^{\infty} \mathrm{d}s' \frac{\operatorname{Im} f_2^{(ii')}(s')}{s'^3(s'-s)(s'-4m_\pi^2)^2}\,, \\
G_0^{(ii')}(s) &= P^4_{G_0^{(ii')}}(s) + \frac{s^3}{\pi}\int_{4m_\pi^2}^{\infty} \mathrm{d}s' \frac{\operatorname{Im} g_0^{(ii')}(s') - \frac{5}{2}\operatorname{Im} g_2^{(ii')}(s')}{s'^3(s'-s)}\,, \\
G_1^{(ii')}(s) &= P^3_{G_1^{(ii')}}(s) + \frac{s^3}{\pi}\int_{4m_\pi^2}^{\infty} \mathrm{d}s' \frac{\operatorname{Im} g_1^{(ii')}(s')}{s'^3(s'-s)(s'-4m_\pi^2)}\,, \\
G_2^{(ii')}(s) &= P^2_{G_2^{(ii')}}(s) + \frac{s^3}{\pi}\int_{4m_\pi^2}^{\infty} \mathrm{d}s' \frac{\operatorname{Im} g_2^{(ii')}(s')}{s'^3(s'-s)(s'-4m_\pi^2)^2}\,.
\end{aligned} \tag{6.81}$$

Here, $P^l_A(s)$ denotes the polynomial corresponding to the function A. The order of the polynomial l is determined by the order of the polynomial in the symmetrized dispersion relation $P_4^{(ii')}$ taking into account the pre-factors in the reconstruction theorem. It is easy to check that the parameters in $P_4^{(ii')}$ can indeed be expressed in terms of the parameters in the polynomials $P^l_A(s)$.

The functions $G_j^{(ii')}$ can be expressed in terms of $F_j^{(ii')}$ by using Eq. (6.36). The results are given in App. B.1.

6.7.2 Imaginary parts of the single-variable functions

In order to obtain the imaginary parts of the single-variable functions, we plug the reconstruction theorems into the unitarity relations Eqs. (6.54) and (6.55). The phase-space integrals involving the s-channel single-variable functions can be performed straightforwardly and for the ones involving the t- and u-channel functions we define the angular averages

$$\langle z^p F_j^{(ii')}\rangle := \frac{1}{2}\int_{-1}^{1} dz z^p F_j^{(ii')}\left(-\frac{1}{2}(s-4m_\pi^2)(1-z)\right) . \tag{6.82}$$

We note that in this integral the single-variable function is evaluated on the real axis below the cut so that the angular averages are real. Finally, we project the results onto partial waves and calculate the imaginary parts of the single-variable functions according to Eq. (6.81).

The results receive three contributions

$$\operatorname{Im} F_j^{(ii')}(s) = \operatorname{Im}^{\text{hom}} F_j^{(ii')}(s) + \operatorname{Im}^{\text{av}} F_j^{(ii')}(s) + \operatorname{Im}^{\text{sing}} F_j^{(ii')}(s) \tag{6.83}$$

containing terms linear in the functions $F_j^{(ii')}(s)$, terms linear in angular averages of the functions $F_j^{(ii')}$ and terms from the inhomogeneous contributions in Eq. (6.62), respectively. The homogeneous contributions read

$$\begin{aligned}
\operatorname{Im}^{\text{hom}} F_0^{(10)} &= \frac{\sigma_\pi(s)}{64\pi}\Big(2s\sigma_\pi^2(s)F_1^{(01)}(s)(t_2^0(s)^* - t_0^0(s)^*) + 2F_0^{(10)}(s)t_0^0(s)^* + 2F_0^{(10)}(s)^* t_1^1(s) \\
&\qquad + s^2\sigma_\pi^4(s)(5F_2^{(10)}(s)(t_0^0(s)^* - t_2^0(s)^*) + 3F_2^{(10)}(s)^* t_1^1(s))\Big) , \\
\operatorname{Im}^{\text{hom}} F_2^{(10)} &= \frac{\sigma_\pi(s)}{32\pi} F_2^{(10)}(s)t_2^0(s)^* , \\
\operatorname{Im}^{\text{hom}} F_1^{(01)} &= \frac{\sigma_\pi(s)}{32\pi}\Big(t_1^1(s)^*\left(F_1^{(01)}(s) - s\sigma_\pi(s)^2 F_2^{(10)}(s)\right) + F_1^{(01)}(s)^* t_2^0(s)\Big) , \\
\operatorname{Im}^{\text{hom}} F_0^{(12)} &= \frac{\sigma_\pi(s)}{64\pi}\Big(2s\sigma_\pi^2(s)F_1^{(21)}(s)(t_2^2(s)^* - t_0^2(s)^*) + 2F_0^{(12)}(s)t_0^2(s)^* + 2F_0^{(12)}(s)^* t_1^1(s) \\
&\qquad + s^2\sigma_\pi^4(s)(5F_2^{(12)}(s)(t_0^2(s)^* - t_2^2(s)^*) + 3F_2^{(12)}(s)^* t_1^1(s))\Big) , \\
\operatorname{Im}^{\text{hom}} F_2^{(12)} &= \frac{\sigma_\pi(s)}{32\pi} F_2^{(12)}(s)t_2^2(s)^* , \\
\operatorname{Im}^{\text{hom}} F_1^{(21)} &= \frac{\sigma_\pi(s)}{32\pi}\Big(t_1^1(s)^*\left(F_1^{(21)}(s) - s\sigma_\pi(s)^2 F_2^{(12)}(s)\right) + F_1^{(21)}(s)^* t_2^2(s)\Big) ,
\end{aligned}$$

$$\begin{aligned}
\mathrm{Im}^{\mathrm{hom}}\, F_0^{(11)} &= \frac{\sigma_\pi(s)}{32\pi}\Big(F_0^{(11)}(s) t_1^1(s)^* + F_0^{(11)}(s)^* t_1^1(s)\Big)\,,\\
\mathrm{Im}^{\mathrm{hom}}\, F_2^{(11)} &= 0\,,\\
\mathrm{Im}^{\mathrm{hom}}\, F_1^{(22)} &= \frac{\sigma_\pi(s)}{32\pi}\Big(F_1^{(22)}(s) t_2^2(s)^* + F_1^{(22)}(s)^* t_2^2(s)\Big)
\end{aligned} \tag{6.84}$$

and the contributions from the singular pieces follow directly from Eq. (6.62). The results for $\mathrm{Im}^{\mathrm{av}}\, F_j^{(ii')}(s)$ are lengthy and therefore not displayed here. For the function $F_2^{(11)}(s)$, all three contributions to the imaginary part vanish.

6.7.3 Omnès solution

We now derive an inhomogeneous Omnès solution, similarly to what has been done e.g. for $\eta \to 3\pi$ in Ref. [197]. The imaginary parts in Eq. (6.84) do not yet have the form of an Omnès problem since the right-hand sides involve complex conjugates of the single-variable functions. To get rid of these, we write

$$F_j^{(ii')}(s)^* = F_j^{(ii')}(s) - 2\,\mathrm{Im}\, F_j^{(ii')}(s) \tag{6.85}$$

and solve the resulting system for $\mathrm{Im}\, F_j^{(ii')}(s)$. Leaving aside $F_2^{(11)}(s)$ whose imaginary part vanishes and using matrix notation with

$$\vec{F}(s) = \Big(F_0^{(10)}(s), F_2^{(10)}(s), F_1^{(01)}(s), F_0^{(12)}(s), F_2^{(12)}(s), F_1^{(21)}(s), F_0^{(11)}(s), F_1^{(22)}(s)\Big)^T\,, \tag{6.86}$$

we can write

$$\mathrm{Im}\, \vec{F}(s) = H(s)\vec{F}(s) + \vec{A}(s) + \vec{I}(s) \tag{6.87}$$

with a matrix $H(s)$, a vector $\vec{I}(s)$ depending only on $\pi\pi$-scattering partial waves and a vector $\vec{A}(s)$ linear in angular averages of $F_j^{(ii')}(s)$ with prefactors depending on $\pi\pi$-scattering partial waves.

We can diagonalize the system by a matrix $M(s)$ given in App. B.2

$$\mathrm{Im}\, F_D^n(s) = e^{-i\delta_n(s)} \sin\delta_n(s)(F_D^n(s) + A_D^n(s) + I_D^n(s)) \tag{6.88}$$

with

$$\begin{aligned}
\vec{F}_D(s) &= M(s)\vec{F}(s)\,,\\
\vec{A}_D(s) &= \mathrm{diag}(e^{-i\delta_n(s)}\sin\delta_n(s))^{-1} M(s)\vec{A}(s)\,,\\
\vec{I}_D(s) &= \mathrm{diag}(e^{-i\delta_n(s)}\sin\delta_n(s))^{-1} M(s)\vec{I}(s)
\end{aligned} \tag{6.89}$$

and the phase shifts

$$\begin{aligned}
&\delta_1(s) = \delta_0^0(s) + \delta_1^1(s)\,, && \delta_2(s) = \delta_2^0(s)\,, && \delta_3(s) = 2\delta_1^1(s)\,,\\
&\delta_4(s) = \delta_2^0(s) + \delta_1^1(s)\,, && \delta_5(s) = \delta_0^2(s) + \delta_1^1(s)\,, && \delta_6(s) = \delta_2^2(s)\,,\\
&\delta_7(s) = 2\delta_2^2(s)\,, && \delta_8(s) = \delta_2^2(s) + \delta_1^1(s)\,.
\end{aligned} \tag{6.90}$$

As required for an inhomogeneous Omnès problem, these phase shifts $\delta_n(s)$ are real, the expressions for $A_D^n(s)$ are real and independent of $\pi\pi$-scattering phase shifts and the inhomogeneous pieces $I_D^n(s)$ are real as can be seen from the explicit expressions in App. B.2. This provides a strong consistency check on our calculation.

The solution of these equations for fixed angular averages is given by (see e.g. Ref. [197])

$$F_D^n(s) = \Omega_n(s)\left[\tilde{P}_n(s) + \frac{s^{p_n}}{\pi}\int \frac{\mathrm{d}s'}{s'^{p_n}}\frac{\sin\delta_n(s')(A_D^n(s') + I_D^n(s'))}{|\Omega_n(s')|(s'-s-i\epsilon)}\right] \tag{6.91}$$

with the Omnès functions

$$\Omega_n(s) = \exp\left[\frac{s}{\pi}\int_{4m_\pi^2}^{\infty}\frac{\mathrm{d}s'}{s'}\frac{\delta_n(s')}{s'-s-i\epsilon}\right]. \tag{6.92}$$

The subtraction polynomials $\tilde{P}_n(s)$ are the subject of the following section.

The function $F_2^{(11)}(s) =: F_D^9(s)$ is just given by a polynomial

$$F_D^9(s) = \tilde{P}_9(s)\,. \tag{6.93}$$

6.7.4 Subtraction polynomials and ambiguities

6.7.4.1 General case

We have the freedom to shift polynomial contributions between the single-variable functions in such a way that the physical functions $\mathcal{M}^{(ii')}$ are unchanged. To quantify this freedom, we consider again the polynomial in Eq. (6.77). The 6 polynomials corresponding to the 6 isospin amplitudes have in total 45 free parameters since there are 3 symmetric and 3 antisymmetric amplitudes. Imposing the crossing relations Eq. (6.36) on them reduces the number of independent parameters to 15. We then demand that these polynomials agree with the reconstruction theorem, where we plug in polynomials with arbitrary parameters for F_D^n. This leaves 27 parameters undetermined, i.e. there is a 27-parameter family of polynomials that we can add to the single-variable functions without changing physical observables.

Next, we repeat this with additional constraints on the polynomials at $s \to \infty$ and $s = 0$. A set of constraints that has a unique solution for all parameters is given by

$$\begin{aligned}
&F_D^1(s) = \mathcal{O}(s^4)\,, && F_D^2(s) = \mathcal{O}(s^2)\,, && F_D^3(s) = \mathcal{O}(s^4)\,,\\
&F_D^4(s) = \mathcal{O}(s^3)\,, && F_D^5(s) = \mathcal{O}(s^4)\,, && F_D^6(s) = \mathcal{O}(s^2)\,,\\
&F_D^7(s) = \mathcal{O}(s^3)\,, && F_D^8(s) = \mathcal{O}(s^3)\,, && F_D^9(s) = \mathcal{O}(s^2)
\end{aligned} \tag{6.94}$$

at $s \to \infty$ and

$$\begin{aligned}
&F_D^1(s) = \mathcal{O}(s^0)\,, && F_D^2(s) = \mathcal{O}(s^3)\,, && F_D^3(s) = \mathcal{O}(s)\,,\\
&F_D^4(s) = \mathcal{O}(s^3)\,, && F_D^5(s) = \mathcal{O}(s^2)\,, && F_D^6(s) = \mathcal{O}(s^3)\,,\\
&F_D^7(s) = \mathcal{O}(s^4)\,, && F_D^8(s) = \mathcal{O}(s^2)\,, && F_D^9(s) = \mathcal{O}(s^3)
\end{aligned} \tag{6.95}$$

at $s = 0$. We have chosen these constraints for the following reasons:

- We chose the asymptotic constraints in accordance with the asymptotic behavior in Eq. (6.81). In this way, we ensure that the ambiguities do not introduce terms growing faster at $s \to \infty$ that would have to cancel between different single-variable functions.
- If we neglect D-wave $\pi\pi$-scattering partial waves, the dispersion integrals drop out of 4 single-variable functions. We imposed constraints at the origin such that those functions do neither receive contributions from the subtraction polynomials.
- We imposed as many constraints as possible on the origin of the single-variable functions that receive no S-wave contribution. In this way, we obtain the simplest possible result in χPT. It is, however, not possible to fix all ambiguities without also constraining the ones that do receive an S-wave contribution.

The chosen constraints lead to

$$F_D^9(s) = F_2^{(11)}(s) = 0\,. \tag{6.96}$$

For $\lim_{s\to\infty} \delta_n(s) = a_n\pi$, the Omnès function behaves as $\Omega_n(s) = \mathcal{O}(s^{-a_n})$. In our numerical study we will use phase shifts with

$$\lim_{s\to\infty} \delta_0^0(s) = \pi\,, \quad \lim_{s\to\infty} \delta_0^2(s) = 0\,, \quad \lim_{s\to\infty} \delta_1^1(s) = \pi\,, \quad \lim_{s\to\infty} \delta_2^0(s) = \pi\,, \quad \lim_{s\to\infty} \delta_2^2(s) = 0\,. \tag{6.97}$$

This implies

$$\begin{aligned}
&\Omega_1(s) = \mathcal{O}(s^{-2})\,, && \Omega_2(s) = \mathcal{O}(s^{-1})\,, && \Omega_3(s) = \mathcal{O}(s^{-2})\,, && \Omega_4(s) = \mathcal{O}(s^{-2})\,, \\
&\Omega_5(s) = \mathcal{O}(s^{-1})\,, && \Omega_6(s) = \mathcal{O}(s^{0})\,, && \Omega_7(s) = \mathcal{O}(s^{0})\,, && \Omega_8(s) = \mathcal{O}(s^{-1})
\end{aligned} \tag{6.98}$$

for $s \to \infty$. The most general polynomials obeying the constraints are thus

$$\begin{aligned}
\tilde{P}_1(s) &= A_1 + B_1 s + C_1 s^2 + D_1 s^3 + E_1 s^4 + F_1 s^5 + G_1 s^6\,, \\
\tilde{P}_2(s) &= A_2 s^3\,, \\
\tilde{P}_3(s) &= A_3 s + B_3 s^2 + C_3 s^3 + D_3 s^4 + E_3 s^5 + F_3 s^6\,, \\
\tilde{P}_4(s) &= A_4 s^3 + B_4 s^4 + C_4 s^5\,, \\
\tilde{P}_5(s) &= A_5 s^2 + B_5 s^3 + C_5 s^4 + D_5 s^5\,, \\
\tilde{P}_6(s) &= 0\,, \\
\tilde{P}_7(s) &= 0\,, \\
\tilde{P}_8(s) &= A_8 s^2 + B_8 s^3 + C_8 s^4\,.
\end{aligned} \tag{6.99}$$

According to the argument in Ref. [197], fixing the enlarged set of 24 subtraction constants in these polynomials is expected to ensure that the integral equations in Eq. (6.91) have a unique solution.

The dispersion integral in Eq. (6.91) behaves as s^{p_n-1} for $s \to \infty$ and as s^{p_n} for $s \to 0$. Thus, in order for the integrals not to mess up the imposed constraints, we have to choose suitable values for the p_n. We choose the values such that the asymptotic behavior of the dispersion integral matches that of the highest term in the subtraction polynomial[2]

$$p_1 = 7\,, \quad p_2 = 4\,, \quad p_3 = 7\,, \quad p_4 = 6\,, \quad p_5 = 6\,, \quad p_6 = 3\,, \quad p_7 = 4\,, \quad p_8 = 5\,. \tag{6.100}$$

The system with 24 independent subtraction constants is clearly unsuited for a numerical study since there are no experimental data for $\pi\pi \to \gamma\pi\pi$ in the right kinematic limit available to constrain these. Also, the χPT one-loop representation is not sufficient to reliably constrain such a large number of parameters. We will thus next discuss additional constraints on the asymptotic behavior of the single-variable functions. This corresponds to the single-variable functions fulfilling a set of sum rules, which allows us to reduce the number of subtraction constants.

6.7.4.2 Imposing additional constraints on the asymptotic behavior of the single-variable functions

Assuming a uniform scaling, the form of the reconstruction theorems allow the most restrictive assumption to be that the $\mathcal{M}^{(ii')}$ grow quadratically in the Mandelstam variables and we have checked that the integral equations remain consistent with this constraint. However, if we allow for a non-uniform scaling, we can put much stronger constraints on the asymptotic behavior of the single-variable functions.

In order to determine the most restrictive scaling that still leads to consistent integral equations, we first calculate the asymptotic behavior of the inhomogeneous contributions to the dispersion integrals. Assuming that the phase shifts approach their asymptotic values as $1/s$, we obtain that $\sin\delta_n I_D^n/|\Omega_n|$ behaves as s^{i_n} with $i_1 = i_3 = -2$ and $i_4 = i_5 = -3$, whereas for the other n there is no inhomogeneous contribution. This means that the dispersion integrals would converge even without any subtractions if A_D^n vanished.

We then assume that F_D^n behaves asymptotically in the same way as the Omnès function divided by s. Plugging this into A_D^n, $\sin\delta_n A_D^n/|\Omega_n|$ behaves as s^{i_n} with $i_1 = i_3 = 2$, $i_4 = i_5 = 1$ and $i_8 = 0$ whereas the remaining i_n are negative. This implies that we have to introduce 11 subtractions in total to make all integrals converge. With this new asymptotic behavior of the F_D^n, we recalculate the asymptotic behavior of the angular averages and obtain that with the same number of subtractions the integrals still converge. The asymptotic behavior we finally

[2]As explained in Ref. [197], the solution is independent of the chosen values of p_n since the difference between different choices can be absorbed in the subtraction constants.

obtain from this is

$$
\begin{aligned}
&F_D^1(s) = \mathcal{O}(s^0)\,, && F_D^2(s) = \mathcal{O}(s^{-2})\,, && F_D^3(s) = \mathcal{O}(s^0)\,, \\
&F_D^4(s) = \mathcal{O}(s^{-1})\,, && F_D^5(s) = \mathcal{O}(s^0)\,, && F_D^6(s) = \mathcal{O}(s^{-1})\,, \\
&F_D^7(s) = \mathcal{O}(s^{-1})\,, && F_D^8(s) = \mathcal{O}(s^{-1})\,, && F_D^9(s) = \mathcal{O}(s^{-1})
\end{aligned}
\tag{6.101}
$$

and

$$
p_1 = 3\,, \quad p_2 = 0\,, \quad p_3 = 3\,, \quad p_4 = 2\,, \quad p_5 = 2\,, \quad p_6 = 0\,, \quad p_7 = 0\,, \quad p_8 = 1\,. \tag{6.102}
$$

With this asymptotic behavior, there is a reduced set of shifts $F_D^n(s) \to F_D^n(s) + \Delta F_D^n(s)$ that leave the physical amplitudes $\mathcal{M}^{(ii')}$ invariant

$$
\Delta F_D^1(s) = a_1\,, \qquad \Delta F_D^3(s) = a_3\,, \qquad \Delta F_D^5(s) = \frac{1}{10}(3a_1 - 12a_3) \tag{6.103}
$$

and $\Delta F_D^n(s) = 0$ for $n \notin \{1, 3, 5\}$. We can thus remove two further subtraction constants by imposing the constraints

$$
\begin{aligned}
&F_D^1(s) = \mathcal{O}(s^1)\,, && F_D^2(s) = \mathcal{O}(s^0)\,, && F_D^3(s) = \mathcal{O}(s^1)\,, \\
&F_D^4(s) = \mathcal{O}(s^0)\,, && F_D^5(s) = \mathcal{O}(s^0)\,, && F_D^6(s) = \mathcal{O}(s^0)\,, \\
&F_D^7(s) = \mathcal{O}(s^0)\,, && F_D^8(s) = \mathcal{O}(s^0)\,, && F_D^9(s) = \mathcal{O}(s^0)
\end{aligned}
\tag{6.104}
$$

at $s = 0$. The subtraction polynomials then become

$$
\begin{aligned}
&\tilde{P}_1(s) = A_1 s + B_1 s^2\,, && \tilde{P}_2(s) = 0\,, && \tilde{P}_3(s) = A_3 s + B_3 s^2\,, \\
&\tilde{P}_4(s) = A_4 + B_4 s\,, && \tilde{P}_5(s) = A_5 + B_5 s\,, && \tilde{P}_6(s) = 0\,, \\
&\tilde{P}_7(s) = 0\,, && \tilde{P}_8(s) = A_8\,, && \tilde{P}_9(s) = 0\,.
\end{aligned}
\tag{6.105}
$$

with 9 independent subtraction constants. We will use this set of polynomials and p_i for the numerical study in the next section.

One could even further restrict the asymptotic behavior by assuming that the dispersion integrals behave as the imaginary parts in the integrands, i.e. that they can decay faster than $1/s$ if the integrand allows it. Since, however, a set of sum rules would be needed to ensure that, which would make the numerical implementation more difficult, we refrain here from following this approach.

6.8 Numerical solution

Here, we solve the integral equations (6.91) numerically. If both the polynomials $\tilde{P}_n$ and the inhomogeneous contributions I_D^n were absent, then the solution would be given by all scalar functions vanishing. The polynomial is linear in each of the subtraction constant and if we

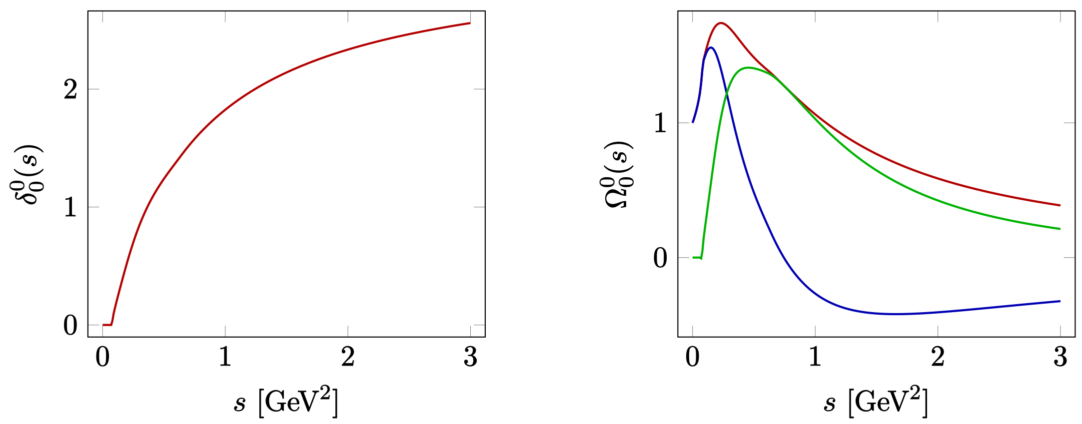

Figure 6.5: Left: $I = 0$ S-wave phase shift from Ref. [182] guided to π asymptotically, right: Omnès function obtained from this phase shift. Red corresponds to the absolute value, blue to the real part and green to the imaginary part.

introduce a parameter i in front of I_D^n in Eq. (6.91), then the system is also linear in this parameter. We can thus calculate a set of basis functions given by the solution if one of the parameters is set to 1 and all others to 0. The full solution is then given by

$$F_D^n(s) = B_I^n(s) + \sum_{p \in P} p B_p^n(s)\,, \tag{6.106}$$

where P is the set of parameters of the polynomials and B_p^n is the basis function for $p = 1$ and all other parameters vanishing.

We will now explain how we calculate the basis functions before discussing how the subtraction constants can be fixed.

6.8.1 Calculation of the basis functions

For each basis function, we solve the system of integral equations by an iterative procedure. Initially, we set the angular averages contained in A_D^n to zero. We calculate the single-variable functions F_D^n in the space-like regime and from this we obtain an updated evaluation of the angular averages in the time-like domain. We repeat these steps until convergence is observed.

For the S- and P-wave phase shifts, we use the results of Ref. [182] based on Roy equations [183]. We guide the $I = 0$ S-wave to the asymptotic value π by using the function

$$\delta_{\text{asymp}} = \pi + \frac{a}{s+b} \tag{6.107}$$

above $s = (0.8\,\text{GeV})^2$ with the parameters a and b chosen such that the function and its first derivative are continuous at the matching point. The low matching point is chosen in order to cut off the effect of the $f_0(980)$ resonance and the closely related effect of the $K\bar{K}$ threshold.

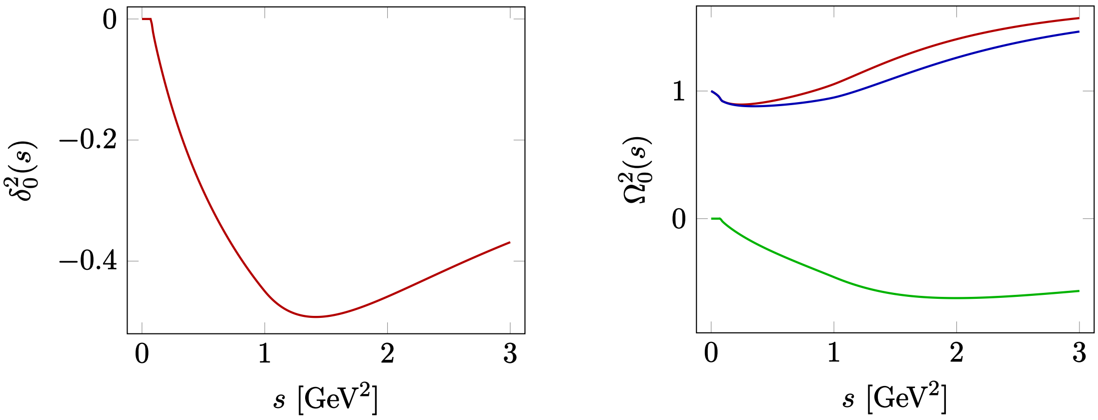

Figure 6.6: Left: $I = 2$ S-wave phase shift from Ref. [182] guided to 0 asymptotically, right: Omnès function obtained from this phase shift. Red corresponds to the absolute value, blue to the real part and green to the imaginary part.

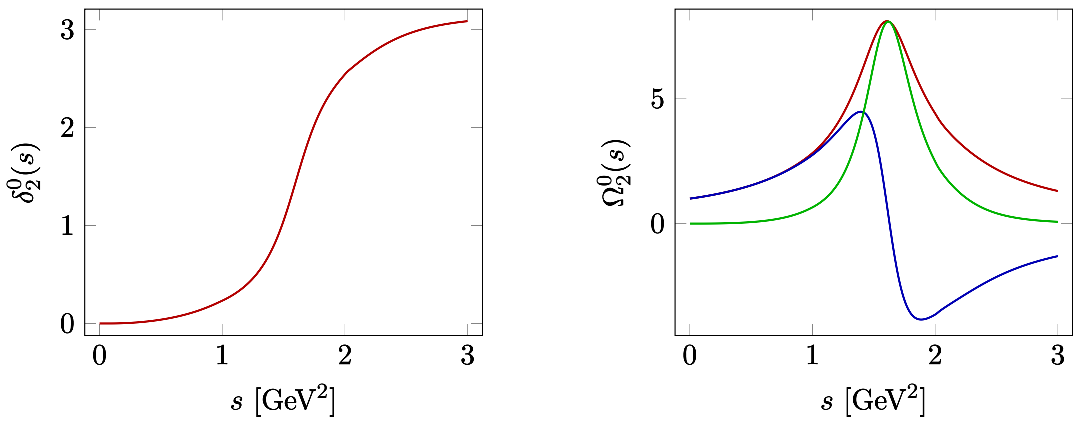

Figure 6.7: Left: $I = 0$ D-wave phase shift from Ref. [182] guided to π asymptotically, right: Omnès function obtained from this phase shift. Red corresponds to the absolute value, blue to the real part and green to the imaginary part.

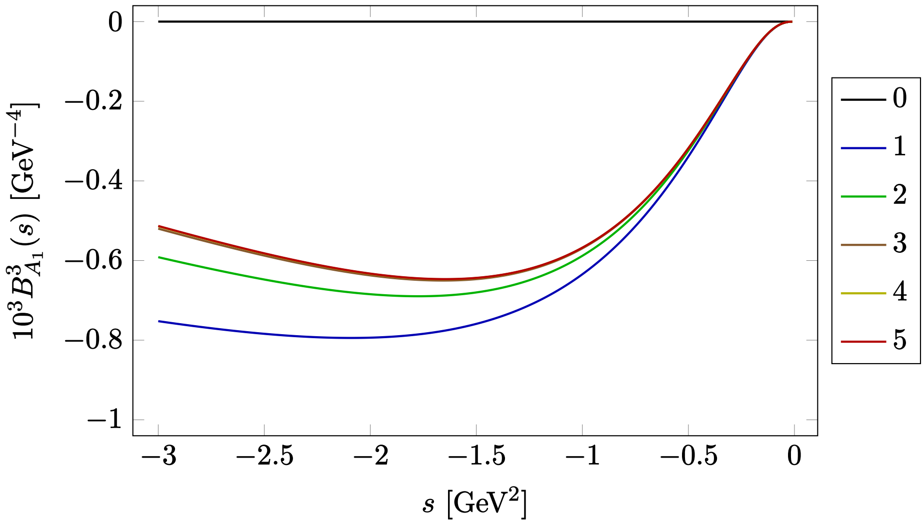

Figure 6.8: Results for the basis function $B^3_{A_1}(s)$ after successive iterations at space-like s. 0 denotes the starting value and the result after four iterations is hidden behind the final one after 5 iterations.

The $I = 1$ P-wave is matched to the same asymptotic function, but this time at $s = (1\,\text{GeV})^2$, which has also been used in Ch. 4. For the exotic $I = 2$ S-wave, we match to

$$\delta'_{\text{asymp}} = \frac{a + bs}{s^2 + (1\,\text{GeV})^4} \tag{6.108}$$

to avoid poles in the asymptotic function. The matching is again performed at $s = (1\,\text{GeV})^2$. Finally, for the $I = 0$ D-wave, we use the phase shift from Ref. [198], which already approaches π. Plots of the S- and D-wave phase shifts and the corresponding Omnès functions are provided in Figs. 6.5, 6.6 and 6.7. The analogous ones for the P-wave can be found in Fig. 4.6.

An example of the convergence behavior is shown in Fig. 6.8. We see there that only very few iterations are required to obtain a stable result. This pattern is observed also for the other single-variable functions and the other basis solutions, most of which converge even faster. For our final results, we thus use the functions obtained after five iterations. As an example, the functions $B^4_{A_1}$ in the region above threshold can be found in Fig. 6.9. Since the phase δ_4 receives contributions from both the $I = 1$ P-wave and the $I = 0$ D-wave, the ρ- and f_2-resonances can both be seen as peaks in the absolute value of this function. Above the peaks, it approaches zero due to the asymptotic constraint in Eq. (6.101).

6.8.2 Fixing the subtraction constants

Since we do not consider additional sum rules here, we have to fix all subtraction constants from low-energy input. In the absence of a measurement or a lattice QCD calculation that can be used here, we only have the χPT expressions at our disposal. Indeed, the result in

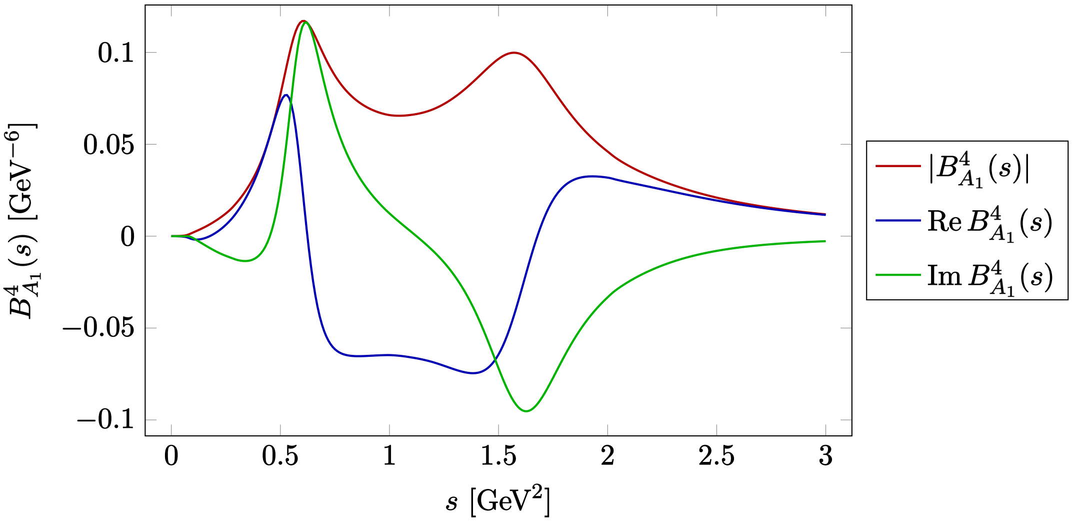

Figure 6.9: Result for the basis function $B^4_{A_1}(s)$ after convergence has been observed.

Eq. (6.66) can be reconstructed from Eq. (6.80) with the three non-vanishing single-variable functions

$$\begin{aligned}
F^1_D(s) &= \frac{2(s^2 - 14m_\pi^2 s - 2m_\pi^4)}{9F^4 s(s-4m_\pi^2)} \bar{J}_{\pi\pi}(s) + \frac{31s + 2m_\pi^2}{432\pi^2 F^4(s-4m_\pi^2)} \,, \\
F^3_D(s) &= -\frac{s-4m_\pi^2}{12F^4 s} \bar{J}_{\pi\pi}(s) - \frac{1}{288\pi^2 F^4} \,, \\
F^5_D(s) &= \frac{s^2 + 4m_\pi^2 s - 20m_\pi^4}{6F^4 s(s-4m_\pi^2)} \bar{J}_{\pi\pi}(s) - \frac{53s - 122m_\pi^2}{1440\pi^2 F^4(s-4m_\pi^2)} \,.
\end{aligned} \tag{6.109}$$

We have fixed the ambiguity by imposing Eqs. (6.101) and (6.104).

Of course, in a realistic study, one should not extract information on higher-order coefficients in the expansion around $s = 0$ from these expressions. Instead, sum rules could be assumed to reduce the number of subtraction constants, the χPT calculation could be extended to the two-loop level, models could be considered or eventually experimental or lattice QCD [190–192] input might become available. To demonstrate the approach, we nevertheless fix all subtraction constants from Eq. (6.109). There are different possibilities, which coefficients to use to fix the 9 subtraction constants. We choose to use the ones corresponding to the subtraction polynomials in Eq. (6.105), i.e. the linear and quadratic coefficients of F^1_D and F^3_D, the constant and linear coefficients of F^4_D and F^5_D as well as the constant coefficient from F^8_D. In order to obtain numerically stable results, we perform the s-expansion of the basis solutions before the dispersive integral in Eq. (6.91). The vanishing χPT results for F^4_D and F^8_D immediately lead to $A_4 = B_4 = A_8 = 0$ and for the remaining ones we obtain with $F = 93\,\text{MeV}$

$$\begin{aligned}
A_1 &= -(0.338\,\text{GeV})^{-6} \,, & B_1 &= -(0.346\,\text{GeV})^{-8} \,, & A_3 &= -(0.550\,\text{GeV})^{-6} \,, \\
B_3 &= -(0.878\,\text{GeV})^{-8} \,, & A_5 &= -(0.493\,\text{GeV})^{-4} \,, & B_5 &= (0.371\,\text{GeV})^{-6} \,.
\end{aligned} \tag{6.110}$$

The single-variable functions that we obtain from this are displayed in Fig. 6.10. We see that those functions that get a contribution from the phase δ_1^1 in Eq. (6.90), i.e. F_D^n with $n \in \{1,3,4,5,8\}$ exhibit a clear peak due to the ρ-resonance. Similarly, the effect of the tensor resonance $f_2(1270)$ can be seen in F_D^2 and F_D^4. A small effect of the $f_2(1270)$ is also visible in F_D^1, which is caused by the dependence of the inhomogeneity on the phase-shift δ_2^0. In F_D^1 and F_D^5, the $(s-4m_\pi^2)^{-1/2}$ behavior at threshold reveals itself through the divergence at low s.

It is likely that these results have large uncertainties due to missing higher orders in χPT, which would be needed to reliably extract the subtraction constants. In addition, the effect of uncertainties in the $\pi\pi$-scattering phase shifts, especially at high energies, should be studied.

6.9 Conclusions

In this chapter, we presented a dispersive formalism for the process $\pi\pi \to \gamma\pi\pi$ in the limit of a soft photon. This process is required as a nested sub-process for the inclusion of two-pion rescattering into the triangle-kinematics formalism to HLbL, see Ch. 5. After studying the constraints from Lorentz, crossing and isospin symmetry, we discussed the soft-photon limit, in which the amplitude diverges. Using the techniques introduced in Sec. 5.3, we defined a gauge-invariant splitting into a singular part given solely in terms of $\pi\pi$-scattering amplitudes and a regular part. We calculated the two-pion discontinuity of the regular part through unitarity relations. In this way, we also proved that additional singularities from radiation of the soft photon from internal pions cancel between the two cuts. This cancellation also has to happen in the case of two-pion intermediate states in HLbL, see Sec. 5.1.2, so that the calculation here can be seen as a proof of concept also for that case.

Then, we derived reconstruction theorems to obtain the real parts of the amplitudes from these discontinuities and discussed the role of ambiguities in them. We constructed an inhomogeneous Omnès solution and calculated the basis solutions through an iterative numerical algorithm. Finally, we provided a preliminary determination of the subtraction constants from χPT. Although further work is required to improve this last step, the results presented here show that it is possible to derive dispersion relations for five-particle processes with a soft photon and obtain numerical results. The techniques developed in this analysis will prove useful in a similar dispersive study of the other sub-process required for the inclusion of two-pion rescattering into the formalism introduced in Ch. 5, $\gamma^*\gamma^* \to \gamma\pi\pi$. Since $\pi\pi \to \gamma\pi\pi$ enters there as a sub-process, see Fig. 5.5, the results presented here opens the way to perform this study.

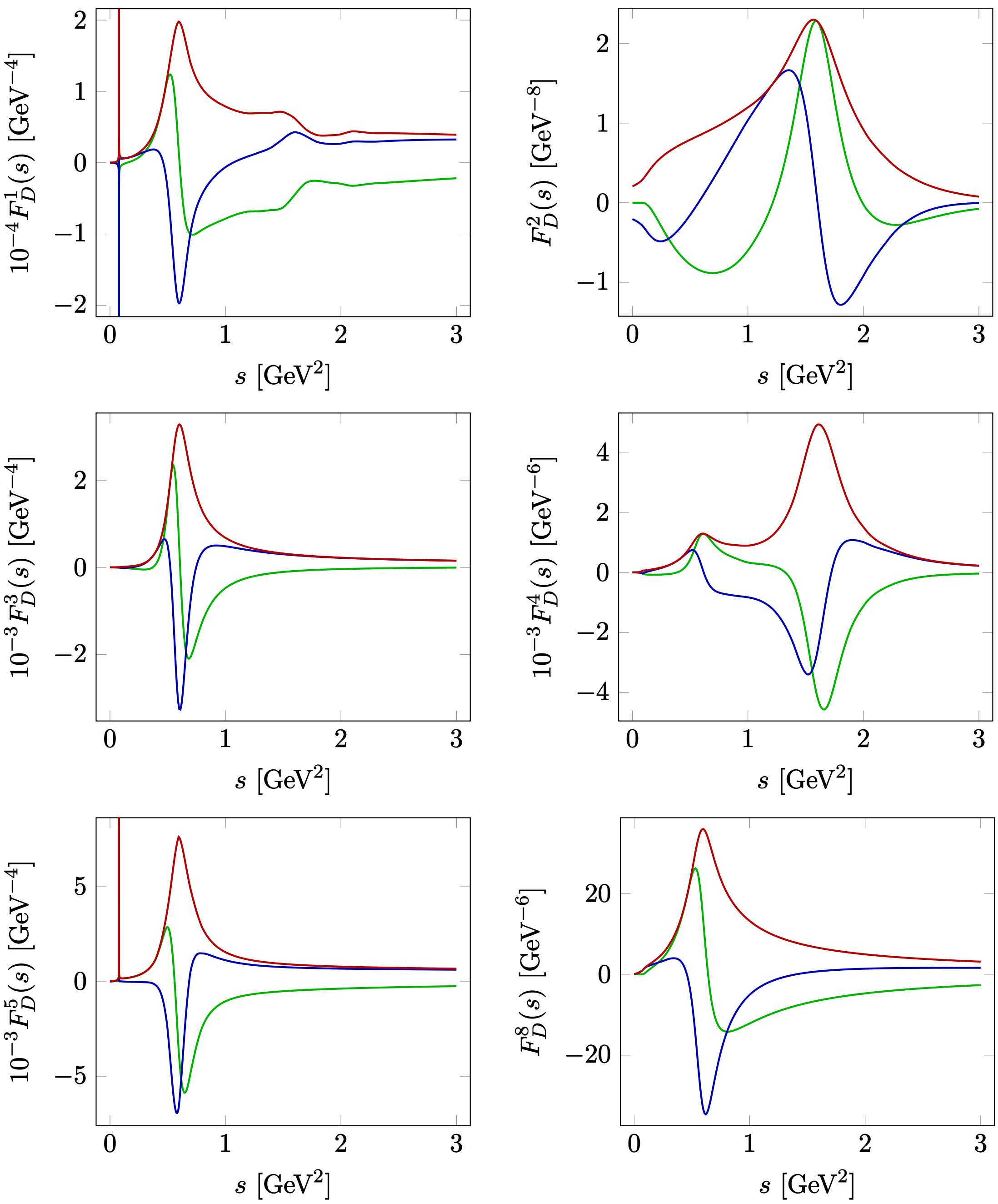

Figure 6.10: Final results for the non-vanishing single-variable functions in the diagonal basis. Red corresponds to the absolute value, blue to the real part and green to the imaginary part.

7 Summary and Outlook

The anomalous magnetic moment of the muon is one of very few observables in particle physics characterized by a long-standing tension between the SM prediction and its measurement. Ongoing progress in the experimental determination demands similar improvements on the theory side. This thesis provides advances in the dispersive data-driven evaluation of the HLbL contribution to the SM prediction, which is responsible for a considerable part of the theory uncertainty. While the most important intermediate-state contributions are under excellent control, the uncertainty of HLbL is presently dominated by intermediate states in the 1–2 GeV mass range and the matching to SDCs. Both points have been addressed in this thesis.

We first provided a new method to incorporate longitudinal SDCs in the HLbL evaluation. The approach is based on the observation that the low-energy space-like regime is well described by the dispersive evaluation of the lightest intermediate states, for which precise input exists. At higher energies, truncating the sum over intermediate states in the unitarity relation after the first few terms ceases to be a good approximation. Instead, at high enough and mixed energy scales, pQCD and the OPE can be used to obtain precise predictions. It is thus the regions where neither of the representations is valid that are most uncertain. However, since at space-like values for the virtualities the scalar functions are free of singularities, the connection between the constrained regions must be smooth. This motivated us to consider general interpolants that match smoothly to the known representations in the regions where they are assumed to be valid.

Previously, only hadronic models including infinite towers of intermediate states had been used to describe the intermediate energy region. Within our approach, we could show that the constraints together with the expectation of a smooth connection between the various kinematic regions are sufficient to reach the required precision and the details of the complicated hadron dynamics as described by these models are not necessary. This relatively simple procedure allowed us to perform a detailed assessment of all possible uncertainties. In accordance with earlier studies, we found that control over intermediate states in the 1–2 GeV mass range is mandatory to considerably reduce the uncertainties of the HLbL contribution to a_μ. Conversely, refinements of the effect of the lightest intermediate states or the SDCs are not required for an improvement in the matching.

We found that the effect of longitudinal SDCs is to shift a_μ^{long} by

$$\Delta a_\mu^{\text{long}} = (10.4 \pm 8.3) \times 10^{-11} \tag{7.1}$$

with respect to the ground-state pseudoscalar poles. This result relies on the assumption that at low energies the longitudinal component of the HLbL tensor is well approximated by the ground-state pseudoscalar poles alone. Using model-dependent hQCD input for the lightest isovector axial-vector meson a_1 as a guidance, we demonstrated that it will be possible to include these additional contributions to the low-energy input if model-independent analyses confirm their non-negligible effect at low energies.

Two issues currently limit the control over intermediates states in the 1–2 GeV mass range. On the one hand, both direct and indirect experimental input on their form factors is in general very scarce, which prevents data-driven analyses. On the other hand, in the established CHPS approach, the redundancies in the Lorentz decomposition of the HLbL tensor lead to kinematic singularities in individual contributions to the scalar functions, which only cancel if entire sets of intermediate states that fulfill certain sum rules are considered. This can be avoided for intermediate states with spin ≤ 1, but is unavoidable using only the minimal set of sum rules if higher-spin states are included. For this reason, model-independent evaluations of the effect of D-wave $\pi\pi$-rescattering and narrow tensor resonances are currently not possible in the CHPS formalism.

The CHPS approach is based on dispersion relations in the Mandelstam variables while keeping the photon virtualities fixed. The soft-photon limit needed for a_μ is taken only at the end. Since there exists a Lorentz basis free of redundancies and kinematic singularities in the soft-photon limit, dispersion relations written directly in this limit are free of these issues, but the constraints from unitarity become more complicated. Due to these additional complications, we first worked out the formalism for the simpler case of the VVA correlator. We derived expressions for pseudoscalar, axial-vector and vector poles as well as the contribution from two-pion rescattering. We saw that in a dispersive formalism with fixed photon virtualities, i.e. the analogue of the CHPS formalism for HLbL, vector-poles and two-pion rescattering do not contribute to the VVA unitarity relation, but enter if the pseudoscalar and axial-vector TFFs are reconstructed dispersively. This implies a reshuffling of contributions between the two approaches. E.g., what is denoted as pion pole in the CHPS-like formalism contains not only the pure pole singularity from single-pion exchange, but also singularities due to intermediate states in the pion TFF within the new formalism, mainly vector poles and a two-pion cut. By performing a detailed comparison, we saw that the CHPS-like formalism does not fully capture the two-pion cut in $g-2$ kinematics due to neglected heavier intermediate states. Thus, whereas the new formalism correctly incorporates all singularities up to the neglected ones, the dispersion relations with fixed photon virtualities miss parts of the cuts in the photon virtualities after taking the soft-photon limit. These considerations also translate to the two dispersive approaches to HLbL.

We also provided preliminary numerical implementations of both dispersive representations in the isovector channel. We took into account SDCs by adding a single effective pole in the new dispersive formalism. This is not possible in the CHPS-like approach since each individual pole drops off too quickly at high energies to saturate the SDC. In this case, infinite towers of intermediate states are required for an accurate description at high energies, which resembles the situation in HLbL. Instead of modeling these infinite towers, we applied the method based on general interpolants to the case of VVA. The numerical evaluation revealed a clear advantage of the new approach because the CHPS-like approach suffers from the fast asymptotic fall-off of the exclusive contributions already below the matching point, before the interpolants can guide the functions to the correct asymptotic limits. Compared to the hadronic model calculations available in the literature, the new dispersive representation is in good agreement within uncertainties. For the transversal component, a χPT calculation of the normalization favors the representation based on dispersion relations in $g-2$ kinematics with respect to the models. These observations are also reflected in the hadronic electroweak contribution to a_μ due to the first-family part of the VVA correlator, which can be calculated from a weighted integral over the scalar functions. We obtained a value that is compatible within uncertainties with the hadronic model used so far and our uncertainty is similar to the one estimated in the model calculation.

Afterwards, we returned to HLbL and applied the new formalism to that case. We provided results for single-particle intermediate-state contributions due to pseudoscalar, scalar, axial-vector, vector and tensor mesons. The first three of these can also be described in the CHPS formalism, but in order to understand the reshuffling, a calculation in the new approach is also required. Vector-meson poles do not contribute in the CHPS framework, but are hidden in the form factors. Finally, tensor-meson poles contribute in four-point kinematics, but are affected by the kinematic singularities. Therefore, the new approach enables the first model-independent definition of these contributions. In addition, we studied two-pion intermediate states in the unitarity relations. We found that compared to the CHPS approach the new sub-processes $\gamma^*\gamma^* \to \gamma\pi\pi$ and $\pi\pi \to \gamma\pi\pi$ are required. Crucially, their tensor decompositions are free of issues with kinematic singularities. This opens a path towards the first complete data-driven evaluation of all exclusive hadronic contributions to HLbL that are relevant at an accuracy adequate for the comparison with the forthcoming measurements of a_μ.

In the examination of two-pion intermediate states, we encountered a new subtlety that is not present in the considered contributions to VVA, namely singularities in the soft-photon limit. These arise if sub-processes involve charged particles together with the soft photon. Since HLbL is finite in that limit, the singularities have to cancel and this cancellation is guaranteed to happen separately for each intermediate state, in contrast to the kinematic singularities in the CHPS approach whose cancellation relies on sum rules. The amplitudes can be split into two pieces: one that is singular in the soft-photon limit but related to the corresponding process with the soft photon removed and another one that is non-singular in the limit. We pointed out that a suitable definition of the singular part can be obtained from dispersion relations. For the non-singular part, dispersion relations directly in the soft-photon limit can be derived.

Finally, we considered the sub-process $\pi\pi \to \gamma\pi\pi$ with a soft photon. This is a five-particle process, which leads to a significant complexity. After deriving symmetry constraints and the Lorentz decomposition, we provided a definition of the singular part that preserves all symmetries of the full amplitude. Then, we calculated the discontinuities of the non-singular parts from unitarity relations. We showed explicitly that the soft-photon singularities of the sub-processes cancel. The limit is well-defined and consistent with the one-loop result in χPT. In order to obtain the real parts, we derived reconstruction theorems including $\pi\pi$ D-waves in the soft-photon limit, where the problem reduces to four-point kinematics. The unitarity relations for the single-variable functions could be reduced to the form of an inhomogeneous Omnès problem, which we solved using dispersion relations. In order to obtain numerical results, we implemented an iterative algorithm. The solution depends on a set of subtraction constants, for which external input is required. As a preliminary strategy, we fixed them from the one-loop χPT expressions.

The dispersive study of $\pi\pi \to \gamma\pi\pi$ represents an important step towards the inclusion of D-wave $\pi\pi$ rescattering into HLbL. It is needed as an input in the dispersive reconstruction of $\gamma^*\gamma^* \to \gamma\pi\pi$ for which a similar analysis can now be performed. Many of the techniques developed in the case of $\pi\pi \to \gamma\pi\pi$ will be applicable to that process. The tensor decomposition is already known but considerably more complicated than in the case of $\pi\pi \to \gamma\pi\pi$. Finally, once this sub-process is under control, it can be plugged into the unitarity relations for HLbL to obtain the $\pi\pi$ rescattering contribution.

In addition, a proper matching to SDCs is mandatory. As briefly mentioned in this thesis, the new formalism provides a new perspective on this because there is a close connection between the dispersion relations for VVA and the ones for HLbL in the mixed region through the OPE. Thus, exactly those intermediate states that are required for an accurate description of the VVA correlator will also lead to an accurate representation for HLbL in that regime. In addition, it might is beneficial for an implementation of the SDCs that the asymptotic fall-off of individual single-particle contributions matches that of the leading SDC. In the strategy for the matching to SDCs introduced in this thesis, the deficit typically observed around the matching point might be reduced due to the slower asymptotic decay of the exclusive low-energy contributions. Implementations with finite numbers of effective poles, as studied in this thesis for VVA, could provide an alternative strategy to fulfill the SDCs that is inapplicable to the CHPS formalism due to the faster asymptotic fall-off.

As sketched already in this thesis, a detailed study of the reshuffling between the two dispersive approaches to HLbL enables their combination. Since the truncation of the unitarity sums is different in the two approaches, a combination will allow us to include as many contributions as possible and thus obtain the most precise data-driven representation for HLbL.

Potentially, a study of the reshuffling could also shed new light on the issue of kinematic singularities in the CHPS formalism and might even provide a way to avoid them. In addition, the different truncations can also be used to better estimate the uncertainties due to neglected heavier intermediate states and the connected matching to SDCs. In this regard, the interplay between the two approaches will be very important to achieve the accuracy goals set by the FNAL experiment.

A Phase-space Integrals

A.1 One-particle phase space

We start with the simplest integral, which appears in single-particle intermediate states,

$$P_1(p^2, m^2) = \int \widetilde{\mathrm{d}q_1} (2\pi)^4 \delta^{(4)}(p - q_1) \tag{A.1}$$

with m the mass of the particle with momentum q_1. The phase-space element can be rewritten as a four-dimensional integral with an on-shell δ-function

$$P_1(p^2, m^2) = \int \frac{\mathrm{d}^4 q_1}{(2\pi)^4} 2\pi\delta(q_1^2 - m^2)\theta(q_1^0)(2\pi)^4\delta^{(4)}(p - q_1)\,. \tag{A.2}$$

Now, it is straightforward to perform the integral

$$P_1(p^2, m^2) = 2\pi\delta(p^2 - m^2)\theta(p^0) = 2\pi\delta(p^2 - m^2)\,, \tag{A.3}$$

where we have dropped the θ-function as in the physical region the energy is always positive.

Due to the momentum-conserving δ-function, it is clear that additional factors of q_1 in the integrand lead to corresponding factors of p in the result, e.g.

$$\int \widetilde{\mathrm{d}q_1} q_1^\mu (2\pi)^4\delta^{(4)}(p - q_1) = p^\mu \int \widetilde{\mathrm{d}q_1} (2\pi)^4\delta^{(4)}(p - q_1) = 2\pi\delta(p^2 - m^2)p^\mu\,. \tag{A.4}$$

A.2 Scalar two-particle phase space

We next consider the scalar integral appearing in a two-pion intermediate state of a $2 \to 2$-process

$$P_2^{ll'} = \int \widetilde{\mathrm{d}q_1}\widetilde{\mathrm{d}q_2}(2\pi)^4\delta^{(4)}(p_1 + p_2 - q_1 - q_2)P_l(z')P_{l'}(z'') \tag{A.5}$$

with

$$\begin{aligned} z' &= \cos\measuredangle(\boldsymbol{p}_1, \boldsymbol{q}_1) = \frac{(p_1 - q_1)^2 - (p_2 - q_1)^2}{\lambda^{1/2}(s, p_1^2, p_2^2)\sigma_\pi(s)}\,, \\ z'' &= \cos\measuredangle(-\boldsymbol{p}_3, \boldsymbol{q}_1) = \frac{(p_3 + q_1)^2 - (p_4 + q_1)^2}{\lambda^{1/2}(s, p_3^2, p_4^2)\sigma_\pi(s)}\,, \end{aligned} \tag{A.6}$$

where $p_1 + p_2 + p_3 + p_4 = 0$ and the angles are defined in the center-of-mass frame. The angles fulfill

$$z'' = zz' + \sqrt{1 - z^2}\sqrt{1 - z'^2}\cos\phi'\,, \tag{A.7}$$

where

$$z = \cos\measuredangle(\boldsymbol{p}_1, -\boldsymbol{p}_3) = \frac{(p_1+p_2)^2((p_1+p_3)^2-(p_1+p_4)^2)+(p_1^2-p_2^2)(p_3^2-p_4^2)}{\lambda^{1/2}(s,p_1^2,p_2^2)\lambda^{1/2}(s,p_3^2,p_4^2)} \tag{A.8}$$

is the external scattering angle and ϕ' the azimuthal angle of $\boldsymbol{q}_1$.

We perform the integral over q_2 by the spatial part of the δ-function to obtain in the center-of-mass frame

$$P_2^{ll'} = \int \widetilde{\mathrm{d}q_1} \frac{1}{2\sqrt{\boldsymbol{q}_1^2+m_\pi^2}}(2\pi)\delta\left(p_1^0+p_2^0-\sqrt{\boldsymbol{q}_1^2+m_\pi^2}\right)P_l(z')P_{l'}(z'')\,. \tag{A.9}$$

Next, we use the remaining δ-function to perform the integral over $|\boldsymbol{q}_1|$

$$P_2^{ll'} = \frac{1}{32\pi^2}\sigma_\pi\left((p_1^0+p_2^0)^2\right)\int \mathrm{d}\Omega_1 P_l(z')P_{l'}(z'') = \frac{\sigma_\pi(s)}{32\pi^2}\int \mathrm{d}\Omega_1 P_l(z')P_{l'}(z'')\,, \tag{A.10}$$

where in the last step we have introduced $s=(p_1+p_2)^2$. The remaining integral is over the angles ϕ' and θ' with $z'=\cos\theta'$ and z'' given by Eq. (A.7). The addition theorem for Legendre polynomials then leads to

$$P_2^{ll'} = \frac{\sigma_\pi(s)}{8\pi}\delta_{ll'}\frac{P_l(z)}{2l+1}\,. \tag{A.11}$$

Since this result only depends on Lorentz-invariant quantities, it is valid in any frame.

The case of $1\to 2$ can be understood as the limit of the above expressions for $q_2\to 0$. The angle z' is ill-defined in that limit and thus only $l=0$ is meaningful. Then, the result is independent of z, which is also ill-defined in that limit. We thus obtain

$$\int \widetilde{\mathrm{d}q_1}\widetilde{\mathrm{d}q_2}(2\pi)^4\delta^{(4)}(p_1-q_1-q_2)P_{l'}(z'') = \frac{\sigma_\pi(p_1^2)}{8\pi}\delta_{0l'}\,. \tag{A.12}$$

A.3 Two-particle phase space with additional momenta

In the unitarity relations for $\pi\pi\to\gamma\pi\pi$, phase-space integrals with additional momenta are needed, see Eq. (6.61). As explained in Ref. [17], these can be related to derivatives of the scalar integral. One starts by expressing the uncontracted integration momenta as a derivative of an angle, in this case e.g.

$$P_{l'}'(z_s'')(q_1-q_2)_\mu = -\frac{\sigma_\pi(s)\lambda^{1/2}(s,p_3^2,w_4)}{2}\frac{\partial}{\partial p_4^\mu}P_{l'}(z_s'')\bigg|_{p_1,p_2,q} + A_\mu(z_s'')\,, \tag{A.13}$$

where A_μ depends on the integration variables only via the angle z_s'' so that the integral over this contribution can be performed as in the previous section. For the other term, the derivative can be pulled out of the integral since the derivative of z_s' vanishes. Then, this integral also has the form considered in the previous section and finally the derivative can be performed. In the case of more uncontracted momenta as in $I_{ll'}^{2\mu\nu}$, higher derivatives are needed.

When calculating these derivatives, we consistently allow the external pions to be off-shell. E.g., in the definitions of the angle z_s'', we write $\lambda(s, p_3^2, (p_4+q)^2)$ and take into account derivatives acting on p_3^2 and $(p_4+q)^2$. One could also consider calculating the derivatives under the additional constraint that all pions are on-shell. For the five independent momenta p_1, p_2, p_4, q and q_1, there are 15 scalar products, but only 14 of them are independent in four space-time dimensions due to the Schouten identity. Putting all internal and external pions on the mass shell gives six constraints and fixing p_1, p_2, q and q_1 implies six additional relations between the scalar products. This reduces the number of independent scalar products to two. These should be chosen to be independent of q_1 since otherwise the derivative cannot be pulled out of the loop integral. Then, however, the derivative of z_s'' cannot lead to terms proportional to $q_{1,2}$ with uncontracted indices. This issue does not show up in the case of four-particle processes as considered in Ref. [17].

We have checked that our prescription leads to correct results by choosing low values for l and l'. The Cutkosky rule relates the phase-space integral to the discontinuity of a loop integral, which is easy to perform in that case. Naively replacing p_i^2 by m_π^2 before calculating the derivative leads to wrong results. We stress that working with off-shell pions is only a trick to calculate the phase-space integrals and does not imply that non-perturbative matrix elements have to be defined away from on-shell kinematics.

A.4 Two-particle phase space with internal soft-photon singularity

In addition to the two types of integrals considered in the previous two sections, in the unitarity relations for $\pi\pi \to \gamma\pi\pi$ also the combination of phase-space integrals $\hat{I}^\mu_{ll'} + \mathcal{C}_{13}\mathcal{C}_{24}\hat{I}^\mu_{l'l}$ with $\hat{I}^\mu_{ll'}$ defined in Eq. (6.59) is needed. It can be written as

$$\begin{aligned}\hat{I}^\mu_{ll'} + \mathcal{C}_{13}\mathcal{C}_{24}\hat{I}^\mu_{l'l} = \int \frac{\mathrm{d}^4 q_1}{(2\pi)^4}\frac{\mathrm{d}^4 q_2}{(2\pi)^4}(2\pi)^6\delta(q_1^2-m_\pi^2)\delta(q_2^2-m_\pi^2)\frac{(2p_1+2p_2+q-2q_2)^\mu}{q^2+2q\cdot(p_1+p_2-q_2)} \\ \times P_l\left(\frac{(p_2-q_2)^2-(p_1-q_2)^2}{s-4m_\pi^2}\right)P_{l'}\left(\frac{(p_4+q_2)^2-(p_3+q_2)^2}{\tilde{s}-4m_\pi^2}\right) \\ \times\left[\delta^{(4)}(q_1+q_2-p_1-p_2)-\delta^{(4)}(q_1+q_2-p_1-p_2-q)\right], \qquad \text{(A.14)}\end{aligned}$$

where we suppressed the Heaviside step functions for notational convenience. Now, it is straightforward to perform the q_1 integral

$$\begin{aligned}\hat{I}^\mu_{ll'} + \mathcal{C}_{13}\mathcal{C}_{24}\hat{I}^\mu_{ll'} = \int \frac{\mathrm{d}^4 q_2}{(2\pi)^4}(2\pi)^2\delta(q_2^2-m_\pi^2)\frac{(2p_1+2p_2+q-2q_2)^\mu}{q^2+2q\cdot(p_1+p_2-q_2)} \\ \times P_l\left(\frac{(p_2-q_2)^2-(p_1-q_2)^2}{s-4m_\pi^2}\right)P_{l'}\left(\frac{(p_4+q_2)^2-(p_3+q_2)^2}{\tilde{s}-4m_\pi^2}\right) \\ \times\left[\delta\left((p_1+p_2-q_2)^2-m_\pi^2\right)-\delta\left((p_1+p_2+q-q_2)^2-m_\pi^2\right)\right]. \qquad \text{(A.15)}\end{aligned}$$

We are only interested in the result to order q, which allows us to expand the difference of δ-functions in the square bracket. If we expand around the symmetric point, only odd orders contribute so that the leading term is sufficient. To the required order, the result can be written as

$$\begin{aligned}\hat{I}^{\mu}_{ll'} + \mathcal{C}_{13}\mathcal{C}_{24}\hat{I}^{\mu}_{l'l} = -\frac{1}{2}\int \frac{\mathrm{d}^4 q_2}{(2\pi)^4}(2\pi)^2\delta(q_2^2 - m_\pi^2)(2p_1 + 2p_2 + q - 2q_2)^\mu \\ \times P_l\left(\frac{(p_2-q_2)^2 - (p_1-q_2)^2}{s - 4m_\pi^2}\right) P_{l'}\left(\frac{(p_4+q_2)^2 - (p_3+q_2)^2}{\tilde{s} - 4m_\pi^2}\right) \\ \times \left[\delta'\left((p_1+p_2-q_2)^2 - m_\pi^2\right) + \delta'\left((p_1+p_2+q-q_2)^2 - m_\pi^2\right)\right] + \mathcal{O}(q^2)\,.\end{aligned} \tag{A.16}$$

We notice that the q_2-dependent denominator has canceled. Expressed in terms of the momenta

$$S = p_1 + p_2\,, \qquad \tilde{S} = p_3 + p_4\,, \qquad P = p_1 - p_2\,, \qquad \tilde{P} = p_4 - p_3\,, \tag{A.17}$$

this simplifies to

$$\begin{aligned}\hat{I}^{\mu}_{ll'} + \mathcal{C}_{13}\mathcal{C}_{24}\hat{I}^{\mu}_{l'l} = -\frac{1}{2}\int \frac{\mathrm{d}^4 q_2}{(2\pi)^4}(2\pi)^2\delta(q_2^2 - m_\pi^2)(S - \tilde{S} - 2q_2)^\mu \\ \times P_l\left(\frac{2q_2\cdot P}{S^2 - 4m_\pi^2}\right) P_{l'}\left(\frac{2q_2\cdot \tilde{P}}{\tilde{S}^2 - 4m_\pi^2}\right) \\ \times \left[\delta'\left((S-q_2)^2 - m_\pi^2\right) + \delta'\left((\tilde{S}+q_2)^2 - m_\pi^2\right)\right] + \mathcal{O}(q^2)\,.\end{aligned} \tag{A.18}$$

We can then rewrite the derivatives using

$$\frac{\partial}{\partial S_\mu}\delta\left((S-q_2)^2 - m_\pi^2\right)\Bigg|_{\tilde{S},P,\tilde{P}} = 2(S-q_2)^\mu \delta'\left((S-q_2)^2 - m_\pi^2\right) \tag{A.19}$$

and similarly for the other one. This allows us to remove the additional term q_2^μ in the integrand whereas the terms proportional to $S - \tilde{S}$ turn out to be of higher order in q and can thus be neglected. We then pull the derivatives out of the integral taking into account that they also act on the Legendre polynomials. By reintroducing the q_1 integral, we write the result in terms of the integrals considered in the previous two sections and evaluate them. Finally, we perform the derivatives. Similarly to the previous section, the derivatives have to be performed allowing the pions to be off-shell. As before, we checked the result for low values of l and l' against the difference of discontinuities of the corresponding loop integrals expanded to linear order in q.

B Reconstruction theorems for $\pi\pi \to \gamma\pi\pi$

In this appendix, we provide explicit expressions for some objects used in Sec. 6.7.

B.1 Crossing relations

The crossing relations Eq. (6.36) relate the t- and u-channel single-variable functions to the s-channel ones

$$
\begin{aligned}
G_0^{(10)}(s) &= -\frac{1}{3}F_0^{(10)}(s) - \frac{5}{9}F_0^{(12)}(s) - \frac{2}{3}F_0^{(11)}(s)\,,\\
G_1^{(10)}(s) &= -\frac{1}{3}F_1^{(01)}(s) - \frac{5}{9}F_1^{(21)}(s) - \frac{10}{3}F_1^{(22)}(s)\,,\\
G_2^{(10)}(s) &= -\frac{1}{3}F_2^{(10)}(s) - \frac{5}{9}F_2^{(12)}(s) - \frac{2}{3}F_2^{(11)}\,,\\
G_0^{(01)}(s) &= -\frac{1}{3}F_0^{(10)}(s) - \frac{5}{9}F_0^{(12)}(s) + \frac{2}{3}F_0^{(11)}(s)\,,\\
G_1^{(01)}(s) &= -\frac{1}{3}F_1^{(01)}(s) - \frac{5}{9}F_1^{(21)}(s) + \frac{10}{3}F_1^{(22)}(s)\,,\\
G_2^{(01)}(s) &= -\frac{1}{3}F_2^{(10)}(s) - \frac{5}{9}F_2^{(12)}(s) + \frac{2}{3}F_2^{(11)}\,,\\
G_0^{(12)}(s) &= -\frac{1}{4}F_0^{(10)}(s) + \frac{1}{3}F_0^{(12)}(s) + F_0^{(11)}(s)\,,\\
G_1^{(12)}(s) &= -\frac{1}{4}F_1^{(01)}(s) + \frac{1}{3}F_1^{(21)}(s) - F_1^{(22)}(s)\,,\\
G_2^{(12)}(s) &= -\frac{1}{4}F_2^{(10)}(s) + \frac{1}{3}F_2^{(12)}(s) + F_2^{(11)}\,,\\
G_0^{(21)}(s) &= -\frac{1}{4}F_0^{(10)}(s) + \frac{1}{3}F_0^{(12)}(s) - F_0^{(11)}(s)\,,\\
G_1^{(21)}(s) &= -\frac{1}{4}F_1^{(01)}(s) + \frac{1}{3}F_1^{(21)}(s) + F_1^{(22)}(s)\,,\\
G_2^{(21)}(s) &= -\frac{1}{4}F_2^{(10)}(s) + \frac{1}{3}F_2^{(12)}(s) - F_2^{(11)}\,,\\
G_0^{(11)}(s) &= -\frac{1}{8}F_0^{(10)}(s) + \frac{5}{12}F_0^{(12)}(s)\,,\\
G_1^{(11)}(s) &= \frac{1}{8}F_1^{(01)}(s) - \frac{5}{12}F_1^{(21)}(s)\,,\\
G_2^{(11)}(s) &= -\frac{1}{8}F_2^{(10)}(s) + \frac{5}{12}F_2^{(12)}(s)\,,\\
G_0^{(22)}(s) &= -\frac{1}{8}F_0^{(10)}(s) - \frac{1}{12}F_0^{(12)}(s)\,,
\end{aligned}
$$

$$
\begin{aligned}
G_1^{(22)}(s) &= \frac{1}{8} F_1^{(01)}(s) + \frac{1}{12} F_1^{(21)}(s)\,, \\
G_2^{(22)}(s) &= -\frac{1}{8} F_2^{(10)}(s) - \frac{1}{12} F_2^{(12)}(s)\,.
\end{aligned} \tag{B.1}
$$

B.2 Diagonalization

The matrix $M(s)$ that diagonalizes the homogeneous contributions to the imaginary parts of the single-variable functions reads

$$
M(s) = \begin{pmatrix}
1 & \frac{5}{2}\left(s-4m_\pi^2\right)^2 & 4m_\pi^2 - s & 0 & 0 & 0 & 0 & 0 \\
0 & 1 & 0 & 0 & 0 & 0 & 0 & 0 \\
0 & 0 & 0 & 0 & 0 & 0 & 1 & 0 \\
0 & 4m_\pi^2 - s & 1 & 0 & 0 & 0 & 0 & 0 \\
0 & 0 & 0 & 1 & \frac{5}{2}\left(s-4m_\pi^2\right)^2 & 4m_\pi^2 - s & 0 & 0 \\
0 & 0 & 0 & 0 & 1 & 0 & 0 & 0 \\
0 & 0 & 0 & 0 & 0 & 0 & 0 & 1 \\
0 & 0 & 0 & 0 & 4m_\pi^2 - s & 1 & 0 & 0
\end{pmatrix}. \tag{B.2}
$$

In the diagonal basis, the angular-average contributions are given by

$$
A_D^n(s) = \sum_{p=0}^{5} \sum_{m=1}^{8} A_{pm}^n(s) \langle z^p F_D^m \rangle \tag{B.3}
$$

with

$$
\begin{aligned}
A_{0m}^1(s) &= \Big(-\frac{2}{3},\, 38m_\pi^2 s - 20m_\pi^4 - \frac{53s^2}{4},\, -\frac{4}{3},\, \frac{1}{3}(20m_\pi^2 - 11s),\, -\frac{10}{9}, \\
&\qquad -\frac{5}{12}(-152m_\pi^2 s + 80m_\pi^4 + 53s^2),\, 40m_\pi^2 - 30s,\, \frac{5}{9}(20m_\pi^2 - 11s) \Big)\,, \\
A_{1m}^1(s) &= \Big(\frac{2}{3},\, \frac{1}{4}(19s - 36m_\pi^2)(4m_\pi^2 + s),\, -\frac{4}{3},\, \frac{8}{3}(s - m_\pi^2),\, \frac{10}{9}, \\
&\qquad \frac{5}{12}(19s - 36m_\pi^2)(4m_\pi^2 + s),\, -40(s - 2m_\pi^2),\, \frac{40}{9}(s - m_\pi^2) \Big)\,, \\
A_{2m}^1(s) &= (s - 4m_\pi^2)\Big(0,\, \frac{29s}{4} - 9m_\pi^2,\, 0,\, 1,\, 0,\, \frac{5}{12}(29s - 36m_\pi^2),\, -10,\, \frac{5}{3}\Big)\,, \\
A_{3m}^1(s) &= (s - 4m_\pi^2)^2\Big(0,\, \frac{5}{4},\, 0,\, 0,\, 0,\, \frac{25}{12},\, 0,\, 0\Big)\,, \\
A_{0m}^2(s) &= \frac{1}{(s - 4m_\pi^2)^2}\Big(\frac{1}{3},\, -19m_\pi^2 s + 10m_\pi^4 + \frac{53s^2}{8},\, \frac{2}{3},\, \frac{1}{6}(11s - 20m_\pi^2),\, \frac{5}{9}, \\
&\qquad \frac{5}{24}(-152m_\pi^2 s + 80m_\pi^4 + 53s^2),\, 5(3s - 4m_\pi^2),\, \frac{5}{18}(11s - 20m_\pi^2) \Big)\,, \\
A_{1m}^2(s) &= \frac{1}{(s - 4m_\pi^2)^2}\Big(-1,\, 33m_\pi^2 s - 2m_\pi^4 - \frac{125s^2}{8},\, 2,\, 8m_\pi^2 - 5s,\, -\frac{5}{3}, \\
&\qquad 55m_\pi^2 s - \frac{10m_\pi^4}{3} - \frac{625s^2}{24},\, 50s - 80m_\pi^2,\, -\frac{5}{3}(5s - 8m_\pi^2) \Big)\,,
\end{aligned}
$$

$$
\begin{aligned}
A^2_{2m}(s) &= \frac{1}{(s-4m_\pi^2)^2}\Big(-1,\, -4(-31m_\pi^2 s + 26m_\pi^4 + 8s^2),\, -2,\, 16m_\pi^2 - 7s,\, -\frac{5}{3},\\
&\qquad -\frac{20}{3}(-31m_\pi^2 s + 26m_\pi^4 + 8s^2),\, -30s,\, \frac{5}{3}(16m_\pi^2 - 7s)\Big)\,,\\
A^2_{3m}(s) &= \frac{1}{(s-4m_\pi^2)^2}\Big(\frac{5}{3},\, \frac{37s^2}{2} - 8m_\pi^2(8m_\pi^2 + s),\, -\frac{10}{3},\, \frac{1}{3}(23s - 32m_\pi^2),\, \frac{25}{9},\\
&\qquad \frac{5}{6}(37s^2 - 16m_\pi^2(8m_\pi^2 + s)),\, 160m_\pi^2 - 90s,\, \frac{5}{9}(23s - 32m_\pi^2)\Big)\,,\\
A^2_{4m}(s) &= \frac{1}{s-4m_\pi^2}\Big(0,\, \frac{5}{8}(31s - 44m_\pi^2),\, 0,\, \frac{5}{2},\, 0,\, \frac{25}{24}(31s - 44m_\pi^2),\, -25,\, \frac{25}{6}\Big)\,,\\
A^2_{5m}(s) &= \Big(0,\, \frac{25}{8},\, 0,\, 0,\, 0,\, \frac{125}{24},\, 0,\, 0\Big)\,,\\
A^3_{0m}(s) &= \Big(-\frac{3}{8},\, \frac{9}{64}(24m_\pi^2 s + 48m_\pi^4 - 29s^2),\, 0,\, \frac{3}{16}(7s - 4m_\pi^2),\, \frac{5}{4},\\
&\qquad \frac{15}{32}(29s^2 - 24m_\pi^2(2m_\pi^2 + s)),\, 0,\, \frac{5}{8}(4m_\pi^2 - 7s)\Big)\,,\\
A^3_{1m}(s) &= (s-4m_\pi^2)\Big(0,\, -\frac{9}{32}(13s - 12m_\pi^2),\, 0,\, \frac{9}{16},\, 0,\, \frac{15}{16}(13s - 12m_\pi^2),\, 0,\, -\frac{15}{8}\Big)\,,\\
A^3_{2m}(s) &= \Big(\frac{3}{8},\, \frac{9}{8}(s - 2m_\pi^2)(8m_\pi^2 + 3s),\, 0,\, \frac{3}{16}(4m_\pi^2 - 7s),\, -\frac{5}{4},\\
&\qquad -\frac{15}{4}(s - 2m_\pi^2)(8m_\pi^2 + 3s),\, 0,\, \frac{5}{8}(7s - 4m_\pi^2)\Big)\,,\\
A^3_{3m}(s) &= (s-4m_\pi^2)\Big(0,\, \frac{9}{32}(13s - 12m_\pi^2),\, 0,\, -\frac{9}{16},\, 0,\, \frac{45m_\pi^2}{4} - \frac{195s}{16},\, 0,\, \frac{15}{8}\Big)\,,\\
A^3_{4m}(s) &= (s-4m_\pi^2)^2\Big(0,\, \frac{45}{64},\, 0,\, 0,\, 0,\, -\frac{75}{32},\, 0,\, 0\Big)\,,\\
A^4_{0m}(s) &= \frac{1}{s-4m_\pi^2}\Big(-\frac{1}{3},\, 19m_\pi^2 s - 10m_\pi^4 - \frac{53s^2}{8},\, -\frac{2}{3},\, \frac{1}{6}(20m_\pi^2 - 11s),\, -\frac{5}{9},\\
&\qquad -\frac{5}{24}(-152m_\pi^2 s + 80m_\pi^4 + 53s^2),\, 20m_\pi^2 - 15s,\, \frac{50m_\pi^2}{9} - \frac{55s}{18}\Big)\,,\\
A^4_{1m}(s) &= \frac{1}{s-4m_\pi^2}\Big(-\frac{2}{3},\, 62m_\pi^2 s - 48m_\pi^4 - \frac{35s^2}{2},\, \frac{4}{3},\, \frac{1}{6}(52m_\pi^2 - 25s,\, -\frac{10}{9},\\
&\qquad -\frac{5}{6}(5s - 12m_\pi^2)(7s - 8m_\pi^2),\, 5(5s - 4m_\pi^2),\, -\frac{5}{18}(25s - 52m_\pi^2)\Big)\,,\\
A^4_{2m}(s) &= \frac{1}{s-4m_\pi^2}\Big(1,\, \frac{43s^2}{4} - 4m_\pi^2(9m_\pi^2 + s,\, 2,\, \frac{9s}{2} - 6m_\pi^2,\, \frac{5}{3},\, \frac{5}{12}(43s^2 - 16m_\pi^2(9m_\pi^2 + s)),\\
&\qquad 55s - 100m_\pi^2,\, \frac{5}{2}(3s - 4m_\pi^2)\Big)\,,\\
A^4_{3m}(s) &= \Big(0,\, \frac{23s}{2} - 16m_\pi^2,\, 0,\, \frac{3}{2},\, 0,\, \frac{5}{6}(23s - 32m_\pi^2),\, 15,\, \frac{5}{2}\Big)\,,\\
A^4_{4m}(s) &= (s-4m_\pi^2)\Big(0,\, \frac{15}{8},\, 0,\, 0,\, 0,\, \frac{25}{8},\, 0,\, 0\Big)\,,\\
A^5_{0m}(s) &= \Big(-\frac{1}{2},\, -\frac{3}{16}(-152m_\pi^2 s + 80m_\pi^4 + 53s^2),\, 2,\, 5m_\pi^2 - \frac{11s}{4},\, \frac{2}{3},\\
&\qquad -38m_\pi^2 s + 20m_\pi^4 + \frac{53s^2}{4},\, 12m_\pi^2 - 9s,\, \frac{1}{3}(11s - 20m_\pi^2)\Big)\,,
\end{aligned}
$$

$$
\begin{aligned}
A^5_{1m}(s) &= \Big(\frac{1}{2},\, \frac{3}{16}(19s-36m_\pi^2)(4m_\pi^2+s),\, 2,\, 2(s-m_\pi^2),\, -\frac{2}{3},\, -\frac{1}{4}(19s-36m_\pi^2)(4m_\pi^2+s),\\
&\qquad -12(s-2m_\pi^2),\, -\frac{8}{3}(s-m_\pi^2)\Big)\,,\\
A^5_{2m}(s) &= (s-4m_\pi^2)\Big(0,\, \frac{3}{16}(29s-36m_\pi^2),\, 0,\, \frac{3}{4},\, 0,\, 9m_\pi^2-\frac{29s}{4},\, -3,\, -1\Big)\,,\\
A^5_{3m}(s) &= (s-4m_\pi^2)^2\Big(0,\, \frac{15}{16},\, 0,\, 0,\, 0,\, -\frac{5}{4},\, 0,\, 0\Big)\,,\\
A^6_{0m}(s) &= \frac{1}{(s-4m_\pi^2)^2}\Big(\frac{1}{4},\, \frac{3}{32}(-152m_\pi^2 s+80m_\pi^4+53s^2),\, -1,\, \frac{11s}{8}-\frac{5m_\pi^2}{2},\, -\frac{1}{3},\\
&\qquad 19m_\pi^2 s-10m_\pi^4-\frac{53s^2}{8},\, \frac{9s}{2}-6m_\pi^2,\, \frac{1}{6}(20m_\pi^2-11s)\Big)\,,\\
A^6_{1m}(s) &= \frac{1}{(s-4m_\pi^2)^2}\Big(-\frac{3}{4},\, -\frac{3}{32}(-264m_\pi^2 s+16m_\pi^4+125s^2),\, -3,\, 6m_\pi^2-\frac{15s}{4},\, 1,\\
&\qquad -33m_\pi^2 s+2m_\pi^4+\frac{125s^2}{8},\, 3(5s-8m_\pi^2),\, 5s-8m_\pi^2\Big)\,,\\
A^6_{2m}(s) &= \frac{1}{(s-4m_\pi^2)^2}\Big(-\frac{3}{4},\, 93m_\pi^2 s-78m_\pi^4-24s^2,\, 3,\, 12m_\pi^2-\frac{21s}{4},\, 1,\\
&\qquad 4(-31m_\pi^2 s+26m_\pi^4+8s^2),\, -9s,\, 7s-16m_\pi^2\Big)\,,\\
A^6_{3m}(s) &= \frac{1}{(s-4m_\pi^2)^2}\Big(\frac{5}{4},\, \frac{111s^2}{8}-6m_\pi^2(8m_\pi^2+s),\, 5,\, \frac{23s}{4}-8m_\pi^2,\, -\frac{5}{3},\\
&\qquad 8m_\pi^2 s+64m_\pi^4-\frac{37s^2}{2},\, 48m_\pi^2-27s,\, \frac{1}{3}(32m_\pi^2-23s)\Big)\,,\\
A^6_{4m}(s) &= \frac{1}{s-4m_\pi^2}\Big(0,\, \frac{15}{32}(31s-44m_\pi^2),\, 0,\, \frac{15}{8},\, 0,\, \frac{5}{8}(44m_\pi^2-31s),\, -\frac{15}{2},\, -\frac{5}{2}\Big)\,,\\
A^6_{5m}(s) &= \Big(0,\, \frac{75}{32},\, 0,\, 0,\, 0,\, -\frac{25}{8},\, 0,\, 0\Big)\,,\\
A^7_{1m}(s) &= \frac{1}{s-4m_\pi^2}\Big(-\frac{5}{8},\, \frac{15}{64}(24m_\pi^2 s+48m_\pi^4-29s^2),\, 0,\, \frac{5}{16}(7s-4m_\pi^2),\, -\frac{5}{12},\\
&\qquad \frac{5}{32}(24m_\pi^2 s+48m_\pi^4-29s^2),\, 0,\, \frac{5}{24}(7s-4m_\pi^2)\Big)\,,\\
A^7_{2m}(s) &= \Big(0,\, \frac{45m_\pi^2}{8}-\frac{195s}{32},\, 0,\, \frac{15}{16},\, 0,\, \frac{15m_\pi^2}{4}-\frac{65s}{16},\, 0,\, \frac{5}{8}\Big)\,,\\
A^7_{3m}(s) &= \frac{1}{s-4m_\pi^2}\Big(\frac{5}{8},\, \frac{15}{8}(s-2m_\pi^2)(8m_\pi^2+3s),\, 0,\, \frac{5}{16}(4m_\pi^2-7s),\, \frac{5}{12},\\
&\qquad \frac{5}{4}(s-2m_\pi^2)(8m_\pi^2+3s),\, 0,\, \frac{5}{24}(4m_\pi^2-7s)\Big)\,,\\
A^7_{4m}(s) &= \Big(0,\, \frac{15}{32}(13s-12m_\pi^2),\, 0,\, -\frac{15}{16},\, 0,\, \frac{5}{16}(13s-12m_\pi^2),\, 0,\, -\frac{5}{8}\Big)\,,\\
A^7_{5m}(s) &= (s-4m_\pi^2)\Big(0,\, \frac{75}{64},\, 0,\, 0,\, 0,\, \frac{25}{32},\, 0,\, 0\Big)\,,\\
A^8_{0m}(s) &= \frac{1}{s-4m_\pi^2}\Big(-\frac{1}{4},\, -\frac{3}{32}(-152m_\pi^2 s+80m_\pi^4+53s^2),\, 1,\, \frac{5m_\pi^2}{2}-\frac{11s}{8},\, \frac{1}{3},\\
&\qquad -19m_\pi^2 s+10m_\pi^4+\frac{53s^2}{8},\, 6m_\pi^2-\frac{9s}{2},\, \frac{1}{6}(11s-20m_\pi^2)\Big)\,,
\end{aligned}
$$

$$
\begin{aligned}
A^8_{1m}(s) &= \frac{1}{s-4m_\pi^2}\Big(-\frac{1}{2},\, -\frac{3}{8}(5s-12m_\pi^2)(7s-8m_\pi^2),\, -2,\, \frac{1}{8}(52m_\pi^2-25s),\, \frac{2}{3},\\
&\qquad -62m_\pi^2 s+48m_\pi^4+\frac{35s^2}{2},\, \frac{15s}{2}-6m_\pi^2,\, \frac{1}{6}(25s-52m_\pi^2)\Big)\,,\\
A^8_{2m}(s) &= \frac{1}{s-4m_\pi^2}\Big(\frac{3}{4},\, \frac{129s^2}{16}-3m_\pi^2(9m_\pi^2+s),\, -3,\, \frac{9}{8}(3s-4m_\pi^2),\, -1,\\
&\qquad 4m_\pi^2 s+36m_\pi^4-\frac{43s^2}{4},\, \frac{33s}{2}-30m_\pi^2,\, 6m_\pi^2-\frac{9s}{2}\Big)\,,\\
A^8_{3m}(s) &= \Big(0,\, \frac{69s}{8}-12m_\pi^2,\, 0,\, \frac{9}{8},\, 0,\, 16m_\pi^2-\frac{23s}{2},\, \frac{9}{2},\, -\frac{3}{2}\Big)\,,\\
A^8_{4m}(s) &= (s-4m_\pi^2)\Big(0,\, \frac{45}{32},\, 0,\, 0,\, 0,\, -\frac{15}{8},\, 0,\, 0\Big)
\end{aligned}
\tag{B.4}
$$

and the entries that are not given explicitly vanish. The inhomogeneous contributions become

$$
\begin{aligned}
I^1_D(s) &= \frac{64\pi}{3s^2\sigma_\pi^5(s)}\csc\left(\delta^0_0(s)+\delta^1_1(s)\right)\\
&\quad\times\Big[2s\sigma_\pi^2(s)\left(5\delta^{0\prime}_2(s)\sin\left(\delta^0_0(s)-2\delta^0_2(s)+\delta^1_1(s)\right)-3\delta^{1\prime}_1(s)\sin\left(\delta^0_0(s)-\delta^1_1(s)\right)\right)\\
&\qquad -5\cos\left(\delta^0_0(s)-2\delta^0_2(s)+\delta^1_1(s)\right)+3\cos\left(\delta^0_0(s)-\delta^1_1(s)\right)+2\cos\left(\delta^0_0(s)+\delta^1_1(s)\right)\Big]\,,\\
I^2_D(s) &= 0\,,\\
I^3_D(s) &= -\frac{24\pi\tan\delta^1_1(s)}{s^2\sigma_\pi^3(s)}\,,\\
I^4_D(s) &= \frac{640\pi}{3s^3\sigma_\pi^7(s)}\csc\left(\delta^0_2(s)+\delta^1_1(s)\right)\Big[s\sigma_\pi^2(s)\delta^{0\prime}_2(s)\sin\left(\delta^0_2(s)-\delta^1_1(s)\right)+\sin\delta^0_2(s)\sin\delta^1_1(s)\Big]\,,\\
I^5_D(s) &= \frac{16\pi}{s^2\sigma\pi(s)^5}\csc\left(\delta^1_1(s)+\delta^2_0(s)\right)\\
&\quad\times\Big[2s\sigma_\pi^2(s)\left(3\delta^{1\prime}_1(s)\sin\left(\delta^1_1(s)-\delta^2_0(s)\right)+5\delta^{2\prime}_2(s)\sin\left(\delta^1_1(s)+\delta^2_0(s)-2\delta^2_2(s)\right)\right)\\
&\qquad -5\cos\left(\delta^1_1(s)+\delta^2_0(s)-2\delta^2_2(s)\right)+3\cos\left(\delta^1_1(s)-\delta^2_0(s)\right)+2\cos\left(\delta^1_1(s)+\delta^2_0(s)\right)\Big]\,,\\
I^6_D(s) &= 0\,,\\
I^7_D(s) &= -\frac{40\pi\tan\delta^2_2(s)}{s^3\sigma_\pi^5(s)}\,,\\
I^8_D(s) &= \frac{160\pi}{s^3\sigma\pi(s)^7}\csc\left(\delta^1_1(s)+\delta^2_2(s)\right)\Big[\sin\delta^1_1(s)\sin\delta^2_2(s)-s\sigma_\pi^2(s)\delta^{2\prime}_2(s)\sin\left(\delta^1_1(s)-\delta^2_2(s)\right)\Big]\,.
\end{aligned}
\tag{B.5}
$$

The singularities at points where linear combinations of phase shifts approach multiples of π are canceled by the term $\sin\delta_n(s')$ in Eq. (6.91).

References

[1] **Muon g-2** Collaboration, G. W. Bennett *et al.*, "Final report of the muon E821 anomalous magnetic moment measurement at BNL," *Phys. Rev. D* **73** (2006) 072003, `arXiv:hep-ex/0602035 [hep-ex]`.

[2] M. Davier and W. J. Marciano, "The theoretical prediction for the muon anomalous magnetic moment," *Ann. Rev. Nucl. Part. Sci.* **54** (2004) 115–140.

[3] T. Aoyama *et al.*, "The anomalous magnetic moment of the muon in the Standard Model," *Phys. Rept.* **887** (2020) 1–166, `arXiv:2006.04822 [hep-ph]`.

[4] T. Aoyama, M. Hayakawa, T. Kinoshita, and M. Nio, "Complete Tenth-Order QED Contribution to the Muon $g-2$," *Phys. Rev. Lett.* **109** (2012) 111808, `arXiv:1205.5370 [hep-ph]`.

[5] T. Aoyama, T. Kinoshita, and M. Nio, "Theory of the Anomalous Magnetic Moment of the Electron," *Atoms* **7** no. 1, (2019) 28.

[6] A. Czarnecki, W. J. Marciano, and A. Vainshtein, "Refinements in electroweak contributions to the muon anomalous magnetic moment," *Phys. Rev. D* **67** (2003) 073006, `arXiv:hep-ph/0212229 [hep-ph]`. [Erratum: Phys. Rev. D 73 (2006) 119901(2006)].

[7] C. Gnendiger, D. Stöckinger, and H. Stöckinger-Kim, "The electroweak contributions to $(g-2)_\mu$ after the Higgs boson mass measurement," *Phys. Rev. D* **88** (2013) 053005, `arXiv:1306.5546 [hep-ph]`.

[8] M. Davier, A. Hoecker, B. Malaescu, and Z. Zhang, "Reevaluation of the hadronic vacuum polarisation contributions to the Standard Model predictions of the muon $g-2$ and $\alpha(m_Z^2)$ using newest hadronic cross-section data," *Eur. Phys. J. C* **77** no. 12, (2017) 827, `arXiv:1706.09436 [hep-ph]`.

[9] A. Keshavarzi, D. Nomura, and T. Teubner, "Muon $g-2$ and $\alpha(M_Z^2)$: a new data-based analysis," *Phys. Rev. D* **97** no. 11, (2018) 114025, `arXiv:1802.02995 [hep-ph]`.

[10] G. Colangelo, M. Hoferichter, and P. Stoffer, "Two-pion contribution to hadronic vacuum polarization," *JHEP* **02** (2019) 006, `arXiv:1810.00007 [hep-ph]`.

[11] M. Hoferichter, B.-L. Hoid, and B. Kubis, "Three-pion contribution to hadronic vacuum polarization," *JHEP* **08** (2019) 137, `arXiv:1907.01556 [hep-ph]`.

[12] M. Davier, A. Hoecker, B. Malaescu, and Z. Zhang, "A new evaluation of the hadronic vacuum polarisation contributions to the muon anomalous magnetic moment and to $\alpha(m_Z^2)$," *Eur. Phys. J. C* **80** no. 3, (2020) 241, `arXiv:1908.00921 [hep-ph]`. [Erratum: Eur.Phys.J.C 80, 410 (2020)].

[13] A. Keshavarzi, D. Nomura, and T. Teubner, "$g-2$ of charged leptons, $\alpha(M_Z^2)$, and the hyperfine splitting of muonium," *Phys. Rev. D* **101** no. 1, (2020) 014029, `arXiv:1911.00367 [hep-ph]`.

[14] A. Kurz, T. Liu, P. Marquard, and M. Steinhauser, "Hadronic contribution to the muon anomalous magnetic moment to next-to-next-to-leading order," *Phys. Lett. B* **734** (2014) 144–147, `arXiv:1403.6400 [hep-ph]`.

[15] K. Melnikov and A. Vainshtein, "Hadronic light-by-light scattering contribution to the muon anomalous magnetic moment reexamined," *Phys. Rev. D* **70** (2004) 113006, `arXiv:hep-ph/0312226 [hep-ph]`.

[16] P. Masjuan and P. Sanchez-Puertas, "Pseudoscalar-pole contribution to the $(g_\mu - 2)$: a rational approach," *Phys. Rev. D* **95** no. 5, (2017) 054026, `arXiv:1701.05829 [hep-ph]`.

[17] G. Colangelo, M. Hoferichter, M. Procura, and P. Stoffer, "Dispersion relation for hadronic light-by-light scattering: two-pion contributions," *JHEP* **04** (2017) 161, `arXiv:1702.07347 [hep-ph]`.

[18] M. Hoferichter, B.-L. Hoid, B. Kubis, S. Leupold, and S. P. Schneider, "Dispersion relation for hadronic light-by-light scattering: pion pole," *JHEP* **10** (2018) 141, `arXiv:1808.04823 [hep-ph]`.

[19] A. Gérardin, H. B. Meyer, and A. Nyffeler, "Lattice calculation of the pion transition form factor with $N_f = 2 + 1$ Wilson quarks," *Phys. Rev. D* **100** no. 3, (2019) 034520, `arXiv:1903.09471 [hep-lat]`.

[20] J. Bijnens, N. Hermansson-Truedsson, and A. Rodríguez-Sánchez, "Short-distance constraints for the HLbL contribution to the muon anomalous magnetic moment," *Phys. Lett. B* **798** (2019) 134994, `arXiv:1908.03331 [hep-ph]`.

[21] G. Colangelo, F. Hagelstein, M. Hoferichter, L. Laub, and P. Stoffer, "Longitudinal short-distance constraints for the hadronic light-by-light contribution to $(g-2)_\mu$ with large-N_c Regge models," *JHEP* **03** (2020) 101, `arXiv:1910.13432 [hep-ph]`.

[22] T. Blum, N. Christ, M. Hayakawa, T. Izubuchi, L. Jin, C. Jung, and C. Lehner, "Hadronic Light-by-Light Scattering Contribution to the Muon Anomalous Magnetic Moment from Lattice QCD," *Phys. Rev. Lett.* **124** no. 13, (2020) 132002, `arXiv:1911.08123 [hep-lat]`.

[23] G. Colangelo, M. Hoferichter, A. Nyffeler, M. Passera, and P. Stoffer, "Remarks on higher-order hadronic corrections to the muon $g-2$," *Phys. Lett. B* **735** (2014) 90–91, `arXiv:1403.7512 [hep-ph]`.

[24] **Muon g-2** Collaboration, J. Grange *et al.*, "Muon $g-2$ technical design report," `arXiv:1501.06858 [physics.ins-det]`. unpublished.

[25] **Muon g-2** Collaboration, B. Abi *et al.*, "Measurement of the Positive Muon Anomalous Magnetic Moment to 0.46 ppm," *Phys. Rev. Lett.* **126** no. 14, (2021) 141801, `arXiv:2104.03281 [hep-ex]`.

[26] **Muon g-2** Collaboration, T. Albahri *et al.*, "Measurement of the anomalous precession frequency of the muon in the Fermilab Muon $g-2$ Experiment," *Phys. Rev. D* **103** no. 7, (2021) 072002, `arXiv:2104.03247 [hep-ex]`.

[27] **Muon g-2** Collaboration, T. Albahri *et al.*, "Magnetic-field measurement and analysis for the Muon $g-2$ Experiment at Fermilab," *Phys. Rev. A* **103** no. 4, (2021) 042208, `arXiv:2104.03201 [hep-ex]`.

[28] **Muon g-2** Collaboration, T. Albahri *et al.*, "Beam dynamics corrections to the Run-1 measurement of the muon anomalous magnetic moment at Fermilab," *Phys. Rev. Accel. Beams* **24** no. 4, (2021) 044002, `arXiv:2104.03240 [physics.acc-ph]`.

[29] S. Borsanyi *et al.*, "Leading hadronic contribution to the muon magnetic moment from lattice QCD," *Nature* **593** no. 7857, (2021) 51–55, `arXiv:2002.12347 [hep-lat]`.

[30] T. Blum *et al.*, "An update of Euclidean windows of the hadronic vacuum polarization," `arXiv:2301.08696 [hep-lat]`.

[31] C. Alexandrou *et al.*, "Lattice calculation of the short and intermediate time-distance hadronic vacuum polarization contributions to the muon magnetic moment using twisted-mass fermions," `arXiv:2206.15084 [hep-lat]`.

[32] C. Alexandrou *et al.*, "Probing the R-ratio on the lattice," `arXiv:2212.08467 [hep-lat]`.

[33] M. Cè *et al.*, "Window observable for the hadronic vacuum polarization contribution to the muon $g-2$ from lattice QCD," `arXiv:2206.06582 [hep-lat]`.

[34] **Fermilab Lattice, MILC, HPQCD** Collaboration, C. T. H. Davies *et al.*, "Windows on the hadronic vacuum polarization contribution to the muon anomalous magnetic moment," *Phys. Rev. D* **106** no. 7, (2022) 074509, `arXiv:2207.04765 [hep-lat]`.

[35] A. Bazavov *et al.*, "Light-quark connected intermediate-window contributions to the muon $g-2$ hadronic vacuum polarization from lattice QCD," `arXiv:2301.08274 [hep-lat]`.

[36] **CMD-3** Collaboration, F. V. Ignatov *et al.*, "Measurement of the $e^+e^- \to \pi^+\pi^-$ cross section from threshold to 1.2 GeV with the CMD-3 detector," `arXiv:2302.08834 [hep-ex]`.

[37] G. Colangelo *et al.*, "Prospects for precise predictions of a_μ in the Standard Model," `arXiv:2203.15810 [hep-ph]`.

[38] G. Colangelo, M. Hoferichter, M. Procura, and P. Stoffer, "Dispersive approach to hadronic light-by-light scattering," *JHEP* **09** (2014) 091, `arXiv:1402.7081 [hep-ph]`.

[39] G. Colangelo, M. Hoferichter, M. Procura, and P. Stoffer, "Dispersion relation for hadronic light-by-light scattering: theoretical foundations," *JHEP* **09** (2015) 074, `arXiv:1506.01386 [hep-ph]`.

[40] G. Colangelo, F. Hagelstein, M. Hoferichter, L. Laub, and P. Stoffer, "Short-distance constraints on hadronic light-by-light scattering in the anomalous magnetic moment of the muon," *Phys. Rev. D* **101** no. 5, (2020) 051501, `arXiv:1910.11881 [hep-ph]`.

[41] L. Cappiello, O. Catà, G. D'Ambrosio, D. Greynat, and A. Iyer, "On axials and pseudoscalars in the hadronic light-by-light contribution to the muon $(g-2)$," `arXiv:1912.02779 [hep-ph]`.

[42] J. Leutgeb and A. Rebhan, "Axial vector transition form factors in holographic QCD and their contribution to the anomalous magnetic moment of the muon," `arXiv:1912.01596 [hep-ph]`.

[43] J. Leutgeb and A. Rebhan, "Hadronic light-by-light contribution to the muon $g-2$ from holographic QCD with massive pions," *Phys. Rev. D* **104** no. 9, (2021) 094017, `arXiv:2108.12345 [hep-ph]`.

[44] J. Leutgeb, J. Mager, and A. Rebhan, "Hadronic light-by-light contribution to the muon $g-2$ from holographic QCD with solved $U(1)_A$ problem," `arXiv:2211.16562 [hep-ph]`.

[45] J. Lüdtke and M. Procura, "Effects of longitudinal short-distance constraints on the hadronic light-by-light contribution to the muon $g-2$," *Eur. Phys. J. C* **80** no. 12, (2020) 1108, `arXiv:2006.00007 [hep-ph]`.

[46] G. Colangelo, F. Hagelstein, M. Hoferichter, L. Laub, and P. Stoffer, "Short-distance constraints for the longitudinal component of the hadronic light-by-light amplitude: an update," *Eur. Phys. J. C* **81** no. 8, (2021) 702, `arXiv:2106.13222 [hep-ph]`.

[47] J. Bijnens, N. Hermansson-Truedsson, L. Laub, and A. Rodríguez-Sánchez, "Short-distance HLbL contributions to the muon anomalous magnetic moment beyond perturbation theory," *JHEP* **10** (2020) 203, `arXiv:2008.13487 [hep-ph]`.

[48] J. Bijnens, N. Hermansson-Truedsson, L. Laub, and A. Rodríguez-Sánchez, "The two-loop perturbative correction to the $(g-2)_\mu$ HLbL at short distances," *JHEP* **04** (2021) 240, `arXiv:2101.09169 [hep-ph]`.

[49] J. Bijnens, N. Hermansson-Truedsson, and A. Rodríguez-Sánchez, "Constraints on the hadronic light-by-light in the Melnikov-Vainshtein regime," `arXiv:2211.17183 [hep-ph]`.

[50] M. Hoferichter, B.-L. Hoid, B. Kubis, S. Leupold, and S. P. Schneider, "Pion-pole contribution to hadronic light-by-light scattering in the anomalous magnetic moment of the muon," *Phys. Rev. Lett.* **121** no. 11, (2018) 112002, `arXiv:1805.01471 [hep-ph]`.

[51] I. Danilkin, M. Hoferichter, and P. Stoffer, "A dispersive estimate of scalar contributions to hadronic light-by-light scattering," *Phys. Lett. B* **820** (2021) 136502, `arXiv:2105.01666 [hep-ph]`.

[52] V. Pauk and M. Vanderhaeghen, "Single meson contributions to the muon's anomalous magnetic moment," *Eur. Phys. J. C* **74** no. 8, (2014) 3008, `arXiv:1401.0832 [hep-ph]`.

[53] I. Danilkin and M. Vanderhaeghen, "Light-by-light scattering sum rules in light of new data," *Phys. Rev. D* **95** no. 1, (2017) 014019, `arXiv:1611.04646 [hep-ph]`.

[54] P. Roig and P. Sanchez-Puertas, "Axial-vector exchange contribution to the hadronic light-by-light piece of the muon anomalous magnetic moment," *Phys. Rev. D* **101** no. 7, (2020) 074019, `arXiv:1910.02881 [hep-ph]`.

[55] P. Masjuan, P. Roig, and P. Sanchez-Puertas, "A different viewpoint on the hadronic light-by-light tensor short-distance constraints," `arXiv:2005.11761 [hep-ph]`.

[56] F. Jegerlehner, *The anomalous magnetic moment of the muon*, vol. 274 of *Springer Tracts in Modern Physics*. Springer, Cham, second ed., 2017.

[57] M. Knecht, S. Narison, A. Rabemananjara, and D. Rabetiarivony, "Scalar meson contributions to a_μ from hadronic light-by-light scattering," *Phys. Lett. B* **787** (2018) 111–123, `arXiv:1808.03848 [hep-ph]`.

[58] S. Peris, M. Perrottet, and E. de Rafael, "Two loop electroweak corrections to the muon $g-2$: A New class of hadronic contributions," *Phys. Lett. B* **355** (1995) 523–530, `arXiv:hep-ph/9505405`.

[59] M. Knecht, S. Peris, M. Perrottet, and E. De Rafael, "Electroweak hadronic contributions to the muon $(g-2)$," *JHEP* **11** (2002) 003, `arXiv:hep-ph/0205102 [hep-ph]`.

[60] J. Lüdtke, M. Procura, and P. Stoffer, "Dispersion relations for hadronic light-by-light scattering in triangle kinematics," `arXiv:2302.12264 [hep-ph]`.

[61] J. E. Nafe, E. B. Nelson, and I. I. Rabi, "The Hyperfine Structure of Atomic Hydrogen and Deuterium," *Phys. Rev.* **71** (1947) 914–915.

[62] J. S. Schwinger, "On Quantum electrodynamics and the magnetic moment of the electron," *Phys. Rev.* **73** (1948) 416–417.

[63] S. L. Glashow, "Partial Symmetries of Weak Interactions," *Nucl. Phys.* **22** (1961) 579–588.

[64] S. Weinberg, "A Model of Leptons," *Phys. Rev. Lett.* **19** (1967) 1264–1266.

[65] A. Salam, "Weak and Electromagnetic Interactions," *Conf. Proc. C* **680519** (1968) 367–377.

[66] C.-N. Yang and R. L. Mills, "Conservation of Isotopic Spin and Isotopic Gauge Invariance," *Phys. Rev.* **96** (1954) 191–195.

[67] H. Fritzsch, M. Gell-Mann, and H. Leutwyler, "Advantages of the Color Octet Gluon Picture," *Phys. Lett. B* **47** (1973) 365–368.

[68] **ATLAS** Collaboration, G. Aad *et al.*, "Observation of a new particle in the search for the Standard Model Higgs boson with the ATLAS detector at the LHC," *Phys. Lett. B* **716** (2012) 1–29, `arXiv:1207.7214 [hep-ex]`.

[69] **Particle Data Group** Collaboration, R. L. Workman and Others, "Review of Particle Physics," *PTEP* **2022** (2022) 083C01.

[70] R. S. Van Dyck, P. B. Schwinberg, and H. G. Dehmelt, "New High Precision Comparison of Electron and Positron G Factors," *Phys. Rev. Lett.* **59** (1987) 26–29.

[71] D. Hanneke, S. Fogwell, and G. Gabrielse, "New Measurement of the Electron Magnetic Moment and the Fine Structure Constant," *Phys. Rev. Lett.* **100** (2008) 120801, `arXiv:0801.1134 [physics.atom-ph]`.

[72] R. H. Parker, C. Yu, W. Zhong, B. Estey, and H. Müller, "Measurement of the fine-structure constant as a test of the Standard Model," *Science* **360** (2018) 191, `arXiv:1812.04130 [physics.atom-ph]`.

[73] L. Morel, Z. Yao, P. Cladé, and S. Guellati-Khélifa, "Determination of the fine-structure constant with an accuracy of 81 parts per trillion," *Nature* **588** no. 7836, (2020) 61–65.

[74] A. Pich, "Precision Tau Physics," *Prog. Part. Nucl. Phys.* **75** (2014) 41–85, `arXiv:1310.7922 [hep-ph]`.

[75] **CMS** Collaboration, A. Jofrehei, "Observation of τ lepton pair production in ultra-peripheral nucleus-nucleus collisions with the CMS experiment and the first limits on $(g-2)_\tau$ at the LHC," `arXiv:2205.05312 [hep-ex]`.

[76] **CMS** Collaboration, "Observation of τ lepton pair production in ultraperipheral lead-lead collisions at $\sqrt{s_{\mathrm{NN}}} = 5.02$ TeV," `arXiv:2206.05192 [nucl-ex]`.

[77] A. Crivellin, M. Hoferichter, and J. M. Roney, "Towards testing the magnetic moment of the tau at one part per million," `arXiv:2111.10378 [hep-ph]`.

[78] G. Charpak, F. J. M. Farley, R. L. Garwin, T. Muller, J. C. Sens, V. L. Telegdi, and A. Zichichi, "Measurement of the anomalous magnetic moment of the muon," *Phys. Rev. Lett.* **6** (1961) 128–132.

[79] G. Charpak, F. J. M. Farley, and R. L. Garwin, "A New Measurement of the Anomalous Magnetic Moment of the Muon," *Phys. Lett.* **1** (1962) 16.

[80] G. Charpak, P. J. M. Farley, E. L. Garwin, T. Muller, J. C. Sens, and A. Zichichi, "The anomalous magnetic moment of the muon," *Nuovo Cim.* **37** (1965) 1241–1363.

[81] F. J. M. Farley, J. Bailey, R. C. A. Brown, M. Giesch, H. Jöstlein, S. van der Meer, E. Picasso, and M. Tannenbaum, "The anomalous magnetic moment of the negative muon," *Nuovo Cim. A* **45** no. 1, (1966) 281–286. `https://doi.org/10.1007/BF02738104`.

[82] J. Bailey, W. Bartl, G. Von Bochmann, R. C. A. Brown, F. J. M. Farley, H. Joestlein, E. Picasso, and R. W. Williams, "Precision measurement of the anomalous magnetic moment of the muon," *Phys. Lett. B* **28** (1968) 287–290.

[83] J. Bailey, W. Bartl, G. von Bochmann, R. C. A. Brown, F. J. M. Farley, M. Giesch, H. Jostlein, S. van der Meer, E. Picasso, and R. W. Williams, "Precise Measurement of the Anomalous Magnetic Moment of the Muon," *Nuovo Cim. A* **9** (1972) 369–432.

[84] **CERN-Mainz-Daresbury** Collaboration, J. Bailey *et al.*, "Final Report on the CERN Muon Storage Ring Including the Anomalous Magnetic Moment and the Electric Dipole Moment of the Muon, and a Direct Test of Relativistic Time Dilation," *Nucl. Phys. B* **150** (1979) 1–75.

[85] M. Abe *et al.*, "A New Approach for Measuring the Muon Anomalous Magnetic Moment and Electric Dipole Moment," *PTEP* **2019** no. 5, (2019) 053C02, `arXiv:1901.03047 [physics.ins-det]`.

[86] P. J. Mohr, B. N. Taylor, and D. B. Newell, "CODATA Recommended Values of the Fundamental Physical Constants: 2010," *Rev. Mod. Phys.* **84** (2012) 1527–1605, `arXiv:1203.5425 [physics.atom-ph]`.

[87] S. Laporta, "High-precision calculation of the 4-loop contribution to the electron $g-2$ in QED," *Phys. Lett. B* **772** (2017) 232–238, `arXiv:1704.06996 [hep-ph]`.

[88] S. Volkov, "Calculating the five-loop QED contribution to the electron anomalous magnetic moment: Graphs without lepton loops," *Phys. Rev. D* **100** no. 9, (2019) 096004, `arXiv:1909.08015 [hep-ph]`.

[89] G. Colangelo, A. X. El-Khadra, M. Hoferichter, A. Keshavarzi, C. Lehner, P. Stoffer, and T. Teubner, "Data-driven evaluations of Euclidean windows to scrutinize hadronic vacuum polarization," *Phys. Lett. B* **833** (2022) 137313, `arXiv:2205.12963 [hep-ph]`.

[90] G. Colangelo, M. Hoferichter, and P. Stoffer, "Constraints on the two-pion contribution to hadronic vacuum polarization," *Phys. Lett. B* **814** (2021) 136073, `arXiv:2010.07943 [hep-ph]`.

[91] M. Davier, D. Díaz-Calderón, B. Malaescu, A. Pich, A. Rodríguez-Sánchez, and Z. Zhang, "The Euclidean Adler Function and its Interplay with $\Delta\alpha_{\rm QED}^{\rm had}$ and α_s," `arXiv:2302.01359 [hep-ph]`.

[92] T. DeGrand, "Remarks about weighted energy integrals over Minkowski spectral functions from Euclidean lattice data," *Phys. Rev. D* **106** no. 1, (2022) 014504, `arXiv:2203.04393 [hep-lat]`.

[93] K. Melnikov and A. Vainshtein, "On dispersion relations and hadronic light-by-light scattering contribution to the muon anomalous magnetic moment," `arXiv:1911.05874 [hep-ph]`.

[94] M. Knecht, "On some properties of the fourth-rank hadronic vacuum polarization tensor and the anomalous magnetic moment of the muon," `arXiv:2005.09929 [hep-ph]`.

[95] E.-H. Chao, R. J. Hudspith, A. Gérardin, J. R. Green, H. B. Meyer, and K. Ottnad, "Hadronic light-by-light contribution to $(g-2)_\mu$ from lattice QCD: a complete calculation," *Eur. Phys. J. C* **81** no. 7, (2021) 651, `arXiv:2104.02632 [hep-lat]`.

[96] E.-H. Chao, R. J. Hudspith, A. Gérardin, J. R. Green, and H. B. Meyer, "The charm-quark contribution to light-by-light scattering in the muon $(g-2)$ from lattice QCD," `arXiv:2204.08844 [hep-lat]`.

[97] M. Hoferichter and T. Teubner, "Mixed Leptonic and Hadronic Corrections to the Anomalous Magnetic Moment of the Muon," *Phys. Rev. Lett.* **128** no. 11, (2022) 112002, `arXiv:2112.06929 [hep-ph]`.

[98] G. Abbiendi *et al.*, "Measuring the leading hadronic contribution to the muon $g-2$ via μe scattering," *Eur. Phys. J. C* **77** no. 3, (2017) 139, `arXiv:1609.08987 [hep-ex]`.

[99] G. Abbiendi *et al.*, "Results on multiple Coulomb scattering from 12 and 20 GeV electrons on carbon targets," *JINST* **15** no. 01, (2020) 01, `arXiv:1905.11677 [physics.ins-det]`.

[100] P. Banerjee *et al.*, "Theory for muon-electron scattering @ 10 ppm: A report of the MUonE theory initiative," *Eur. Phys. J. C* **80** no. 6, (2020) 591, `arXiv:2004.13663 [hep-ph]`.

[101] G. Abbiendi *et al.*, "A study of muon-electron elastic scattering in a test beam," *JINST* **16** no. 06, (2021) P06005, `arXiv:2102.11111 [hep-ex]`.

[102] B.-L. Hoid, M. Hoferichter, and B. Kubis, "Hadronic vacuum polarization and vector-meson resonance parameters from $e^+e^- \to \pi^0\gamma$," *Eur. Phys. J. C* **80** no. 10, (2020) 988, `arXiv:2007.12696 [hep-ph]`.

[103] J. Bijnens, E. Pallante, and J. Prades, "Hadronic light by light contributions to the muon $g-2$," *Phys. Rev. Lett.* **75** (1995) 1447–1450, `arXiv:hep-ph/9505251`. [Erratum: Phys.Rev.Lett. 75, 3781 (1995)].

[104] M. Hayakawa, T. Kinoshita, and A. I. Sanda, "Hadronic light by light scattering effect on muon $g-2$," *Phys. Rev. Lett.* **75** (1995) 790–793, `arXiv:hep-ph/9503463`.

[105] M. Hayakawa, T. Kinoshita, and A. I. Sanda, "Hadronic light by light scattering contribution to muon $g-2$," *Phys. Rev. D* **54** (1996) 3137–3153, `arXiv:hep-ph/9601310`.

[106] J. Bijnens, E. Pallante, and J. Prades, "Analysis of the hadronic light by light contributions to the muon $g-2$," *Nucl. Phys. B* **474** (1996) 379–420, `arXiv:hep-ph/9511388`.

[107] M. Hayakawa and T. Kinoshita, "Pseudoscalar pole terms in the hadronic light by light scattering contribution to muon $g-2$," *Phys. Rev. D* **57** (1998) 465–477, `arXiv:hep-ph/9708227`. [Erratum: Phys.Rev.D 66, 019902 (2002)].

[108] J. Prades, E. de Rafael, and A. Vainshtein, "The hadronic light-by-light scattering contribution to the muon and electron anomalous magnetic moments," in *Lepton dipole moments*, vol. 20 of *Advanced series on directions in high energy physics*, pp. 303–317. World Scientific, 2009. `arXiv:0901.0306 [hep-ph]`.

[109] F. Jegerlehner and A. Nyffeler, "The muon $g-2$," *Phys. Rept.* **477** (2009) 1–110, `arXiv:0902.3360 [hep-ph]`.

[110] V. Pauk and M. Vanderhaeghen, "Anomalous magnetic moment of the muon in a dispersive approach," *Phys. Rev. D* **90** no. 11, (2014) 113012, `arXiv:1409.0819 [hep-ph]`.

[111] F. Hagelstein and V. Pascalutsa, "Dissecting the hadronic contributions to $(g-2)_\mu$ by Schwinger's sum rule," *Phys. Rev. Lett.* **120** no. 7, (2018) 072002, `arXiv:1710.04571 [hep-ph]`.

[112] W. A. Bardeen and W.-K. Tung, "Invariant amplitudes for photon processes," *Phys. Rev.* **173** no. 5, (1968) 1423–1433. [Erratum: Phys. Rev. D 4 (1971) 3229].

[113] R. Tarrach, "Invariant amplitudes for virtual Compton scattering off polarized nucleons free from kinematical singularities, zeros and constraints," *Nuovo Cim. A* **28** (1975) 409–422.

[114] J. Aldins, S. J. Brodsky, A. J. Dufner, and T. Kinoshita, "Photon-photon scattering contribution to the sixth-order magnetic moments of the muon and the electron," *Phys. Rev. D* **1** no. 8, (1970) 2378–2395.

[115] R. Barbieri and E. Remiddi, "Electron and muon $\frac{1}{2}(g-2)$ from vacuum polarization insertions," *Nucl. Phys. B* **90** (1975) 233–266.

[116] J. L. Rosner, "Higher-order contributions to the divergent part of Z_3 in a model quantum electrodynamics," *Annals Phys.* **44** (1967) 11–34.

[117] M. J. Levine and R. Roskies, "Hyperspherical approach to quantum electrodynamics: sixth-order magnetic moment," *Phys. Rev. D* **9** no. 2, (1974) 421–429.

[118] P. Stoffer, *Dispersive Treatments of $K_{\ell 4}$ Decays and Hadronic Light-by-Light Scattering.* Phd thesis, Philosophisch-naturwissenschaftliche Fakultät der Universität Bern, 12, 2014. `arXiv:1412.5171 [hep-ph]`.

[119] G. Eichmann, C. S. Fischer, and W. Heupel, "Four-point functions and the permutation group S_4," *Phys. Rev. D* **92** no. 5, (2015) 056006, `arXiv:1505.06336 [hep-ph]`.

[120] M. Hoferichter, B. Kubis, S. Leupold, F. Niecknig, and S. P. Schneider, "Dispersive analysis of the pion transition form factor," *Eur. Phys. J. C* **74** (2014) 3180, `arXiv:1410.4691 [hep-ph]`.

[121] M. Hoferichter, B.-L. Hoid, B. Kubis, and J. Lüdtke, "Improved Standard-Model prediction for $\pi^0 \to e^+e^-$," *Phys. Rev. Lett.* **128** no. 17, (2022) 172004, `arXiv:2105.04563 [hep-ph]`.

[122] G. Eichmann, C. S. Fischer, E. Weil, and R. Williams, "Single pseudoscalar meson pole and pion box contributions to the anomalous magnetic moment of the muon," *Phys. Lett. B* **797** (2019) 134855, `arXiv:1903.10844 [hep-ph]`.

[123] K. Raya, A. Bashir, and P. Roig, "Contribution of neutral pseudoscalar mesons to a_μ^{HLbL} within a Schwinger-Dyson equations approach to QCD," *Phys. Rev. D* **101** no. 7, (2020) 074021, `arXiv:1910.05960 [hep-ph]`.

[124] J. Leutgeb, J. Mager, and A. Rebhan, "Pseudoscalar transition form factors and the hadronic light-by-light contribution to the anomalous magnetic moment of the muon from holographic QCD," *Phys. Rev. D* **100** no. 9, (2019) 094038, `arXiv:1906.11795 [hep-ph]`.

[125] C. Hanhart, A. Kupść, U.-G. Meißner, F. Stollenwerk, and A. Wirzba, "Dispersive analysis for $\eta \to \gamma\gamma^*$," *Eur. Phys. J. C* **73** no. 12, (2013) 2668, `arXiv:1307.5654 [hep-ph]`. [Erratum: Eur. Phys. J. C 75 (2015), no. 6 242].

[126] S. Holz, C. Hanhart, M. Hoferichter, and B. Kubis, "A dispersive analysis of $\eta' \to \pi^+\pi^-\gamma$ and $\eta' \to e^+e^-\gamma$," *Eur. Phys. J. C* **82** no. 5, (2022) 434, `arXiv:2202.05846 [hep-ph]`.

[127] S. Holz, J. Plenter, C. W. Xiao, T. Dato, C. Hanhart, B. Kubis, U. G. Meißner, and A. Wirzba, "Towards an improved understanding of $\eta \to \gamma^*\gamma^*$," *Eur. Phys. J. C* **81** no. 11, (2021) 1002, `arXiv:1509.02194 [hep-ph]`.

[128] B. Kubis, "Towards a dispersive determination of the η and η' transition form factors," *EPJ Web Conf.* **166** (2018) 00012.

[129] S. Holz, *The Quest for the η and η' Transition Form Factors: A Stroll on the Precision Frontier.* PhD thesis, Rheinische Friedrich-Wilhelms-Universität Bonn, 2022.

[130] G. Eichmann, C. S. Fischer, and R. Williams, "Kaon-box contribution to the anomalous magnetic moment of the muon," *Phys. Rev. D* **101** no. 5, (2020) 054015, `arXiv:1910.06795 [hep-ph]`.

[131] M. Hoferichter and P. Stoffer, "Asymptotic behavior of meson transition form factors," *JHEP* **05** (2020) 159, `arXiv:2004.06127 [hep-ph]`.

[132] M. Knecht, M. Perrottet, E. de Rafael, and S. Peris, "New nonrenormalization theorems for anomalous three point functions," *JHEP* **03** (2004) 035, `arXiv:hep-ph/0311100 [hep-ph]`.

[133] S. L. Adler, "Axial vector vertex in spinor electrodynamics," *Phys. Rev.* **177** (1969) 2426–2438.

[134] J. Bell and R. Jackiw, "A PCAC puzzle: $\pi^0 \to \gamma\gamma$ in the σ model," *Nuovo Cim. A* **60** (1969) 47–61.

[135] S. L. Adler and W. A. Bardeen, "Absence of higher-order corrections in the anomalous axial-vector divergence equation," *Phys. Rev.* **182** no. 5, (1969) 1517–1536.

[136] G. 't Hooft, "Naturalness, chiral symmetry, and spontaneous chiral symmetry breaking," in *Recent developments in gauge theories. Proceedings, Nato Advanced Study Institute, Cargese, France, August 26 – September 8, 1979*, vol. 59, pp. 135–157. Springer, 1980.

[137] V. A. Novikov, M. A. Shifman, A. I. Vainshtein, M. B. Voloshin, and V. I. Zakharov, "Use and misuse of QCD sum rules, factorization and related topics," *Nucl. Phys. B* **237** (1984) 525–552.

[138] A. V. Manohar, "The decays $Z \to W\pi$, $Z \to \gamma\pi$, and the pion form factor," *Phys. Lett. B* **244** no. 1, (1990) 101–106.

[139] H. Leutwyler, "On the $1/N$-expansion in chiral perturbation theory," *Nucl. Phys. B (Proc. Suppl.)* **64** (1998) 223–231, `arXiv:hep-ph/9709408 [hep-ph]`.

[140] R. Kaiser and H. Leutwyler, "Pseudoscalar decay constants at large N_c," in *Nonperturbative methods in quantum field theory. Proceedings, Workshop, Adelaide, Australia, February 2-13, 1998*, pp. 15–29. 1998. `arXiv:hep-ph/9806336 [hep-ph]`.

[141] R. Kaiser and H. Leutwyler, "Large N_c in chiral perturbation theory," *Eur. Phys. J. C* **17** (2000) 623–649, `arXiv:hep-ph/0007101 [hep-ph]`.

[142] S. S. Agaev, V. M. Braun, N. Offen, F. A. Porkert, and A. Schäfer, "Transition form factors $\gamma^*\gamma \to \eta$ and $\gamma^*\gamma \to \eta'$ in QCD," *Phys. Rev. D* **90** no. 7, (2014) 074019, `arXiv:1409.4311 [hep-ph]`.

[143] P. Sanchez-Puertas, *A theoretical study of meson transition form factors*. PhD thesis, Mainz U., Inst. Phys., 2016. `arXiv:1709.04792 [hep-ph]`.

[144] E. Braaten, "Quantum-chromodynamic corrections to meson-photon transition form factors," *Phys. Rev. D* **28** (1983) 524–533.

[145] M. B. Voloshin, "QCD calculation of $\pi^0\gamma\gamma$ vertex at equal Euclidean q^2 of both photons," *ITEP-8-1982* (1982) . Unpublished.

[146] G. 't Hooft and M. Veltman, "Regularization and Renormalization of Gauge Fields," *Nucl. Phys. B* **44** (1972) 189–213.

[147] P. Breitenlohner and D. Maison, "Dimensional Renormalization and the Action Principle," *Commun. Math. Phys.* **52** (1977) 11–38.

[148] G. Lepage and S. J. Brodsky, "Exclusive processes in perturbative quantum chromodynamics," *Phys. Rev. D* **22** no. 9, (1980) 2157–2198.

[149] S. J. Brodsky and G. P. Lepage, "Large-angle two-photon exclusive channels in quantum chromodynamics," *Phys. Rev. D* **24** no. 7, (1981) 1808–1817.

[150] J. Bijnens, E. Gamiz, E. Lipartia, and J. Prades, "QCD short-distance constraints and hadronic approximations," *JHEP* **04** (2003) 055, `arXiv:hep-ph/0304222 [hep-ph]`.

[151] J. Leutgeb, J. Mager, and A. Rebhan, "Holographic QCD and the muon anomalous magnetic moment," *Eur. Phys. J. C* **81** no. 11, (2021) 1008, `arXiv:2110.07458 [hep-ph]`.

[152] J. M. Maldacena, "The Large N limit of superconformal field theories and supergravity," *Adv. Theor. Math. Phys.* **2** (1998) 231–252, `arXiv:hep-th/9711200`.

[153] E. de Rafael, "Hadronic contributions to the muon $g-2$ and low-energy QCD," *Phys. Lett. B* **322** (1994) 239–246, `arXiv:hep-ph/9311316 [hep-ph]`.

[154] **PrimEx** Collaboration, I. Larin *et al.*, "A new measurement of the π^0 radiative decay width," *Phys. Rev. Lett.* **106** (2011) 162303, `arXiv:1009.1681 [nucl-ex]`.

[155] **BaBar** Collaboration, B. Aubert *et al.*, "Measurement of the $\gamma\gamma^* \to \pi^0$ transition form factor," *Phys. Rev. D* **80** (2009) 052002, `arXiv:0905.4778 [hep-ex]`.

[156] **Belle** Collaboration, S. Uehara *et al.*, "Measurement of $\gamma\gamma^* \to \pi^0$ transition form factor at Belle," *Phys. Rev. D* **86** (2012) 092007, `arXiv:1205.3249 [hep-ex]`.

[157] I. Danilkin, C. F. Redmer, and M. Vanderhaeghen, "The hadronic light-by-light contribution to the muon's anomalous magnetic moment," *Prog. Part. Nucl. Phys.* **107** (2019) 20–68, `arXiv:1901.10346 [hep-ph]`.

[158] G. Ecker, J. Gasser, A. Pich, and E. de Rafael, "The role of resonances in chiral perturbation theory," *Nucl. Phys. B* **321** (1989) 311–342.

[159] K. Kampf and J. Novotný, "Resonance saturation in the odd-intrinsic parity sector of low-energy QCD," *Phys. Rev. D* **84** (2011) 014036, `arXiv:1104.3137 [hep-ph]`.

[160] **L3** Collaboration, M. Acciarri *et al.*, "Resonance formation in the $\pi^+\pi^-\pi^0$ final state in two-photon collisions," *Phys. Lett. B* **413** (1997) 147–158.

[161] **OBELIX** Collaboration, P. Salvini *et al.*, "anti-$\bar{p}p$ annihilation into four charged pions at rest and in flight," *Eur. Phys. J. C* **35** (2004) 21–33.

[162] B. Efron, “Bootstrap methods: another look at the jackknife,” *Ann. Statist.* **7** no. 1, (01, 1979) 1–26.

[163] J. Hirn and V. Sanz, “Interpolating between low and high energy QCD via a 5D Yang-Mills model,” *JHEP* **12** (2005) 030, `arXiv:hep-ph/0507049 [hep-ph]`.

[164] **L3** Collaboration, P. Achard *et al.*, “$f_1(1285)$ formation in two photon collisions at LEP,” *Phys. Lett. B* **526** (2002) 269–277, `arXiv:hep-ex/0110073`.

[165] **L3** Collaboration, P. Achard *et al.*, “Study of resonance formation in the mass region 1400–1500 MeV through the reaction $\gamma\gamma \to K_S^0 K^\pm \pi^\mp$,” *JHEP* **03** (2007) 018.

[166] J. Mondejar and K. Melnikov, “The VVA correlator at three loops in perturbative QCD,” *Phys. Lett. B* **718** (2013) 1364–1368, `arXiv:1210.0812 [hep-ph]`.

[167] A. Vainshtein, “Perturbative and nonperturbative renormalization of anomalous quark triangles,” *Phys. Lett. B* **569** (2003) 187–193, `arXiv:hep-ph/0212231`.

[168] W. H. Furry, “A Symmetry Theorem in the Positron Theory,” *Phys. Rev.* **51** (1937) 125–129.

[169] G. P. Lepage and S. J. Brodsky, “Exclusive Processes in Quantum Chromodynamics: Evolution Equations for Hadronic Wave Functions and the Form-Factors of Mesons,” *Phys. Lett. B* **87** (1979) 359–365.

[170] P. Stoffer. private communication.

[171] M. Hoferichter, B. Kubis, and D. Sakkas, “Extracting the chiral anomaly from $\gamma\pi \to \pi\pi$,” *Phys. Rev. D* **86** (2012) 116009, `arXiv:1210.6793 [hep-ph]`.

[172] M. Hoferichter, B. Kubis, and M. Zanke, “Radiative resonance couplings in $\gamma\pi\to\pi\pi$,” *Phys. Rev. D* **96** no. 11, (2017) 114016, `arXiv:1710.00824 [hep-ph]`.

[173] J. Wess and B. Zumino, “Consequences of anomalous Ward identities,” *Phys. Lett. B* **37** (1971) 95–97.

[174] E. Witten, “Global Aspects of Current Algebra,” *Nucl. Phys. B* **223** (1983) 422–432.

[175] J. Bijnens, A. Bramon, and F. Cornet, “Three Pseudoscalar Photon Interactions in Chiral Perturbation Theory,” *Phys. Lett. B* **237** (1990) 488–494.

[176] M. Jacob and G. C. Wick, “On the General Theory of Collisions for Particles with Spin,” *Annals Phys.* **7** (1959) 404–428.

[177] R. Omnes, “On the Solution of certain singular integral equations of quantum field theory,” *Nuovo Cim.* **8** (1958) 316–326.

[178] J. Bijnens, L. Girlanda, and P. Talavera, "The Anomalous chiral Lagrangian of order p^6," *Eur. Phys. J. C* **23** (2002) 539–544, `arXiv:hep-ph/0110400`.

[179] M. Zanke, M. Hoferichter, and B. Kubis, "On the transition form factors of the axial-vector resonance $f_1(1285)$ and its decay into e^+e^-," *JHEP* **07** (2021) 106, `arXiv:2103.09829 [hep-ph]`.

[180] M. Knecht, S. Peris, M. Perrottet, and E. de Rafael, "New nonrenormalization theorems for anomalous three point functions," *JHEP* **03** (2004) 035, `arXiv:hep-ph/0311100`.

[181] G. S. Bali, F. Bruckmann, M. Constantinou, M. Costa, G. Endrodi, S. D. Katz, H. Panagopoulos, and A. Schafer, "Magnetic susceptibility of QCD at zero and at finite temperature from the lattice," *Phys. Rev. D* **86** (2012) 094512, `arXiv:1209.6015 [hep-lat]`.

[182] G. Colangelo, J. Gasser, and H. Leutwyler, "$\pi\pi$ scattering," *Nucl. Phys. B* **603** (2001) 125–179, `arXiv:hep-ph/0103088`.

[183] S. M. Roy, "Exact integral equation for pion pion scattering involving only physical region partial waves," *Phys. Lett. B* **36** (1971) 353–356.

[184] **PrimEx-II** Collaboration, I. Larin *et al.*, "Precision measurement of the neutral pion lifetime," *Science* **368** no. 6490, (2020) 506–509.

[185] N. N. Khuri and S. B. Treiman, "Pion-Pion Scattering and $K^{\pm} \to 3\pi$ Decay," *Phys. Rev.* **119** (1960) 1115–1121.

[186] F. Niecknig, B. Kubis, and S. P. Schneider, "Dispersive analysis of $\omega \to 3\pi$ and $\phi \to 3\pi$ decays," *Eur. Phys. J. C* **72** (2012) 2014, `arXiv:1203.2501 [hep-ph]`.

[187] M. Adam, J. Lüdtke, and M. Procura, "Short-distance constraints on hadronic light-by-light scattering in triangle kinematics,". to appear.

[188] M. Adam, "Short-distance constraints on hadronic light-by-light scattering in triangle kinematics," Master's thesis, University of Vienna, 2023. to appear.

[189] M. Hoferichter and P. Stoffer, "Dispersion relations for $\gamma^*\gamma^* \to \pi\pi$: helicity amplitudes, subtractions, and anomalous thresholds," *JHEP* **07** (2019) 073, `arXiv:1905.13198 [hep-ph]`.

[190] A. Baroni, R. A. Briceño, M. T. Hansen, and F. G. Ortega-Gama, "Form factors of two-hadron states from a covariant finite-volume formalism," *Phys. Rev. D* **100** no. 3, (2019) 034511, `arXiv:1812.10504 [hep-lat]`.

[191] R. A. Briceño, M. T. Hansen, and A. W. Jackura, "Consistency checks for two-body finite-volume matrix elements: I. Conserved currents and bound states," *Phys. Rev. D* **100** no. 11, (2019) 114505, `arXiv:1909.10357 [hep-lat]`.

[192] R. A. Briceño, A. W. Jackura, A. Rodas, and J. V. Guerrero, "Prospects for $\gamma^*\gamma^* \to \pi\pi$ via lattice QCD," *Phys. Rev. D* **107** no. 3, (2023) 034504, `arXiv:2210.08051 [hep-lat]`.

[193] F. E. Low, "Bremsstrahlung of very low-energy quanta in elementary particle collisions," *Phys. Rev.* **110** (1958) 974–977.

[194] S. L. Adler and Y. Dothan, "Low-energy theorem for the weak axial-vector vertex," *Phys. Rev.* **151** (1966) 1267–1277.

[195] J. H. Kuhn, "The Tau lepton: Particle physics in a nutshell," *Nucl. Phys. B Proc. Suppl.* **76** (1999) 21–42, `arXiv:hep-ph/9812399`.

[196] R. Unterdorfer, "The One loop functional of chiral SU(2)," *JHEP* **07** (2002) 053, `arXiv:hep-ph/0205162`.

[197] G. Colangelo, S. Lanz, H. Leutwyler, and E. Passemar, "Dispersive analysis of $\eta \to 3\pi$," *Eur. Phys. J. C* **78** no. 11, (2018) 947, `arXiv:1807.11937 [hep-ph]`.

[198] R. Garcia-Martin, R. Kaminski, J. R. Pelaez, J. Ruiz de Elvira, and F. J. Yndurain, "The Pion-pion scattering amplitude. IV: Improved analysis with once subtracted Roy-like equations up to 1100 MeV," *Phys. Rev. D* **83** (2011) 074004, `arXiv:1102.2183 [hep-ph]`.